Utilizing lumped coupled tracer-aided modelling to identify temporal trends in basin-scale evapotranspiration partitioning

by

Aaron Smith

A Thesis submitted to the Faculty of Graduate Studies of

The University of Manitoba

in partial fulfilment of the requirements of the degree of

DOCTOR OF PHILOSOPHY

Department of Civil Engineering

University of Manitoba

Winnipeg

Abstract

Evapotranspiration is a primary hydrologic flux in catchment hydrology, significantly decreasing watershed storage available for discharge. High-latitude watersheds are highly-seasonal where climate change is expected to change sub-surface storage availability, which may consequently result in different evaporation and transpiration fluxes from storages. Temporal variability of the evapotranspiration partitioning in high-latitude large-scale remote watersheds has not been studied but is imperative for assessment of future water availability. Stable water isotopes (SWIs) have been successfully used to separate sources of watershed discharge using both hydrograph separation and modelling techniques as well as evaporative fluxes from total evapotranspiration in small scale modelling studies. The primary objective of this thesis was to identify the temporal changes in evapotranspiration partitioning within high-latitude watersheds, and the influence these fluxes have on watershed storage. A combination of statistical analysis and tracer-aided modelling was used to identify the primary storages contributing to watershed discharge, and the temporal uncertainty of these estimates. Generally, the unsaturated soil zone and rapid overland flow dominated summer discharge, while wetlands and groundwater were the primary contributors during winter. Quantifying temporal contributions of sources and their uncertainties, tracer-aided modelling and hydrograph separation were used to characterize the evaporation fractionation, and thereby evaporation to evapotranspiration (E/ET), within storage to temperature. Model results indicate higher E/ET during spring and fall, annually higher evaporation in wetlands than unsaturated soils, and further increases with soil moisture. Finally, as an additional analysis of the effect of evaporation and transpiration on watershed storage,

transit time distributions were used to estimate evaporation and transpiration flux ages. Separating ET into its components using the temperature dependent model revealed similar results to the tracer-aided modelling. Furthermore, mean evaporation age was less than one month, and showed inverse correlation to watershed transit time. Decreases in transpiration age do not directly influence discharge age, however, they resulted in more enriched simulated isotopic composition during the winter. This thesis identifies the importance of evaporation and transpiration fluxes on storage, and provides a framework by which tracer-aided models may be used to identify evaporation and transpiration influences in data-scarce regions.

Acknowledgements

I would like to utilize this section to thank those who have helped make this research possible. Firstly, my supervisor, Dr. Tricia Stadnyk; who has provided great support throughout my undergraduate and graduate degrees. Trish has encouraged learning and exploring new research areas (including meeting at lunch to discuss isotope and hydrology articles) which has given me the inspiration to pursue a career in research. I'd also like to thank you for your encouragement, during, and since my move overseas.

Secondly, Dr. Chani Welch, who has also supported my continuing education since arriving in Winnipeg in 2015. Those sampling trips were always entertaining, particularly those excursions through the woods to get elusive samples. Thank you for making time at odd hours while I was overseas to discuss ideas. You've become a good friend in the processes and I'm very grateful.

To my committee members Drs. Genevieve Ali, and Shawn Clark. Thank you for being available to discuss concepts when I needed, I am very appreciative of your support.

I would like to acknowledge the sources of financial support I have received throughout my degree, which has greatly helped with data collection and analysis to make this research possible. Manitoba Hydro, University of Manitoba, Natural Sciences and Engineering Research Council, without the support you have provided this thesis would not have been feasible.

My gratitude is extended also to the hydrometrics crew in Thompson, MB, for data collection, prior to the commencement of this degree as well as during this degree. Discussions with you all have provided insight into these remote basins that only years of experience may bring.

Thank you to everybody from the HRTF that I've worked with throughout the years: Alex, Parsa, Greg, Kian, Tegan, Andrew, Carly, Steve, Bill, Shane, Zach. Beer'o'clock Fridays are continuing overseas, though beer'o'clock has changed from 2:30-3:00 to 5:00-5:30.

Finally, to my mom, Helen, dad, Robert, sisters, Rachel and Rebecca, and my girlfriend Karlee, thank you for listening patiently to me discuss math, hydrological concepts, and modelling throughout my degree. I apologize if I bored any of you too much, I think you've all helped me improve my elevator pitch. I am immensely grateful to have you all in my life. Thank you.

Table of Contents

List of Tables

List of Figures

List of Appendices

Use of Copyrighted Material

Chapter 2

Figure 2-1. The theoretical isotopic framework of meteoric waters based on Gibson (1993) Adapted from *Hydrology Research* Volume 24, Issue number 2-3, pages 79-94, with permission from the copyright holders, IWA Publishing…… 18

Chapter 3

Chapter 3 of this thesis has been reproduced with minor modifications to formatting from Smith *et al*., 2015, Identification of geographical influences and flow regime characteristics using regional water isotope surveys in the lower Nelson River, Canada. Canadian Water Resource Journal, 40 (1): 23-35. This section has been reprinted with permission.

Chapter 4

Chapter 4 of this thesis has been reproduced with minor modifications to formatting from Smith *et al.*, 2016, Assessment of a lumped coupled flow-isotope model in data scarce Boreal catchments. Hydrological Processes, 30: 3871-3884. This section has been reprinted with permission.

Contributions of Co-Authors

This thesis was aided by the contributions of multiple co-authors, most notably for the manuscripts presented below. The overall analysis, discussion, and results shown are chiefly of my own work.

Chapter 3

***Identification of geographical influences and flow regime characteristics using regional water isotope surveys in the lower Nelson River, Canada*. (Smith, A., Delavau, C., and Stadnyk, T.)**

Dr. Carly Delavau aided with the writing, narrowing of research scope, and discussion through her extensive previous work and sampling in the lower Nelson River basin. She was also involved with the conceptualization of some of the manuscript figures. Dr. Tricia Stadnyk provided the opportunity to observe the lower Nelson River basin during a summer synoptic survey which greatly improved my understanding of the physiography. Dr. Stadnyk also aided with valuable insights into the flow regime and isotopic controls with regulation. All authors contributed to editing the manuscript prior to publication.

Chapters 4

***Assessment of a lumped coupled flow-isotope model in data scarce Boreal catchments*. (Smith, A., Welch, C., and Stadnyk, T.)**

Dr. Chani Welch aided in the interpretation of model results. She also aided in shaping the discussion of the manuscript. Dr. Tricia Stadnyk provided indispensable expertise in development of hydrologic model, and assessment of model structure. All authors aided in the review and editing of the manuscript, prior to and during the submission process to Hydrological Processes.

Chapters 5

Assessing seasonality and uncertainty in evapotranspiration partitioning using a tracer-aided model. **(Smith, A., Welch, C., and Stadnyk, T.)**

Dr. Chani Welch provided invaluable insights and guidance on improvements to the representation of the subsurface in model development, essential for optimizing flow pathways in final model version (HELIOS). Dr. Welch also provided detailed land cover input data that distinguished between connected and disconnected wetlands, essential for the evaluation of evaporative effects within the storage components of the watersheds. Dr. Tricia Stadnyk provided direction on key improvements for cold-region specific processes, and aided with the interpretation of the model results. She also aided in the auto-calibration which greatly improved the model's capabilities. Both authors contributed to the editing of the manuscript text.

Chapters 6

Examination of storage variant transit time distributions in highly seasonal watersheds. **(Smith, A., Welch, C., and Stadnyk, T.)**

Drs. Welch and Stadnyk provided insight into the storage relationships established, essential for the model. Both authors were also involved with providing feedback on model results. All authors contributed to the editing and framing of the manuscript text.

CHAPTER 1: INTRODUCTION

1.1 RESEARCH MOTIVATION AND BACKGROUND

Evaporation and transpiration are important components of watershed hydrology, affecting stored water availability in the upper-zone soil, interception by vegetation, and open water. These fluxes result in 25-150% annual loss of precipitation in watersheds worldwide (Byrne and O'Gorman 2015). In high-latitude (> 50^{o}) northern watersheds, evaporation and transpiration are highly seasonal processes, with winter months experiencing freezing conditions that limit the growing season and alter water mobility. Evaporation and transpiration fluxes are some of the most difficult to independently measure over large domains (>1 ha), however, resulting in their lumping into a single term: evapotranspiration (ET) (Granger 1989). Eddy covariance towers and energy-balance methods may compute ET with relatively high accuracy over small spatial domains (<10 km^2; Bowen 1926). In contrast, at large scales relevant to assessment of regional water supply, limited energy-flux data have necessitated the use of empirical methods to estimate ET (Thornthwaite 1948; Monteith 1965; Priestley and Taylor, 1972). Evaporation and transpiration are likely to change independently due to climate change. Therefore, lumped empirical methods may no longer be appropriate. Rising temperatures and increasing precipitation due to climate change will likely be the most prominent in high-latitude watersheds, and result in decreasing permafrost extent (Camill 2005; Jorgenson and Osterkamp 2005; St. Jacques and Sauchyn 2009), changes in soil water storage (Taylor et al., 2012), and decreasing stability of the water supply (Whitfield et al 2012). Therefore, simulations of changes in water

availability in response to changing rates of evaporation and transpiration require the temporal partitioning of ET into its components.

Hydrologic modelling has greatly improved comprehension of hydrological processes in regional watersheds worldwide. These models are essential tools for effective water management and planning, particularly under climate change. Where insufficient gauge density and record length exist, models are a tool for stream flow projection, assessment of water availability, and gap-filling hydrometric networks (Spence et al., 2013; Hrachowitz et al., 2013). In Canada, stream flow gauge density does not meet WMO standards across 88% of the country (Coulibaly et al., 2013), which is of significant concern due to data requirements for planning, design, and operation of water control structures in complex, highly seasonal environments. Limited data availability inhibits modelling efforts, specifically by limiting data available for model calibration and verification (Kavetski et al., 2011). Complex physiography and climate in high-latitude watersheds limit the applicability of small-scale meteorological observations for effective regional water management. Therefore, estimation of regional hydrologic processes with partially physically-based equations from sparse observational datasets typically requires empiricism and model calibration. Selection of parameters that best replicate observed conditions complicates analysis of model calibration (Beven 1993). Parameter selection is best addressed through the analysis of multiple parameter permutations, and by identifying the likelihood of each permutation (Beven and Binley 1992; Genereux 1998; Gupta et al., 1998; Wagener et al., 2003; Kavetski et al., 2006; Tolson and Shoemaker 2007). Evaluation of hydrologic model parameter permutations may reveal many potential statistically equivalent parameter combinations, resulting in highly uncertain process identification (Beven and Freer 2001; Kirchner 2006). Highly parameterised empirical estimates of evaporation and transpiration

severely limit the ability of any model calibration to identify statistically likely parameter sets; therefore, partitioning ET with greater certainty requires new methods, and novel use of different observations.

Previous attempts to partition ET into its components have focused on small-scale, highly instrumented study areas during the growing season using multiple measurement techniques to estimate ET, and one component (i.e., evaporation or transpiration) independently (Kool et al., 2014). Direct observation of ET and one component of ET depends on the spatial extent of instrument footprint (<10 km^2). As this density of instrumentation is generally not feasible, supplementary approaches to ET partitioning include: parameterisation of soil and vegetation conditions (Simunek et al., 2008; Moran et al., 2009), spatially variable energy balance estimation (Lascano et al., 1987; Thompson et al., 1993; Daamen and Simmonds 1994), and tracer-aided flux separation (Zhang et al., 2010; Sutanto et al., 2012; Jasechko et al., 2013; Evaristo et al., 2015). Tracers, including the stable water isotopes (SWIs) oxygen-18 ($\delta^{18}O$) and deuterium ($\delta^{2}H$), have effectively identified evaporation flux, while not requiring independent measurement of either evaporation or transpiration (Gibson and Edwards 1996; Gibson 2002). In tracer-aided hydrologic modelling, the relationship of evaporation fractionation (physical changes of composition) (Craig and Gordon 1965) and non-fractionating transpiration (no change to the composition) (Ehleringer and Dawson 1992) may help identify evaporation and transpiration losses from storage. In addition, SWIs have previously identified source water components in hydrologic modelling; aiding in the reduction of equifinality and simulation uncertainty (Sklash and Farvolden 1979; McDonnell et al., 1990; Birkel et al., 2010; Stadnyk et al., 2013; Delavau et al., 2017). Introducing the additional complexity that comes with modelling SWI tracers is necessary to best understand how changes in water storage affect water

availability (Sklash et al., 1976; Hrachowitz et al., 2010). However, including temporally-varying ET partition models requires consideration of new equations, which increases the number of parameters requiring calibration without increasing the data available for calibration. To better address data scarcity, an alternative method to partition ET may make use of modelling techniques and known relationships of SWIs to evaporation (E) and transpiration (TR).

1.2 RESEARCH SCOPE AND OBJECTIVES

The volume of water in watershed storage reduces greatly due to evapotranspiration and its components (i.e., E and TR). Large, high-latitude, watersheds are generally very remote, with limited accessibility; therefore, observation of atmospheric fluxes are difficult and often impractical. The overall goal of this research is the identification of E and TR fluxes and their significance on watershed water age and water availability in regional (>100 km^2), high-latitude watersheds using a tracer-aided hydrologic model. The specific objectives of this research are to:

1) Develop a means to identify the primary flow components of regional stream flow, their temporal variability, and uncertainty in estimation;
2) Develop a new method for partitioning ET into its components using SWI techniques and tracer-aided modelling; and
3) Identify a method to estimate evaporation and transpiration flux age and uncertainty from the various hydrologic storage compartments.

The results of these objectives are not specific to the model developed, and pertain to all tracer-aided models using $\delta^{18}O$ and $\delta^{2}H$. The main research scope is constrained as follows:

- Develop a tracer-aided lumped hydrologic model with the specific intention of capturing the complex processes (e.g., wetland interactions and snowmelt) that occur in high-latitude, Canadian watersheds. A lumped model is selected due to limited data and to

reduce model parameterisation. A tracer-aided model is selected to use stable isotopes to aid in calibration. Isotopes are used since the measurement and instrumentation of an isotope network is cheaper than increasing hydrometric measurements on large scales (Gibson et al., 2010; Tetzlaff et al., 2015).

- Estimate isotopic phase change effects using previously established methods (e.g. snowmelt and evaporation with Craig and Gordon (1965) and transpiration with Ehleringer and Dawson (1992)).
- Use well-established parameters for simulations where possible (e.g. Penman-Monteith vegetation leaf area index) to minimize calibration parameters and reduce the potential for additional equifinality.
- Evaluate evaporation flux by optimizing riverine $\delta^{18}O$ and $\delta^{2}H$ simulations that act as pseudo-observations of evaporation and transpiration flux. ET fluxes are typically unavailable in high-latitude watersheds at appropriate resolutions.
- Estimate ET partitioning using simple methods that minimize additional parameters so as not to over-parameterise the model.
- Simulate output isotope compositions ($\delta^{18}O$ and $\delta^{2}H$), discharge, and parameter uncertainty of discharge and isotopic parameters.

1.3 THESIS ORGANIZATION

This thesis is comprised of seven chapters consisting of an introduction, literature review, research compiled in four manuscripts, and conclusions.

Chapter 1 presents the motivation for, objectives, and scope of this research.

Chapter 2 reviews relevant background literature. This includes the theory and background of research in isotope hydrology as it relates to modelling uncertainty, tracer-aided hydrologic

modelling, transit time analysis, and evapotranspiration partitioning. Additionally, the limitations for application of each of the methods presented for regional modelling of ET partitioning are identified. Study site descriptions and methodologies for this work are provided within each manuscript, and will not be delivered as individual sections of this thesis.

Chapter 3 examines the temporal and spatial variability of riverine isotopic compositions in the high-latitude lower Nelson River Basin (LNRB), focused on its two primary flow systems (Nelson and Burntwood River) and their headwater basins. The variability of $\delta^{18}O$ is examined against discharge anomaly to identify the dependency of isotopic compositions on strong seasonal flow effects for the LNRB, and their likely influence on the variability of isotope fractionation resulting from evaporation. Chapter 3 partially fulfills the first objective, and has been published in the *Canadian Water Resources Journal*

Smith A., Delavau C., and Stadnyk., T., 2015. *Identification of geographical influences and flow regime characteristics using regional water isotope surveys in the lower Nelson River, Canada*. Canadian Water Resource Journal, 40 (1): 23-35.

Chapter 4 assesses the development and use of a lumped tracer-aided ($\delta^{18}O$) hydrologic model to identify the primary stream flow components in high-latitude regional Canadian watersheds. The temporal identifiability of the stream flow components is examined to determine the relative uncertainty of each source, and to identify which storages are most important during evapotranspiration-dominant months. Chapter 4 completes the first objective and partially completes the second objective, and has been published in *Hydrological Processes:*

Smith A., Welch C., and Stadnyk., T., 2016. *Assessment of a lumped coupled flow-isotope model in data scarce Boreal catchments*. Hydrological Processes, 30: 3871-3884.

Chapter 5 identifies a method to temporally partition ET using a tracer-aided model. The method identifies the amount of enrichment that occurs within a watershed throughout the year relative to a no evaporation scenario. The sensitivity of parameters partitioning ET in soils and wetlands, and the effect of storage parameters on ET partition parameters are examined within four high-latitude, Canadian watersheds which undergo seasonal changes in climate and soil conditions. Intra-annual variability of the simulated E/ET is assessed, comparing unsaturated soil storage, wetland storage, and ponded water storage. Additionally, the sensitivity of evaporative fractionation to different hydrologic storages is explored at the catchment outlet (i.e., stream flow observation location). Chapter 5 fulfills objective 2 and partially fulfills objective 3. The manuscript has been submitted to the *Journal of Hydrology*.

Chapter 6 evaluates partitioning ET using storage selection functions and investigates the impact of various evaporation and transpiration distribution functions on simulated mean watershed discharge age. Intra-annual changes in storage availability are identified (winter to summer), as is the effect of storage variability on the isotopic composition of discharge. The variability of mean evaporation and transpiration flux age is analyzed inter-annually to identify how changing ET fluxes may influence storage. This manuscript fulfils objective 3 and has been submitted to *Water Resources Research.*

Chapter 7 summarizes the conclusions of this research and identifies valuable lessons learned through development of tracer-aided hydrologic modelling and provides recommendations for future work.

1.4 REFERENCES

Beven, K., Binley, A. 1992. The future of distributed models: Model calibration and uncertainty prediction. *Hydrological Processes,* **Volume 6**: 279-298.

Beven, K. 1993. A manifesto for the equifinality thesis. *Journal of Hydrology*. **Volume 320(1)**: 18-36.

Beven, K., Freer, J. 2001. Equifinality, data assimilation, and uncertainty estimation in mechanistic modelling of complex environmental systems using the GLUE methodology. *Journal of Hydrology*, **Volume 249**: 11-29.

Birkel, C., Dunn, S. M., Tetzlaff, D., Soulsby, C. 2010, Assessing the value of high-resolution isotope tracer data in the stepwise development of a lumped conceptual rainfall–runoff model. *Hydrological Processes*, **Volume 24**: 2335–2348. DOI:10.1002/hyp.7763

Bowen, I.S. 1926: The ratio of heat losses by conduction and by evaporation from any water surface. *Physical Review*, **Volume 27**: 779–787

Byrne, M., O'Gorman P.A. 2015. The Response of Precipitation Minus Evapotranspiration to Climate Warming: Why the ''Wet-Get-Wetter, Dry-Get-Drier'' Scaling Does Not Hold over Land. *Journal of Climate*, **Volume 28**: 8078-8092.

Camill, P. 2005. Permafrost Thaw Accelerates in Boreal Peatlands During Late-20th Century Climate Warming. *Climatic Change*. **Volume 68**: 135-152. DOI:10.1007/s10584-005-4785-y.

Craig, H., Gordon, L.I. 1965. Deuterium and oxygen 18 variations in the ocean and marine atmosphere. *Stable Isotopes in Oceanographic Studies and Paleotemperatures*, **Spoleto**: 9-130.

Coulibaly, P., Samuel, J., Pietroniro, A., Harvey, D. 2013. Evaluation of Canadian National Hydrometric Network density based on WMO 2008 standards. *Canadian Water Resources Journal*, **Volume 38(2)**: 159-167.

Daamen, C.C., Simmonds, L.P. 1994. Soil water, energy and transpiration – a numerical model on water and energy fluxes in soil profiles and sparse canopies. *Department of Soil Science*, University of Reading

Delavau, D., Stadnyk, T., Holmes, T. 2017. Examining the impacts of precipitation isotope products ($\delta^{18}O_{ppt}$) on distributed, tracer-aided hydrological modeling. *Hydrology and Earth System Sciences*. **Volume 21**: 2595-2614. DOI:10.5194/hess-2016-539

Ehleringer, J.R., Dawson, T.E. 1992. Water uptake by plants: perspectives from stable isotope composition. *Plant, Cell & Environment*, **Volume 15**: 1073–1082.

Evaristo, J., Jasechko, S., McDonnell, J.J. 2015. Global separation of plant transpiration from groundwater and streamflow. *Nature*. **Volume 525**: 91-94.

Genereux, D. 1998. Quantifying uncertainty in tracer-based hydrograph separations. Water *Resources Research*, **Volume 34(4)**: 915-919.

Gibson, J.J., Edwards., T.W.D. 1996. Development and Validation of An Isotopic Method For Estimating Lake Evaporation. *Hydrological Processes*. **Volume 10**: 1369–1382.

Gibson, J.J. 2002. Short-term evaporation and water budget comparisons in shallow arctic lakes using non-steady isotope mass balance. *Journal of Hydrology*. **Volume 264**: 247-266.

Gibson, J.J. Reid, R. 2010. Stable isotope fingerprint of open-water evaporation losses and effective drainage area fluctuations in a subarctic shield watershed. *Journal of Hydrology*. **Volume 381**: 142-150.

Granger, R. J. 1989. An examination of the concept of potential evaporation. *Journal of Hydrology*, **Volume 111**: 9-19.

Gupta, H. V., Sorooshian, S., Yapo, P.O. 1998. Toward improved calibration of hydrologic models: Multiple and non-commensurable measures of information. *Water Resources Research*, **Volume 34(4)**: 751-763.

Hrachowitz, M., Soulsby, C., Tetzlaff, D., Speed, M. 2010. Catchment transit times and landscape controls - does scale matter? *Hydrological Processes*, **Volume 24**: 117-125.

Hrachowitz, M., Savenije, H.H.G., Blöschl, G., McDonnell, J.J., Sivapalan, M., Pomeroy, J.W., Arheimer, B., Blume, T., Clark, M.P., Ehret, U., Fenicia, F., Freer, J.E., Gelfan, A., Gupta, H.V., Hughes, D.A., Hut, R.W., Montanari, A., Pande, S., Tetzlaff, D., Troch, P.A., Uhlenbrook, S., Wagener, T., Winsemius, H.C., Woods, R.A., Zehe, E., Cudennec, C. 2013. A decade of Predictions in Ungauged Basins (PUB)—a review. *Hydrological Sciences Journal*, **Volume 58(6)**: 1198-1255.

Jasechko, S., Sharp, Z.D., Gibson, J.J., Birks, S.J., Yi, Y., Fawcett, P.J. 2013. Terrestrial water fluxes dominated by transpiration. *Nature*, **Volume 496**: 347-350.

Jorgenson, M.T., Osterkamp, T.E. 2005. Response of boreal ecosystems to varying modes of permafrost degradation. *Canadian Journal of Forest Research*, **Volume 35(9)**: 2100-211.

Lascano, R.J., van Bavel, C.H.M., Hatfield, J.L., Upchurch, D.R. 1987. Energy and water balance of a sparse crop: Simulated and measured soil and crop evaporation. *Soil Science Society of America Journal,* **Volume 51**: 1113-1121.

Kavetski, D., Kuczera, G., Franks, S.W. 2006. Bayesian analysis of input uncertainty in hydrological modeling: 1. Theory. *Water Resources Research*, **Volume 42(3)**: 03407-1-9. DOI:10.1029/2005WR004368.

Kavetski, D., Fenicia, F., Clark, M.P. 2011. Impact of temporal data resolution on parameter inference and model identification in conceptual hydrological modeling: Insights from an experimental catchment. *Water Resources Research*, **Volume 47(5)**: DOI: 10.1029/2010WR009525.

Kirchner, J.W., 2006. Getting the right answers for the right reasons: Linking measurements, analysis, and models to advance the science of hydrology. *Water Resources Research*, **Volume 42**: W03S04-1-5. DOI:10.1029/2005WR004362.

Kool, D., Agam, N., Lazarovitch, N., Heitman, J.L., Sauer, T.J., Ben-Gal, A. 2014. A review of approaches for evapotranspiration partitioning. *Agricultural and Forest Meteorology*, **Volume 184**: 56-70.

McDonnell, J.J., Bonell, M., Stewart, M.K., Pearce, A.J. 1990. Deuterium variations in storm rainfall: Implications for stream hydrograph separation. *Water Resources Research*, **Volume 26(3)**: 455-458. DOI: 10.1029/WR026i003p00455

Monteith JL. 1965. Evaporation and environment. In: The state and movement of water in living organism. *19th Symposia of the Society for Experimental Biol*ogy, 205-234.

Moran, M.S., Scott, R.L., Keefer, T.O., Emmerich, W.E., Hernandez, M., Nearing, G.S., Paige, G.B., Cosh, M.H., O'Neill, P.E. 2009. Partitioning evapotranspiration in semiarid grassland and shrubland ecosystems using time series of soil surface temperature, *Agricultural and Forest Meteorology*, **Volume 149**: 59-72. DOI:10.1016/j.agrformet.2008.07.004.

Priestley, C.H.B., Taylor, R.J. 1972. On the assessment of surface heat flux and evaporation using large-scale parameters. *Monthly Weather Review*, **Volume 100(2)**: 81–92.

Simunek, J., Van Genuchten, M.T., Sejna, M. 2008. Development and Applications of the HYDRUS and STANMOD Software Packages and Related Codes. *Vadose Zone Journal VZJ*, **Volume 7(2)**:587-600

Sklash, M.G., Farvolden, R.N., Fritz, P. 1976. A conceptual model of watershed response to rainfall, developed through the use of oxygen-18 as a natural tracer. *Canadian Journal of Earth Science*, **Volume 13**: 271-283.

Sklash, M.G., Farvolden, R.N. 1979. The role of groundwater in storm runoff. *Journal of Hydrology*, **Volume 43(1)**: 45-65.

Spence, C., Whitfield, P.H., Pomeroy, J.W., Pietroniro. A., Burn, D.H., Peters, D.L., St-Hilaire, A. 2013. A review of the Prediction in Ungauged Basins (PUB) decade in Canada. *Canadian Water Resource Journal*, **Volume 38(4)**: 253-262.

St. Jacques, J.-M., Sauchyn, D. J. 2009. Increasing winter baseflow and mean annual streamflow from possible permafrost thawing in the Northwest Territories, Canada, *Geophysical Research Letters*, **Volume 36**: L01401-1-6, DOI: 10.1029/2008GL035822.

Stadnyk, T.A., Delavau, C., Kouwen, N., Edwards, T.W.D. 2013, Towards hydrological model calibration and validation: simulation of stable water isotopes using the isoWATFLOOD model. *Hydrological Processes*, **Volume 27**: 3791–3810.

Sutanto, S., Wenninger, J., Coender S-Gerrits, A., Uhlenbrook, S. 2012. Partitioning of evaporation into transpiration, soil evaporation and interception: a comparison between isotope measurements and a HYDRUS-1D model. *Hydrology and Earth System Sciences*, **Volume 16(8)**: 2605-2616.

Taylor, R.G., Scanlon, B., Döll, P., Rodell, M., Van Beek, R., Wada, Y., Longuevergne, L., Leblanc, M., Famiglietti, J.S., Edmunds, M., Konikow, L., Green, T.R., Chen, J., Taniguchi, M., Bierkens, M.F.P., Macdonald, A., Fan, Y., Maxwell, R.M., Yechieli, Y., Gurdak, J.J., Allen, D.M., Shamsudduha, M., Hiscock, K., Yeh, P.J.F., Holman, I., Treidel, H. 2012. Ground water and climate change. *Nature*, **Volume 3(4)**: 322.

Tetzlaff, D., Buttle, J., Carey, S.K., van Huijgevoort, M.H.J., Laudon, H., McNamara, J.P., Mitchell, C.P.J., Spence, C., Gabor, R.S., Soulsby, C. 2015. A preliminary assessment of water partitioning and ecohydrological coupling in northern headwaters using stable isotopes and conceptual runoff models. *Hydrological Processes*, **Volume 29(25)**: 5153-5173.

Thompson, R., Whitock, C., Bartlein, P., Harrison, S., Spaulding, G. 1993. Climate change in the western United States since 18,000 yr B.P. *in Global Climates Since the Last Glacial Maximum*. Minneapolis; University of Minnesota Press: 468-513.

Thornthwaite, C.W. 1948. An approach toward a rational classification of climate. *Geographical Review*, **Volume 38(1)**: 55–94.

Tolson, B. A., Shoemaker, C. A. 2007. Dynamically dimensioned search algorithm for computationally efficient watershed model calibration. *Water Resource Research*, **Volume 43(1)**:W01413-1-16. DOI:10.1029/2005WR004723.

Wagener, T., McIntyre, N., Lees, M.J., Wheater, H.S., Gupta, H.V., 2003. Toward reduced uncertainty in conceptual rainfall-runoff modelling: Dynamic identifiability analysis. *Hydrological Processes*, **Volume 17**: 455-476.

Whitfield, P. 2012. Floods in future climates: a review. *Journal of Flood Risk Management*, **Volume 5(4)**: 336-365. DOI: 10.1111/j.1753-318X.2012.01150.x.

Zhang S., Wang, X., Wang, J., Yu, G., Sun, X. 2010. The use of stable isotopes to partition evapotranspiration fluxes into evaporation and transpiration. *Acta Ecologica Sinica*. **Volume 30**: 201-209.

CHAPTER 2: THEORY AND BACKGROUND LITERATURE

High latitude watersheds, particularly in Canada, are of significant interest to water resource practitioners due to the large quantities of water potentially available for allocation and environmental sustainability. However, these watersheds incur highly seasonal evaporation and transpiration fluxes, which can significantly reduce the total water available to be released from storage during the spring, summer and fall months. Watersheds of operational interest are notoriously complex, and studies of these watersheds are further burdened by limited accessibility, and, consequently, low temporal and spatial data resolution. Hydrologic modelling is one tool that may be applied to mitigate some of these data concerns within these watersheds. The challenge with hydrologic modelling is understanding the 'correctness' of the models estimation of physical processes. Model correctness is essential due to the uncertainty of hydrologic non-linearities, non-stationarities, and non-uniqueness that influence water availability. Source separation using tracers (e.g. hydrograph separation and mass-balance) may mitigate model uncertainty. Evapotranspiration (ET) may have a significant impact on the water availability, although its components may also independently affect water availability. Complexities of large watersheds reduce the applicability of simple methods (e.g. hydrograph separation) to partition ET into its components, which introduces the use of tracer-aided modelling as a tool for partitioning ET. The partitioning of ET may yield further understanding of watershed storage dynamics, particularly the mean age of water that evaporation and transpiration may act to remove from hydrologic storage.

2.1. HYDROLOGIC MODEL CALIBRATION AND UNCERTAINTY

Historically, hydrologic modellers have largely focused on efficiency criteria to assess how well a model replicates observed values (Krause et al., 2005). This presents a fundamental issue being addressed in current research: the identification and quantification of water sources and their corresponding uncertainty. Even with improved process understanding, full diagnosis of model fit and performance for operational predictions requires significant consideration of uncertainty. However, hydrological uncertainty is a proverbial hydrologic hurdle, propagating from input, parameters, model structure, and output in space and time. Klemeš (2002) classified such uncertainty as a struggle between known uncertainties (KUNK), unknown uncertainties (UNKUNK) and a known that stinks (SKUNK). There have been many attempts to address the enduring concern of known model uncertainty; however, there is still not likely a best method for assessing all simultaneously. Beven and Young (2013) suggested that uncertainty may be either aleatory (natural randomness) or epistemic (model process), and both must be considered to address full model uncertainty.

Comprehensive uncertainty analysis considers the four main types of uncertainty: (1) input uncertainty (Kavetski et al., 2006), (2) output uncertainty, (3) parameterisation uncertainty (Beven and Freer, 2001; Wagener et al., 2003), and (4) model structure uncertainty (Wagener et al., 2003; Kavetski et al., 2006). Observed model forcing (i.e., input) data are assessed through instrumentation/interpolation uncertainty and are more easily quantifiable than spatial or temporal uncertainty (i.e. due to orographic and topographic effects, Kavetski et al., 2006). Parameter uncertainty is the likelihood a parameter set best represents a behavioural characteristic. The behavioural characteristics of a model may be defined using a specific statistical criterion (e.g. minimum Nash-Sutcliffe efficiency), which helps to reduce the total number of 'viable' (i.e., meeting the statistical criterion) parameter sets. Parameter uncertainty is

synonymous with equifinality, which is the likelihood that many different parameter sets will produce statistically equal output. Therefore, it is widely accepted that a single best parameter set is not feasible for models and that multiple parameterisations are required (Beven and Freer 2001). Model structural uncertainty, or structural inadequacy, is uncertainty that originates from misrepresentation of processes from expected watershed behaviour. Structural uncertainties originate from insufficient parameters (i.e. unable to capture all event processes), over parameterisation (no means of measuring the structural uncertainty, Wagener et al., 2003), and lack of important process inclusion, and is assessed through the failure of model process estimation through direct comparison to observations. Structural uncertainty is one of the most difficult model uncertainties to account for and reduce since it generally cannot be reduced through further calibration or reduced parameter ranges.

Statistically-based uncertainty estimation methods experience significant limitations due to use of both non-physically and physically based parameters. There have been numerous attempts to address hydrologic modelling uncertainty, focusing on Bayesian theory to address uncertainty through the estimation of a simulation's likelihood of 'acting' behavioural relative to observations (Beven and Binley 2013). Beven and Binley (1992) developed one of the most widely used methods for assessing uncertainty and parameter likelihoods using a goodness-of-fit measure called the Generalized Likelihood Uncertainty Estimation (GLUE). GLUE parameter uncertainty develops cumulative distribution functions (CDFs) of the efficiency parameter and assesses the likelihood of each parameter value to provide an estimation of Bayesian analysis. While the method does not address input or model strucuture uncertainty, applications of this method are common in hydrologic studies and have been sucessful in the identification of parameter likelihoods (Beven and Freer 2001; Hrachowitz et al., 2009; Jost et al., 2012; Timbe et

al., 2014). To attain the CDFs required for likelihood functions, numerous model runs must be performed to evaluate different parameter sets. GLUE was originally developed for use with Monte Carlo parameter sampling, and is dependent on a relatively large number of parameter sets meeting the efficiency criteria. However, the applicability of GLUE is not limited to assess modelled discharge: Birkel et al. (2010, 2011) have shown its utility to assess the uncertainty of tracer-aided modelling, and Joerin et al. (2002) used the method to assess uncertainty in hydrograph separation modelling.

Monte Carlo simulations have widely been used as a means of producing high volumes of output to assess behavioural parameters (i.e. physically realistic hydrologic limits) and calibration. Monte Carlo analysis was derived as a method to randomly sample parameters over a given distribution (e.g. uniform, normal, etc). To appropriately identify hydrologic parameters, Monte Carlo methods typically need tens of thousands of model runs, which is computationally expensive when simulation periods and calculation times are long. While these challenges can be significant, they are less important when model runtimes are not significantly long (e.g. lumped models). Though model runtimes may not be significantly long, the Monte Carlo simulation is not always efficient as it does not preferentially select behavioural parameter sets.

Other calibration methods have focused on auto-calibration, which continuously updates the probability of parameter selection. Optimization of the Monte Carlo method has been attempted on numerous occasions with the objective of reducing the number of 'non-behavioural' parameter sets sampled, using methods such as the Markov Chain Monte Carlo (Metropolis et al., 1953). This method has been adapted in numerous ways to improve the randomization of sampling including non-symmetric probabilistic sampling (Hastings 1970) and high-dimensional search algorithms (Vrugt 2016). Tolson and Shoemaker (2007) further

advanced the field of auto-calibration through the development of the Dynamically Dimensioned Search (DDS) algorithm and further developed DDS into DDS-AU (approximation of uncertainty) for uncertainty assessment (Tolson and Shoemaker 2008). Similar to the other calibration techniques mentioned, DDS requires a large number of Monte Carlo simulations but reduces the range of parameter randomization using previous simulations. This results in fewer required simulations; though to ensure optimization is not held to a local optimum, multiple trials are required to compare parameter and efficiency optimization. The development of DDS-AU merged the GLUE approach with DDS to include pseudo-likelihood (combined probability) functions rather than the traditional likelihood functions. Though the method shows significantly fewer simulations are required for the DDS-AU method, relative to traditional GLUE and Monte Carlo, the use of DDS for uncertainty analysis is not limited to pseudo-likelihood functions and GLUE is still applicable. DDS has been used successfully in numerous hydrologic and tracer-aided approaches, notably in high-latitude watersheds (Holmes 2016; Eum et al., 2016a,b; Qi et al., 2016).

Incorporation of additional validation data into models (i.e. tracers, storage-discharge measurements) has aided with parameter identifiability in conditions where the additional data significantly increase the information content for the model (Sklash 1976). The inclusion of tracers, for example, may aid in reducing the model's calibration uncertainty (McMillan et al., 2012), while providing information on structural uncertainties present in the model (Gupta et al., 1998; Holmes 2016).

Finally, output uncertainty adds the uncertainty in measurements (i.e., discharge, isotopic) to all other sources of uncertainty to give a measure of the total uncertainty related to the observations. Quantifying each type of uncertainty is imperative to the full understanding of the

model's capability to simulate fluxes. Uncertainty related to hydrological modelling, however, may be eased through the separation of the hydrograph into its source components, which helps to inform model structure and first estimates of parameterisation.

2.2. HYDROLOGY OF STABLE ISOTOPES OF WATER

Stable isotopes of water consist of heavy and light hydrogen and oxygen molecules, ranging from light to heavy water ($H_2^1O^{16}$ and $H_2^3O^{18}$, respectively). The use of isotopes in hydrologic analysis is dependent on the abundance of light isotopes oxygen-16 (99.759%) and hydrogen-1 (99.985%) relative to their rarer isotopes oxygen-18 (0.204%) and hydrogen-2 (deuterium: 0.0155%) (Buttle 1994; International Atomic Energy Agency 2001). With the historical exception of tritium (^{3}H), the remaining isotopes of hydrogen and oxygen are not typically used in hydrology due to low abundance (oxygen-17: 0.031%) or rapid decay rates (oxygen-19 and oxygen-20 have half-lives less than one day) unsuitable for hydrologic studies with transit times weeks to years in length (International Atomic Energy Agency 2001). Some of the first studies conducted with stable isotopes include correlations between meteoric oxygen-18 and deuterium (Craig 1961), fractionation through phase change as described by Rayleigh distillation (Posey and Smith 1957; Craig et al., 1963; Ehhalt et al., 1963; Craig and Gordon, 1965; Rodhe 1981), and spatial variation of isotopes in meteoric waters (Dansgaard 1964). Craig (1961) identified difficulties associated with directly comparing water samples of varying spatial and temporal origins, and introduced standardization of water samples with ocean water, Standard Mean Ocean Water (SMOW), enabling a world-wide comparison of water samples and sources. Samples are standardized (Equation 2-1) using the abundance ratio of heavy to light isotope (i.e. H^2/H^1 or O^{18}/O^{16}), R, for the sample and standard, and δ is the isotopic composition in parts per thousand (per mil, ‰).

$$\delta = \left(\frac{R_{SAMPLE}}{R_{STANDARD}} - 1\right) \cdot 1000 \qquad 2\text{-}1$$

SMOW was later revised by the International Atomic Energy Agency (IAEA) into four standard values: Vienna Standard Mean Ocean Water (VSMOW), Vienna Standard Mean Ocean Water 2 (VSMOW2) (IAEA, 2009), Standard Light Antarctic Precipitation (SLAP), and Standard Light Antarctic Precipitation 2 (SLAP2) (IAEA, 2009), for more consistent isotopic comparisons between studies. In addition to monitoring the standard practices for isotopic analysis, the IAEA has also established two large monitoring networks: Global Network for Isotopes in Precipitation (GNIP) and the Global Network for Isotopes in Rivers (GNIR) to provide large spatial and temporal datasets. GNIP was introduced to help expand the understanding of the hydrologic cycle at a multitude of different scales. GNIR was developed as a network to enhance the understanding of hydrological processes while providing a sampling protocol for isotope data from both small and large basins (IAEA, 2012). Samples from GNIR and GNIP have assisted with kinetic and equilibrium fractionation relationship development for hydrologic cycle components (e.g. evaporated water, precipitation) for direct comparison with measured atmospheric and moisture composition relationships.

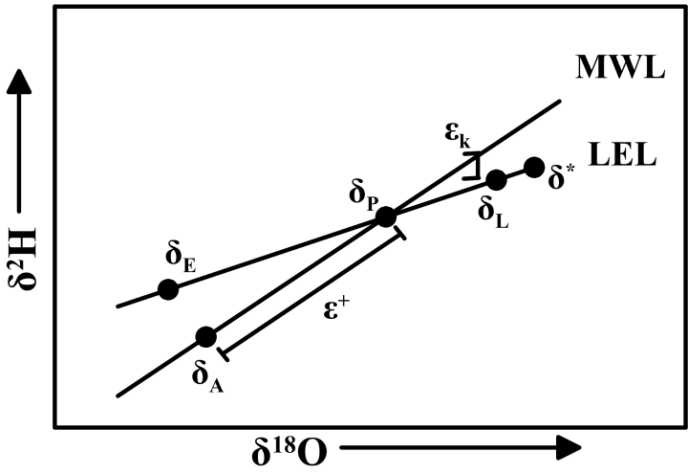

Figure 2-1. The theoretical isotopic framework of meteoric waters (after Gibson, 1993).

Through his work, Craig (1961) established a linear relationship between deuterium and oxygen-18 on an isotopic framework called the delta-delta (δ^2H vs. $\delta^{18}O$) space (Figure 2-1). Kinetic fractionation effects (i.e. temperature, wind speed, and relative humidity) within the watershed define the separation between the meteoric water line (MWL) and the local evaporation line (LEL). Each watershed has its own MWL, referred to as the local MWL (LMWL). The LMWL is determined through the linear regression of precipitation compositions. Deep groundwater compositions are generally similar to flux weighted long-term average precipitation (δ_P), while snowpack is similar to the ambient atmosphere composition (δ_A). Both δ_P and δ_A lie along the LMWL. These two values are separated by equilibrium fractionation (ε^*), a process that does not preferentially select light isotopes. As the name implies, equilibrium fractionation undergoes equal fractionation of oxygen-18 and deuterium, when sufficient energy or a closed, well-mixed system occur. The atmospheric composition of water vapour that has undergone evaporation (δ_E), isotopic composition of stored water (δ_L), and the limiting enrichment (δ^*) fall along the local evaporation line (LEL), determined by water samples that have undergone both kinetic (ε_k) and equilibrium fractionation during the evaporation process. Similar to δ_A, δ_E and δ^* are measurable though not commonly attainable for large study areas due difficulty of sampling over remote, inaccessible areas, but can be estimated using empirical equations. The limiting enrichment (δ^*) is the theoretical isotopic composition of the last drop of water evaporated. The distinct differences between the LMWL and LEL show the potential for the identification of evaporation using SWIs. Due to differences in precipitation source and evaporative fractionation, watershed storages may have different and distinct isotopic compositions. Due to these observable differences, stable water isotopes are commonly used to perform hydrograph separation (e.g. Sklash et al., 1976), referred to as isotope hydrograph

separation (IHS). This separation is used to identify the sources of storage water contributing to stream discharge.

2.2.1. TRACER-BASED HYDROGRAPH SEPARATION

Hydrograph separation has long been a method used by hydrologists in attempts to identify source components of discharge and appropriate (i.e. correct) flow paths using basic mathematical methods (Hall, 1968). Early attempts focused on the separation of baseflow from the hydrograph, which assumed that pre-event water could be characterized by baseflow sampled prior to an event. Each mathematical approach requires an assessment of hydrograph rising and falling limbs, and separation of baseflow from event water via inflection points or recursive filtering techniques (Eckhardt 2005). Additional approaches have i) utilized unit hydrograph recession limbs (Su 1995), ii) established physical relationships between baseflow and rating curves (Kliner and Knezek 1974), iii) introduced the use of tracers to solve mass-balance equations of source components at the catchment outlet (Klaus et al., 2013), and iv) used principal component analysis (end-member mixing analysis, EMMA) (Barthold et al., 2011). Comparisons of these methods generally show that studies using environmental tracers have been the most consistent with observed data (Gonzales et al., 2009; Lott and Stewart 2016).

Dinçer et al. (1970) was one of the first to apply a tracer-based mass-balance approach, where oxygen-18 and tritium were used to assess snowmelt contributions to total streamflow (i.e., percent meltwater versus percent old water/baseflow). Results suggested that significant contributions of water from the subsurface contribute to streamflow (i.e., approximately two-thirds). Following Dinçer's (1970) mass-balance approach, several studies used two component separation models to establish storm water runoff (i.e., new or event water) and baseflow (i.e., old or pre-event water) components (e.g. Sklash et al., 1976; Sklash and Farvolden 1979;

Metcalfe and Buttle 2001; Brock et al., 2007). Sklash (1976) and Sklash and Farvolden (1979) presented five primary assumptions for valid tracer hydrograph separation including: (1) distinct and measurable differences between event and pre-event water, (2) event water variability is accounted for in space and time, (3) pre-event water variability is accounted for in space and time, (4) vadose zone water is negligible, and (5) contributions from surface storage are negligible. The use of isotopes in tracer aided hydrograph separation (i.e. IHS) has identified that these assumptions are generally violated even in small catchments (Kennedy et al., 1986; Moore 1989; McDonnell et al., 1990; Buttle 1994; Klaus and McDonnell 2013). Studies have continued despite limiting assumptions, given the lack of other viable methods to quantify source waters and the prohibitive cost and feasibility of implementing high temporal and spatial monitoring programs. Testing the limitations of IHS are often more prohibitive in high-latitude, large watersheds, however, because of the substantial costs of sample analysis, equipment implementation (e.g. auto samplers), and issues surrounding site accessibility and transportation to remote sampling sites. IHS assumptions may lead to percent contributions greater than 100% or less than 0% if measured compositions at the outlet are not bound by the expected event and pre-event water compositions (McDonnell et al., 1991). McDonnell et al. (1990) showed temporal variability violating the IHS assumptions in a 3.1 km^2 basin using the incremental mean against the event weighted average (62 to 76% pre-event water). Spatial variations in isotopic composition have been observed for hydrologic inputs (i.e., soil water, groundwater; Moore 1989), and precipitation where catchments have larger elevation change (McGuire et al., 2005). While these errors are easily identifiable through measurement, comprehensive measurements of isotopic compositions to assess spatial and temporal variability are not always available.

In larger basins, additional difficulties arise with the simple IHS assumptions due to longer response times (potential evaporative effects) and large-scale mixing patterns combining water of multiple ages and sources. This has led to the consideration of additional sources (>2 components) (McDonnell et al., 1991; Merot et al., 1995; Rice and Hornberger 1998; Lee and Krothe 2001), and end member mixing analysis (Christopherson and Hooper 1992). Stadnyk et al. (2005) and St Amour et al. (2005) circumvented the required additional tracer to assess more than two components through use of a step-wise, temporally variant two-component separation distinguishing between ice-off and ice-on baseflow conditions. However, even multi-component IHS decomposes in high-latitude watersheds due to the complexities of physiographic variations (e.g., slope, depth of soil, vegetation), temporal periods of sub-surface water immobility caused by frozen ground and permafrost (Laudon et al., 2004; Carey and Quinton 2004; Carey and Quinton 2005), and snowmelt and sublimation fractionation. Snowmelt has a similar influence to that of evaporation on residual water in storage where melt water initially and preferentially releases lighter (depleted) isotopes. This generally results in more enriched snowmelt as the residual snowpack decreases (Moser and Stichler 1975; Taylor et al., 2001, 2002), although the process remains difficult to estimate as instantaneous snowmelt measurements are not easily attainable (Penna et al., 2014); particularly in high latitude regions. EMMA relies on the use of principal component analysis to correlate end members to tracers at the catchment outlet. However, EMMA breaks down with temporal and spatial changes in end members (Barthold et al., 2010), and is unable to appropriately identify sources. Despite positive results in small watersheds, neither IHS nor EMMA can independently account for the large-scale spatial and temporal variability of water composition (event or pre-event).

2.2.2. PARTITIONING OF EVAPOTRANSPIRATION USING HYDROGRAPH SEPARATION

Besides catchment IHS, stable isotopes of water have also been utilized in mass-balance studies of multi-outflow control volume modelling (i.e., lakes) where evaporation is a significant process (e.g. Gibson et al., 1993; Gibson 2002; Gibson et al., 2008). Gibson et al. (1993) first showed the effectiveness of stable isotopes of water to estimate lake evaporation by comparing mass-balance approaches with evaporation pan measurements and mass-transfer estimates. Gibson et al. (1993, 1996, 2002) expanded the mass-balance approach by conducting step-wise mass-balance estimations, estimating between collection periods. Step-wise mass-balance estimations significantly advanced the use of stable isotopes in flux identification by removing the requirement for high temporal resolution data previously limiting flux estimation. Gibson et al. (2008) applied similar methods to an arid, irrigation-driven river in Australia using steady-state reach mass balances. Monthly isotope samples were used to derive the total monthly evaporation flux; however, some downstream reaches incurred more complex mixing patterns resulting in over-estimation of evaporation and violation of the steady-state assumption ($\Delta V \cong 0$) . This emphasizes the limitation of steady-state assumptions of simplified mass-balance approaches, similar to more typical IHS (Jasechko et al., 2013; Good et al., 2015, Evaristo et al., 2016). Identifying lake fluxes and isotopic compositions (inflow, outflow, and precipitation) provided sufficient information for the partitioning of evaporation and transpiration fluxes, showing that transpiration is globally the dominant component of ET (Jasechko et al., 2013). However, unlike other IHS attempts, partitioning ET using IHS has been temporally limited to the identification of average annual fluxes. Partitioning ET is more complex in high latitudes due to temporal periods of ice-on and frozen ground conditions. Evaporative effects are generally most observable during the summer months with smaller effects of evaporative enrichment

(smaller deviation from the LMWL) observed during winter. Progression of storage compositions toward the LWML indicates hysteresis of summer enrichment (no winter evaporation) as storage is repleneshed with meteoric waters. These mixing dynamics of enrichment and hysteresis are observable via annual cycles of isotopic compositions between the LMWL and LEL.

2.2.3. WATERSHED MIXING ON THE LOCAL EVAPORATION LINE

Despite the complexities of the Craig and Gordon (1965) model, spatial and temporal variations in kinetic fractionation are still most easily observed via changes in the MWL and LEL. LMWL slopes are typically lower than the GMWL slope in semi-arid watersheds because of factors such as re-evaporation of rainwater (Ehhalt et al., 1963) and continental precipitation originating from ET (International Atomic Energy Agency 2001). Changes in evaporation not only occur spatially, but also temporally most notably in cold regions where evaporation ceases during ice-on periods, resulting in higher LEL slopes relative to lakes undergoing year-round evaporation (Gibson et al., 2008). For a given evaporative body, the LEL slope may be estimated using the Craig and Gordon (1965) model:

$$\boldsymbol{S_{LEL}} = \frac{\left[\dfrac{\boldsymbol{h(\delta_A - \delta_P) + (1 + \delta_P) \cdot (\varepsilon_K + \varepsilon^*/\alpha^*)}}{\boldsymbol{h - \varepsilon_K - \varepsilon^*/\alpha^*}}\right]}{\left[\dfrac{\boldsymbol{h(\delta_A - \delta_P) + (1 + \delta_P) \cdot (\varepsilon_K + \varepsilon^*/\alpha^*)}}{\boldsymbol{h - \varepsilon_K - \varepsilon^*/\alpha^*}}\right]} \qquad \text{2-2}$$

Use of the LEL for watershed-scale analysis is limited since it is generally only applicable to lakes, wetlands and other stagnant, open and evaporating water bodies. Yi et al. (2010) suggests the use of a local mixing line (LML) as a more appropriate means of analyzing riverine isotopic compositions, as this suggests mixing between evaporated and non-evaporated (groundwater) sources. This concept was shown in earlier work by St. Amour et al. (2005), where seasonal cycles of riverine waters vary between depleted snowmelt, between the MWL and LEL, and

along the MWL around weighted δ_P values. St. Amour et al. (2005) most simply showed this temporal variability of source water using the IHS method (Section 2.3.1).

2.3. TRACER-AIDED HYDROLOGIC MODELLING

Poor temporal resolution of hydrologic data, and a lack of available forcing data, have limited the understanding of regional hydrologic processes and evolution of these processes, resulting in the use of mathematical and statistical models to 'gap-fill' missing data (Crawford and Linsley 1966; Bras and Rodriguez-Iturbe 1976). Despite achieving high efficiencies, calibrations can still result in high uncertainty, and model uncertainty tends to increase with increased parameterisation. To constrain parameter uncertainty with calibration, the use of additional validation methods was considered (Beven and Binley 1992; Beven and Young 2013). The success of IHS component identification and external verification methods using isotopes as 'soft data' have naturally led to incorporating isotopes as tracers in hydrological models to validate models and reduce uncertainty.

Including tracers in hydrological studies is not a new concept, and tracers have been used in water quality modelling to determine advection, diffusion, and dispersion through aqueous substances (Chapra 1997). Development of such models involved simplifying reality to an ideal reactor, and a control volume that accounts for mass flux including: continuous flow stirred tank reactor (CSTR), plug-flow reactor (PFR), or mixed flow reactor (MFR), among others. The CSTR is the most frequently used mass balance model due to the simplifying assumption of a completely mixed system. Gibson (2002) was one of the first to model hydrologically-driven isotopic change with the CSTR model with the objective of quantifying the evaporative flux from the lake. Using steady-state (time-dependent) and non-steady-state (fraction-dependent) models, he showed that since the residual volume remained relatively equal to the initial volume

over a single time-step ($0.95 \leq (f = V/V_o) \leq 1$) for high-latitude lakes, results between models were relatively similar. Seasonality was, however, captured slightly better using the fraction-dependent model. This model was applied to small scale areas (0.22 - 2.2 km^2), and has proven useful for improved process understanding on both small and large-scale areas (Belachew et al., 2016).

A significant development in tracer-aided modelling came with the development of the isotope module for the partially physically-based routing model, WATFLOOD (Stadnyk-Falcone, 2008). The isoWATFLOOD routine was built off the CFSTR steady- and non-steady state equations described in Gibson (2002) to perform internal mass-balance calculations for fluxes and storage. Included as part of the tracer mass-balance are snowpack and snowmelt fractionation, surface storage/runoff, wetland hydrology and routing, open water fractionation, and upper and lower zone storage and runoff (more detail available in Stadnyk et al., 2013). Stadnyk et al. (2013) applied the isoWATFLOOD module to five study areas within the Mackenzie River Basin near Fort Simpson to test calibration and validation of the model using both hydrologic and isotopic data, comparing to previous IHS completed in the same region (Stadnyk et al., 2005; St. Amour et al., 2005). Although high goodness-of-fit results were found for modelled isotopic compositions, goodness-of-fit values for modelled discharge were poorer than pre-isotope model calibration (i.e., flow-only calibration). These results indicate calibration without isotopes or other tracers may produce high goodness-of-fit, but not necessarily achieve a set of physically-based parameters that are representative of basin hydrology. At the time, the decrease in hydrologic efficiency criteria was primarily attributed to model forcing data availability (annual average isotopic composition) and limitations of a minimum spatial scale. Holmes (2016) expanded the isoWATFLOOD model to include deuterium and deuterium-excess

calculations. While there was not a noticeable improvement (or decrease) in efficiency when calibrating with both oxygen-18 and deuterium, the use of isotopic calibration resulted in the best prediction of discharge over long time periods and aided in verifying and improving evaporative components (parameters) of the model. The study showed that evaporation was originally over-estimated (identified by too much isotopic fractionation); however, the ET component in WATFLOOD was not partitioned temporally in this study, and was instead held constant despite the seasonality of the study region's climate. IsoWATFLOOD was additionally calibrated with simulated monthly isotopic precipitation compositions, which reduced the number of behavioral parameters from previous discharge-only calibration (Delavau et al., 2017). The reduction of behavioral parameters indicated improved identifiability of parameters. This highlights the utility of tracer-aided modelling for estimating subsurface flow paths.

Additional attempts in developing tracer-aided hydrologic models have been undertaken in the form of conceptual lumped tracer-aided models (Birkel et al., 2010; Birkel et al., 2011). These models, however, do not account for the physics of water routing, variability in physiographic characteristics (e.g. land cover), high-latitude dominating processes (snowpack and snowmelt), or fractionation of evaporation in storage. Progression from five to 10 parameter lumped models showed improved efficacy of simulated daily isotopic variations (for a 2.3 km^2 basin), specifically with incorporation of a simple lake evaporation module (Birkel et al., 2011); however, fractionation of ET was still not considered. The primary components of the model are the storage units: two for both upper and lower zone storage; linearly relating storage to discharge. The model was later expanded from a lumped to a distributed model to better assess spatial resolution of water age and catchment mixing (van Huijgevoort et al., 2016). Unlike the lumped model, the distributed model addresses snowmelt using the degree-day method to divide

total precipitation into rain and snow, though little snowmelt within the basin limits examination of its impact. Increased resolution helped to identify rapid flow paths within the basin that were not previously identifiable. Neither the lumped model nor the distributed model were tested on a poorly gauged basin to assess whether parameterisation and calibration of the model perform as well in data sparse regions. While some tracer-aided models implement particle tracking techniques to identify potential flow paths, other methods such as distribution functions have been used as a simplified method to estimate watershed flow paths and mixing patterns. These simplified methods estimate mean watershed transit time and aid in the understanding of the dynamics of watershed storage. These methods may be used to identify how the transit time of different fluxes may influence long-term storage availability.

2.4. TRANSIT TIME MODELLING

In addition to tracer-aided hydrologic modelling, mean transit time (MTT) analysis has aided in the understanding of watershed storage and flow dynamics. The inputs to MTT modelling typically require precipitation fluxes and their accompanying isotopic composition. The selection of transit time distributions and evaporative fractionation (i.e. total evaporative flux), however, directly impact the simulation of streamflow isotopes. Appropriate selection of transit time and fractionation effects may serve as a multifunction tool for determining watershed effective storage (mean storage contributing to discharge), and a means to identify how storage changes with time.

2.4.1. APPLICATION OF TRANSIT TIME MODELS

Modelling MTT has played an integral part in understanding basin dynamics by helping to assess the connectivity of storage. Most studies have used MTT estimates to assess connectivity within a basin (Frederickson and Criss 1999; Asano et al., 2002; McDonnell et al., 2010; Tetzlaff

et al., 2014), or to establish physiographic correlations to MTTs (McGlynn et al., 2003; McGuire et al., 2005; Rodgers et al., 2005; McGuire and McDonnell 2010) to provide an estimate of how a watershed may respond to changes in precipitation. To verify information received from MTT estimations, Rodhe et al. (1996) controlled input (i.e., sprinkler) and measured total time for the input to dominate outlet composition. Rodhe et al. (1996) found that independent measures of input (i.e., evaporation and input water flux) were close to estimates provided by the transit time assessment. These studies have examined the effectiveness of correlating MTTs with basin characteristics (McGlynn et al., 2003; Rodgers et al., 2005; McGuire et al., 2005), total storage capacity (Rodhe et al., 1996), effects of input and output variability on the storage (Soulsby et al., 2014) and location of storage units (Tetzlaff et al., 2014). Through these studies, MTTs are not strongly correlated to basin size, but rather to the mean contributing area (McGlynn et al., 2003; Rodgers et al., 2005) and basin slope (McGuire et al., 2005). Simple MTT models, however, require limiting assumptions, including i) time-invariant solutions, ii) one-dimensional flow, iii) uniform recharge, iv) linear relationships, and v) no stagnation zones in the basin (McGuire and McDonnell 2006; McDonnell et al., 2010). Attempts to maintain valid transit time assumptions have resulted in many studies continuing with research catchment size basins (<100 km^2) and relatively high basins slopes to maintain assumptions ii), iii), and v) (Figure 2-2). For most study regions, oxygen-18 is the preferred isotope, with some studies using deuterium and tritium (McGuire and McDonnell 2006). Deuterium and tritium have preferentially been used for extreme basin areas (i.e., less than 0.01 and greater than 10,000 km^2) due to very short and very long transit times, respectively.

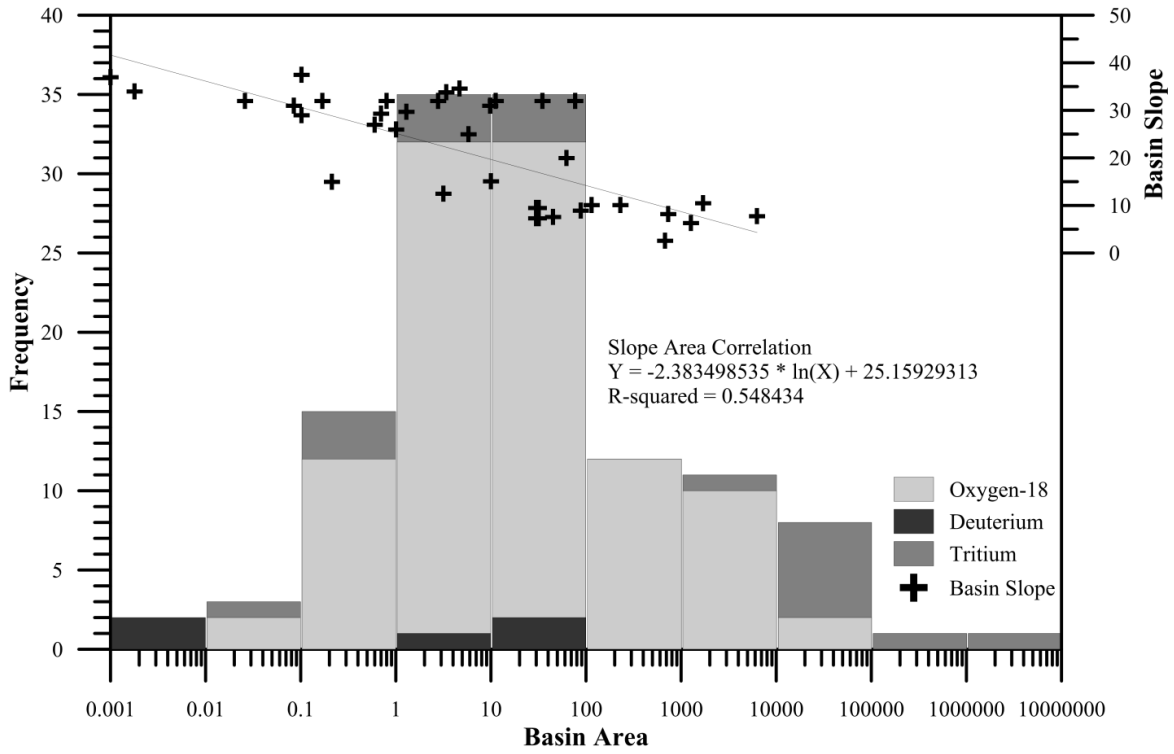

Figure 2-2. Histogram of transit time distribution studies with log-basin area and the corresponding basin slope-area relationship

The primary concern with transit time modelling is the steady-state assumption within watershed storage. Maloszweski and Zuber (1992) showed that this assumption may be valid for some basins where short periods of wet or dry conditions are unlikely to influence flow paths. As some basins have small sub-surface storage, temporal variability in precipitation and ET processes will do not exclusively undergo steady-state conditions and therefore cannot be considered time-invariant systems. Soulsby et al. (2006) demonstrated non-stationarity, showing that catchment residence times depend highly on antecedent moisture conditions, where wet basin conditions (high storage) produced transit times of hours or days compared to the long-term basin mean transit time. Conditions such as long-term wetting or drying of a watershed require significant consideration, such as through the solution of Niemi's (1977) non-steady-state transit time proposal.

2.4.2. INVESTIGATING WATERSHED STORAGE USING TRANSIT TIME DISTRIBUTIONS

MTT estimations are strongly tied to appropriate transit time distribution (TTD) selection and application of the TTD (McGuire and McDonnell 2006). The selection of TTD depends on data availability and expected correlations with physiography. Methodologies to solve for the MTT include the convolution equation (Maloszewki and Zuber 1982; Maloszewski and Zuber 1992; Rodhe et al., 1996; McGlynn et al., 2003; McGuire et al., 2005), sine-wave (Asano et al., 2002; Rodgers et al., 2005), mixing model (Michel 1992), and exponential average (Frederickson and Criss 1999). The most frequently used methods are convolution and sine-wave methods, though the sine-wave method is derived from the convolution equation (McGuire and McDonnell 2006) (Equation 2-3):

$$\boldsymbol{\delta_{out}(t) = \int_0^{\infty} g(\tau) \cdot \delta_{in}(t-\tau) d\tau = g(t) \cdot \delta_{in}(t)} \quad 2\text{-}3$$

where t is the current time-step, τ is the time of input, and $g(\tau)$ is the TTD. In addition to model structure, TTD selection has been widely explored in attempts to better capture the MTT of catchments (e.g. Timbe et al., 2014).

TTDs used most frequently include exponential (EM) (e.g. Zuber et al., 1986; Asano et al., 2002), piston-flow (PM) (McGlynn et al., 2003), exponential piston-flow (EPM) (McGuire et al., 2002; Vitvar et al., 2002), dispersion (DM) (Maloszewski and Zuber 1982; Vitvar and Balderer 1997), two parallel linear reservoir (TPLR) (Weiler et al., 2003). and gamma (GM) (Kirchner et al., 2001; Timbe et al., 2014) distributions. The EM and PM were the first two models used in transit time analysis due to their simplicity (i.e., 1 parameter models), although PM is widely recognized as non-representative of physical flow-path behaviours (Danckwerts 1953; Maloszewki and Zuber 1982). Each model is represented by two components, the timing and

duration of storage release. Of the TTDs presented above, the gamma distribution is a feasible simplification for a 1-D hillslope advection-dispersion model, widely consistent between watersheds (Kirchner et al., 2000; Hrachowitz et al., 2010). Kirchner et al. (2000) found that the GM outperformed the EM and DM models for a small catchment due to the lag of peak concentration (shape) and length of the tail (scale). Through uncertainty analysis of seven TTDs to identify the best model performance (based on Nash-Sutcliffe), Timbe et al. (2014) showed that heterogeneity in soil structures is a key factor in TTD identification. Overall, the EPM, GM, and TPLR distributions produced the most consistent efficiencies; however, higher model complexity also created larger parameter uncertainties over using simpler models. Although efficiency criteria were reasonable, the concern remained that the time-invariance assumption does not appropriately capture peak and low flow events (i.e. wet and dry conditions). Since storage is known to be temporally variable in many systems, it is important to understand and to better assess the long-term impacts of changes in storage.

2.4.3. THE EVOLUTION OF TIME-VARIANT TRANSIT TIME SOLUTIONS

Botter et al. (2010) and Hrachowitz et al. (2010) each examined how inclusion of time-variance to Niemi's (1977) model influences the mean water age exiting a watershed. Niemi (1977) proposed that a non-steady state solution of transit time was possible by integrating mass flux of multiple ages and a control volume. Botter et al. (2010) and Hrachowitz et al. (2010) differed on non-steady state storage solutions, where Botter focused on the probabilistic movement of water and Hrachowitz focused on the time-variance of TTD parameters. Botter et al. (2010) noted that much older water would leave the basin during dry conditions, compared to during wet conditions when water is younger. They derived the cumulative probability of water of specific ages that has moved through the watershed based on the probability that water resides

within the storage. Van der Velde et al. (2012) expanded on Botter's (2010) approach by examining advection-dispersion, suggesting that the beta distribution may best represent hillslope storage. Hrachowitz et al. (2010) approached time-variant TTD solutions through the probability of exceedance of precipitation in a given year to define wet and dry conditions for the watershed. They found a high correlation between precipitation and the scale parameter (β for gamma distributions), indicating temporal variability of the parameter is essential. Harman (2015) applied Botter's approach in accounting for the probabilistic selection of water from storage, while accounting for temporal variability of β found by Hrachowitz et al (2010) using a linear relationship with storage. While these and additional time-variant studies (Botter 2011; Birkel et al., 2012; Botter et al., 2012; Birkel et al., 2015; Soulsby et al., 2016; Benettin et al., 2017) have continued to identify methods to solve Niemi's (1977) model with the inclusion of temporal dependency, they all lack the ability to partition ET into its components. This is of significant concern for tracer-aided modelling where stable isotopes are utilized in high latitude watersheds given evaporative effects may occur for water of any age in storage, rather than just the newest water.

2.5. EVAPOTRANSPIRATION PARTITIONING

The partitioning of ET is of significant interest to hydrologists because while the individual components may not always be significant to watershed runoff (i.e. observable), changes in the ratio of its components may greatly influence storage recharge and hence discharge. To date, two approaches have been identified for ET partitioning: correlation-based partitioning and stable water isotopes (Kool et al., 2014). Correlation-based partitioning relies on CO_2 measurement from transpiration and ET flux to establish stomatal flux (transpiration) and non-stomatal flux (evaporation) (Scanlon and Sahu 2008). Evaporation and transpiration may be estimated separately to partition ET, though partitioning then requires continuous energy-based flux

estimation over large spatial scales. Eddy covariance systems may provide ET and evaporation observations; however, measurement range and location of the tower limits the potential to partition ET over large areas. The difficulties in obtaining representative and continuous (both spatially and temporally) observation data have driven the examination of alternative methods for ET partitioning.

Sheppard (1958) and Bunker (1949) were the first to estimate evaporative flux with the use of tracers. Estimation of partitioning via stable water isotopes may, however, be applied over larger regions than energy-based or correlation based measurements (Kool et al., 2014). SWI partitioning depends on abundance of the more rare, heavy isotopes of water (oxygen-18 and deuterium), where the ratio of isotopes is used to identify the total flux of evaporation. Although the method requires further temporal validation, it has had success in both small (Souch et al., 1996; Wenninger et al., 2010; Sutanto et al., 2012) and global-scale studies (Jasechko et al., 2013). Significant differences in methodology are apparent in small-scale (field) studies relative to large-scale (watershed) studies. Small-scale studies have focused on atmospheric fluxes and sub-daily variations in water composition; whereas large-scale studies have focused on the changes in isotopic composition of water in storage. Each method has its limitations: small-scale studies have large data requirements, and large-scale studies are based on relatively sparse data which assume that isotopic fractionation is relatively similar over the storage area. Significant difficulties arise when combining these approaches, namely a mismatch in available and required data and upscaling over different land covers (Liu et al., 2016). Despite these difficulties, the use of SWIs has the inherent benefit of distinguishing evaporative flux from transpired flux through observational data and physical relationships. Isotopes help to identify transpiration losses to the atmosphere utilizing mass-balance of storage and atmosphere flux via the Craig and Gordon

model (Farquhar et al., 2007). The mass-balance of ET flux (Equation 2-4) describes the water flux of each source (F) in addition to the mass (δ):

$$\boldsymbol{\delta_{ET} \cdot F_{ET} = \delta_E \cdot F_E + \delta_T \cdot F_T} \quad 2\text{-}4$$

where, the subscripts ET, E, and T denote evapotranspiration, evaporation and transpiration, respectively. Rearranging the equation for F_E and F_T gives the flux of each component as a function of the isotopic composition and total ET flux (Zhang et al., 2010):

$$\boldsymbol{F_E = \frac{\delta_T - \delta_{ET}}{\delta_T - \delta_E} \cdot F_{ET}} \quad 2\text{-}5$$

$$\boldsymbol{F_T = \frac{\delta_{ET} - \delta_E}{\delta_T - \delta_E} \cdot F_{ET}} \quad 2\text{-}6$$

The inherent issue with Equations 2-5 and 2-6 is the number of unknowns, where δ_T, δ_E, and δ_{ET} are all typically unknown. Numerous methods have been proposed for estimating δ_{ET} (Yepez et al., 2003; Williams et al., 2004; Sun et al., 2005), and similarly δ_T (Dongman et al., 1974; Farquhar and Cernusak 2005; Lee et al., 2008) so that the above equations may be solved.

2.5.1 ESTIMATION OF ISOTOPIC COMPOSITION OF EVAPORATION

Using the relationships of kinetic and equilibrium isotopic fractionation, Craig and Gordon (1965) developed a model to quantify the isotopic composition of evaporative vapour over a readily available water source (e.g. open water). The model considers several boundary conditions including the turbulent and laminar layers of both vapour and liquid phases of water, and identifies an interface between the two volumes (i.e., liquid and gas). Craig and Gordon (1965) also included resistance factors for the laminar liquid, interface, laminar and turbulent gas sections of the model. Measurement of all layers is, however, not feasible in the field or

regionally, and the relationship for the isotopic composition of evaporative flux is commonly therefore simplified by neglecting liquid mixing phase resistance (Gonfiantini 1986):

$$\boldsymbol{\delta_E = \frac{\delta_L - RH \cdot \delta_A - \varepsilon}{1 - RH + \varepsilon_K/1000}} \quad \text{2-7}$$

where ε is the total isotopic separation [‰] and RH is relative humidity [%]. The total isotopic separation is the summation of the kinetic and equilibrium fractionation ($\varepsilon = \varepsilon^* + \varepsilon_k$). Similarly, measurement of δ_A is not always feasible, in which case equilibrium with precipitation over larger regions may be assumed (Gat and Levy 1978; Gat 1981). The compositions of δ_A and δ_P are linearly correlated using the liquid-vapour equilibrium fractionation (α^*) defined by Rayleigh`s law (Majoube 1971; Horita and Wesolowski 1994):

$$\boldsymbol{\delta_A = \frac{\delta_P - \varepsilon^*}{\alpha^*}} \quad \text{2-8}$$

Estimation of ε_K depends on turbulence parameters that consider atmospheric conditions above the evaporating surface, including the effect of evaporative flux on ambient moisture (n), the ratio of molecular diffusivity of heavy to light isotopes (C_d), and advection of humidity accumulation (θ):

$$\boldsymbol{\varepsilon_k = n \cdot C_d \cdot \theta \cdot (1 - RH)} \quad \text{2-9}$$

Typically, studies simplify variables of Equation 2-9 into two simple bulk terms:

$$\boldsymbol{\varepsilon_k = C_k(n, \theta) \cdot (1 - RH)} \quad \text{2-10}$$

where $C_k(n, \theta)$ incorporates n, and atmospheric advection and turbulence (θ) assuming n is 0.5 and θ is 1 (Gat 2010). C_d of oxygen-18 and deuterium is generally considered to be 28.5‰ and 25.1‰, respectively (Gat 2010). The parameter for ambient moisture flux (n) is typically found to be low (0.5) when the evaporative surface is freely evaporating (i.e. open water) and high ($0.9 \leq n \leq 1$) when evaporation is restricted (i.e. soils) (Gat 2010). However, measurement of RH at

varying heights from the surface is typically not available, therefore atmospheric layers are assumed to be fully mixed, simplifying θ to one (Gat 2010).

2.5.2 ESTIMATION OF ISOTOPIC COMPOSITION OF TRANSPIRATION

Transpiration fluxes are evaporation that occurs through stomatal pores of vegetation. The difference between evaporation and transpiration is significant because transpiration relationships require two additional components: water availability and stomatal resistance. While it is possible to measure stomatal resistance and plant water availability (Monteith et al., 1965; Oosterhuis and Walker 1987), the difficulty with measuring these resistances and δ_T over large regions has led to numerous approaches to estimate the flux and isotopic composition of the flux. For the composition of transpired water, the general Craig and Gordon model (Equation 2-7) is modified:

$$\boldsymbol{\delta_T = \frac{\delta_{L,e}/\alpha^* - RH \cdot \delta_A - \varepsilon^* - (1 - RH) \cdot \varepsilon_k}{(1 - RH) + (1 - RH) \cdot \varepsilon_k/1000}} \qquad 2\text{-}11$$

where $\delta_{L,e}$ is the composition of evaporative leaf water in place of the composition of open, evaporating water. Equation 2-11 specifically focuses on atmospheric conditions within the canopy (at the stomatal pores), most notably for correction of ε_K. Kinetic fractionation within leaf stoma is estimated separately from evaporation (Equation 2-9), dependent on leaf resistance:

$$\textit{For } \boldsymbol{\delta^{18}O}\text{:} \qquad \boldsymbol{\varepsilon_k = \frac{32r_s + 21r_b}{r_s + r_b}} \text{ [‰]} \qquad 2\text{-}12$$

$$\textit{For } \boldsymbol{\delta^{2}H} \qquad \boldsymbol{\varepsilon_k = \frac{16r_s + 11r_b}{r_s + r_b}} \text{ [‰]} \qquad 2\text{-}13$$

where r is the leaf resistance and subscripts s and b denote soil and boundary layers. While $\delta_{L,e}$ is not directly measurable, it is directly correlated to the composition of xylem water (δ_x). Farquhar and Lloyd (1993) established relationships between δ_x and the $\delta_{L,e}$ using the ratio of enrichment of evaporative water to source water ($\Delta_{L,e}$):

$$\boldsymbol{\delta_{L,e}} = \Delta_{\boldsymbol{L,e}}\left(\mathbf{1} + \frac{\boldsymbol{\delta_x}}{\mathbf{1000}}\right) + \boldsymbol{\delta_x} \quad \text{2-14}$$

where $\Delta_{L,e}$ is a function of the Péclet number (*P*é) and the ratio of bulk water to source water ($\Delta_{L,b}$):

$$\Delta_{\boldsymbol{L,e}} = \frac{\Delta_{\boldsymbol{L,b}} \cdot \boldsymbol{P}\text{é}}{(\mathbf{1} - \boldsymbol{e}^{-\boldsymbol{P}\text{é}})} \quad \text{2-15}$$

The Péclet number is a function of vapour density (ρ_v), heat capacity (C_p), air velocity (v_a), temperature gradient from the ground to the atmosphere ($T_1 - T_0$), characteristic length of the gradient (L), and the heat transfer coefficient (k):

$$\boldsymbol{P}\text{é} = \frac{\boldsymbol{\rho_v \cdot C_p \cdot v_a \cdot (T_1 - T_0)/L}}{\boldsymbol{k \cdot (T_1 - T_0)/L^2}} \quad \text{2-16}$$

Finally, $\Delta_{L,b}$ is estimated using the δ_x and the composition of bulk leaf water ($\delta_{L,b}$), which are both measureable:

$$\Delta_{\boldsymbol{L,b}} = (\boldsymbol{\delta_{L,b} - \delta_x})/(\mathbf{1} + \boldsymbol{\delta_x}/\mathbf{1000}) \quad \text{2-17}$$

Transpiration composition (at any time-step) may be solved by substituting Equations 2-14 and either Equation 2-12 or 2-13 into Equation 2-11. Consideration of atmospheric variability in this relationship (i.e., temperature, wind speed, air density) results in large temporal changes of the Péclet number, and therefore isotopic composition. During periods of steady-state (longer than a few hours), the composition of the xylem water may be assumed equal to the composition of transpired water (Yakir 1998; Yakir et al., 2000; Gan et al., 2002). This is beneficial for large regions as the isotopic composition of xylem water may be assumed to be equal to the composition of shallow soil water, and hence transpiration may be considered a non-fractionating process with respect to soil water compositions (e.g. Ehleringer and Dawson 1992; Yepez et al., 2003; Koeniger et al., 2010).

2.5.3 ESTIMATION OF ISOTOPIC COMPOSITION OF EVAPOTRANSPIRATION

Finally, the solution of Equations 2-6 and 2-7 requires the composition of evapotranspired water (δ_{ET}), observations of which are not always available. Kahmen et al. (2008) estimated δ_{ET} using the Keeling plot with water ratios (w) in the canopy and in the atmosphere (w_b), and isotopic samples of surface vapour (δ_v). Estimation of vapour composition for the Keeling plot method may be obtained from temperature (Jacob and Sonntag 1991; Gat 1996), or mixing water ratios (Lee et al., 2006). The Keeling plot method assumes i) background conditions and δ_{ET} are constant in model space and time-step, ii) atmospheric changes are in steady state (occur only due to ET fluxes), and iii) no condensation occurs (Zhang et al., 2010). The Keeling plot cannot directly account for regional rainout processes due to the general nature of the relationship (Lee et al., 2006). This requires atmospheric stability conditions (w and δ_v) to be known or measured, which is not always feasible across large regions. Additionally, since estimation of δ_{ET} from the Keeling plot generally requires extrapolation, small changes in atmospheric input (w and δ_v) may result in large changes in δ_{ET} (Yakir and Sternberg 2000).

Though the isotopic method presented above shows promise (Zhang et al., 2011), there are several assumptions required for this direct method to be used when observation data are not readily available. While these assumptions may hold true for smaller areas, larger regions and watersheds violate model assumptions due to large spatial heterogeneity (i.e. vegetation and atmospheric conditions). Of course, remotely sensed data or general circulation models (GCMs) may be used to gap-fill information where no data are observed, but this introduces additional input data uncertainty that is difficult to quantify. With these concerns, estimation of δ_{ET} through the mass-balance method is not practical for regional-scale studies with limited observational data. Therefore, a new method is required to specifically address the temporal changes of the

partition in ET in large watersheds, quantifiably partitioning ET with limited observed data such as more potentially available data sources that combine storage fractionation over large scales.

2.6. SUMMARY OF GAPS IN EXISTING LITERATURE

Despite significant advancement in improving the simulations made by hydrologic models in high-latitude regions, large-scale applications are still limited by the need for process-based conceptualizations where data are lacking to utilize a full, physically-based set of equations. Poor representation of the seasonality of evaporation and transpiration is important to hydrologic models in data-sparse, high latitude watersheds given the potential these processes can have to significantly impact seasonal water availability. Modelling hydrological processes and isotopes simultaneously has the potential to account for the temporal and spatial variability of flow paths and associated storages. To date, empirical methods for partitioning ET with respect to vegetation and moisture on large scales is limited. Consideration of evaporative fractionation in primary source waters has the potential to influence the identification of flow paths within a watershed, similar to the precipitation influence observed by McDonnell et al. (1991); but such a method has yet to be developed.

Understanding of evaporation and transpiration fluxes has been significantly improved in recent years, including tracer-aided application evaporation and transpiration flux estimations (Zhang et al., 2010; Jasechko et al., 2013; Good et al., 2015). However, large spatial scales currently do not lend themselves to temporal partitioning of ET using mass-balance or hydrograph separation. This leaves a significant gap in ET partitioning research, a method of temporally partitioning ET at large scales with limited observed data. Additionally, highly seasonal mid-to-high-latitude watersheds are under-represented in ET partition studies. These watersheds exhibit extreme seasonal effects on ET fluxes, rendering an understanding of ET processes and seasonality critical to effective regional water management.

In addition to hydrologic models, transit time distributions have used tracers to help identify storage availability in watersheds. Although transit time models have been applied to snowmelt-dominated catchments, these studies have not included high-latitude regions where the availability of storage changes throughout the year due to soil freeze-thaw cycles. Transit time studies have generally not focused on the inclusion of ET, or the fractionation of evaporation from storage. Seasonality and frozen ground has a much larger influence on evaporation in high-latitudes than low-latitude wet watersheds that rapidly replenish evaporative losses; and therefore, must be accounted for. Lastly, transit time modelling studies have not yet considered the influence that differences in evaporation and transpiration fluxes may have on flow pathways, which is critical when assessing both inter and intra -annual changes in water availability.

2.7 REFERENCES

Asano, Y., Uchida, T., Ohte, N. 2002. Residence times and flow paths of water in steep unchannelled catchments, Tanakami, Japan. *Journal of Hydrology*, **Volume 261**: 173-192.

Barthold, F.K., Wu, J. Vaché, K.B., Schneider, K., Frede, H., Breuer, L. 2010. Identification of geographic runoff sources in a data sparse region: Hydrological processes and the limitations of tracer-based approaches. *Hydrological Processes*, **Volume 24**: 2313-2327. DOI: 10.1002/hyp.7678.

Barthold, F.K., Tyralla, C., Schneider, K., Vaché, K.B., Frede, H., Breuer, L. 2011. How many tracers do we need for end member mixing analysis (EMMA)? A sensitivity analysis. *Water Resources Research*, **Volume 47**, W08519-1-14. DOI: 10.1029/2011/WR010604

Benettin, P., Soulsby, C., Birkel, C., Tetzlaff, D., Botter, G., Rinaldo, A., 2017. Using SAS functions and high-resolution isotope data to unravel travel time distributions in headwater catchments. *Water Resources Research*, **Volume 53(3)**: 1864-1878.

Belachew, D.L., Leavesley, G., David, O., Patterson, D., Aggarwal, P., Araguas, L., Terzer, S., Carlson, J. 2016. IAEA Isotope-enabled coupled catchment-lake water balance model, IWBMIso: description and validation. *Isotopes in Environmental and Health Studies*, **Volume 52(4-5)**: 1-16. DOI: 10.1080/10256016.2015.1113959

Beven, K., Binley, A. 1992. The future of distributed models: Model calibration and uncertainty prediction. *Hydrological Processes*, **Volume 6**: 279-298.

Beven, K., Freer, J., 2001. Equifinality, data assimilation, and uncertainty estimation in mechanistic modelling of complex environmental systems using the GLUE methology. *Journal of Hydrology*, **Volume 249**: 11-29.

Beven, K., Binley, A. 2013. GLUE: 20 years on. *Hydrological Processes*, **Volume 28(24)**: 5897-5918.

Beven, K., Young, P. 2013. A guide to good practice in modelling semantics for authors and referees. *Water Resources Research*, **Volume 49**: 5092-5098.

Birkel, C., Dunn, S.M., Tetzlaff, D., Soulsby, C. 2010. Assesing the value of high-resolution isotope tracer data in the stepwise development of a lumped conceptual rainfall-runoff model. *Hydrological Processes*, **Volume 24**: 2335-2348.

Birkel, C., Tetzlaff, D., Dunn, S.M., Soulsby, C. 2011. Using lumped conceptual rainfall-runoff models to simulate daily isotope variability with fractionation in a nested mesoscale catchment. *Advances in Water Resources*, **Volume 34(3)**: 383-394.

Birkel, C., Soulsby, C., Tetzlaff, D., Dunn, S., Spezia, L. 2012. High-frequency storm event isotope sampling reveals time-variant transit time distributions and influence of diurnal cycles. *Hydrological Processes*, **Volume 26(2):** 308–316. DOI:10.1002/hyp.8210.

Birkel, C., Soulsby, C., Tetzlaff, D. 2015. Conceptual modelling to assess how the interplay of hydrological connectivity, catchment storage and tracer dynamics controls nonstationary water age estimates. *Hydrological Processes*, **Volume 29**: 2956–2969.

Botter, G., Bertuzzo, E., Rinaldo, A. 2010. Transport in the hydrologic response: Travel time distributions, soil moisture dynamics, and the old water paradox. *Water Resources Research*, **Volume 46**: W03514-1-18. DOI: 10.1029/2009WR008371.

Botter, G. 2012. Catchment mixing processes and travel time distributions. *Water Resources Research*, **Volume 48**: W05545-1-15. DOI: 10.1029/2011WR011160.

Bras, R.L., Rodriguez-Iturbe, I. 1976. Rainfall Generation: A nonstationary time-varying multidimensional model. *Water Resources Research*, **Volume 12(3)**: 450-456.

Brock, B., Wolfe, B., Edwards, T. 2007. Characterizing the Hydrology of Shallow Floodplain Lakes in the Slave River Delta, NWT, Canada, Using Water Isotope Tracers. *Arctic, Antarctic and Alpine Research*, **39(3):** 388-401.

Buttle, J.M. 1994. Isotope Hydrograph separations and rapid delivery of pre-event water from drainage basins. *Progress in Physical Geography*, **Volume 18(1)**: 16-41.

Carey, S.K., Quinton, W.L. 2004. Evaluating snowmelt runoff generation in a discontinuous permafrost catchment using stable isotope, hydrochemical and hydrometric data. *Nordic Hydrology*, **Volume 35**: 309-324

Carey, S.K., Quinton, W.L. 2005. Evaluation of runoff generation during summer using hydrometric, stable isotope and hydrochemical methods in a discontinuous permafrost environment. *Hydrological Processes*, **Volume 19**: 95-114.

Chapra, S.C., 1997. Surface Water-Quality Modelling. 2nd (reissued) ed. s.l.:Waveland Press Inc..

Christophersen, N., Hooper, R.P. 1992. Multivariate analysis of stream water chemical data: The use of principal components analysis for the end-member mixing problem, *Water Resources Research*, **Volume 28(1)**, 99–107. DOI:10.1029/91WR02518.

Craig, H. 1961. Isotopic Variations in Meteoric Waters. *Science*, **Volume 133(26)**: 1702.

Craig, H., Gordon, L. 1965. Deuterium and oxygen-18 variations in the ocean and marine atmosphere. *Stable Isotopes in Oceanographic Studies and Paleotemperatures*: 9-130.

Craig, H., Gordon, L. I., Horibe, Y. 1963. Isotopic exchange effects in the evaporation of water: 1. Low-temperature experimental results. *Journal of Geophysical Research*, **Volume 68(17)**: 5079-5087.

Crawford, N.H., Linsley, R.K. 1966. Digital Simulation in Hydrology: Stanford Watershed Model IV, Stanford: Department of Civil Engineering: Stanford University.

Danckwerts, P.V. 1953. Continous flow systems. Distribution of residence times. *Chemical Engineering Science*, **Volume 2(1)**: 1-13.

Dansgaard, W. 1964. Stable isotopes in Precipitation. In: Y. Kitano, ed. Geochemistry of Water 1975. Stroudsburg: Dowden, Hutchinson & Ross, Inc.: 436-468.

Dinçer, T., Payne, B.R., Florkowski, T., Martinec, J., Tongiorgi, E. 1970. Snowmelt runoff from measurements of tritium and oxygen-18. *Water Resources Research*, **Volume 6**: 110–124.

Dongmann G, Nürnberg, H.W., Förstel, H., Wagener, K. 1974. On the enrichment of H2 18O in the leaves of transpiring plants. Radiation and Environmental Biophysics. **Volume 11**: 41–52.

Eckhardt, K. 2005. How to construct recursive digital filters for baseflow separation. *Hydrological Processes*, **Volume 19(2)**: 507-515.

Ehhalt, D., Knott, K., Nagel, J.F., Vogel, J.C. 1963. Deuterium and Oxygen-18 in Rain Water. *Journal of Geophysical Research*, **Volume 68(13)**: 3775-3780.

Ehleringer, J.R., Dawson, T.E. 1992. Water uptake by plants: Perspectives from stable isotope composition. *Plant, Cell and Environment*, **Volume 15**: 1073-1082.

Eum, H., Dibike, Y., Prowse, T. 2016a. Climate-induced alteration of hydrologic indicators in the Athabasca River Basin, Alberta, Canada. *Journal of Hydrology*, **Volume 544**: 327-342.

Eum, H., Dibike, Y., Prowse, T. 2016b. Comparative evaluation of the effects of climate and land-cover changes on hydrologic responses of the Muskeg River, Alberta, Canada. *Journal of Hydrology*: *Regional Studies*, **Volume 8**: 198-221.

Evaristo, J., Jasechko, S., McDonnell, J., 2015. Global separation of plant tranispiation from groundwater and streamflow. *Nature*, **Volume 525**: 91-94. DOI: 10.1038/nature14983

Farquhar, G.D., Cernusak, L.A. 2005. On the isotopic composition of leaf water in the non-steady state. *Functional Plant Biology*. **Volume 32**: 293–303

Farquhar, G.D., Lloyd, J. 1993. Carbon and oxygen isotope effects in the exchange of carbon dioxide between terrestrial plants and the atmosphere, in: J.R. Ehleringer, A.E. Hall, G.D. Farquhar (Eds.), *Stable Isotopes and Plant Carbon– Water Relations,* Academic Press, San Diego: 47–70.

Farquhar, G.D., Cernusak, L.A., Barnes., B. 2007. Heavy water fractionation during transpiration, *Plant Physiology*. **Volume 143**: 11–18.

Frederickson, G.C., Criss, R.E. 1999. Isotope hydrology and residence times of the unimpounded Meramec River Basin, Missouri. *Chemical Geology*. **Volume 157(3–4)**: 303–317.

Gan, K.S., Wong, S.C., Yong, J.W.H., Farquhar, D. 2002. ^{18}O spatial patterns of vein xylem water, leaf water, and dry matter in cotton leaves, *Plant Physiology*, **Volume 130**: 1008–1021.

Gat, J. 1981. Lakes. In: Stable Isotope Hydrology-Deuterium and Oxygen-18 in the Water Cycle. Vienna: IAEA: 203-221.

Gat, J.R., Levy, Y. 1978. Isotope Hydrology of inland sabkhas in the Bardawil area, Sinai. *Limnology and Oceanography*, **Volume 23(5)**: 841-850.

Gat, J. 2010. Isotope Hydrology: A study of the water cycle. Imperial College Press. London.

Gibson, J. 2002. Short-term evaporation and water budget comparisons in shallow Arctic lakes using non-steady isotope mass-balance. *Journal of Hydrology*, **Volume 264:** 242-261.

Gibson, J., Edwards, T.W. 1996. Development and Validation of an Isotopic Method for Estimating Lake Evaporation. *Hydrological Processes*: **Volume 10(10):** 1369-1382.

Gibson, J., Edwards, T.W., Bursey, G.G. 1993. Estimating Evaporation Using Stable Isotopes: Quantitative Results and Sensitivity Analysis for Two Catchments in Northern Canada. *Nordic Hydrology*, **Volume 24:** 79-94.

Gibson, J.J., Birks, S.J., Edwards, T.W. 2008. Global predication of dA and d2H-d18O evaporation slopes for lakes and soil water accounting for seasonality. *Global Biochemical Cycles*, **Volume 22**: GB2031-1-12. DOI:10.1029/2007GB002997

Gonfiantini, R. 1986. Environmental isotopes in lake studies. In: P. Fritz & J. C. Fontes, eds. Handbook of Environmental Isotope Geochemistry. New York: Elsevier: 113-168.

Gonzalez, A. L., Nonner, J., Heijkers, J., Uhlenbrook, S. 2009. Comparison of different base flow seperation methods in a lowland catchment. *Hydrology and Earth System Sciences*, **Volume 13**: 2055-2068.

Good, S. P., Noone, D., Bowen, G. 2015. Hydrologic connectivity constrains partitioning of global terrestrial water fluxes. *Science*, **Volume 349 (6244)**: 175-177.

Gupta, H.V., Sorooshian, S., Yapo, P.O. 1998. Toward improved calibration of hydrologic models: Multiple and noncommensurable measures of information. *Water Resources Research*, **Volume 34(4)**: 751-763. DOI: 10.1029/97WR03495.

Hall, F.R. 1968. Base-flow recessions: A review. *Water Resources Research*, **Volume 4(5):** 973-983.

Harman, C. 2015. Time-variable transit time distribution and transport: Theory and application to storage-dependent transport of chloride in a watershed. *Water Resources Research*, **Volume, 51**:1-30. DOI:10.1002/2014WR015707

Hastings, W.K. 1970. Monte Carlo Sampling Methods using Markov Chains and their Applications. *Biometrika*, **Volume 57(1)**: 97-109.

Holmes, T. 2016. Assessing the value of stable water isotopes in Hydrologic Modelling: A Dual-Isotope Approach. MSc Thesis. University of Manitoba.

Hortia, J., Wesolowski, D. 1994. Liquid-vapour fractionation of oxygen and hydrogen isotopes of water form the freezing to the critical temperature. *Geochimica et Cosmochimica Acta*, **Volume 58(16)**: 3425-3437.

Hrachowitz, M., Soulsby, C., Tetzlaff, D., Dawson, J.J.C., Dunn, S.M., Malcolm, I.A. 2009. Using long-term data sets to understand transit times in contrasting headwater catchments. *Journal of Hydrology*, **Volume 367**: 237-248.

Hrachowitz, M., Soulsby, C., Tetzlaff, D., Malcolm, I.A., Schoups, G. 2010. Gamma distribution models for transit time estimation in catchments: Physical interpretation of parameters and implications for time-variant transit time assessment. *Water Resources Research*, **Volume 46(10)**: W10536-1-15. DOI: 10.1029/2010WR009148.

IAEA. 2001. Environmental Isotopes in the Hydrological Cycle: Principles and Applications. Vienna: IAEA.

IAEA. 2009a. SLAP2, Water. [Online] Available at: http://nucleus.iaea.org/rpst/ReferenceProducts/ReferenceMaterials/Stable_Isotopes/2H18O-water-samples/SLAP2.htm [Accessed 2014].

IAEA. 2009b. VSMOW2, Water. [Online] Available at: http://nucleus.iaea.org/rpst/ReferenceProducts/ReferenceMaterials/Stable_Isotopes/2H18O-water-samples/VSMOW2.htm [Accessed 2014].

IAEA. 2012. Monitoring Isotopes in Rivers: Creation of the Global Network of Isotopes in Rivers (GNIR), Vienna: International Atomic Energy Agency- *TECDOC* - 1673.

Jacob, H., Sonntag, C. 1991. An 8-year record of the seasonal variation of ^{2}H and ^{18}O in atmospheric water vapor and precipitation at Heidelberg, Germany. Tellus Series B – *Chemical and Physical Meteorology*, **Volume 43**: 291–300.

Jasechko, S., Sharp, Z., Gibson, J., Birks, J., Yi, Y., Fawcett, P. 2013. Terrestrial water fluxes dominated by transpiration. *Nature*, **Volume 496**: 347-350.

Joerin, C., Beven, K.J., Iorgulescu, I., Musy, A. 2002. Uncertainty in hydrograph separations based on geochemical mixing models. *Journal of Hydrology*, **Volume 255 (1–4)**: 90–106.

Jost, G., Moore, R.D., Menounos, B., Wheate, R. 2012. Quantifying the contribution of glacier runoff to streamflow in the upper Columbia River Basin, Canada. *Hydrology and Earth System Sciences*, **Volume 16**: 849-860.

Kahmen, A., Simonin, K., Tu, K.P., Merchant, A., Callister, A., Siegwolf, R., Dawson, T.E., Arndt, S.K. 2008. Effects of environmental parameters, leaf physiological properties and leaf water relations on leaf water d18O enrichment in different Eucalyptus species, *Plant Cell and Environment,* **Volume 31**: 738–751.

Kavetski, D., Kuczera, G., Franks, S.W. 2006a. Bayesian analysis of input uncertainty in hydrological modelling: 1. Theory. *Water Resources Research*, **Volume 42(3)**: W03407-1-9. DOI:10.1029/2005WR004368.

Kavetski, D., Kuczera, G., Franks, S.W., 2006b. Bayesian analysis of input uncertainty in hydrological modelling: 2. Application. *Water Resources Research*, **Volume 42(3)**: W03408-1-10. DOI:10.1029/2005WR004376.

Kendall, C., McDonnell, J.J. 2003. *Isotope Tracers in Catchment Hydrology*. 3rd ed. Amsterdam: Elsevier.

Kennedy, V.C., Kendall, C., Zellweger, G.W., Wyerman, T.A., Avanzino, R.J. 1986. Determination of the components of stormflow using water chemistry and environmental isotopes, Mattole Rivr Basin, California. *Journal of Hydrology*, **Volume 84(1-2)**: 107-140.

Kirchner, J.W., Feng, X., Neal, C. 2000. Fractal stream chemistry and its implications for contaminant transport in catchments. *Nature*, **Volume 403(3)**: 524-527.

Kirchner, J.W., Feng, X., Neal, C. 2001. Catchment-scale advection and dispersion as a mechanism for fractal scaling in stream tracer concentrations. *Journal of Hydrology*, **Volume 254**: 82–101.

Klaus, J., McDonnell, J.J., 2013. Hydrograph separation using stable isotopes: Review and evaluation. *Journal of Hydrology*, **Volume 505**: 47-64.

Klemeš, V. 2002. Risk analysis: The unbearable cleverness of bluffing. In: Bogardi, J.J., Kundrewicz, Z.W. (eds) *Risk, reliability, uncertainty and robustness of water resource systems.* Cambridge University Press: 22-29.

Kliner, K., Knezek, M. 1971. The underground runoff separation method making use of the observation of ground water table. *Hydrology and hydromechanics*, **Volume 22(5)**: 457–466.

Koeniger, P., Leibundgut, C., Link, T., Marshall, J.D. 2010. Stable isotopes applied as water tracers in column and field studies. *Organic Geochemistry*, **Volume 41(1)**: 31-40.

Kool, D., Agam, N., Lazarovitch, N., Heitman, J.L., Sauer, T.J., Ben-Gal, A. 2014. A review of approaches for evapotranspiration partitioning. *Agricultural and Forest Meteorology*, **Volume 184**: 56-70.

Krause, P., Boyle, D.P., Bäse, F. 2005. Comparison of difference efficiency criteria for hydrological model assessment. *Advances in Geosciences*, **Volume 5**: 89-97.

Laudon, H., Seibert, J., Köhler, S. and Bishop, K. 2004. Hydrological flow paths during snowmelt: Congruence between hydrometric measurements and oxygen 18 in meltwater, soil water, and runoff. *Water Resources Research*. **Volume 40**: W03102-1-9. DOI: 10.1029/2003WR002455.

Lee, E.S., Krothe, N.C. 2001. A four-component mixing model for water in a karst terrain in south-central Indiana, USA. Using solute concentration and stable isotopes as tracers. *Chemical Geology*, **Volume 179(1-4)**: 129-143.

Lee, X., Smith, R., Williams, J. 2006. Water vapour $^{18}O/^{16}O$ isotope ratio in surface air in New England, USA. *Tellus*, **Volume 58B**: 293-304.

Lee, X.H., Griffis, T.J., Baker, J.M., Billmark, K.A., Kim, K., Welp, L.R. 2008. Canopy-scale kinetic fractionation of atmospheric carbon dioxide and water vapor isotopes. *Global Biogeochemical Cycles*, **Volume 23(1)**: GB1002-1-15. DOI:10.1029/2008gb003331.

Liu, S., Xu, Z., Song, L., Zhao, Q., Ge, Y., Xu, T., Ma, Y., Zhu, Z., Jia, Z., Zhang, F. 2016. Upscaling evapotranspiration measurements from multi-site to the satellite pixel scale over heterogeneous land surfaces. *Agricultural and Forest Meterology*, **Volume 72(3)**: 18-29.

Lott, D.A., Stewart, M.T. 2016. Base flow separation: A comparison of analytical and mass balance methods. *Journal of Hydrology*, **Volume 535**: 525-533.

Majoube, M. 1971. Fractionnement en oxygen-18 et en deuterium entre l'eau et sa vapeur, *Journal de Chimie Physique*, **Volume 68**: 1423–1436.

Maloszewki, P., Zuber, A. 1982. Determining the turnover time of groundwater systems with the aid of environmental tracers. *Journal of Hydrology*, **Volume 57**: 207-231.

Maloszewski, P., Zuber, A. 1992. principles and practice of calibration and validation of mathematical models for the interpretation of environmental tracers. *Advances in Water Resources*, **Volume 16**: 173-190.

McDonnell, J.J., Bonell, M., Stewart, M.K., Pearce, A.J. 1990. Deuterium Variations in Storm Rainfall: Implications for Stream Hydrograph Separation. *Water Resources Research*, **Volume 26(3)**: 455-458.

McDonnell, J.J., McGuire, K., Aggarwal, P., Beven, K., Biondi, D., Destouni, G., Dunn, S., James, A., Kirchner, J., Kraft, P., Lyon, S., Maloszewski, P., Newman, B., Pfister, L., Rinaldo, A., Rodhe, A., Sayama, T., Seiber, J., Solomon, K., Soulsby, C., Stewart, M., Tetzlaff, D., Tobin, C., Troch, P., Weiler, M., Western, A., Worman, A., Wrede, S. 2010. How old is streamwater? Open questions in catchment transit time conceptualization, modelling and analysis. *Hydrological Processes*, **Volume 24**: 1745-1754.

McDonnell, J.J., Stewart, M.K., Owens, I.F. 1991. Effect of catchment-scale subsurface mixing on stream isotopic response. *Water Resources Research*, **Volume 27(12)**: 3065-3073.

McGlynn, B., McDonnell, J.J., Stewart, M., Seibert, J. 2003. On the relationships between catchment scale and streamwater mean residence time. *Hydrological Processes*: **Volume 17(1):** 175-181. DOI: 10.1002/hyp.5085.

McGuire, K.J., McDonnell, J.J. 2006. A review and evaluation of catchment transit time modelling. *Journal of Hydrology*, **Volume 330**: 543-563.

McGuire, K.J., McDonnell, J.J., Weiler, M., Kendall, C., McGlynn, B.L., Welker, J.M., Seiber, J. 2005. The role of topography on catchment-scale water residence time. *Water Resources Research*, **Volume 41(5):** W05002-1-14. DOI: 10.1029/2004WR003657.

McMillan, H., Telzlaff, D., Clark, M., Soulsby, C. 2012. Do time variable tracers aid the evalution of hydrological model structure? A multimodel approach. *Water Resources Research*, **Volume 48**. W05501-1-18. DOI:10.1029/2011WR011688

Merot, P., Durand, P., Morisson, C. 1995. Four-component hydrograph separation using isotopic and chemical determinations in an agricultural catchment in Western France. *Physics and Chemistry of the Earth*, **Volume 20(3)**: 415-425.

Metcalfe, R. A., Buttle, J. M. 2001. Soil partitioning and surface store controls on spring runoff from a boreal peatland basin in north-central Manitoba, Canada. *Hydrological Processes*, **Volume 15(12)**: 2305-2324.

Metropolis, N., Rosenbluth, A.W., Rosenbluth, M.N., Teller, A.H., Teller, E. 1953. Equation of state calculations by faster computing machines. *Journal of Chemical Physics*. **Volume 21**: 1087-1092. DOI: 10.1063/1.1699114.

Michel, R.L. 1992. Residence times in river basins as determined by analysis of long-term tritium records. *Journal of Hydrology*, **Volume 130**: 367-378.

Moore, R.D. 1989. Tracing Runoff Sources with Deuterium and Oxygen-18 during spring melt in a headwater catchment, southern Laurentian, Quebec. *Journal of Hydrology*, **Volume 112(1-2)**: 135-148.

Moser, H., Stichler, W. 1975. Deuterium and oxygen-18 contents as an index of the properties of snow covers. In: *Snow Mechanics; Proceedings of the Grindelwald Symposium.* s.l.:IAHS Publication: 122-135.

Niemi, A.J. 1977. Residence time distributions of variable flow processes. *International Journal of Applied Radiation and Isotopes*, **Volume 28(10-11)**: 855–860.

Oosterhuis, D.M., Walker, S. 1987. Stomatal resistance measurement as an indicator of water deficit stress in wheat and soybeans. *South African Journal of Plant and Soil*, **Volume 4**: 113-120. DOI: 10.1080/02571862.1987.10634956.

Penna, D., Ahmad, M., Birks, S.J., Bouchaou, L., Brencic, M., Butt, S., Holko, L., Jeelani, G., Martinez, D.E., Melikadze, G., Shanley, J.B., Sokratov, S.A., Stadnyk, T., Sugimoto, A., Vreca, P. 2014. A new method of snowmelt sampling for water stable isotopes. *Hydrological Processes,* **Volume 28(22)**: 5637-5644. DOI: 10.1002/hyp.10273.

Posey, J. C., Smith, H.A. 1957. The equilibrium distribution of light and heavy waters in a freezing mixture. *Journal of the American Chemical Society*, **Volume 79**: 555-557.

Qi, W., Zhang, C., Fu, G., Zhou, H., Liu, J. 2016. Quantifying uncertainties in extreme flood predictions under climate change for a medium-sized basin in Northeastern China. *American Meteorological Society*, **Volume 17**: 3099-3112.

Rice, K. C., Hornberger, G.M. 1998. Comparison of hydrochemical tracers to estimate source contributions to peak flow in a small, forested, headwater catchment. *Water Resources Research*, **Volume 34(7)**: 1755-1766.

Rodgers, P., Soulsby, C., Waldron, S. 2005. Using stable isotope tracers as diagnotic tools in upscaling flow path understanding and residence times estimates in a mountainous mesoscale catchment. *Hydrological Processes*, **Volume 19**: 2291-2307.

Rodhe, A. 1981. Spring flood: meltwater or groundwater? *Nordic Hydrology*, **Volume 12**: 21-30.

Rodhe, A., Nyberg, L., Bishop, K. 1996. Transit times for water in a small till catchment from a step shift in the oxygen-18 content of the water input. *Water Resources Research*, **Volume 32(12)**: 2497-3511.

Scanlon, T.M., Sahu, P. 2008. On the correlation structure of water vapor and carbon dioxide in the atmospheric surface layer: a basis for flux partitioning. *Water Resources Research*, **Volume 44**: W10418-1-15. DOI: 10.1029/2008WR006932.

Sheppard, P.A. 1958. Transfer across the earth's surface and through the air above. *Quarterly Journal of the Royal Meteorological Society*. **Volume 84**: 205–224.

Sklash, M.G., Farvolden, R.N., 1979. The role of groundwater in storm runoff. *Journal of Hydrology*, **Volume 43(1)**: 45-65.

Sklash, M.G., Farvolden, R.N., Fritz, P. 1976. A conceptual model of watershed response to rainfall, developed through the use of oxygen-18 as a natural tracer. *Candian Journal of Earth Sciences*, **Volume 13(2)**: 271-283.

Souch, C., Grimmond, C., Wolfe, C. 1996. Wetland evaporation and energy partitioning: Indiana Dunes National Lakeshore. *Journal of Hydrology*, **Volume 184**: 189-208.

Soulsby, C., Birkel, C., Geris, J., Tetzlaff, D. 2014. The isotope hydrology of a large river system regulated for hydropower. *River Research and Applications*, **Volume 31(3):** 335-349.

Soulsby, C., Tetzlaff, D., Dunn, S.M., Waldron, S. 2006. Scaling up and out in runoff process understanding: insights from nested experimental catchment studies. *Hydrological Processes*. **Volume 20**: 2461-2465.

Soulsby, C., Birkel, C., Tetzlaff, D. 2016. Characterizing the age distribution of catchment evaporative losses. *Hydrological processes*, **Volume 30**: 1308-1312.

St. Amour, N., Gibson, J., Edwards, T., Prowse, T. 2005. Isotopic time-series partitioning of streamflow components in wetland-dominated catchments, lower Liard River basin, Northwest Territories, Canada. *Hydrological Processes*, **Volume 19(17)**: 3357-3381.

Stadnyk-Falcone, T. 2008. Mesoscale Hydrological Model validation and Verification using Stable Water Isotopes: The isoWATFLOOD Model, s.l.: University of Waterloo.

Stadnyk, T.A., St Amour, N., Kouwen, N., Edwards, T., Pietroniro, A., Gibson, J. 2005. A groundwater separation study in boreal wetland terrain: The WATFLOOD hydrological model compared with stable isotope tracers. *Isotopes in Environmental and Health Studies*, **Volume 41(1)**: 49-68.

Su, N. 1995. The unit hydrograph model for hydrograph separation. *Environment International*, **Volume 21(5)**: 509-515.

Sun, W., Lin, G.H., Chen, S.P., Huang, J.H. 2005. Applications of stable isotope techniques and Keeling plot approach to carbon and water exchange studies of terrestrial ecosystems, *Acta Phytoecologica Sinica*, **Volume 29**: 851–862.

Sutanto, S.J., Wenninger, J., Coenders-Gerrits, A.M., Uhlenbrook, S. 2012. Partitioning of evaporation into transpiration, soil evaporation and interception: a comparison between isotope measurements and a HYDRUS-1D model. *Hydrology and Earth System Sciences*, **Volume 16**: 2605-2616.

Taylor, S., Feng, X., Kirchner J.W., Osterhuber, R., Klaue, B., Renshaw, C.E. 2001. Isotopic evolution of a seasonal snowpack and its melt. *Water Resources Research*. **Volume 37(3)**: 759-769.

Taylor, S., Feng, X., Renshaw, C.E. 2002. Isotopic evolution of snowmelt 2. Verification and parameterization of a one-dimensional model using laboratory experiments. *Water Resources Research*, **Volume 38(10)**: 36-1-36-8. DOI: 10.1029/2001WR000815.

Tetzlaff, D., Birkel, C., Dick, J., Geris, J., Soulsby, C. 2014. Storage dynamics in hydropedological units control hillslope connectivity, runoff generation, and the evolution of catchment transit time distributions. *Water Resources Research*, **Volume 50(2)**: 969-985. DOI: 10.1002/2013WR014147.

Timbe, E., Windhorst, D., Crespo, P., Frede, H., Feyen, J., Breuer, L. 2014. Understanding uncertainties when inferring mean transit times of water trough tracer-based lumped-parameter models in Andean tropical montane cloud forest catchments. *Hydrology and Earth System Sciences*, **Volume 18**: 1503-1523.

Tolson, B.A., Shoemaker, C.A. 2007. Dynamically dimensioned search algorithm for computationally efficient watershed model calibration. *Water Resources Research,* **Volume 43(1):** W01413-1-16. DOI:10.1029/2005WR004723.

Tolson, B.A., Shoemaker, C.A. 2008. Efficient prediction uncertainty approximation in the calibration of environmental simulation models. *Water Resources Research*, **Volume 44(4)**, W044111-19. DOI: 10.1029/2007WR005869

Van Huijgevoort, M.H.J., Tetzlaff, D., Sutanudjaja, E.H., Soulsby, C. 2016. Using high resolution tracer data to constrain water storage, flux and age estimates in a spatially distributed rainfall-runoff model. *Hydrological Processes*, **Volume 30(25)**: 4761-4778.

Vitvar, T., Balderer, W. 1997. Estimation of mean water residence times and runoff generation by 18O measurements in a pre-Alpine catchment (Rietholzbach, eastern Switzerland). *Applied Geochemistry*, **Volume 12(6):** 787 –796.

Vitvar, T., Burns, D.A., Lawrence, G.B., McDonnell, J.J., Wolock, D.M. 2002. Estimation of baseflow residence times in watersheds from the runoff hydrograph recession: method and application in the Neversink watershed, Catskill Mountains, New York. *Hydrological Processes,* **Volume 16 (9)**: 1871–1877

Vrugt, J.A. 2016 Markov chain Monte Carlo simulation using the DREAM software package: Theory, concepts, and MATLAB implementation. *Environmental Modelling & Software*, **Volume 75**: 273-316.

Wagener, T., McIntyre, N., Lees, M.J., Wheater, H., Gupta, H. 2003. Toward reduced uncertainty in conceptual rainfall-runoff modelling: Dynamic identifiability analysis. *Hydrological Processes*, **Volume 17**: 455-476.

Weiler, M., McGlynn, B.L., McGuire, K., McDonnell, J.J. 2003. How does rainfall become runoff? A combined tracer and runoff transfer function approach, *Water Resources Research*, **Volume 39(11)**: 1315-1328. DOI:10.1029/2003WR002331.

Wenninger, J., Beza, D.T., Uhlenbrook, S. 2010. Experimental investigations of water fluxes within the soil-vegetation-atmosphere system: Stable isotope mass-balance approach to partition evaporation and transpiration. *Physics and Chemistry of the Earth*, **Volume 35**: 565-570.

Williams, D.G., Cable, W., Hultine, K., Hoedjes, J., Yepez, E., Simonneaux, V., Er-Raki, S., Boulet, G., de Bruin, H.A.R., Chehbouni, A., Hartogensis, O., Timouk, F. 2004. Evapotranspiration components determined by stable isotopes, sap flow and eddy covariance techniques. *Agricultural and Foret Meteorology,* **Volume 125**: 241-258.

Yakir, D., Sternberg, L.D.L., 2000. The use of stable isotopes to study ecosystem gas exchange, *Oecologia*, **Volume 123**: 297–311.

Yakir, D. 1998. Oxygen-18 of leaf water: a crossroad for plant-associated isotopic signals, in: H. Griffiths (Ed.), *Stable Isotopes: Integration of Biological, Ecological and Geochemical Processes*, BIOS Scientific Publishers Ltd., Oxford: 147–168.

Yepez, E.A., Williams, D.G., Scott, R.L., Lin, G. 2003. Partitioning overstor and understory evapotranspiration in a semiarid savanna woodland from the isotopic composition of water vapor. *Agricultural and Forest Meteorology,* **Volume 119**: 53-69.

Yi, Y., Gibson, J.J., Helie, J.-F., Dick, T.A. 2010. Synoptic and time-series stable isotope surveys of the Mackenzie River from Great Slave Lake to the Arctic Ocean, 2003 to 2006. *Journal of Hydrology,* **Volume 383(1)**: 223-232.

Zhang, S., Wen, X., Wang, J., Yu, G., Sun, X. 2010. The use of stable isotopes to partition evapotranspiration fluxes into evaporation and transpiration. *Acta Ecologica Sinica,* **Volume 30**: 201-209.

Zhang, Y., Shen, Y., Sun, H., Gates, J.B., 2011. Evapotranspiraiton and its partitioning in an irrigated winter wheat field: A combined isotopic and micrometeorologic approach. *Journal of Hydrology,* **Volume 408**: 203-2011.

CHAPTER 3: IDENTIFICATION OF GEOGRAPHICAL INFLUENCES AND FLOW REGIME CHARACTERISTICS USING REGIONAL WATER ISOTOPE SURVEYS IN THE LOWER NELSON RIVER, CANADA

Aaron Smith[1], Carly Delavau[1], and Tricia Stadnyk[1]

[1]Department of Civil Engineering, University of Manitoba, Winnipeg, Manitoba

Published in 2015 in the Canadian Water Resources Journal (DOI: 10.1080/07011784.2014.985512). Submitted November 2013, accepted August 2014.

This chapter examines the isotopic regime of the Lower Nelson River Basin through statistical analysis of spatial and temporal trends of main stem and tributaries. Riverine isotopic data are highly useful for the identification of primary sources of water. The linear regression of riverine deuterium and oxygen-18 compositions additionally provides qualitative evidence of evaporative effects within watershed storages.

CHAPTER 3

3.1 ABSTRACT

Results are reported from a 3-year monitoring initiative (2010–2013) of stable water isotopes ($\delta^{18}O$ and $\delta^{2}H$) at over 50 hydrometric sites in the lower portion of the Nelson River Basin, a key freshwater–marine corridor in Canada with global significance. Data are collected from annual synoptic surveys and a time-series monitoring program. Water isotope signals exhibit significant long-term average (with reported standard deviation) differences between the upper Nelson River (–10.5‰ $\delta^{18}O \pm 0.18$‰) and Burntwood River (i.e. Churchill Basin; –12.8‰ $\delta^{18}O \pm 0.4$‰) regions which are attributed to the geographic extent and origin of the water. Upper Nelson River flow-isotope signals suggest a more temperate climate, and exhibit reverse seasonal cycling (i.e. ice-on isotope enrichment; ice-off isotope depletion) due to the connectivity with and influence of Lake Winnipeg. In contrast, the Burntwood River behaves like a snowmelt-dominated river heavily influenced by wetland storage and enrichment during ice-off periods, exhibiting isotopic signals negatively correlated with headwater river discharge. Flow-weighted $\delta^{18}O$ and $\delta^{2}H$ show decreased variability in both regions at extreme low- and high-flow regimes, indicating a tendency towards a single dominant end member: wetland release (low-flow regime) or snowmelt/rainfall (high-flow regime). Mid- to normal-flow regimes exhibit increased isotopic variability, as do small headwater catchments resulting from varied source water contributions, residence times, mixing patterns and the role of landscape-specific features. The Stable Water Isotope Monitoring Network (SWIMN) presented enables the closure of water-isotope mass balance modelling that will facilitate the understanding of changes to freshwater–marine linkages.

3.2 INTRODUCTION

Recent studies by the Canadian National Hydrometric Network (CNHN) determined that only 12% of Canadian watersheds meet the minimum gauge density recommended by the World Meteorological Organization (WMO), while the remainder of the country is considered either poorly gauged or ungauged (Mishra and Coulibaly 2010; Coulibaly et al. 2013). Due to difficulties in establishing and maintaining an adequate hydrometric network in Canada, there is a need for additional "soft" data sources (e.g. stable water isotopes and water chemistry data) to facilitate water-mass balance modelling to understand changes in flow regime using minimal gauging or sampling. Stable isotope tracers provide a method for labelling and disaggregating total flow contributions at both local and regional scales, provided isotopic compositions of water sources are well defined and quantified. The operational value of tracers used in conjunction with hydrometric networks has resulted in a global initiative by the International Atomic Energy Agency (IAEA) to develop a Global Network for Isotopes in Rivers (GNIR), and other regional initiatives in Canada and the United States (Coplen and Kendall 2000). To accomplish this, more regional Canadian networks, particularly with global water cycle linkage through the Arctic, are required to advance global mapping of isotopic variability, interpolation methods and isotope mass balance modelling efforts (Gibson et al. 2010).

The heavy water isotopes of hydrogen and oxygen (^{2}H and ^{18}O) are ideal tracers for "soft" data applications as they exhibit well-understood and systematic changes due to isotopic fractionation during phase changes and diffusion (Posey and Smith 1957; Craig 1961; Dansgaard 1964; Craig and Gordon 1965). The use of such complementary data (Fenicia et al. 2008) to better understand the variability and complexity of hydrological processes has been extensively explored, primarily through smaller-scale, short-duration studies (reviewed by Kendall and

McDonnell 1998). These studies have utilized isotopic tracers to facilitate a more comprehensive understanding of water source and residence time, surface-groundwater exchanges, precipitation variability, snowmelt, and evaporation-transpiration processes in both scientific and operational contexts. Emerging across larger spatial scales and time periods, the integration of water isotopes in hydrological modelling has been shown to constrain parameters driving changes in runoff, reducing uncertainty in model predictions (Kuczera 1983; Beven and Binley 1992; Kuczera and Mroczkowski 1998; Siebert and McDonnell 2002; Kirchner 2003, 2006; Dunn et al. 2008; Fenicia et al. 2008).

The focus of integrated hydrometric-isotope programs has increased over the last decade to include macro-scale (> 10,000 km^2) basin analysis. In 2002, the IAEA initiated a Coordinated Research Project (IAEA-CRP) entitled "Design criteria for a network to monitor isotope compositions of runoff in large rivers," or GNIR, as described in Gibson et al. (2002) and Vitvar et al. (2007). Macro-scale projects have been established in Canada, within the Canadian Arctic (Cooper et al. 2008; McClelland et al. 2008; Yi et al. 2012) and the Canadian tundra (Yi et al. 2010). Results from the aforementioned studies demonstrate the utility of the large-scale isotope monitoring networks in Canada for enhancing the understanding of water cycling in remote regions at both regional and continental scales.

Based on the success of previous isotope networks in Canada, the need to improve network coverage across Canada and the inadequacy of hydrometric data in the northern and central regions of Canada, a Stable Water Isotope Monitoring Network (SWIMN) within the lower Nelson River Basin (LNRB) was launched to establish a record of isotope data to supplement existing hydrometric data for hydrologic assessment and modelling purposes. Understanding hydrologic change and variability within the LNRB is essential to the operation of six generating

stations (GS) within the basin, totalling 75% of the generating capacity of Manitoba Hydro (MH, a major Canadian hydroelectric utility). The addition of naturally occurring tracers into an existing operational hydrometric program (operated by MH) provides a viable low-cost integration option for improved understanding and efficient water management within a remote, large-scale basin.

This study examines the large-scale application to two major river regimes in a northern Canadian basin using a coupled hydrometric and water isotope approach. The objectives of this study are to investigate: (1) geographic influence and variability in water isotope signals within LNRB rivers, (2) temporal and flux-weighted evolution of source water contributions to streamflow, and (3) mixing characteristics occurring within and between river reaches along the Nelson River en route to Hudson Bay, contributing to initiatives within Canada to enhance regional water isotope data in tandem with hydrometric measurements. Data collected will assist water regulators in the LNRB in understanding regional and inter-annual variability, and will provide a comprehensive data set for hydrologic modelling purposes.

3.3 BACKGROUND

3.3.1 STUDY REGION

Fresh water from the Saskatchewan River to the west, the Red River to the south and the Winnipeg River system to the east culminates in Lake Winnipeg before it flows north along the Nelson River and drains into Hudson Bay, forming the boundary of the Nelson River basin (Figure 3-1a). The LNRB (90,580 km^2) is the downstream segment of the Nelson River basin fed by Lake Winnipeg (minimum and maximum discharges from 2010 to 2013 were 1350 to 5615 m^3/s, respectively) and discharging to Hudson Bay (Figure 3-1b), receiving a majority of the outflow from the drainage area upstream of the Nelson River (970,000 km^2). On the

northwestern watershed boundary, MH operates the Churchill River Diversion (CRD). Starting in 1977, a portion of the Churchill River Basin (CRB) (license maximum of 850 m^3/s) is diverted into the LNRB, regulated at Notigi Lake by the Notigi Control Structure (NCS) on the Rat River, before joining the Burntwood River and entering the Nelson River further downstream at Split Lake (Figure 3-1).

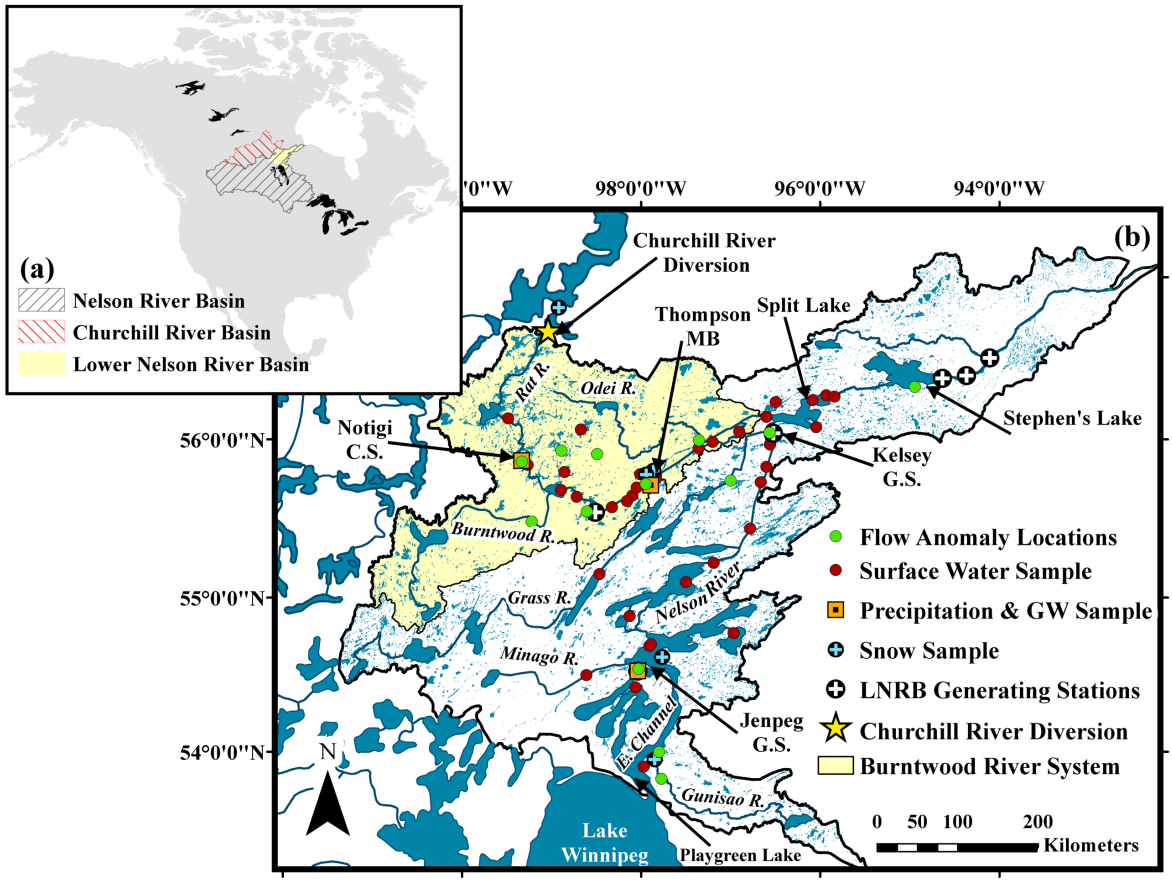

Figure 3-1. (a) The Nelson River Basin (NRB), Churchill River Basin (CRB) and Lower Nelson River Basin (LNRB) with respect to North America. Watershed boundaries of the NRB, the LNRB and the portion of the CRB from which flow is diverted into the LNRB. (b) The established Stable Water Isotope Monitoring Network (SWIMN) in the LNRB. Locations of the isotope collection sites for the various sources of water are denoted by the indicated symbols. The drainage areas of the major river systems within the LNRB are delineated as marked. Important lakes and rivers are indicated along the main stem of the river or detailed with an arrow. Major rivers and lakes and administrative boundaries are also indicated. Generating stations (GS) are denoted by a circle with a cross in the centre, and the Notigi Control Structure is represented by a star symbol. The Churchill River diversion is indicated with a yellow star and an arrow. GW: groundwater.

3.3.2 BASIN PHYSIOGRAPHY

Situated in the boreal forest, Canadian Shield region of Canada, the LNRB has extremely low relief, with approximately 330 m of topographical relief in the main direction of drainage (south to north). Due to this low gradient, large regions of surface water in the form of small lakes and wetlands are interspersed about the basin in addition to many sections of channelized lakes along the main stems of the Rat and Nelson Rivers (Figure 3-1b). Satellite land cover imagery of the basin obtained through GeoBase® (http://www.geobase.ca) indicates that land cover within the LNRB is predominantly coniferous forest of varying densities (34%), followed by a combination of fens and bogs (i.e. connected and disconnected wetlands, respectively; 25%). Shrubland and open water are also prevalent, comprising 16% and 13% of the basin, respectively. The LNRB is located within a sporadic discontinuous permafrost region (10–50% permafrost), predominantly poorly draining fine-grained lacustrine clays, with the most downstream portion of the basin situated in extensive discontinuous permafrost (50–90% permafrost).

3.3.3 CLIMATE AND WATER REGIME

The LNRB has a continental sub-arctic cool climate as it is located in the subhumid mid-to-high Boreal Ecoclimatic Region of Canada (Ecoregions Working Group 1989). Climate normals (1981–2010) from two Class "A" Environment Canada meteorological stations (i.e. stations adhering to WMO standards) within the LNRB are summarized in Table 3-1 (locations indicated on Figure 3-1). Summers are typically cool and approximately 5 months long with moderate amounts of rainfall (300– 500 mm). Winters are very cold, experiencing average daily temperatures below –20°C and –15°C between December and February at Thompson and Cross Lake Jenpeg, respectively.

Table 3-1. Weather data obtained from the Thompson (Manitoba) Airport station and Jenpeg Generating Station at Cross Lake. Totals and averages are shown for both the study period (January 2010 to October 2013) and climate normals (1981–2010).

Thompson Airport (Climate ID: 5062922)					
Parameter	**2010**	**2011**	**2012**	**2013**	**Climate normal**
Mean daily temperature (°C)	–0.2	-2.0	-1.9	0.1	-2.85
Annual total precipitation (mm)	624.0	551.3	550.8	340.1	509.15
Annual snowfall (cm)	171.8	110.5	196.1	51.9	186.97
Annual rainfall (mm)	484.9	465.0	399.5	301.2	340.18
Average annual relative humidity (1500 LST, %)	59.9	59.0	61.3	67.0	57.85
Cross Lake Jenpeg (Climate ID; 5060623)					
Parameter	**2010**	**2011**	**2012**	**2013**	**Climate normal**
Mean daily temperature (°C)	1.5	0.0	0.3	1.4	-0.43
Annual total precipitation (mm)	505.4	565.2	438.6	315.5	469.44
Annual snowfall (cm)	96.6	84.2	153.3	75.2	119.51
Annual rainfall (mm)	408.8	481.0	285.3	240.3	349.92

During the study period, temperatures were warmest in 2010, while 2011 and 2012 showed similar yet slightly (i.e. 2°) cooler temperatures (Table 3-1). These warmer-than-average winters resulted in less snowfall accumulation (and therefore snowmelt) due to shortened winter periods. The wettest winter during the study period was 2011–2012 with a total snowfall of 182 cm at Thompson and 130 cm at Jenpeg; the driest was 2010–2011 where total snowfall only reached 130 cm at Thompson and 62 cm at Jenpeg. The 2010 and 2011 summers were wet (~135% of normal precipitation) and resulted in high soil moisture content prior to winter freeze-up.

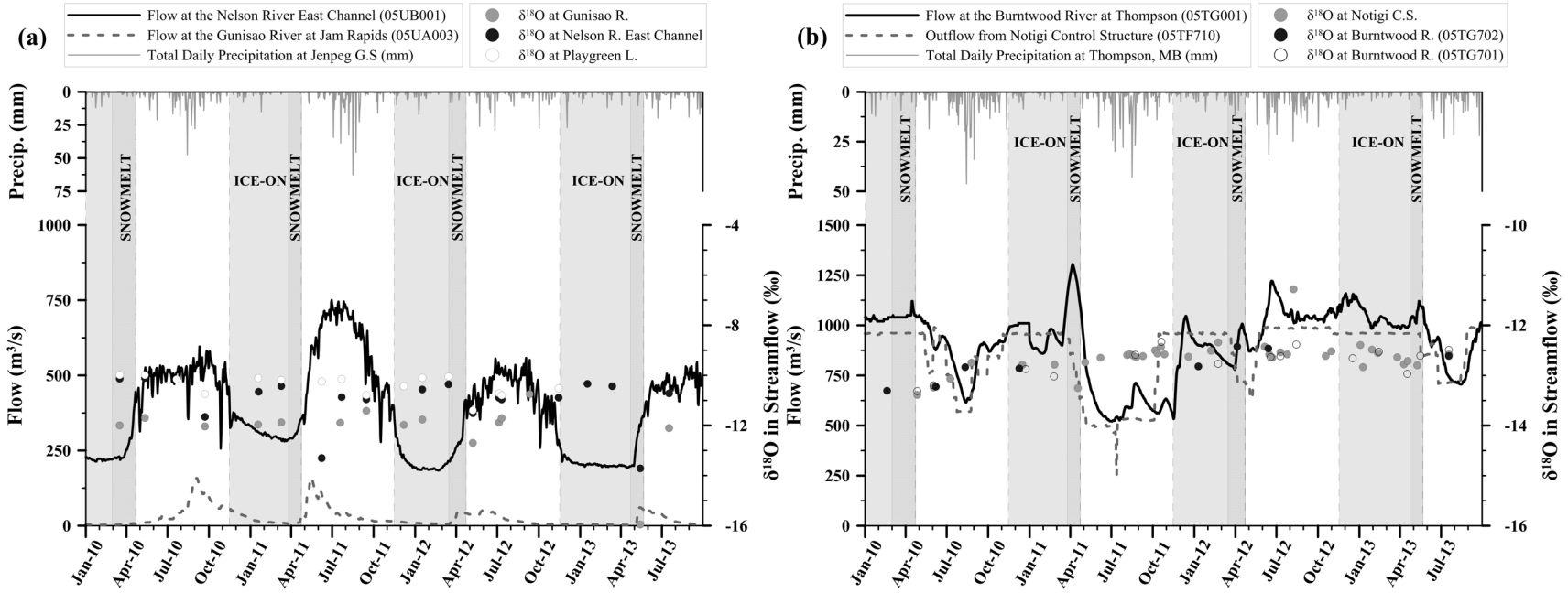

Figure 3-2. Total daily precipitation amount from the nearest collection site, daily average streamflow and isotopic composition of oxygen-18 ($\delta^{18}O$) for three locations along each of the Nelson and Burntwood Rivers over the study period. Ice-on periods and snow-melt periods are gray shaded and hatched areas, respectively. Note the different scales for the Nelson and Burntwood River isotopic compositions. G.S., Generating Station; C.S., Control Structure.

The majority of streamflow in the lower Burntwood and upper Nelson Rivers comes from the CRD and Lake Winnipeg Regulation (LWR) operations, respectively, which govern the Nelson River main stem flow regime. Beginning in May 2011 and throughout the summer of 2011, Jenpeg GS was operated at maximum capacity due to provincial regulation of high water levels on Lake Winnipeg. CRD operations in 2011 showed the opposite trend due to MH significantly decreasing releases through the NCS to mitigate further flooding within the lower Nelson system. The 2012 melt was more gradual than 2011, due to earlier warming and a series of melt and refreeze events throughout March and April that gradually reduced the snowpack. The gauged headwater basins within the LNRB showed varying streamflow response for both timing and magnitude of the 2011 and 2012 spring freshets. In 2013, cooler conditions delayed the start of the melt period by almost 1 month from observations in 2010–2012, and resulted in both a rapid response time for the melt and a reduction in peak runoff. These flow regimes from January 2010 to October 2013 of both the Nelson River near the outlet of Lake Winnipeg and the Burntwood River are displayed in Figure 3-2.

Discharges at NCS are measured from the outlet of the control structure. From Figure 3-2, significant correlations between changes in flow and isotopic signature are present and consistent for each location and year of study, indicating isotopic variability is not overly damped or missed by low-resolution temporal sampling.

3.4 METHODS

3.4.1 STABLE WATER ISOTOPE MONITORING NETWORK (SWIMN)

The SWIMN was established at hydrometric gauge locations throughout the LNRB beginning in March 2010. Currently, there are over 50 sites where surface waters from rivers and lakes are sampled, four sites collecting composite isotopes in precipitation, three drive-point piezometers collecting shallow groundwater samples (1.0–1.3m depth) and one Class "A" evaporation pan sampling isotope-enriched surface water (δ*; locations indicated on Figure 3-1). After each precipitation sample is taken, the bucket is emptied and new oil is added to prevent evaporation from occurring. Due to the remoteness of the basin and penetration of frost, winter sampling of piezometers, precipitation buckets and the evaporation pan is not possible. Composite snow samples are collected at five locations within the basin. Starting in 2011, as part of an IAEA-CRP initiative (IAEA 2012), depth-dependent snow sampling was incorporated into the program as a means to evaluate best practices for isotope-based snow and snowmelt sampling. Early results indicate that composite snow samples are generally representative of snowmelt compositions in the LNRB (Penna et al. 2014).

3.4.2 SAMPLING DISTRIBUTION

In addition to sampling during routine hydrometric visits, annual basin-wide synoptic surveys are conducted each summer to provide a snapshot of the isotopic and hydrologic state of the entire LNRB within a 2-day period following the spring freshet (i.e. June or July). Similar to other large-scale river isotope networks, each surface water site is sampled bimonthly on average (6–7 times per year). Precipitation stations (located near cities or at generating stations) are generally sampled at the same frequency as surface water for consistency.

3.4.3 SAMPLING METHODS

Site locations were selected based on existing hydrometric maintenance schedules and routes. Field technicians fill two 30 mL water samples in high-density polyethylene Nalgene® bottles at each site from a filled 500-mL sampling bottle attached to an extendable pole that enables sampling from the section of the river experiencing turbulent flow. During ice-on, river and lake samples are collected by auguring through the ice and filling 30 mL sample bottles via a plastic bailer. Grab samples from the near-surface of rivers are considered representative of the isotopic composition of the entire water column so long as flow is turbulent and not within near-shore stagnation zones (Raymond et al. 2007). Samples are analyzed by the University of Victoria Environmental Isotope Laboratory managed by Alberta Innovates Technology Futures (AITF) for ^{2}H and ^{18}O. Isotope compositions are analyzed using a Delta V Advantage stable isotope mass spectrometer, using a GasBench II peripheral for $\delta^{18}O$, and an HDevice peripheral for $\delta^{2}H$ (Nelson 2000). Standardization is accomplished by analyzing in-house internal standards with Vienna Standard Mean Ocean Water (VSMOW2) allowing results to be reported relative to VSMOW as delta (δ) values of per mil (‰). Results are reproducible to ± 0.2‰ and ± 1‰ for $\delta^{18}O$ and $\delta^{2}H$, respectively. Additional use was made of the relationship between $\delta^{18}O$ and $\delta^{2}H$ through the determination of deuterium excess (d-excess) using Equation 3-1 (Craig 1961):

$$\boldsymbol{d - excess = \delta^{2}H - 8 \cdot \delta^{18}O} \qquad 3\text{-}1$$

D-excess represents the deviation of isotopic compositions from the global meteoric water line (GMWL), which has a d-excess of 10‰ and corresponds to global patterns of evaporation and condensation of oceanic origin water vapour. Deviations of d-excess from the GMWL are the result of other evaporative conditions influenced by relative humidity, re-evaporation from

wetlands, repeated evaporation and condensation over large landscape scales, lake surfaces, and other processes that can imprint d-excess values consistent with the identification of geographical influences (i.e. land cover and topography), moisture source identification and riverine mixing.

3.4.4 ANALYSIS METHODS

Annual synoptic survey data are used to derive contours of isotopic composition at the time of sampling (Figure 3-4). Similar to other large-scale isotope studies (e.g. Kendall and Coplen 2001), interpolation and extrapolation are used to describe isotopic variation throughout the entire basin. Interpolations represent modelled estimates of isotopic signals in rivers or lakes where samples are not collected. Spline interpolation with barriers (i.e. basin boundaries) is used to contour $\delta^{18}O$ in streamflow signals. From 2011 to 2013, the number of locations sampled during the synoptic survey increased from 24 to 54 locations to improve spatial distribution throughout the basin. Sampling density is dependent on weather conditions (i.e. wind speed and direction) during the survey, with the maximum sampling coverage at the outlet of Lake Winnipeg downstream to Stephens Lake, and from the Rat River inflow at Southern Indian Lake downstream of the junction of the Burntwood and Nelson Rivers (Figure 3-4).

Averaged surface water samples are used with ordinary least squares (OLS) linear regression for rivers within the LNRB on a plot of $\delta^{18}O$ versus $\delta^{2}H$ (Figure 3-3b). Regression lines are derived from mixed surface waters, and will hereafter be referred to as mixing lines. The extent of each mixing line is set by the maximum and minimum weighted value sampled within that reach. The Nelson River is divided into two distinct reaches: Nelson River upstream of Kelsey GS and Nelson River downstream of Kelsey GS. The Burntwood and Grass Rivers join the Nelson downstream of the Kelsey GS spillway where significant mixing of riverine

systems occurs.

3.5 RESULTS

3.5.1 ISOTOPIC SOURCE IDENTIFICATION

The isotopic framework developed from data collected over the study period is shown in Figure 3-3. Various water sources are denoted by symbols indicating snow, rainfall, groundwater, isotope-enriched waters from the evaporation pan and surface waters (river and lake samples). The number of samples collected from each source, the average ($\bar{X}$), standard deviation (S) and range (min, max) of $\delta^{18}O$ and d-excess are provided in Table 3-2.

Discharge/level measurement locations are not available for all isotope-sampling locations, so it is not possible to flux-weight all samples. To verify the effect of flux-weighting, isotope-discharge locations are flux-weighted and analyzable against the geometric mean of location composition ($\delta^{2}H$, $\delta^{18}O$ and d-excess) with no significant differences among methods found. The regression of evaporation pan samples was described by the following equation:

$$\boldsymbol{\delta^{2}H = 4.2 \cdot \delta^{18}O - 52.1} \qquad 3\text{-}2$$

A slope of 4.2 suggests high amounts of seasonal evaporation and is comparable with the observed local evaporation line (LEL) slopes from lakes and shallow wetlands sampled at similar latitudes across Canada (Gibson et al. 2005).

Table 3-2. Statistical summary of $\delta^{18}O$ and deuterium excess (d-excess) for water sources sampled from March 2010–July 2013 from the SWIMN program. Isotopic averages are not flux- or amount-weighted. The sample mean and standard deviation are represented by the $\overline{X}$ and S symbols, respectively.

Water source	$\delta^{18}O$ (‰)					D-excess (‰)	
	n	$\overline{X}$	S	Minimum	Maximum	$\overline{X}$	S
Snow	110	-25.29	3.03	-33.32	-10.52	10.2	3.5
Rain	56	-13.32	2.78	-21.29	-8.40	4.4	6.0
Groundwater	50	-15.34	2.17	-21.25	-8.33	6.2	2.2
Surface waters:							
Evap. Pan	24	-4.98	2.55	-11.92	0.36	-33.5	10.3
Burntwood	269	-12.74	0.41	-14.84	-11.54	-7.8	1.8
Nelson	344	-10.64	0.52	-13.73	-9.79	-2.3	1.4
Headwater	205	-12.85	1.48	-17.60	-9.65	-2.5	3.9

Precipitation samples show substantial variability in isotopic composition, which is typical of mid- to high-latitude regions in Canada (Dansgaard 1964; Araguas-Araguas et al. 2000; Yi et al. 2012) (Figure 3-2a, Table 3-2). OLS linear regression of rain and snowpack compositions indicated that the unweighted local meteoric water line (LMWL) for the LNRB is described by the following equation (Figure 3-3):

$$\boldsymbol{\delta^2 H = 7.47 \cdot \delta^{18} O \; - \; 3.0} \qquad 3\text{-}3$$

Since δ^2H and $\delta^{18}O$ of snowfall are not sampled, weighting by precipitation volume (i.e. the LMWL) would inaccurately skew the composition towards isotope enriched summer rainfall. The LNRB isotopes in precipitation data are consistent, however, with long-term records from the Canadian Network for Isotopes in Precipitation (CNIP; Birks et al. 2004; Delavau et al. 2011) at Churchill, ($\delta^2H = 7.5 \cdot \delta^{18}O - 0.5$) and the Pas ($\delta^2H = 7.6 \cdot \delta^{18}O + 0.62$), and the LMWL for Canada ($\delta^2H = 7.8 \cdot \delta^{18}O + 5.2$; derived from amount-weighted monthly precipitation; Gibson et al. 2005).

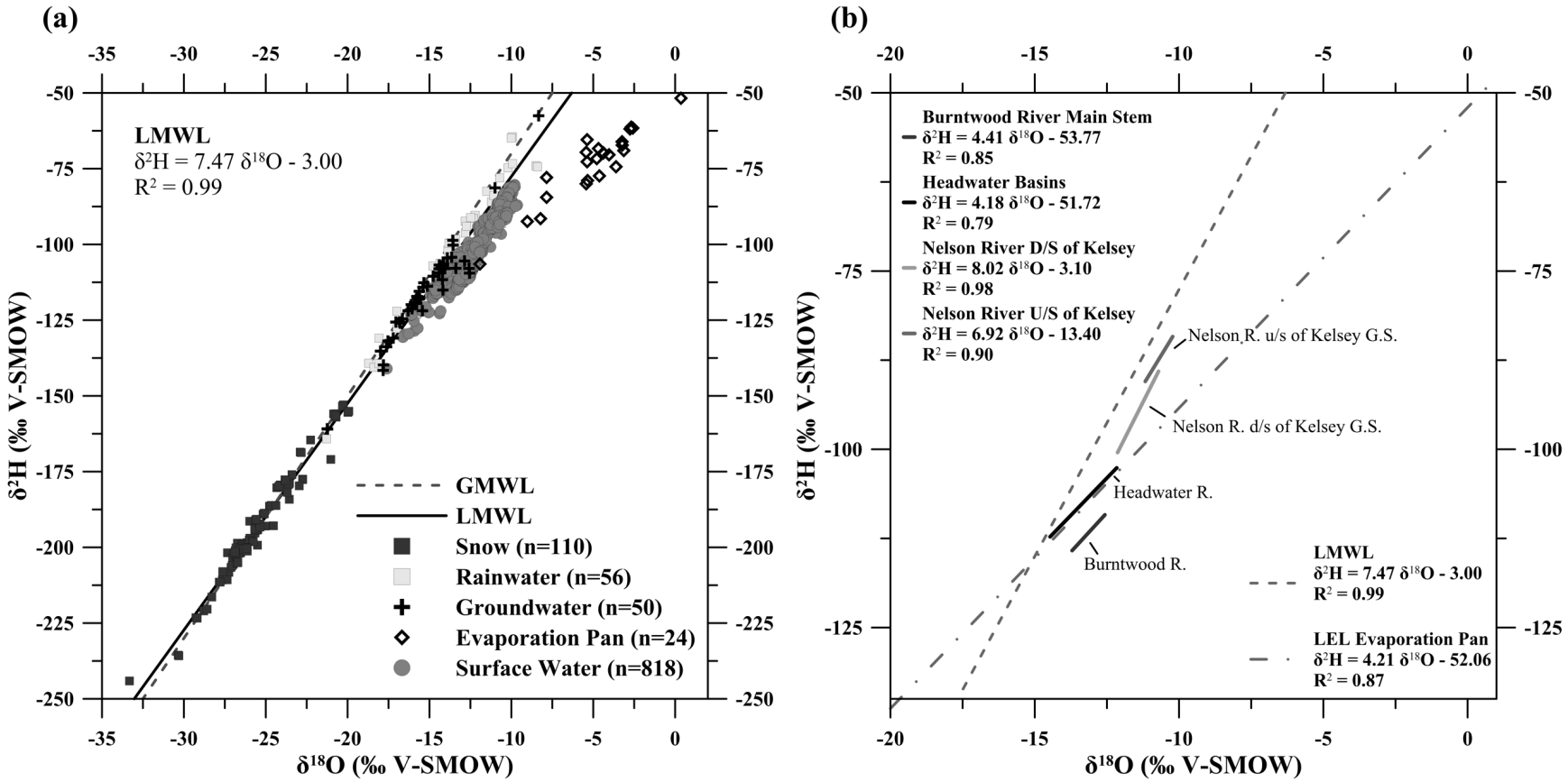

Figure 3-3. (a) The global isotope framework for the Lower Nelson River Basin (LNRB) with water sample categories represented by symbols. The number of measurements for each water source (n) is indicated in brackets to the right of the symbol and source water description on the isotope framework. (b) Regression slopes of averaged surface waters within the isotope framework, separated into four different water sources: Nelson River upstream of Kelsey Generating Station (GS), Nelson River downstream of Kelsey GS, Rat/ Burntwood River main stem, and headwater basins. Regression lines and equations for the evaporation pan local evaporation line (LEL), and the LNRB Local Meteoric Water Line (LMWL) are displayed. The average isotopic composition of Stephens Lake is also indicated on the figure. GMWL, global meteoric water line; V-SMOW, Vienna Standard Mean Ocean Water.

Shallow groundwaters sampled at Thompson are consistent with the LMWL ($\delta^2H = 7.56 \cdot \delta^{18}O + 1.15$, $R^2 = 0.98$), while samples from Jenpeg and Notigi show more variability, with some samples plotting below the LMWL. This pattern is attributed to the shallow sampling depth at Jenpeg (1.0 m piezometer depth, and assuming that if ponding surrounding the piezometer occurs during wet conditions, the pond waters are sampled) and possible evaporation of shallow soil moisture and/or ponded waters. Notigi similarly shows heavy, isotopically enriched piezometer signals with a similar sampling technique to Jenpeg where the piezometer occasionally floods, potentially causing standing water infiltration and evaporation. Additional variability is seen at the beginning of the year where groundwater samples typically deviate from the LMWL to the GMWL, showing a strong relationship with the measured snowpack composition (i.e. snowmelt signature), as opposed to mid-summer (average values) that appear to be a mixture of summer precipitation and snowmelt.

3.5.2 ISOTOPIC DISTRIBUTION FROM SYNOPTIC SAMPLING

Three synoptic surveys (2011, 2012 and 2013) were conducted within the LNRB to complement ongoing time-series sampling and to provide a regional perspective of the spatial distribution in isotopic compositions across the basin. Synoptic surveys were performed at approximately the same time each year (post-freshet) for interannual comparison of river and headwater basin δ^2H and $\delta^{18}O$. In 2011, the survey was conducted at the beginning of June, versus 2012 and 2013 when it was completed in mid-July due to later spring melts.

Sampling earlier in the year shows a greater influence (i.e. homogenized isotopic signature) of heavy isotope-depleted snowmelt contributions from the melting snow pack (Figure 3-4a), particularly in headwater basins with lower runoff volumes. Prior to the synoptic survey in 2011, cumulative precipitation within the basin was lower than normal (based on 1981–2010

records) in June, resulting in conditions that were not significantly influenced by rainfall events. An increased sampling density and later survey date in 2012 show spatial trends in streamflow $\delta^{18}O$ values emerging for each river and sub-basin system relative to 2011. Samples from upstream, lake-dominated portions of the Nelson system show the same isotopic range as the channelized section of the Nelson River near Thompson ($\delta^{18}O$ values of –10 to –11‰), validating the homogeneity in interpolated contours in the 2011 survey. Increased station density in 2012 and 2013 surveys capture progressive downstream isotope enrichment occurring along the Grass River ($\delta^{18}O$ values ranging from –12 to –13‰ up to –11 to –12‰ in 2012 and 2013, respectively), suggesting an increasing influence of evaporation along the flow path from the numerous wetlands in this part of the basin. Interpolated $\delta^{18}O$ compositions are generally consistent from year to year, with noticeable differences only in the headwater basin composition. Headwater lakes on the east side of the Nelson River show increased isotope enrichment in 2013 over previous years' surveys, and a larger extent of isotope-enriched surface waters ($\delta^{18}O$ values of –10 to –11‰) within the Nelson River near Lake Winnipeg. Similar isotope distributions were observed in both the Grass River and the headwater rivers north of NCS, indicating persistence of the enrichment trend in both the upper Nelson and Burntwood systems. Some headwater locations in the Burntwood and upper Nelson basins show more depleted isotope compositions in 2013 relative to 2011 and 2012, indicating that timing and retention of snowmelt is highly variable from year to year and persistent for at least 1 month post-freshet. This indicates relatively long residence times and a likelihood for high storage capacities along the headwater basin flow paths. It is important to note that $\delta^{18}O$ contours in some headwater basins (notably Minago and Gunisao, Figure 1) are the result of extrapolating the isotopic composition of surface waters that are significantly depleted upstream of sampling

locations. Although the heavy-isotope depletion is expected in upstream reaches of headwater basins, the increasing magnitude of the depletion cannot be substantiated by the sampling network and is an artefact of the interpolation model. Discontinuities at basin boundaries were anticipated utilizing spline interpolation model with boundaries, and are representative of different basin waters.

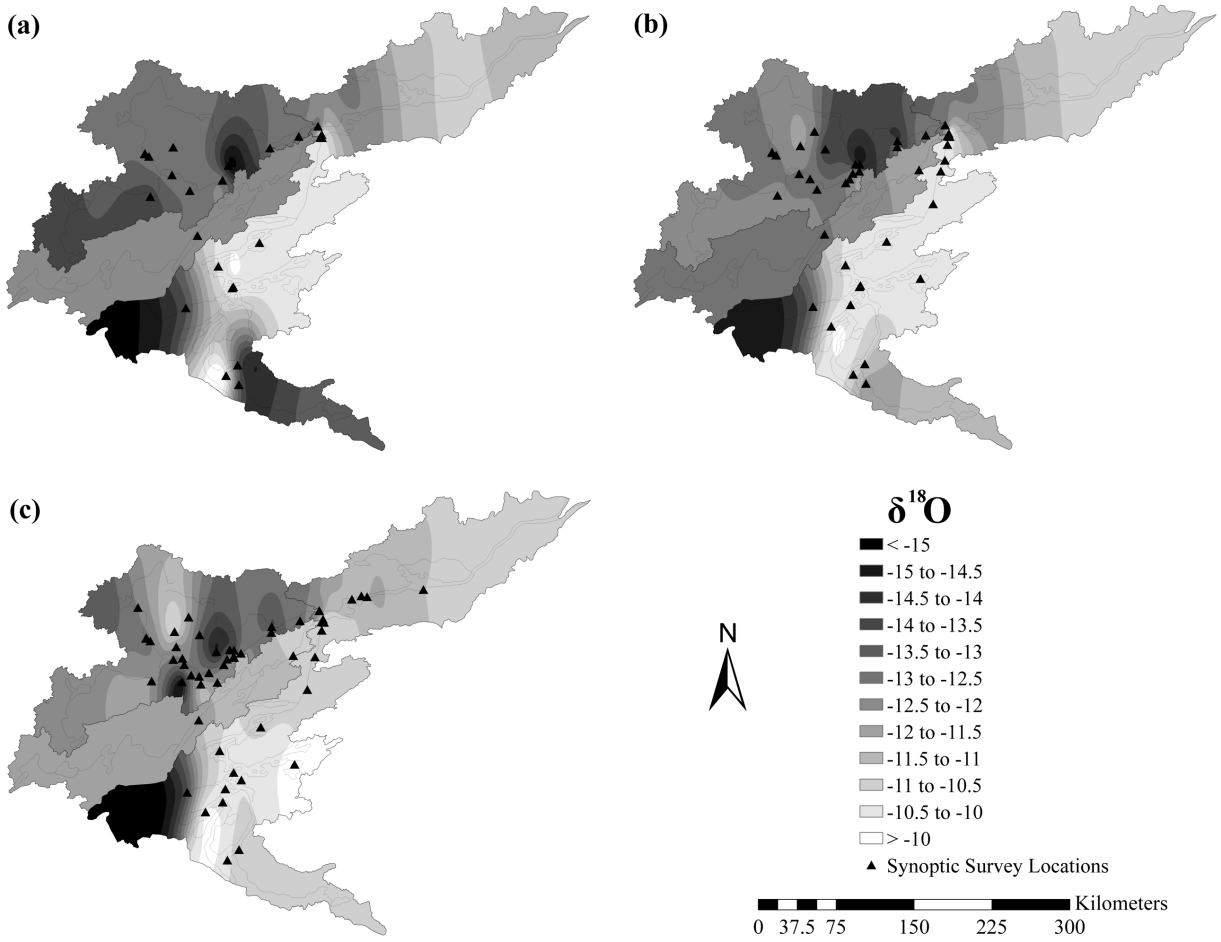

Figure 3-4. Streamflow $\delta^{18}O$ contours derived from synoptic surveys of the lower Nelson River basin (LNRB) with measurements at: (a) 24 locations between 7–8 June 2011; (b) 40 locations between 10–11 July 2012; (c) 54 locations between 17–18 July 2013.

A distinction between headwater tributary and main stem composition is evident in Figure 3-2a and Figures 3-4a and 3-4b, showing the Gunisao tributary as consistently more depleted

relative to the main stem upper Nelson at Playgreen Lake and East Channel (except during the high stage, where backwater effects and downstream-to-upstream mixing occur). Similarly, the Burntwood main stem (Figure 3-2b) shows seasonal ice-on depletion, likely attributed to increased groundwater and baseflow contributions over winter, which is typical of high-latitude isotopic response during ice-on conditions (St. Amour et al. 2005; Yi et al. 2012). In contrast, the upper Nelson (Figure 3-2a) exhibits a seasonal pattern of oxygen-18 enrichment with decreasing ice-on low flow due to the connectivity with late fall evaporatively enriched, under-ice Lake Winnipeg inflows to the upper Nelson system. Similarly, from Figure 3-4, regions of open surface water (upper Nelson River near Lake Winnipeg) show an increase in the evaporation/inflow (E/I) ratio (Gibson 2002) that results in increased heavy-isotope enrichment over time during drier conditions, prevalent in 2013 (Figure 3-2a). The net effect is greater distinction in 2013 between heavy isotope-depleted headwater basins and heavy isotope-enriched main stem rivers relative to the 2011 and 2012 surveys.

3.5.3 ISOTOPIC EVOLUTION WITH FLOW REGIMES

Interannual variability in the LNRB is linked to specific processes, which characteristically occur in different flow regimes. Individual isotopic water samples are limited to a single, low-resolution temporal record but flow data can assist in using isotopic variability to diagnose hydrologic end members and end-member mixing. In Figure 3-5, $\delta^{18}O$ values of surface water compositions from the 13 sites with gauging stations (Figure 3-1) are compared to instantaneous discharge, reported as a discharge anomaly, ΔQ:

$$\boldsymbol{\Delta Q} = \frac{\boldsymbol{Q_i} - \overline{\boldsymbol{Q}}}{\boldsymbol{S}} \qquad 3\text{-}4$$

where Q_i is the instantaneous average daily streamflow on the day the isotope sample was collected and $\bar{Q}$ and S are the average daily streamflow and standard deviation of streamflow

over the period of record. Because the method normalizes data, it allows for direct comparison among sampling locations regardless of flow magnitude. Flow anomalies are grouped into three flow regimes, similar to what was done in an analysis conducted by Yi et al. (2010): $\Delta Q \leq -0.5$ is considered low flow, $-0.5 < \Delta Q < 2.0$ is normal to high flow and $\Delta Q \geq 2.0$ is extremely high flow. The collection sites are grouped into four water sources for interpretation based on geographic differences noted from the synoptic survey data: Nelson River East Channel, Nelson River main stem, Burntwood River main stem, and headwater basins. Averages and standard deviations for each source and flow condition are indicated by a black dashed line and a shaded gray region, respectively. Note that similar trends in the variability of δ^2H are observed, although only trends in $\delta^{18}O$ are presented here (Figure 3-5). Isotopic-flow anomalies show lower (or lowest) variability of oxygen-18 during low-flow regimes ($\Delta Q \leq -0.5$) across all basins, and higher variability during normal- to high-flow regimes ($-0.5 < \Delta Q < 2.0$) and extremely high-flow regimes ($\Delta Q \geq 2.0$) in headwater basins. The greatest isotopic variability (both ^{18}O and ^{2}H) occurs in headwater basins and is attributed to differences in basin response time, mixing characteristics and significantly lower runoff volumes which reduce dilution (or averaging) effects observed in main stem rivers. Low-flow regimes tend toward more positive (heavy isotope-enriched) compositions with lower d-excess than baseflow or shallow groundwater discharge (Figure 3-3a), whereas normal- to high-flow regimes tend toward slightly less heavy isotope-enriched compositions.

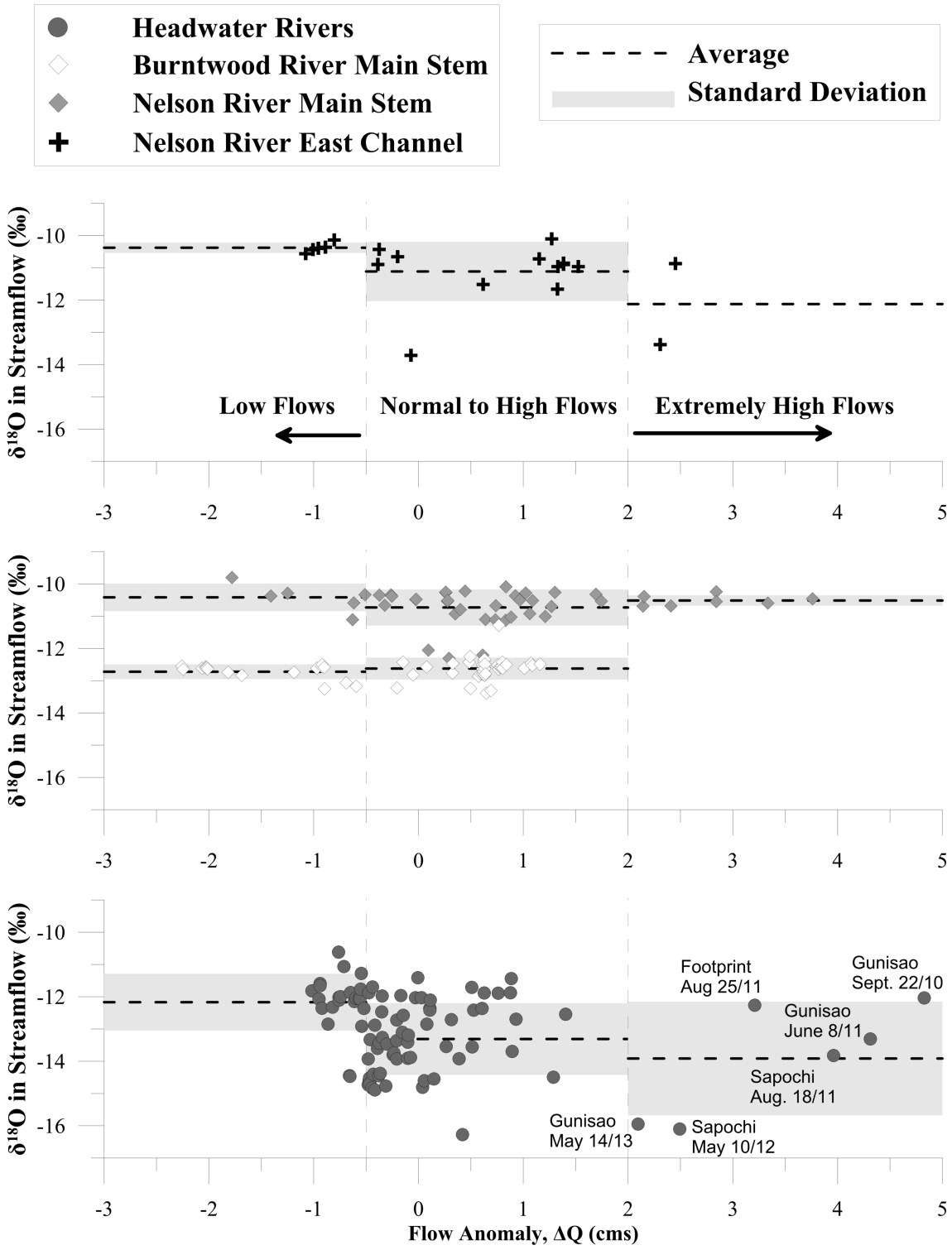

Figure 3-5. Flow anomaly (ΔQ) versus $\delta^{18}O$ composition of streamflow for four surface water sources: Nelson River East and main channels, headwater tributaries and the Burntwood River main stem. Averages and standard deviations for each water source and flow condition are as indicated. Extreme events or significant deviations from the average are detailed on the figure.

Similar to low-flow events (dominated by pre-freshet), extremely high-flow events along the Nelson main stem exhibit lower isotopic variability but are dominated by measurements collected from the spring freshet. However, unlike the low-flow events (–10.4 ± 0.4‰ for $\delta^{18}O$ and –2.0 ± 0.8‰ for d-excess), isotopic composition observed during extremely high-flow regimes show increased variability of d-excess (not shown) while maintaining more consistent $\delta^{18}O$ compositions (–10.5 ± 0.2‰ for $\delta^{18}O$ and –1.8 ± 1.6‰ for d-excess), consistent with a mix of summer storm flow and freshet events. Headwater basins indicate significant variability in isotopic signal during extremely high-flow regimes, and a positive relationship between increasing flow anomaly and $\delta^{18}O$ values (Figure 3-5). This suggests that heavier rainfall events (i.e. as indicated by the date of the high-flow event) also correspond with heavier isotopic compositions, which would be consistent with isolated, convective storm events. During the time frame of this study, the Burntwood main stem was not subject to extremely high-flow conditions; therefore, the isotopic response and associated variability during this flow regime could not be evaluated.

At low- and normal-to-high flows ($\Delta Q \leq 2$), the Nelson River East Channel shows the least variability, followed by both the Burntwood main stem and Nelson main stem (moderated by Lake Winnipeg), and finally the headwater catchments with the largest variability. The standard deviation of the Burntwood main stem isotopic signal increases during normal-to-high flows, but the average composition remains consistent across all flow regimes (for $\delta^{18}O$, $\delta^{2}H$ and d-excess). In contrast, the Nelson main stem average isotopic composition of the low-flow regime is slightly more enriched in $\delta^{18}O$ relative to the normal-to-high flow regime (–10.4‰ vs. – 10.7‰ main stem; –10.4‰ vs. –11.1‰ East Channel). Unlike low- and extremely high-flow regimes, no discernable temporal period is correlated to this regime or the enrichment. Flow anomalies

suggest consistent temporal (seasonal) trends in isotopic variability, and the dominance of single end members at both low- and extremely high-flow regimes. Mid-to-normal flow regimes are expectedly more complex, indicating a myriad of processes and end-member contributions which isotope-mass balance modelling could help to discern.

3.6 DISCUSSION

Both major river systems of the LNRB receive water external from the basin (i.e. the CRB for the Burntwood system, and Lake Winnipeg for the upper Nelson), the drainage areas of which deviate in both size and latitude. Large-scale patterns of isotopes in precipitation result in increasing depletion with increasing latitudes relative to the tropics (Dansgaard 1964; Bowen 2010; Gibson et al. 2010). Therefore, it would be expected that CRB inflows would be more depleted relative to the upper Nelson River, which originates at much lower latitudes (i.e. as far south as the Red River basin, 45°N). The Burntwood River shows heavy-isotope depletion and higher d-excess relative to the Nelson River (Figure 3-3b), likely resulting from a more northerly drainage area (Figure 3-1). The significant and consistent differences in d-excess between the two main stem systems contributing to the LNRB can also be attributed to differences in the air mass source from which meteoric waters are originally derived (Pacific, Gulf of Mexico, or Arctic) (Birks and Edwards 2009).

In conjunction with geographical influence, the variability in flow anomaly and interannual analyses can elicit some understanding of primary source components (i.e. groundwater, snowmelt, surface runoff) contributing to the riverine systems. The Burntwood River basin is the least variable of any of the rivers with consistently low standardized flow. Despite high rainfall recorded within the basin from 2010 to 2012, the river has been neither significantly enriched nor depleted by such rainfall events, indicating an isotopically steady and dominant inflow source

from upstream (i.e. Churchill River basin inflows), as well as longer-term storage from lakes or wetlands. The Burntwood and Nelson Rivers have a high percentage of watershed wetland coverage (> 20% for both fens and bogs). Since wetlands attenuate water until they become saturated (or until no hydraulic gradient is present), delayed release of water in storage would naturally attenuate the contribution of any significant precipitation (or snowmelt) events prior to release into the river. Lower-than-average snowfall over the study period (Table 3-1) would act to increase wetland storage availability (Roulet and Woo 1986), thereby reducing the influence of direct runoff events. In contrast, the upper Nelson River exhibits more isotopic variability (Figure 3-5), but that is limited due to a direct connection with Lake Winnipeg. Enrichment occurs during the winter, and depletion during early- to mid-summer. Lake Winnipeg water is enriched in late summer and fall due to evaporation (i.e. decreasing in d-excess), which discharges to the upper Nelson system during early onset ice-on conditions (November–March). Large sections of open water during the summer (Figure 3-1) in the upper Nelson River provide increased enrichment downstream of Lake Winnipeg. The appreciable differences in isotopic compositions of the Burntwood and upper Nelson River systems provide traceable mixing characteristics downstream of Split Lake (Figure 3-1).

Operationally, riverine mixing is of interest to understand and separate distinct river contributions (i.e. upper Nelson River and Burntwood River) downstream of Kelsey GS for the purpose of understanding turbulence effects and variability in the long-term flow data. Mixing lines developed from stable isotopes are useful tools for diagnosing characteristics of the contributing systems (i.e. volume of contribution and distance required for complete mixing). In the LNRB, mixing of the Burntwood and Nelson Rivers is evident through both the increase in the slope of a mixing line for the Nelson River downstream of Kelsey, and increased variability

of isotopic composition compared to either the Burntwood or Nelson River upstream of Split Lake. Split Lake isotopic compositions are dominated by Burntwood River compositions (more depleted); however, downstream compositions progress toward the ratio of Nelson to Burntwood River flow at Stephens Lake (Figure 3-3b). The spatial lag in mixing extent is caused by Split Lake, a non-channelized reach of the Nelson River. The lack of channel definition calms turbulent velocities and limits complete mixing of the Burntwood and Nelson River until flow is restricted to a channelized reach and velocities increase.

At the headwater basin scale, climate and geography affect isotopic compositions, similar to the larger riverine systems. In contrast, however, the headwater basins have the greatest observed variability (Figure 3-5) across flow regimes and interannual variability among the synoptic surveys (Figure 3-4), which offer additional insight into hydrologic processes. Of the headwater basins sampled in the LNRB, few had temporal isotopic variations similar to each other, suggesting that headwater basins have differing dominant end-members that are linked to specific physiographic features within each basin (e.g. land cover). Generally speaking, headwater basins would be expected to be more depleted during the spring due to snowmelt influence, and progressively enriched with ice-off evaporation. Despite occurrences of distinct high-flow events in several headwater basins, significant variability in basin response was noted among the extremely high-flow events (Figure 3-5). The variability is suggestive of possible hysteretic release of heavy-isotope enriched water from storage (i.e. lakes and wetlands) resulting in a mixture of event and pre-event source water that is time lagged (Hayashi et al. 2004).

The most significant influence of a headwater basin occurs at the confluence of the Gunisao River and the Nelson River East Channel (average flow addition is 6.78%), which is

noticeable in Figure 3-2a and Figure 3-4. High-flow events on the Gunisao strongly influence the observed $\delta^{18}O$ and $\delta^{2}H$ in the East Channel (Figure 3-2a). Mixing is also observed during low-flow periods, based on the deviation of $\delta^{18}O$ in the East Channel from that in Playgreen Lake.

To further identify cause–effect relationships within headwater basins, correlations between isotopic variability and basin physiography (land cover characteristics, residence time and degree of connectivity) should be explored through geographic information system (GIS) or systems-based approaches. These sites are ideal candidates for isotope-mass balance modelling as end members are isotopically distinct, different basins exhibit different characteristic responses and the basins are gauged but unregulated. The capability to continuously simulate both streamflow and isotopic composition using the isoWATFLOOD model (Stadnyk et al. 2013) in the LNRB will additionally facilitate continuous records of isotopic variability in response to hydrologic change, enabling a more thorough understanding of hydrologic– isotopic response and reasons for hydrologic change at various scales.

Flow in the LNRB is sustained by contributions from both Lake Winnipeg (i.e. the greater Nelson River Basin) and the CRD (i.e. Churchill River basin), where spatial progression of isotopic composition results from geographical origin, flow conditions, local inflows and the characteristic mixing of river systems. These factors influence isotopic compositions and are identifiable and traceable throughout the LNRB, which would not be possible from flow records alone.

3.7 CONCLUSIONS

Achieving hydrologic data with adequate spatial and temporal resolution in the LNRB (and many other northern Canadian basins) is generally difficult due to its vast size and the limited access to sampling locations, but there is considerable value in establishing complementary

stable water isotope monitoring networks to supplement existing hydrometric measurements. Isotopic data assist in the identification of geographical origin and changes in flow and mixing regimes. The variability of stable water isotopes within the LNRB is strongly dependent on geography, the size of the basin and the characteristic flow regime. Larger rivers in the LNRB exhibit significantly less isotopic variability than smaller headwater basins, caused by the longer flow paths and residence times. Additionally, mixing characteristics downstream of river confluences exhibiting different isotopic compositions are discernible. This is valuable information for water managers and hydroelectric operators seeking to understand dynamics of the water balance and channel routing mechanisms. To complement hydrologic modelling of the LNRB, and to evaluate reasons for long-term hydrologic change, set-up of a continuous iso-hydrological simulation model (i.e. isoWATFLOOD) within the LNRB has been completed (Chapters 4&5). Furthermore, modelling is aided by the isotopic analysis of headwaters, which identified two primary water storages greatly influencing riverine isotopic compositions, wetlands at low flow and shallow surface storages during high flow (rapid flow paths). Subsequent identification of source waters using flow anomaly analysis during average flow and may be identified through tracer-aided modelling using the SWIMN.

3.8 ACKNOWLEDGEMENTS

We would like to first and foremost acknowledge substantial funding for the SWIMN from Manitoba Hydro. This also includes the in-kind contribution of their hydrometric staff in Thompson, Manitoba, for isotope collection and site/equipment maintenance. We would also like to acknowledge the assistance of Water Survey of Canada personnel in Winnipeg and Thompson for collecting isotope samples at various gauges throughout the LNRB. We are also very thankful to the Environmental Isotope Laboratory in Victoria, BC, run by Alberta Innovates

Technology Futures, for conducting stable water isotope analysis of the collected waters – in particular, Dr. John J. Gibson and Mr. Paul Eby. We acknowledge the contributions of our reviewers whose valuable input has improved this manuscript significantly. This research was partially funded by Natural Sciences and Engineering Research Council (NSERC) Alexander Graham Bell Canada Graduate Scholarships (CGS).

3.9 REFERENCES

Araguas-Araguas, L., Froehlich, K., Rozanski, K. 2000. Deuterium and oxygen-18 composition of precipitation and atmospheric moisture. *Hydrological Processes,* **Volume 14(8)**: 1341–1355.

Beven, K.J., Binley, A.M. 1992. The future of distributed models: Model calibration and uncertainty prediction. *Hydrological Processes,* **Volume 6(3)**: 279–298.

Birks, S.J., Edwards, T.W.D. 2009. Atmospheric circulation controls on precipitation isotope-climate relations in western-Canada. Tellus Series B – *Chemical and Physical Meteorology,* **Volume 61(3)**: 566–576.

Birks, S. J., Edwards, T.W.D., Gibson, J.J., Drimmie, R.J., Michel, F.A. 2004. Canadian Network for Isotopes in Precipitation (CNIP). http://www.science.uwaterloo.ca/~twdedwar/cnip/cniphome.html (accessed October, 2013).

Bowen, G.J. 2010. Isoscapes: Spatial pattern in isotopic biogeochemistry. *Annual Review of Earth and Planetary Sciences,* **Volume 38**: 161–187.

Cooper, L.W., McClelland, J.W., Holmes, R.M., Raymond, P.A., Gibson, J.J., Guay, C.K., Peterson, B.J. 2008. Flow-weighted values of runoff tracers ($\delta^{18}O$, DOC, Ba, alkalinity) from the six largest Arctic rivers. *Geophysical Research Letters,* **Volume 35(18)**: L18606.

Coplen, T. B., Kendall, C. 2000. Stable hydrogen and oxy- gen isotopes ratios for selected sites of the US Geological Survey's NASQAN and benchmark surface-water networks: Open-File Report 00-160. United States Geological Survey.

Coulibaly, P., Samuel, J., Pietroniro, A., Harvey, D. 2013. Evaluation of Canadian National Hydrometric Network density based on WMP 2008 standards. *Canadian Water Resources Journal,* **Volume 39(2)**: 159–167.

Craig, H. 1961. Isotopic variations in meteoric waters. *Science*, **Volume 133**: 1833–1834.

Craig, H., Gordon, L.I. 1965. Deuterium and oxygen-18 variations in the ocean and the marine

atmosphere. In Stable Isotopes in Oceanographic Studies and Paleotemperatures, edited by E. Tongiori, 9–130. Spoleto Meeting on Nuclear Geology, Lab. di Geologia, Pisa.

Dansgaard, W. 1964. Stable isotopes in precipitation. *Tellus,* **Volume 16(4)**: 436–468.

Delavau, C., Stadnyk, T.A., Birks, S.J. 2011. Model based distribution of oxygen-18 isotopes in precipitation across Canada. *Canadian Water Resources Journal,* **Volume 36(4)**: 313–330.

Dunn, S.M., Freer, J., Weiler, M., Kirkby, M.J., Seibert, J., Quinn, P.F., Lischeid, G., Tetzlaff, D., Soulsby, C. 2008. Conceptualization in catchment modelling: simply learning? *Hydrological Processes,* **Volume 22(13)**: 2389–2393.

Ecoregions Working Group. 1989. Ecoclimatic regions of Canada, first approximation (plus map at 1:750,000). Ottawa, ON: Environment Canada.

Fenicia, F., McDonnell, J.J., Savenije, H.H.G. 2008. Learning from model improvement: On the contribution of complementary data to process understanding. *Water Resources Research,* **Volume 44(6)**: W06419.

Gibson, J.J. 2002. Short-term evaporation and water budget comparisons in shallow arctic lakes using non-steady isotope mass balance. *Journal of Hydrology,* **Volume 264**: 242–261.

Gibson, J.J., Fekete, B.M., Bowen, G.J. 2010. Stable isotopes in large scale hydrological applications. In Isoscapes: Understanding movement, pattern, and process on Earth through isotope mapping, Edited by J. B. West, G. J. Bowen, T. E. Dawson, and K. P. Tu, 389–405. New York: Springer.

Gibson, J.J., Aggarwal, P., Hogan, J., Kendall, C., Martinelli, L.A., Stichler, W., Rank, D., Goni, I., Choudhry, M., Gat, J., Bhattacharya, S., Suginoto, A., Fekete, B., Pietroniro, A., Maurer, T., Panarello, H., Stone, D., Seyler, P., Maurice-Bougoin, L., Herczeg, A. 2002. Isotope studies in large river basins: A new global research focus. *EOS,* **Volume 83(52)**: 613–617.

Gibson, J. J., Edwards, T.W.D., Birks, S.J., St.Amour, A.N., Buhay, W.M., McEachern, P., Wolfe, B.B., Peters, D.L. 2005. Progress in isotope tracer hydrology in Canada. *Hydrological Process*, **Volume 19**: 303–327.

Hayashi, M., Quinton, W., Pietroniro, A., Gibson, J.J. 2004. Hydrologic functions of wetlands in a discontinuous permafrost basin indicated by isotopic and chemical signatures. *Journal of Hydrology,* **Volume 296**: 81–97.

International Atomic Energy Agency (IAEA). 2012. Use of environmental isotopes in assessing water resources in snow, glacier, and permafrost dominated areas under changing climatic conditions: First report for CRP F3.2006. Isotope Hydrology Section, IAEA.

Kendall, C., Coplen, T.B. 2001. Distribution of oxygen-18 and deuterium in river waters across

the United States. *Hydrological Processes,* **Volume 15(7)**: 1363–1393.

Kendall, C., McDonnell, J.J. 1998. Isotope tracers in catchment hydrology. *EOS,* **Volume 80**: 260.

Kirchner, J.W. 2003. A double paradox in catchment hydrology and geochemistry. *Hydrological Processes,* **Volume 17(4)**: 871–874.

Kirchner, J.W. 2006. Getting the right answers for the right reasons: Linking measurements, analyses, and models to advance the science of hydrology. *Water Resources Research,* **Volume 42**: W03S04.

Kuczera, G. 1983. Improved parameter inference in catchment models, 2. Combining different kinds of hydrologic data and testing their compatibility. *Water Resources Research,* **Volume 19(5)**: 1163–1172.

Kuczera, G., Mroczkowski, M. 1998. Assessment of hydrologic parameter uncertainty and the worth of multi-response data. *Water Resources Research,* **Volume 34(6)**: 1481–1489.

McClelland, J.W., Holmes, R.M., Peterson, B.J., Amon, R., Brabets, T., Cooper, L., Gibson, J., Gordeev, V.V., Guay, C., Milburn, D., Staples, R., Raymond, P.A., Shiklomanov, I., Striegl, R., Zhulidov, A., Gurtovaya, T., Zimov, S. 2008. Development of a Pan-Arctic Database for River Chemistry. *Eos, Transactions American Geophysical Union,* **Volume 89(24)**: 217–218.

Mishra, A.K., Coulibaly, P. 2010. Hydrometric network evaluation for Canadian watersheds. *Journal of Hydrology,* **Volume 380**: 420–437.

Nelson, S.T. 2000. A simple, practical methodology for routine VSMOW/SLAP normalization of water samples analyzed by continuous flow methods. *Rapid Communications in Mass Spectrometry,* **Volume 14(12)**: 1044–1046.

Penna, D., Ahmad, M., Birks, S.J., Bouchaou, L., Brenčič, M., Butt, S., Holko, L., Jeelani, G., Martínez, D. E., Melikadze, G., Shanley, J. B., Sokratov, S. A., Stadnyk, T., Sugimoto, A., Vreča, P. 2014. A new method of snowmelt sampling for water stable isotopes. *Hydrological Processes*, **Volume 28(22),** pp. 5637-5644.

Posey, J.C., Smith, H.A. 1957. The equilibrium distribution of light and heavy water in a freezing mixture. *Journal of the American Chemical Society,* **Volume 79(3)**: 555–557.

Raymond, P.A., McClelland, J.M., Holmes, R.M., Zhulidov, A.V., Mull, K., Peterson, B.J., Striegl, R.G., Aiken, G.R., Gurtovaya, T.Y. 2007. Flux and age of dissolved organic carbon exported to the Arctic Ocean: A carbon isotopic study of the five largest arctic rivers. *Global Biogeochemical Cycles,* **Volume 21(4)**: GB4011.

Roulet, R.T., Woo, M.-K. 1986. Hydrology of a wetland in the continuous permafrost region. *Journal of Hydrology,* **Volume 89(1)**: 73–91.

Siebert, J., McDonnell, J.J. 2002. On the dialog between experimentalist and modeler in catchment hydrology: Use of soft data for multicriteria model calibration. *Water Resource Research,* **Volume 38(11)**: 23.1–23.14.

Stadnyk, T.A., Delavau, C., Kouwen, N., Edwards, T.W.D. 2013. Towards hydrological model calibration and validation: Simulation of stable water isotopes using the isoWATFLOOD model. *Hydrological Processes,* **Volume 27(25)**: 3791–3810.

St. Amour, N.A., Gibson, J.J., Edwards, T.W.D., Prowse, T.D., Pietroniro, A. 2005. Isotopic time-series partitioning of streamflow components in wetland-dominated catchments, lower Liard river basin, Northwest Territories, Canada. *Hydrological Processes,* **Volume 19(17)**: 3357–3381.

Vitvar, T., Aggarwal, P.K., Herczeg, A.L. 2007. Global network is launched to monitor isotopes in rivers. *EOS,* **Volume 88(33)**: 325–326.

Yi, Y., Gibson, J.J., Hélie, J.F., Dyck, T.A. 2010. Synoptic and time-series stable isotope surveys of the Mackenzie River from Great Slave Lake to the Arctic Ocean, 2003 to 2006. *Journal of Hydrology,* **Volume 383(3)**: 223–232.

Yi, Y., Gibson, J.J., Cooper, L.W., Hélie, J.F., Birks, S.J., McClelland, J.W., Holmes, R.M., Peterson, B.J. 2012. Isotopic signals (^{18}O, ^{2}H, ^{3}H) of six major rivers draining the pan-Arctic watershed. *Global Biogeochemical Cycles,* V**olume 26(1)**: GB1027.

CHAPTER 4: ASSESSMENT OF A LUMPED COUPLED FLOW-ISOTOPE MODEL IN DATA SCARCE BOREAL CATCHMENTS

Aaron Smith[1], Chani Welch[1], and Tricia Stadnyk[1]

[1]Department of Civil Engineering, University of Manitoba, Winnipeg, Manitoba

Published in 2016 in Hydrologic Processes (DOI: 10.1002/hyp.10835). Received December 2014; accepted February 2016.

This chapter investigates the use of a lumped tracer-aided ($\delta^{18}O$) hydrologic model for the identification of the contribution of primary flow paths within two headwater catchments of the LNRB. Identification of the contributions of stream water help to constrain estimation of the flow mechanisms and the influence evaporation and transpiration fluxes may have on the stream flow. Temporal uncertainty of the contributions of streamflow further help to identify influential hydrological processes.

CHAPTER 4

4.1 ABSTRACT

Quantifying streamflow sources within remote, data scarce, Boreal catchments remains a significant challenge because of limited accessibility and complex, flat topography. The coupled use of hydrometric and isotopic data has previously been shown to facilitate quantification of streamflow sources, but application has generally been limited to small basins and short time scales. A lumped flow-isotope model was used to estimate contributing streamflow sources (soil, ground, and wetland water) over a four-year period in two large nested headwater catchments (Sapochi and Odei Rivers) in northern Manitoba, Canada. On average, the primary streamflow source was estimated as soil water (60%) in the Sapochi River, and groundwater (54%) in the Odei River. A strong seasonal influence was observed: soil water was the primary streamflow source in summer, changing to groundwater and wetlands during the winter. Interannual variability in streamflow sources was strongly linked to the presence or absence of late summer rainfall. The greatest uncertainties in source quantification were identified during the spring freshets and high precipitation events, and hence, simulations may be improved through explicit representation of the soil freeze/thaw process and data collection during this period. Assessment of primary streamflow components and qualitative uncertainty estimation using coupled isotope-flow modelling is an effective method for first-order identification of streamflow sources in data sparse remote headwaters.

4.2 INTRODUCTION

Northern Canadian watersheds are some of the most remote and sparsely monitored hydrologic locations in North America and contain complex geographic and topographic features and hydrological processes. Understanding of the hydrodynamics of these basins is critical for operational flow forecasting and water supply projections under climate change (Bohrn 2012; Yip et al., 2012), short-term inflow forecasting for improved management of hydraulic controls (i.e. control structures, generating stations, diversions), and assessment of susceptibility to ecological change. Hydrologic models in ungauged or sparsely monitored basins frequently encounter uncertainty in the simulation of discharge because of complexities in connectivity of land cover, system response, and heterogeneity (Spence et al., 2013; Hrachowitz et al., 2014). Input uncertainty, structural uncertainty, and parameter uncertainty all contribute to uncertainty in the outputs of hydrological models (Wagener et al., 2003). Explicit acknowledgement and assessment of such uncertainty have the potential to increase understanding of hydrologic data and the inferences derived regarding catchment functioning, improve the robustness of predictions of hydrological behaviour, and identify the value of additional data collection (Juston et al., 2013).

Stable water isotopes oxygen-18 ($\delta^{18}O$) and deuterium ($\delta^{2}H$) have long been used in hydrology for improving the understanding of streamflow generation mechanisms using mass balance approaches, including two-component separations (Sklash et al., 1976; McDonnell et al., 1990; Metcalfe and Buttle 2001; Brock et al., 2007) and end member mixing analysis (Merot et al., 1995; Rice and Hornberger 1998; Lee and Krothe 2001). However, while estimates of streamflow components at short time scales are common, multi-year investigations in headwater catchments in northern regions are rare (Carey et al., 2013). Furthermore, consideration of

simultaneous hydrometric and isotope data is necessary to improve identification of streamflow source components (Rice and Hornberger 1998; Birkel et al., 2014).

Modelling approaches that couple flow and tracers have resulted in improved model parameterisations that are representative of basin processes rather than aggregates of model error (Birkel et al., 2010; Stadnyk et al., 2013), and in some cases, rejection of proposed model structures (Vache and McDonnell 2004). Such models are capable of exploiting both the continuous simulation of hydrologic models and the time- and process-knowledge integrated by stable water isotopes as they traverse a catchment. Examples of coupled flow and isotope models (herein referred to as iso-hydrologic models) include lumped conceptual catchment isotope models (CIM) (e.g. Birkel et al., 2010; Birkel et al., 2011), and the physically based routing model, isoWATFLOOD (Stadnyk et al., 2013). The isoWATFLOOD model was designed to be applied at large scales in Canadian catchments where snowmelt processes are important to the annual hydrologic cycle. However, the internal structure of isoWATFLOOD is not designed to be physically realistic at small scales. In contrast, CIM applies storage units that use linear scaling parameters for storage release, shows some sensitivity to the number of model parameters employed, and has generally been applied to small river basins driven by rainfall (Birkel et al., 2011).

In this study, we developed a lumped iso-hydrologic model that incorporates physically based routing and snowmelt processes, with the primary objective of obtaining a first order estimate of the temporal variation in primary streamflow components. Through modelling, we also address the secondary objective, quantifying parameter identifiability and the temporal uncertainty of each model output (flow, $\delta^{18}O$, and components). The model was applied to two large, nested, headwater catchments in northern Manitoba, Canada over a four-year period.

4.3 SITE DESCRIPTION

The Odei River basin is located in the Burntwood River Basin, north of Thompson, Manitoba, Canada (55°44'N; 97°52′W), and has a drainage area of over 6300 km^2 (Figure 4-1). The Sapochi River basin is a headwater of the Odei River with an area of 390 km^2. The Odei River drains into the Burntwood River, which is a major tributary flowing eastward and feeding the Nelson River. Quantification of flow generation mechanisms in these headwater basins is vital as the Nelson River is utilized for 75% of Manitoba Hydro's hydroelectric power generation (Manitoba Hydro 2014).

Table 4-1. Climate data and climate normal (1981-2010) from the Class A meteorological station at Thompson Airport

	Thompson Airport				
	2010	**2011**	**2012**	**2013**	**Normals**
Maximum temperature (^{o}C)	5.8	4.6	4.3	2.5	3.4
Minimum temperature (^{o}C)	-6.3	-8.5	-8.1	-9.6	-9.1
Mean temperature (^{o}C)	-0.2	-1.9	-1.8	-3.1	-2.9
Rainfall (mm)	485	465	400	302	340
Snow water equivalent (mm)	139	87	152	106	169
Total precipitation (mm)	624	552	552	408	509
Relative humidity 0600LST (%)	73.4	82.7	83.8	69.3	79.3

The Sapochi and Odei River basins are located within the Boreal Canadian Shield region of northern Manitoba (Figure 4-1) where the climate is continental sub-arctic (Ecoregions Working Group 1989). The basins receive approximately 500 mm of precipitation annually, 70%

of which occurs as rainfall. The sub- arctic climate of these basins maintains a low mean annual temperature of 3°C and is sub-humid with a mean average relative humidity of 79%. From 2010 to 2012 temperatures were notably warmer than climate normals, specifically in 2010 when mean temperatures were 2°C above normal (Table 4-1). Annual average water balance estimates 325 mm of average watershed water loss because of extensive evapotranspiration in each basin.

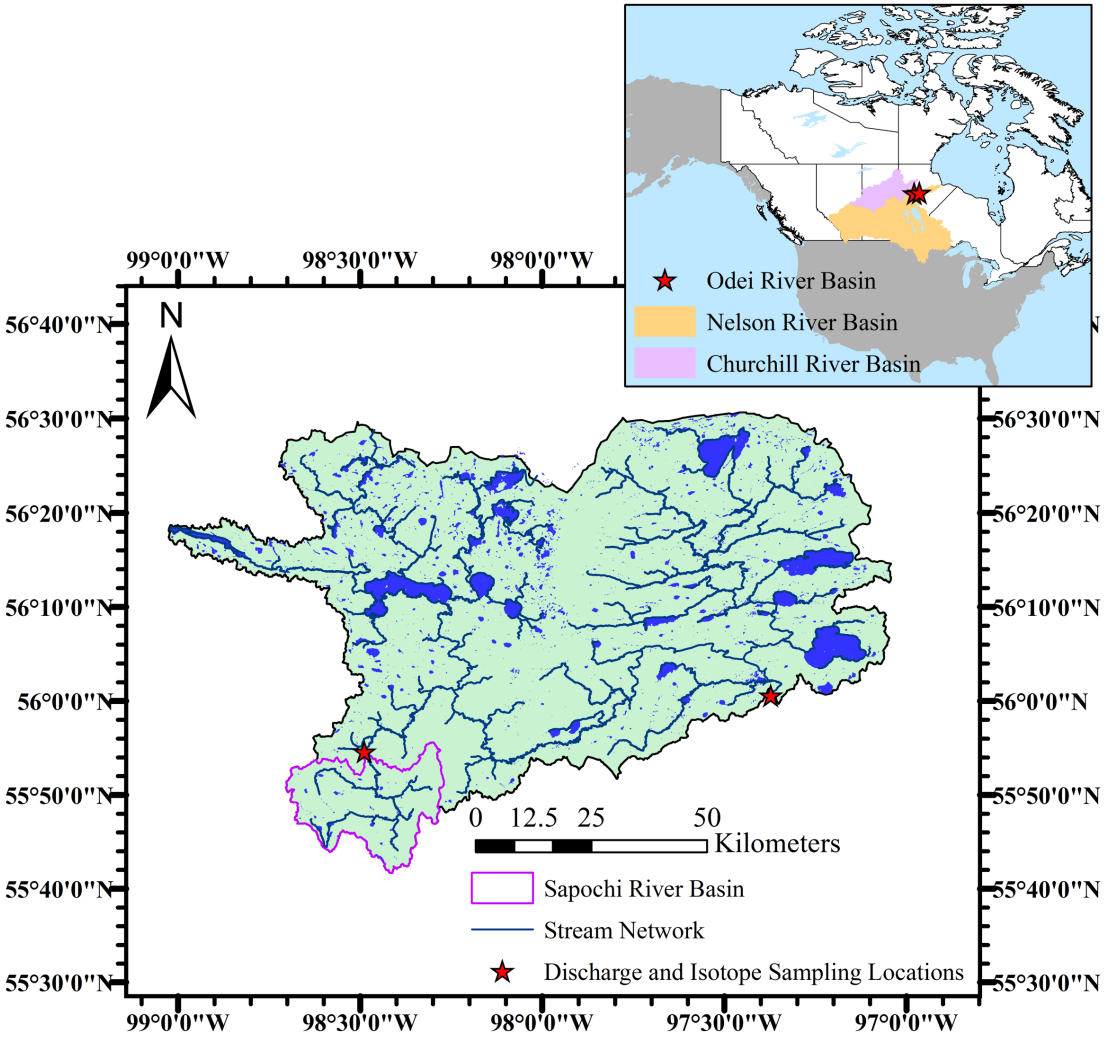

Figure 4-1. The Odei and Sapochi River basins identified with station locations and hydrography. The insert shows the boundary of the Nelson River basin relative to North America, the lower Nelson River basin, the portion of the Churchill River basin feeding into the lower Nelson River basin, and the Odei River basin.

The Sapochi and Odei River basins have minimum elevations of 231 and 167 m above sea level and average stream slopes of 6.5 and 11.1%, respectively. However, average slopes of the basins are substantially lower (2.0 and 1.4% respectively). As with similar northern catchments, connectivity between lakes and surface storage is a function of water level (i.e. fill-and-spill, Spence 2007). Low gradients also increase the importance of land cover for flow attenuation: channel-lined fens retard runoff before it reaches the channel, and lakes increase retention time. The land cover within each basin is shown in Table 4-2.

Table 4-2. Land cover percentages of the Sapochi and Odei River basin from GeoBase (GeoBase 2014)

Land cover classifications	Sapochi River Basin (%)	Odei River Basin (%)
Water	3.7	9.6
Shrubs	37.6	28.8
Wetlands	20.9	21.7
Coniferous forest	24.4	30.0
Broadleaf forests	10.0	3.0
Mixedwood forests	2.5	6.8
Other	0.9	0.1

The basins lie on the Canadian Shield, which is characterized by shallow bedrock. Subsurface storage is further limited by sporadic discontinuous permafrost, present across 10–50% of the basin area (Atlas of Canada 2014), and seasonally frozen ground throughout the remaining areas. Permafrost has been shown to constrain soil flux and reduce the availability of storage, resulting in rapid streamflow peaks, specifically during snowmelt (Roulet and Woo 1986; Woo and Winter 1993).

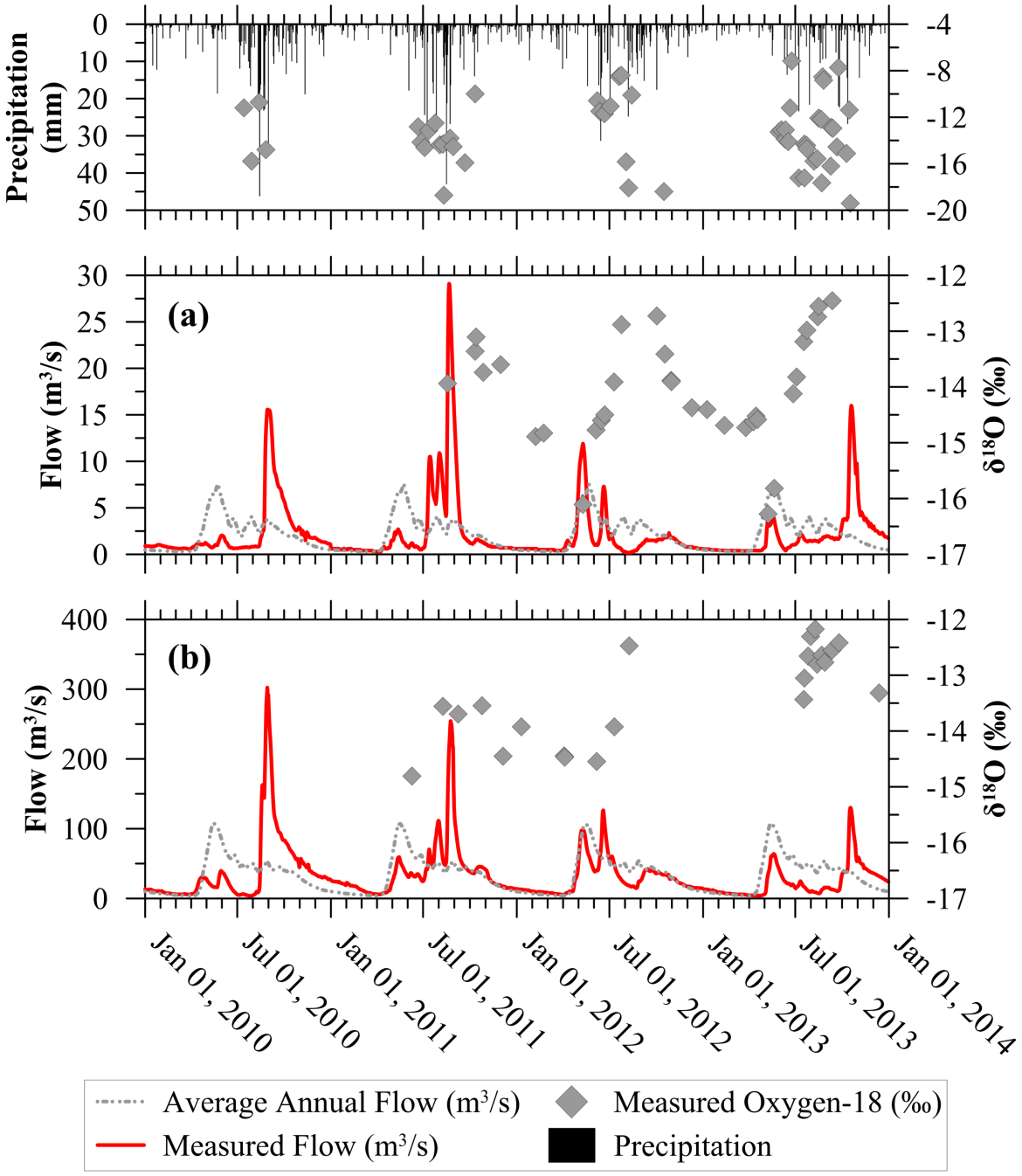

Figure 4-2. Precipitation and measured rainfall $\delta^{18}O$ composition, and the flow and measured streamflow $\delta^{18}O$ composition of the (a) Sapochi and (b) Odei River Basin. The dashed grey line shows the average annual discharge over the period of record.

Annual average flows are 2.18 m^3/s for the Sapochi River (1993 – 2013) and 33.14 m^3/s for the Odei River (1979 – 2013) (Environment Canada 2014). Annual average flows for both basins peak during the spring freshet (late April to late May), with smaller peak flows during the

summer and fall months because of rainfall (Figure 4-2). However, during the study years only 2012 flow data followed this trend. The remaining years (2010, 2011, and 2013), were characterized by smaller, late, melt periods, and the annual peak flow occurred during the late summer (July and August) as a result of rainfall. Each year above normal temperatures also experienced higher rainfall amounts (60 to 140mm, Table 4-1), resulting in high peak flows during the summers of 2010 and 2011 within both river basins (Figure 4-2). Large differences in measured flow occurred between 2011 and 2012, and are directly correlated to the change in precipitation (>50 mm in precipitation). Two large precipitation events occurred in both 2012 and 2013; however only the 2013 event resulted in a peak flow event. Iso-hydrologic modelling of the basins provides an opportunity to understand the causes of event-based responses.

4.4 METHODOLOGY

4.4.1 COLLECTION AND ANALYSIS OF STABLE WATER ISOTOPES

Samples of precipitation, snow, shallow groundwater, and river waters were collected for analysis of isotopic composition between 2010 and 2013. Precipitation samples were collected following large events from 2010 to 2012 and on an event basis in 2013. Depth-dependent and composite snowpack samples were collected prior to melt. Groundwater and river samples were collected approximately once per month. Groundwater samples were not collected during the winter as the ground froze. Meteorological and groundwater samples were collected at a single location 40 km from the outlet. The monitoring network is described in detail in Smith et al. (2015). Water samples were analysed for $\delta^{18}O$ and $\delta^{2}H$ at the University of Victoria Environmental Isotope Laboratory using a Delta V Advantage stable isotope mass spectrometer with a precision of ±0.2 per mille for $\delta^{18}O$ and ±1.0 per mille for $\delta^{2}H$.

4.4.2 HYDROLOGIC MODEL DEVELOPMENT

The University of Manitoba Stable Water Isotope Model (UMSWIM) was designed as a lumped conceptual mathematical model, for flow and $\delta^{18}O$ simulation in unregulated headwater basins. The UMSWIM modelling interface, Stella® (ISEE Systems 2015), provided a systems approach to modelling and multiple distribution Monte Carlo parameterisation and uncertainty analyses. The mathematical relationships for storage and hydrological process dynamics are provided in Table 4-3 and a conceptual diagram of the model in Figure 4-3. The catchment was separated into hydrologic response units (HRU) based on land cover type, and the response was lumped for each HRU. Within the model framework, upper zone soil and wetlands were the only storages that received precipitation and lost water through evapotranspiration. Of the four storage components, upper zone soils were also the only storage directly linked to each of the other storages.

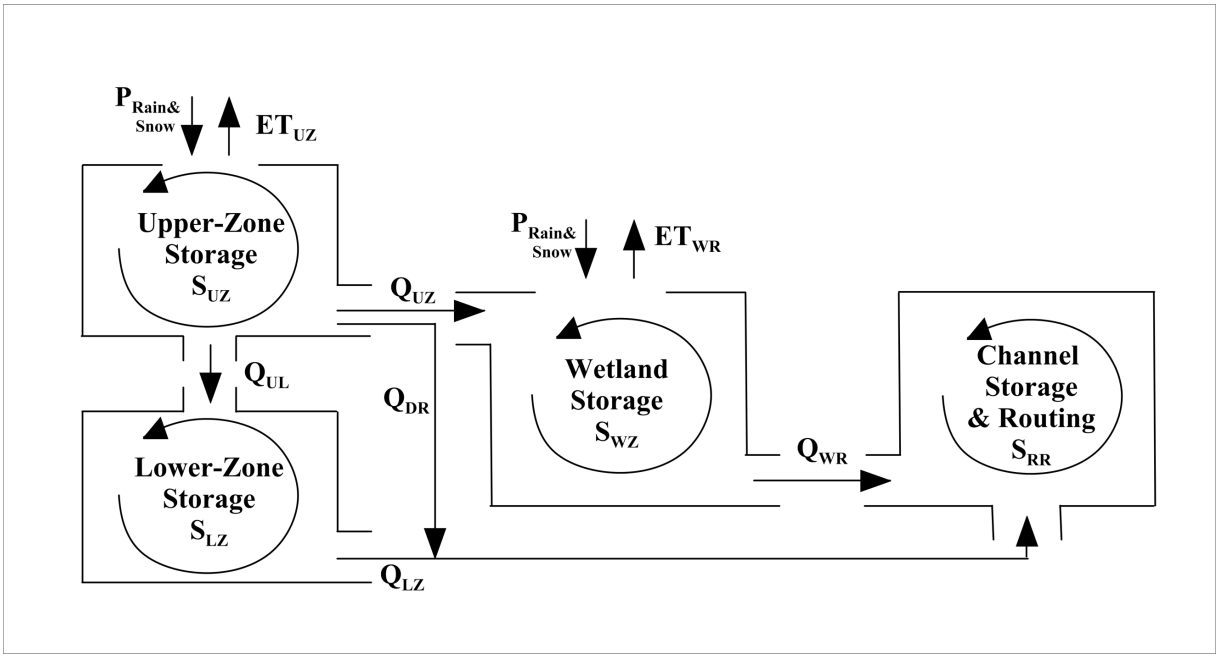

Figure 4-3. Structure of UMSWIM within Stella®. With the exception of the wetlands, each flow component shown is modelled through a power function

Upper zone soil (soil) and lower zone soil (groundwater) storage release functions were

non-linear and followed a power function with storage volume (m^3), power factor a (unitless), and scaling factor c ($m^{-a}day^{-1}$) (Table 4-3, Equations 4-9, 4-10, and 4-12). The wetland release function was based on the two-dimensional Dupuit equation, correlating wetland water level in storage (h_o), length of stream (L), wetland width and conductivity (W_{width} and K), and stream water level (h_r) (Table 4-3, Equation 4-13) (Schwartz and Zhang 2003). Water was released from wetland storage when $h_o > h_r$. The rate of flow was a function of W_{width}, K, head difference ($h_o - h_r$) and L. For hydrologic routing, channel storage was divided into stream orders, and further sub-divided into reaches, where water from storage was added to the channels. Water was routed through the channels using the Muskingum routing equation (Table 4-3, Equation 4-14). This equation assumes that channels have low slopes and attenuate flow, both characteristics of the Sapochi and Odei River basins.

Table 4-3. UMSWIM basin storage relationships, corresponding model parameters, and hydrological functions

Model process	Method	Mathematical/empirical model	Equation
Soil water reservoir	Accumulation of inflow and outflow to determine the change in storage volume	$\frac{dS_{UZ}}{dt} = P_{Rain} + P_{Snow} - ET_{UZ} - Q_{UZ} - Q_{UL} - Q_{DR}$	4-1
Deep soil/groundwater reservoir		$\frac{dS_{LZ}}{dt} = Q_{UL} - Q_{LZ}$	4-2
Wetland reservoir		$\frac{dS_{WR}}{dt} = w \cdot Q_{UL} - ET_{WR} - Q_{WR}$	4-3
River storage		$\frac{dS_{RR}}{dt} = Q_{WR} + Q_{LZ} + Q_{DR} + (1-w) \cdot Q_{UL} + Q_{US} - Q_o$	4-4
Evapotranspiration (ET)	Adjusted mass-transfer estimation	$ET_{UZ} = PE_{Soil} \cdot \big((b_0 + b_1 \cdot v_a) \cdot (e_s - e_a)\big)$	4-5
		$ET_{WR} = PE_{Wet} \cdot \big((b_0 + b_1 \cdot v_a) \cdot (e_s - e_a)\big)$	4-6
Snowmelt	Degree-day snowmelt estimation	$Q_m = 0.011 \cdot \rho_s \cdot (T_a - T_B)$	4-7
Ice formation	Ice forms over sustained cold temperatures, also reduces ET	$\text{if}\big((T_{(t-5\Delta t)} + T_{(t-4\Delta t)} + T_{(t-3\Delta t)} + T_{(t-2\Delta t)} + T_t) < 0\big), 1$	4-8
Runoff generation		$Q_{UZ} = c_{UZ} \cdot {S_{UZ}}^{a_{UZ}}$	4-9
		$Q_{UL} = c_{UL} \cdot {S_{UZ}}^{a_{UL}}$	4-10
		$\text{if}\big(S_{UZ} > S_{UZ(MAX)}\big), Q_{DR} = S_{UZ} - S_{UZ(MAX)}$	4-11
		$Q_{LZ} = c_{LZ} \cdot {S_{LZ}}^{a_{LZ}}$	4-12
Wetland runoff generation	Dupuit groundwater equation	$if(h_o > h_r), Q_{WR} = K \cdot \frac{h_o^2 - h_r^2}{W_{width}} \cdot L \cdot h_o$	4-13
River reach routing	Muskingum routing	$Q_{Out2} = Q_{In2} \cdot R_o + Q_{In1} \cdot R_1 + Q_{Out1} \cdot R_2$	4-14
		$R_o = \frac{-K_M \cdot X_M + 0.5 \cdot \Delta t}{D}$	4-15
		$R_1 = \frac{K_M \cdot X_M + 0.5 \cdot \Delta t}{D}$	4-16
		$R_2 = \frac{K_M - K_M \cdot X_M - 0.5 \cdot \Delta t}{D}$	4-17
		$D = K_M - K_M \cdot X_M + 0.5 \cdot \Delta t$	4-18

* Q: discharge, P: precipitation, ET: evapotranspiration, UZ: upper zone, LZ: lower zone, UL: upper zone to lower zone interface, WR: wetland, DR: direct runoff, w: percent area of wetlands, RR: channels, S: storage, PE: evapotranspiration correction factor, b_o & b_1: weighting parameters, v_a: wind speed, e_s: surface vapour pressure, e_a: atmospheric vapour pressure, ρ_s: density of snow, T_a: air temperature: T_B: melt temperature, T_t: air temperature at time t, c: linear scaling parameter, a: power scaling factor, h_o: wetland water level, h_r: river water level, K: hydraulic conductivity, L: length of stream, W_{width}: wetland width, K_M: Muskingum k value, X_M: Muskingum x value, Δt: change in time.

Table 4-4. Isotope mixing models, model parameters, and fractionation equations used in UMSWIM

Isotope process	Method	Mathematical/empirical model	Equation
Isotope mixing models	Fraction dependent mixing model. Used when volume changes over the time-step	$C(t) = C_{ss} - (C_{ss} - C_o) \cdot f^{-\frac{ET(m-1)+Q_{in}}{Q_{in}-ET-Q_{out}}}$	4-19
	Time dependent mixing model used for constant volume conditions	$C(t) = C_{ss} - (C_o - C_{ss}) \cdot e^{-\frac{(ET \cdot m + Q_{out}) \cdot t}{V}}$	4-20
		$m = \frac{1}{1 - h + \varepsilon_k}$	4-21
Atmospheric composition		$\delta_A = \frac{(\delta_p - \varepsilon^*)}{\alpha^*}$	4-22
Equilibrium separation		$\varepsilon^* = (\alpha^* - 1) \cdot 1000$	4-23
Liquid-vapour equlibrium	Relationship between ambient temperature and isotopic fractionation for liquid-vapour equilibrium (Horita & Wesolowski 1994)	$\alpha^* = \frac{\left(e^{6.7123 \cdot \frac{\left(\frac{10^3}{T_a+273.15}\right)}{1000}}\right) \cdot \left(e^{0.35041 \cdot \frac{\left(\frac{10^9}{(T_a+273.15)^3}\right)}{1000}}\right)}{\left(e^{\frac{7.685}{1000}}\right) \cdot \left(e^{1.6664 \cdot \frac{\left(\frac{10^6}{(T_a+273.15)^2}\right)}{1000}}\right)}$	4-24
Kinetic separation		$\varepsilon_k = n \cdot C_k \cdot \theta \cdot (1 - h)$	4-25
Evaporative composition		$\delta_e = (C(t) - h \cdot \delta_A - \varepsilon) \cdot m$	4-26

*C: composition, SS: steady-state, C_o: initial composition, f: ratio of previous volume to current volume, V: volume in storage, h: relative humidity, ε^*: equilibrium fractionation, δ_p: precipitation composition, T_a: air temperature C_k: transport resistance of heavy isotopes, θ: advection parameter for relative humidity, n: turbulence parameter.

Isotope modelling was based on the method developed by Gibson (2002) in a continuous time-series, using both time and fraction dependent mixing equations for wetland, channel, and soil water storage and evaporative losses (Table 4-4). The fraction dependent mixing equation (Table 4-4, Equation 4-20) was used to calculate the change in volume of storage (increase in volume, f >1, decrease in volume, f <1) over a time-step, and to estimate the $\delta^{18}O$ composition in storage. Simulations were completed on a daily time-step. The assumptions used in UMSWIM were: (1) water was completely mixed by the end of the time-step, (2) precipitation $\delta^{18}O$ was

equal to the flux-weighted average rainfall $\delta^{18}O$, (3) snowmelt $\delta^{18}O$ was equal to the average composite snowpack $\delta^{18}O$, (4) lower zone storage groundwater $\delta^{18}O$ was the long-term average of measured shallow groundwater samples, (5) channel $\delta^{18}O$ was derived from wetland, soil, and groundwater and channel storage mixing, (6) soil and wetland water were influenced by evaporative fractionation, and (7) no distinction between available evaporation or transpiration water storages. The $\delta^{18}O$ values of groundwater (-15.73‰), rain (-14.15‰), and snow (-26.45‰) were set at the measured flux weighted average compositions, similar to previous Canadian studies (Gibson et al., 2002; Hayashi et al., 2004; St. Amour et al., 2005; Mountain et al., 2015). Flux weighted averages were used because of the spatial and temporal limitations of the measured data; hence, the simulated results provide a first order estimate of the source components. Initial $\delta^{18}O$ compositions of soil, wetland, and channel water were set as the mean measured streamflow composition (-14.26‰ Sapochi River and -13.27‰ for the Odei River).

4.4.3 CALIBRATION SET UP AND MONTE CARLO PARAMETERISATION

Calibration of UMSWIM followed a multi-criteria, multi-step process, with the goal of increasing the likelihood of identifying the global optimum parameter set (Ritter and Munoz-Carpen 2013). To best evaluate the model parameters used in UMSWIM (Table 4-4), the Nash–Sutcliffe efficiency (NSE) (Nash and Sutcliffe 1970), percent deviation of flow (Dv), and log percent deviation of flow (LDv) (Efstratiadis & Koutsoyiannis 2010; Li et al. 2010) were used as flow objective functions, and root mean square error (RMSE) was used as the objective function for $\delta^{18}O$. The ranges of criteria were selected to cover the spectrum of flows observed. NSE has a bias towards peak flow, whereas LDv is most appropriate for low flow periods. The NSE, Dv, and LDv efficiency were not considered suitable metrics for $\delta^{18}O$ model performance because isotope data are discontinuous. Calibration was conducted in a step-wise manner:

1. Preliminary manual calibration of model parameters to identify parameter ranges.
2. Generation of 80 000 parameter sets with the Monte Carlo method (uniform distributions).
3. Simulation of both basins with the same parameter sets. Flow and $\delta^{18}O$ were simulated for 2010–2012 and were evaluated using the above efficiency criteria for each Monte Carlo parameter set. To enable model spin up of hydrologic storage and isotopic composition, simulation years contain an initial flow only year (2010) prior to isotope-flow data for remaining years (2011 and 2012).
4. Monte Carlo simulations were evaluated against minimum efficiency criteria. Parameter sets were rejected when acceptable efficiency criteria were not met (NSE > 0.4, |%Dv| < 20, |%LDv| < 20, and RMSE < 3).
5. Selection of behavioural parameter sets was completed by calculating 95% confidence intervals of the acceptable parameter sets (Step 4). Parameter sets not within the confidence intervals were rejected as localized efficiency optima.
6. Parameter sets were evaluated against a weighted minimization function (Equation 4-27) to ensure that both flow and $\delta^{18}O$ results were acceptable. Parameter sets with a minimization function value greater than 0.7 were rejected.

$$\mathbf{min}\left(\frac{\mathbf{4}}{\mathbf{9}}\cdot(\mathbf{1}-\boldsymbol{Nash})+\frac{\mathbf{2}}{\mathbf{9}}\cdot\left(\frac{|\%\boldsymbol{D_v}|}{\mathbf{100}}+\frac{|\%\boldsymbol{LD_v}|}{\mathbf{100}}\right)+\frac{\mathbf{3}}{\mathbf{9}}\cdot\boldsymbol{NRMSE}\right) \quad \text{4-27}$$

Normalized RMSE was used in the minimization function to ensure all metrics were dimensionless. Following the calibration (2010–2012), acceptable parameter sets (Step 6) were simulated for an additional year (2013) for flow and isotopes. Confidence intervals (95%) were calculated for the entire simulation period (2010–2013) using $Q_i^{CI} = \overline{Q_\iota} \pm 1.96 \cdot \sigma_i$, where Q_i^{CI} is the upper/lower confidence bound at time *i*, $\overline{Q_\iota}$ is the average of all acceptable simulation runs at

time i, and σ_i is the standard deviation of all simulation runs at time i.

4.5 RESULTS

4.5.1 MEASURED STABLE WATER ISOTOPE DATA

Stable water isotope results followed a consistent seasonal pattern in both the Sapochi and Odei Rivers (Figure 4-2). Isotopic compositions of river waters were highly depleted during the spring freshet in May and June, enriched throughout summer months, and gradually depleted to an intermediate steady value during ice-on conditions, indicative of temporal changes in dominant source water components.

The isotopic frameworks for the Sapochi and Odei River basins assist with qualitatively assessing the effect of evaporation and mixing on source water components (Figure 4-4). Mixing slopes were developed through ordinary least squares regression of river water samples, and reflect the weighted average of the source components (Simpson and Herczeg 1991; McKenna et al., 1992; St. Amour et al., 2005). The mixing slopes of the Sapochi and Odei River basins were significantly different (p-value of 0.03). However, excluding freshet sampling because of unequal sample numbers (May), resulted in mixing slopes of 4.42 (Sapochi River) and 4.08 (Odei River), which were not significantly different (p-value of 0.46). The difference between the mixing slopes suggests different, though not significant, evaporative effects in both basins. The range observed in surface water composition indicates contributions from groundwater, snowmelt, and precipitation. Shallow groundwater composition (between -11 and -22‰ for $\delta^{18}O$) indicates mixing from snowmelt (-24.4 to -29.2‰ for $\delta^{18}O$) early in the year, and precipitation (-7.2 and -19.4‰ for $\delta^{18}O$) for the remainder. The shallow depth of the fully screened piezometer (0.8 m below ground level in peat) appears to have resulted in partial mixing of soil and groundwaters.

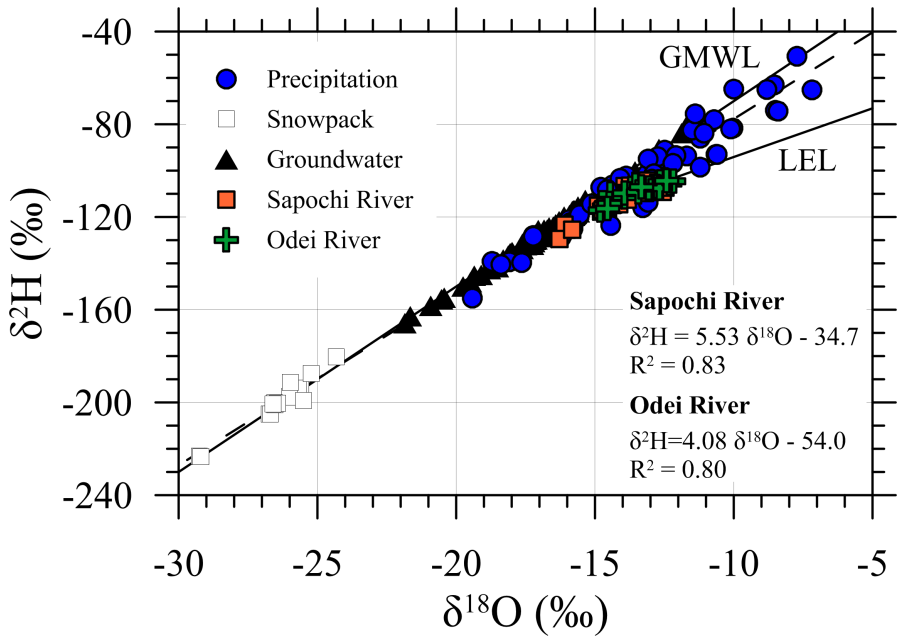

Figure 4-4. Measured streamflow $\delta^{18}O$ versus $\delta^{2}H$ for the Odei and Sapochi River basins. Also shown are the measured precipitation, snowpack, and groundwater compositions. The LMWL of the lower Nelson River Basin (Smith et al., 2015) is shown in relation to the GMWL and LEL.

4.5.2 UMSWIM MODEL RESULTS

Results of the calibration (2010–2012) and test year (2013) of UMSWIM are shown on Figure 4-5. Mean simulated flow (subplots (a) and (d)) and mean simulated $\delta^{18}O$ stream composition (subplots (b) and (e)) are shown (black dotted line) relative to observed flow (red line) and measured $\delta^{18}O$ compositions (red diamonds). The shaded grey region in both plots represents the 5^{th} and 95^{th} confidence intervals of the simulations. The percent contribution of the three primary sources of streamflow, i.e. soil, ground, and wetland water, are shown on Figure 4-5 (subplots (c) and (f)). In the Sapochi River, the confidence bounds of the calibrated simulations generally captured the measured flows. Simulations best captured the first two years of flow and $\delta^{18}O$ data (2010–2011), where the mean daily simulated flow produced the goodness-of-fit metrics: 0.51 (NSE), 6.2% (Dv), 31% (LDv), and 0.64 (RMSE). The peak flow in 2011 was underestimated, and resulted in an overestimation of winter flow (recession of the

hydrograph) as water more slowly drained from the simulated system. The remaining two simulation years had decreased goodness-of-fit of the NSE, LDv, and RMSE, but improved the Dv goodness-of-fit (toward zero). These decreases were because of overestimation of flow after precipitation events in late 2012 and early 2013. The 95% confidence intervals of simulated $\delta^{18}O$ compositions generally capture the measured compositions; however, simulated low flow periods during the fall and winter were over-enriched in $\delta^{18}O$ compared to measured values, indicating excessive enrichment of soil water through the summer months that was progressively flushed out through fall and winter by wetland and groundwater release. Although mean contribution varied between years, the simulated average annual contribution of each source was 60% for soil water, 19% for groundwater, and 21% for wetlands. Seasonal changes in contribution to streamflow were observed for all source waters. Between spring and fall (May–October), soil water was the dominant source (65–98%) of streamflow. The dominant source of streamflow during late fall and winter varied between groundwater (16–46%) and wetland water (8–87%). Interannual variability in source water component was also observed. High summer precipitation resulted in high wetland contribution during the following winter (e.g. 2011 and 2012). Conversely, low summer precipitation was followed by low wetland contribution and higher groundwater contribution (e.g. 2012).

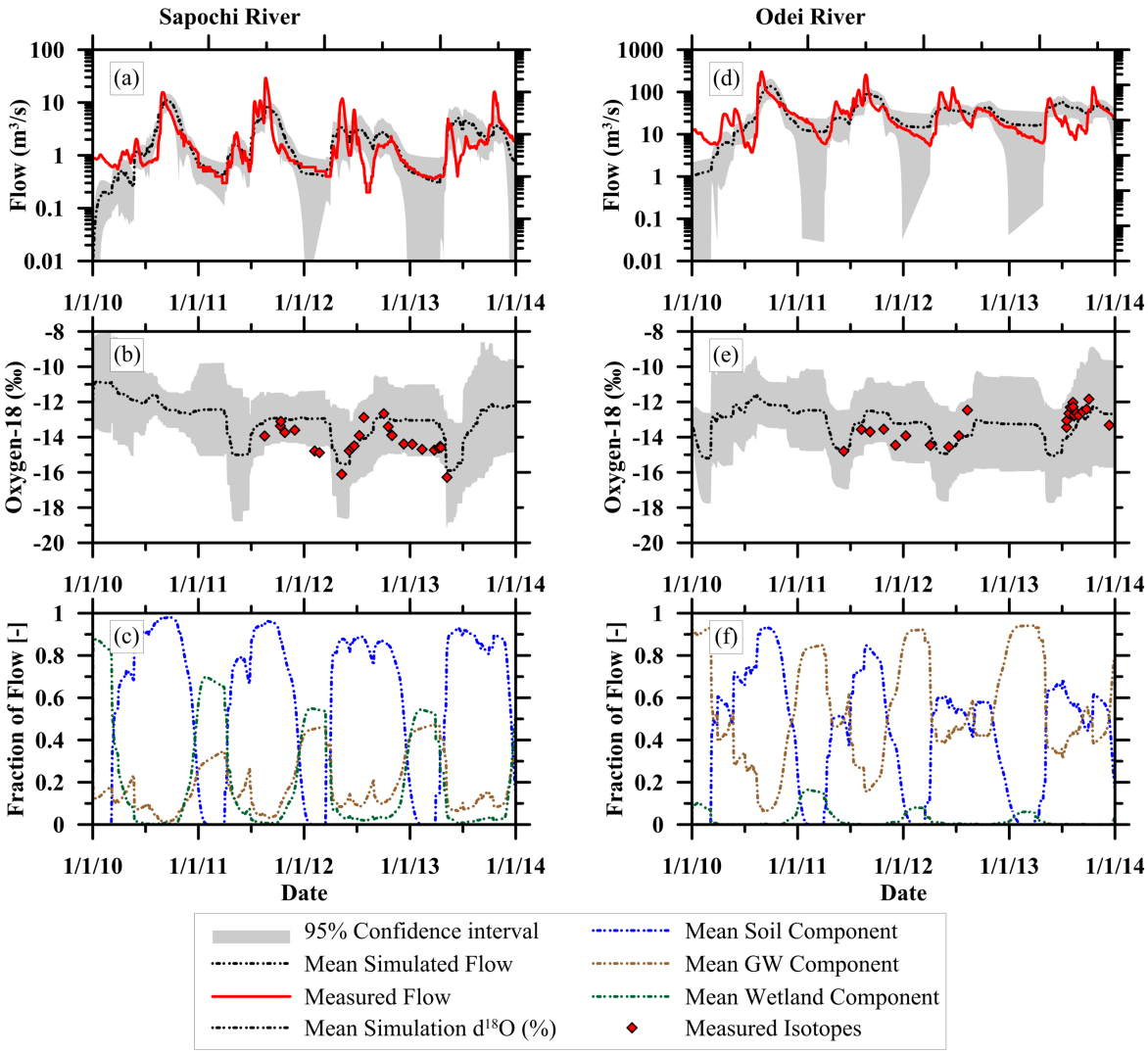

Figure 4-5. Mean simulated flow and $\delta^{18}O$ for the Sapochi River (a and b) and Odei River (d and e). Also included are the mean fraction of flow components for the Sapochi (c) and Odei Rivers (f), broken down into soil, ground, and wetland waters

Similar to the Sapochi River simulations, the Odei River confidence bounds of the simulations generally captured the measured flow. Calibration again best captured the first two years (2010–2011) of flow and $\delta^{18}O$ with goodness-of-fit metrics: 0.45 (NSE), 16.1% (Dv), 9.2% (LDv), and 0.89 (RMSE). Timing of the spring peaks was not well captured by the calibration, which is reflected in a lower NSE in the Odei River relative to the Sapochi River calibration. Simulation goodness-of-fit decreased slightly for the NSE and RMSE in the final two years (2012– 2013) because peak flows were underestimated. However, goodness-of-fit of Dv and

LDv improved during these years, improving the simulation of the total water balance. The mean simulation of $\delta^{18}O$ for the Odei River captured measured temporal trends more effectively than the Sapochi River simulations. Similar to the measured compositions, annual variability of the simulated $\delta^{18}O$ was more damped than the Sapochi River simulations, likely reflecting the larger basin size and increased mixing time. The simulated Odei River average annual contribution of each source differed from the Sapochi River, with groundwater providing the greatest contribution with 54%, followed by soil water with 43%, and wetlands with 3%. Similar to the Sapochi River, seasonal trends in source contributions were observed for the Odei River. Soil water was again the dominant source from spring to fall (May–October), with a minimum contribution of 60% and maximum contribution of 93%. Winter streamflow was consistently dominated by groundwater (47–94%). Wetland contribution also peaked during the winter (1–16%); however, the total flow was significantly less than either soil or groundwater peak contribution.

Initial and calibrated parameter ranges (median, 5th, and 95th percentiles) are presented in Table 4-5 by basin. Qualitatively, reductions in parameter ranges correspond to increased parameter identifiability. Statistically significant reductions in parameter ranges were reported for 10 (Sapochi River) and nine (Odei River) of the 14 calibrated parameters.

In both basins the power factors (a_{UZ}, a_{UL}, and a_{LZ}), which control non-linearity in storage release, were more identifiable than the linear storage release factors (c_{UZ}, c_{UL}, and c_{LZ}, see Table 4-3), with some ranges reduced by over 50%. The upper zone soil power factor (a_{UZ}) was the most identifiable parameter in each basin. Parameter ranges were comparable between basins for a_{UZ} and a_{UL}, however not for a_{LZ}, which controlled the release of groundwater to the stream. The parameter range for a_{LZ} was both more constrained, indicating greater identifiability, and higher,

indicating more groundwater release, in the Odei River than the Sapochi River. The latter was reflected in the greater groundwater contribution to streamflow in the Odei River compared to the Sapochi River (Figure 4-5). Wetland parameters were not identifiable (wetland conductivity and evapotranspiration scaling parameter, not shown).

Table 4-5. Initial and final calibration parameter ranges of the Sapochi and Odei River basin. Parameters shown have greater than 10% decreases in the total parameter range (identifiable). ChanRatio is the scaling factor to describe the size of the wetlands relative to the width of the channel.

	Initial parameter range		Sapochi River calibrated parameter range			Odei River calibrated parameter range		
Parameter	**Min**	**Max**	**5th percentile**	**Median**	**95th percentile**	**5th percentile**	**Median**	**9th percentile**
a_{UZ}	0.0	1.0	0.75	0.97	1.00	0.72	0.93	1.00
c_{UZ}	0.0	2.0	0.55	1.44	2.00	0.40	1.26	2.00
a_{UL}	0.0	2.0	0.00	0.46	1.03	0.00	0.64	1.24
c_{UL}	0.0	2.0	0.00	0.77	1.84	0.02	0.78	1.63
a_{LZ}	0.0	1.0	0.00	0.50	0.81	0.48	0.66	0.82
ChanRatio	0.5	30.0	0.00	2.01	5.20	0.50	3.00	11.50
$Depth_{Soil\_EQ}$	0.0	1.5	0.14	0.68	1.40	[-]	[-]	[-]
$Depth_{GW\_EQ}$	0.0	1.5	0.05	0.55	1.13	[-]	[-]	[-]
PE_{Soil}	0.0	2.5	0.00	1.10	1.70	[-]	[-]	[-]
K_M	1.0	2.0	[-]	[-]	[-]	1.00	1.17	1.50
X_M	0.0	0.5	0.00	0.19	0.40	0.00	0.20	0.44

Temporal uncertainty assessment of the simulation results was conducted to obtain an estimate of the confidence of the simulated flow, $\delta^{18}O$, and estimated source components. Uncertainty was calculated as the normalized difference between the 5th and 95th percentiles, then standardized between 0 (least uncertainty) and 1 (most uncertainty) for direct comparison between stream components independent of volume (Figure 4-6). The average daily uncertainties for flow, $\delta^{18}O$, and source components are presented for each basin (Figure 4-6a, g). Interannual uncertainty is presented for daily simulated flow (Figure 4-6b, h), $\delta^{18}O$ (Figure 4-6c, i), soil contribution (Figure 4-6d, j), groundwater contribution (Figure 4-6e, k), and wetland contribution (Figure 4-6f, l).

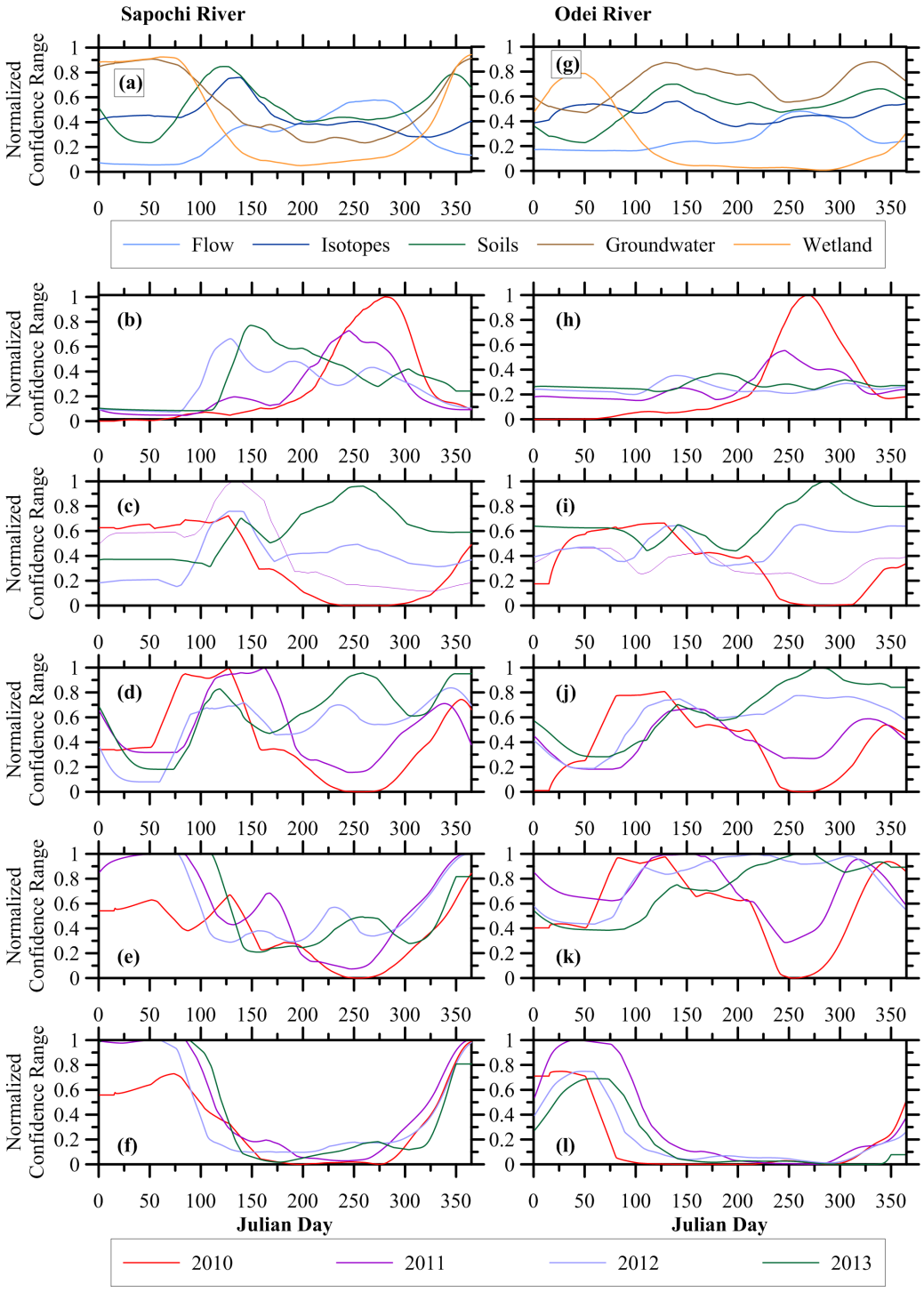

Figure 4-6. Uncertainty values for the Sapochi River showing the uncertainty of (a) the mean daily confidence interval range, and interannual comparisons of (b) flow, (c) $\delta^{18}O$, (d) soil, (e) groundwater, and (f) wetland flow contributions. Uncertainty values for the Odei River are on the right of the figure, (g) mean daily confidence interval range, and interannual comparisons of (h) flow, (i) $\delta^{18}O$, (j) soil, (k) groundwater, and (l) wetland flow contributions for each simulation year (2010–2013). Uncertainty varies from low (0) to high (1).

Annually, distinct differences in uncertainties of flow, $\delta^{18}O$, and flow components were calculated for the Sapochi River simulations (Figure 4-6a). The greatest uncertainties were observed for the groundwater and wetland contributions, beginning during the fall and continuing through to the beginning of the freshet. This coincides with the period when groundwater and wetland contribution to streamflow was highest, and when these components were flushing excessively enriched soil water from the system. Uncertainty in estimated groundwater and wetland contributions decreased during the spring and summer months. Conversely, the soil contribution and isotopic simulations experienced their maximum average daily uncertainty during the freshet, and flow uncertainty peaked in late summer. The most distinct variability in interannual uncertainty was reported for flow (Figure 4-6b). Highest uncertainty was consistently reported during peak flow events, in particular 2010, the first year of simulation (likely attributable to model spin up). The $\delta^{18}O$ and soil water contributions (Figure 4-6c, d) also experienced substantial interannual variability in maximum uncertainty. For each of these simulated components, the increase in uncertainty was directly related to rapid changes in simulated data (flow, $\delta^{18}O$, and soil contribution). For flow and soil water contribution, these rapid changes typically resulted from precipitation. However, during the last two simulation years (2012–2013), large late season precipitation events did not affect the uncertainty of flow, but instead increased $\delta^{18}O$, and soil and groundwater contribution percent (Figure 4-6b–d). These two years corresponded to the two years with the least summer rainfall (Table 4-2), indicating a threshold response in the system. Uncertainties in $\delta^{18}O$ and soil contribution increased as precipitation decreased, which indicated that uncertainty was strongly dependent on water held in storage. Temporal variation in uncertainty of simulated $\delta^{18}O$ and soil contribution was strongly linked, indicating the dependence of $\delta^{18}O$ stream composition on soil water

composition.

Similar to the Sapochi River, highest average daily uncertainty in the Odei River was reported for wetland contribution during the winter months (Figure 4-6g). However, uncertainties of the other components (flow, $\delta^{18}O$, soil, and groundwater contributions) were relatively consistent through the year. Soil and groundwater contributions had the next highest average daily uncertainty, highest during the spring freshet. Interannually, the greatest uncertainties in flow occurred during the first simulation year (largest peak flow event in August), followed by the second year (second largest peak flow event in July). However, the timing of these uncertainties did not translate to uncertainty in $\delta^{18}O$, soils, groundwater, or wetland contribution. During 2012 and 2013, a late summer precipitation event coincided with high uncertainty in $\delta^{18}O$, soil water, and groundwater contribution, likely the result of large contributions from multiple sources and rapid change in flow. Despite the higher identifiability of the groundwater release parameter for the Odei relative to the Sapochi River (Table 4-5), uncertainty in the percentage contribution of groundwater was generally higher in the Odei River than the Sapochi River.

Rapid changes in flow generally corresponded to increased uncertainty in source components. Rapid increases in flow coincided with rapid increases in soil contribution uncertainty. Conversely, rapid decreases in flow coincided with rapid increases in wetland and groundwater contribution uncertainty, although for groundwater in the Odei River this relationship was limited to late fall and winter flows. The strong dependence of uncertainty between $\delta^{18}O$ and source component indicated $\delta^{18}O$ uncertainty originated from the storage. Both basins exhibited the strongest dependence of $\delta^{18}O$ uncertainty on soil contribution.

4.6 DISCUSSION

4.6.1 UNDERSTANDING THE HYDRODYNAMICS OF TWO BASINS

Obtaining detailed understanding of streamflow sources in large (>300km^2) remote areas such as the Odei and Sapochi River basins is complicated by challenges in data collection at adequate spatial and temporal resolutions. Hence, modelling studies provide unique opportunities to enhance hydrodynamic understanding in such catchments. Tracers such as stable water isotopes that integrate responses across time and space aid in quantification of streamflow sources and impacts of physiographic features such as wetlands (Klaus and McDonnell 2013; Tetzlaff et al., 2014) in ways not possible with stream hydrometric measurements alone (Rice and Hornberger 1998). Previous studies that used iso-hydrologic models to quantify streamflow sources have tended to focus on events, short periods, or small (in the Canadian context) catchments (Klaus and McDonnell 2013). In this study, we used an iso-hydrologic model to estimate streamflow and isotopic composition, and subsequently separate streamflow source components for a four-year period that encompassed a variety of climatic conditions.

Model results indicated that streamflow source components varied seasonally and interannually as demonstrated in localized field studies in boreal regions (Tetzlaff et al., 2014). Seasonal variability in contributions was predominantly a function of the timing of precipitation during the study period. High summer rainfall translated into high soil water contributions, and large percentage wetland contributions in the following fall and winter. This is consistent with the understanding of hydrological function of wetlands in boreal catchments, increasing connectivity and streamflow contribution once storage thresholds are filled (Spence et al., 2011). Conversely, low summer rainfall resulted in a greater percentage contribution of groundwater in fall and winter.

4.6.2 INTERPRETING THE UNCERTAINTY OF SIMULATED FLOW, ISOTOPES, AND SOURCES

The uncertainty associated with the simulation results is of significant importance to the interpretation of the model results, because all hydrologic models are simplifications of the physical world (Beven 2013). Our model results exhibited greatest uncertainty when rapid change in flow or isotopic composition occurred. For flow, this was consistently the peak flow event of the season, regardless of whether or not the event was generated by rainfall or snowmelt. Rapid change in isotopic composition occurred during spring snowmelt. These results are consistent with previous catchment assessments that combined flow and tracers (Seibert and McDonnell 2002; Birkel et al., 2010) and relate to the increased number of components that contribute to streamflow, or are active, during high flows.

Improving understanding of flow processes during large events is critical because of potential impacts on operational decisions, and the probability that such events will increase because of climate change in this region. Recent advances in iso-hydrologic models have demonstrated the ability to improve understanding of flow generation mechanisms through incorporation of measurements of internal state variables in addition to measurements at the catchment outlet (Birkel et al., 2014). However, implementation and operation of dense monitoring networks remain impractical in large catchments in hostile environments such as the remote regions of northern Manitoba, Canada. The ability to quantify uncertainty in internal processes through broadscale measurement is therefore limited. The modelling approach presented in this paper, where uncertainty assessment of streamflow components was based on multiple realizations and catchment outlet data, provides a feasible alternative. Results can then be strategically used to design field investigations that target specific temporal periods and processes, or structurally modify models where simplified or absent processes appear to be

affecting results (Capell et al., 2012). Large uncertainties identified during snowmelt periods suggest that additional data and or more physically based snowmelt estimation and representation of the freeze/thaw cycle of soils would be beneficial in the catchments studied. Additional uncertainties, including over-enrichment of the soil water during the summer months, suggest that fractionation likely does not occur as much as estimated by the model. Reducing simulated fractionation may be achieved by splitting evapotranspiration into its components (evaporation and transpiration) and not fractionating water that is transpired. While the timing of events of high uncertainty was similar for both basins, uncertainty was lower overall in the Odei River. This is likely because of physiographic differences between the basins, including slope, land cover, and basin size. In particular, preliminary assessment indicates a larger percentage of disconnected wetlands within the Sapochi River basin. These wetlands may influence peak flow events by adding more flow once storages are full, affecting the uncertainty and isotopic composition of the surface waters (Spence 2007). Explicit inclusion of the connection status of wetlands is therefore also likely to improve simulation results and reduce uncertainty in the estimate of wetland contribution.

In addition to model structural uncertainty, input data can contribute to uncertainty in model results (McDonnell et al., 1990). In the current model, groundwater and precipitation input isotopic compositions were held constant because of the absence of reliable long-term, spatially distributed, datasets across all seasons and basins. Variability in the limited groundwater dataset reflects the shallow installation depth in peat that resulted in mixing of soil water and groundwater. This conclusion was supported by the seasonal trends observed that indicate mixing with snowmelt in spring, and mixing with precipitation in summer and fall. Furthermore, the stream composition approached steady-state during late summer and fall at a

composition between enriched soil and wetland waters, and a more depleted, stable, source. The depleted source is indicative of a deeper groundwater source not captured by the shallow piezometer, which experiences minor temporal variability, and reflects recharge dominated by snow melt over the long-term (Abbott et al., 2000; O'Driscoll et al., 2005; Peralta-Tapia et al., 2015). Consequently, reduction in uncertainty is most likely to be achieved by implementing time-varying precipitation composition in the model and calculating groundwater composition rather than specifying a constant value or time-varying function. Inclusion of temporally varying isotopes in precipitation may additionally help reduce the excessive amount of fractionation simulated in soil water, and subsequent low flow isotopic uncertainty, through the direct addition of more enriched water in late summer and fall. Recently developed methods for empirical estimation of precipitation isotopes across North America (Delavau et al., 2015) will facilitate such an approach in future modelling endeavours.

4.7 CONCLUSIONS

This study has explored the use of iso-hydrologic modelling in sparsely gauged headwater basins to identify the primary sources of streamflow and estimate the uncertainty of each source. Temporal changes to streamflow sources and uncertainties were examined under a variety of climatic conditions. First order estimates of contributions (soil, ground, and wetland water) varied considerably between seasons. Key periods of change were the spring freshet (transition from groundwater and wetland dominated to soil water dominated) and freeze-up (transition from soil water dominated to groundwater and wetland dominated). Interannual variability of wetland and groundwater streamflow contributions during the fall and winter were linked to the presence or absence of summer precipitation events. High precipitation during late summer resulted in greater wetland contribution during fall and winter, whereas low precipitation led to

greater groundwater contribution. The degree of uncertainty in streamflow source was linked to rapid changes in streamflow; the highest uncertainty for all sources typically occurred during the spring freshet and the largest annual precipitation event. Qualitative assessment of streamflow source uncertainty has been shown to be a useful tool for improving the understanding of behavioural responses in remote basins that do not have dense monitoring networks. The tracer-aided modelling identified the significance of evaporative fractionation within the headwater catchments, however a static isotopic partition yielded high streamflow uncertainty despite low uncertainty of source contribution. Furthermore, high uncertainty of source components during peak events (snowmelt and precipitation) indicates additional rapid flow paths are present, separate from soil waters, and unlikely to be influenced significantly by evaporative fractionation due to the relatively short period they remain in the watershed.

4.8 ACKNOWLEDGEMENTS

The authors acknowledge Manitoba Hydro and Water Survey of Canada for funding isotope collection and analysis and maintenance of on-site equipment. Additional project funding was provided by the Natural Sciences and Engineering Research Council (NSERC) of Canada Collaborative Research and Development Grant. Aaron Smith acknowledges a Tri-council Award from the University of Manitoba, and Postgraduate Scholarship-Doctoral Program (PGS-D) from NSERC. We would also like to thank our reviewers Christian Birkel and Christine Stumpp for their constructive comments that greatly improved the clarity of the manuscript.

4.9 REFERENCES

Abbott, M.D., Lini, A., Bierman, P.R. 2000. $\delta^{18}O$, δD and ^{3}H measurements constrain groundwater recharge patterns in an upland fractured bedrock aquifer, Vermont, USA. *Journal of Hydrology,* **Volume 228(1)**: 101–112.

Atlas of Canada. 2014. Natural Resources Canada: The North. [Online] Available at:

http://atlas.gc.ca/site/english/maps/thenorth.html#physicalgeography [Accessed 2014].

Beven, K. 2013. So how much of your error is epistemic? Lessons from Japan and Italy. *Hydrological Processes,* **Volume 27**: 1677–1680.

Birkel, C., Dunn, S.M., Tetzlaff, D., Soulsby, C.. 2010. Assessing the value of high- resolution isotope tracer data in the stepwise development of a lumped conceptual rainfall–runoff model. *Hydrological Processes,* **Volume 24**: 2335–2348.

Birkel, C., Soulsby, C., Tetzlaff, D. 2014. Developing a consistent process- based conceptualization of catchment functioning using measurements of internal state variables. *Water Resources Research*, **Volume 50(4)**: 3481-3501. DOI:10.1002/ 2013WR014925.

Birkel, C., Tetzlaff, D., Dunn, S.M., Soulsby, C. 2011. Using lumped conceptual rainfall–runoff models to simulate daily isotope variability with fractionation in a nested mesoscale catchment. *Advances in Water Resources,* **Volume 34(3)**: 383–394.

Bohrn, S.K. 2012. Climate change impact assessment and uncertainty analysis of the hydrology of a northern, data-sparse catchment using multiple hydrological models. University of Manitoba: Winnipeg.

Brock, B., Wolfe, B., Edwards, T. 2007. Characterizing the hydrology of shallow floodplain lakes in the slave river delta, NWT, Canada, using water isotope tracers. *Arctic, Antarctic, and Alpine Research,* **Volume 39(3)**: 388–401.

Capell, R., Tetzlaff, D., Soulsby, C. 2012. Can time domain and source area tracers reduce uncertainty in rainfall–runoff models in larger heterogeneous catchments? *Water Resources Research,* **Volume 48**: W09544-1-19. DOI:10.1029/2011WR011543.

Carey, S., Boucher, J.L., Duarte, C.M. 2013. Inferring groundwater contributions and pathways to streamflow during snowmelt over multiple years in a discontinuous permafrost subarctic environment (Yukon, Canada). *Hydrogeology Journal,* **Volume 21**: 67–77.

Delavau, C., Chun, K.P., Stadnyk, T.A., Birks, S.J., Welker, J.M. 2015. North American precipitation isotope zones revealed in time series modeling across Canada and northern United States. *Water Resources Research*, **Volume 51(2)**: 1284-1299. DOI:10.1002/2014WR015687.

Ecoregions Working Group. 1989. Ecoclimatic regions of Canada, first approximation (plus map at 1:750,000). Environment Canada: Ottawa. Environment Canada. 2014. Hydrometric data. [Online] Available at: http://www.wsc.ec.gc.ca/applications/H2O/index-eng.cfm?stype=location [Accessed 2014].

GeoBase. 2014. [Online] Available at: http://www.geobase.ca/geobase/en/ [Accessed 2014].

Gibson, J. 2002. Short-term evaporation and water budget comparisons in shallow Arctic lakes

using non-steady isotope mass-balance. *Journal of Hydrology,* **Volume 264**: 242–261.

Gibson, J.J., Prepas, E.E., McEachern, P. 2002. Quantitative comparison of lake throughflow, residency, and catchment runoff using stable isotopes: modelling and results from a regional survey of Boreal Lakes. *Journal of Hydrology,* **Volume 262(1)**: 128–144.

Hayashi, M., Quinton, W.L., Pietroniro, A., Gibson, J.J. 2004. Hydrologic functions of wetlands in a discontinuous permafrost basin indicated by isotopic and chemical signatures. *Journal of Hydrology,* **Volume 296(1)**: 81–97.

Hrachowitz, M., Savenije, H.J., Blöschl, G., McDonnell, J.J., Sivapalan, M., Pomeroy, J.W., Cudennec, C. 2014. A decade of Predictions in Ungauged Basins (PUB)—a review. *Hydrological Sciences Journal,* **Volume 58(6)**: 1198–1255.

ISEE Systems. 2015. Stella: systems thinking for education and research. [Online] Available at: http://www.iseesystems.com/softwares/Education/StellaSoftware.aspx [Accessed 2015].

Juston, J.M., Kauffeldt, A., Quesada Montano, B., Siebert, J., Beven, K.J., Westerberg, I.K. 2013. Smiling in the rain: seven reasons to be positive about uncertainty in hydrological modelling. *Hydrological Processes,* **Volume 27**: 1117–1122.

Klaus, J., McDonnell, J.J. 2013. Hydrograph separation using stable isotopes: review and evaluation. *Journal of Hydrology,* **Volume 505**: 47–64.

Lee, E.S., Krothe, N.C. 2001. A four-component mixing model for water in a karst terrain in south-central Indiana, USA. Using solute concentration and stable isotopes as tracers. *Chemical Geology,* **Volume 179**: 129–143.

Manitoba Hydro. 2014. Generating stations. [Online] Available at: http://www.hydro.mb.ca/corporate/facilities/generating_stations.shtml [Accessed January 2014].

McDonnell, J.J., Bonell, M., Stewart, M.K., Pearce, A.J. 1990. Deuterium variations in storm rainfall: implications for stream hydrograph separation. *Water Resources Research,* **Volume 26(3)**: 455–458.

McKenna, S.A., Ingraham, N.L., Jacobson, R.L., Cochran, G.F. 1992. A stable isotope study of bank storage mechanisms in the Trunkee river basin. *Journal of Hydrology,* **Volume 134**: 203–219.

Merot, P., Durand, P., Morisson, C. 1995. Four-component hydrograph separation using isotopic and chemical determinations in an agricultural catchment in Western France. *Physics and Chemistry of the Earth,* **Volume 20(3)**: 415–425.

Metcalfe, R.A., Buttle, J.M. 2001. Soil partitioning and surface store controls on spring runoff from a boreal peatland basin in north-central Manitoba, Canada. *Hydrological Processes,* **Volume 15(12)**: 2305–2324.

Mountain, N., James, A.L., Chutko, K. 2015. Groundwater and surface water influences on streamflow in a mesoscale Precambrian Shield catchment. *Hydrological Processes,* **Volume 29(18)**: 3941–3953.

Nash, J.E., Sutcliffe, F.V. 1970. Fiver flow forecasting through conceptual models: part 1—a discussion of principles. *Journal of Hydrology,* **Volume 10**: 282–290.

O'Driscoll, M.A., DeWalle, D.R., McGuire, K.J., Gburek, W.J. 2005. Seasonal 18O variations and groundwater recharge for three landscape types in central Pennsylvania, USA. *Journal of Hydrology,* **Volume 303(1)**: 108–124.

Peralta-Tapia, A., Sponseller, R.A., Tetzlaff, D., Soulsby, C., Laudon, H. 2015. Connecting precipitation inputs and soil flow pathways to stream water in contrasting boreal catchments. *Hydrological Processes,* **Volume 29(16)**: 3546–3555.

Rice KC, Hornberger GM. 1998. Comparison of hydrochemical tracers to estimate source contributions to peak flow in a small, forested, headwater catchment. *Water Resources Research,* **Volume 34(7)**: 1755–1766.

Ritter, A., Munoz-Carpena, R. 2013. Performance evaluation of hydrological models: statistical significance for reducing subjectivity in goodness-of-fit assessments. *Journal of Hydrology,* **Volume 480**: 33–45.

Roulet, N.T., Woo, M. 1986. Hydrology of a wetland in the continuous permafrost region. *Journal of Hydrology,* **Volume 89**: 73–91.

Schwartz, F.W., Zhang, H. 2003. Fundamentals of Ground Water. John Wiley & Sons Inc.

Seibert, J., McDonnell, J.J. 2002. On the dialogue between the experimentalist and modeler in catchment hydrology: use of soft data for multi-criteria model calibration. *Water Resources Research,* **Volume 38(11):** 1241–1255.

Simpson, H.J., Herczeg, A.L. 1991. Stable isotopes as an indicator of evaporation in the River Murray, Australia. *Water Resources Research,* **Volume 27(8)**: 1925–1935.

Sklash, M.G., Farvolden, R.N., Fritz, P. 1976. A conceptual model of watershed response to rainfall, developed through the use of oxygen- 18 as a natural tracer. *Canadian Journal of Earth Sciences,* **Volume 13(2)**: 271–283.

Smith, A.A., Delavau, C.J., Stadnyk, T.A. 2015. Hydrologic assessment of the Lower Nelson River Basin using stable water isotope investigations. *Canadian Water Resource Journal,* **Volume 40(1)**: 23–35.

Spence, C. 2007. On the relation between dynamic storage and runoff: a discussion of thresholds, efficiency, and function. *Water Resources Research*, **Volume 43(12)**: W12416-1-11. DOI:10.1029/2006WR005645.

Spence, C., Guan, X.J., Phillips, R. 2011. The hydrological functions of a boreal wetland.

Wetlands, **Volume 31**: 75–85.

Spence, C., Whitfield, P.H., Pomeroy, J.W., Pietroniro, A., Burn, D.H., Peters, D.L., St-Hilaire, A. 2013. A review of the Prediction in Ungauged Basins (PUB) decade in Canada. *Canadian Water Resource Journal,* **Volume 38(4)**: 253–262.

St. Amour, N., Gibson, J., Edwards, T., Prowse, T. 2005. Isotopic time-series partitioning of streamflow components in wetland-dominated catchments, lower Liard River basin, Northwest Territories, Canada. *Hydrological Processes,* **Volume 19(17)**: 3357–3381.

Stadnyk, T.A., Delavau, C.J., Kouwen, N., Edwards, T.W.D. 2013. Towards hydrological model calibration and validation: simulation of stable water isotopes using the isoWATFLOOD model. *Hydrological Processes,* **Volume 27(25)**: 3791–3810.

Tetzlaff, D., Buttle, J., Carey, S.K., McGuire, K., Laudon, H., Soulsby, C. 2014. Tracer-based assessment of flow paths, storage and runoff generation in northern catchments: a review. *Hydrological Processes*, **Volume 29(16)**: 3475-3490. DOI:10.1002/ hyp.10412.

Vache, K.B., McDonnell, J.J. 2004. On the use of multiple criteria for a posteriori model rejection: soft data to characterize model performance. *Geophysical Research Letters,* **Volume 31**: L21504.

Wagener, T., McIntyre, N., Lees, M.J., Wheater, H.S., Gupta, H.V. 2003. Toward reduced uncertainty in conceptual rainfall–runoff modelling: dynamic identifiability analysis. *Hydrological Processes,* **Volume 17**: 455–476.

Woo, M-K, Winter, T.C. 1993. The role of permafrost and seasonal frost in the hydrology of northern wetlands in North America. *Journal of Hydrology,* **Volume 141**: 5–31.

Yip, K.K., Burn, D.H., Seglenieks, F., Peitroniro, A., Soulis, E.D. 2012. Climate impacts on hydrological variables in the Mackenzie River Basin. *Canadian Water Resources Journal,* **Volume 37(3)**: 209–230.

CHAPTER 5: ASSESSING THE SEASONALITY AND UNCERTAINTY IN EVAPOTRANSPIRATION PARTITIONING USING A TRACER-AIDED MODEL

Aaron Smith[1,2], Chani Welch[1], Tricia Stadnyk[1]

[1]Department of Civil Engineering, University of Manitoba, Winnipeg, Manitoba

[2]Department of Geosciences, University of Aberdeen, Aberdeen, UK

This manuscript has been submitted to Journal of Hydrology

This chapter examines a novel method for partitioning evapotranspiration on a watershed scale using the stable isotopes of $\delta^{18}O$ and $\delta^{2}H$ of streamflow and groundwater in data scarce northern catchments. A combination of hydrograph separation techniques and tracer-aided modelling are used to calibrate a multi-step optimisation with a multi-objective function with the objective of quantifying the isotopic evaporation enrichment relative to total evapotranspiration in sub-surface storage.

CHAPTER 5

5.1 ABSTRACT

Evapotranspiration (ET) partitioning is a growing field of research in hydrology due to the significant fraction of watershed water loss it represents. The use of tracer-aided models has improved understanding of watershed processes, but few tracer-aided models have focused on time-variable partitioning of evaporation (E) from ET. A tracer-aided model was used to establish a time-series of E/ET using differences in riverine $\delta^{18}O$ and $\delta^{2}H$ and air temperature within four northern Canadian watersheds (lower Nelson River, Manitoba, Canada). On average E/ET follows a parabolic trend ranging from 0.7 in the spring and fall to 0.15 during the growing season for three of the basins, and 0.5 for the growing season in the fourth basin where wetlands and shrubs dominate land cover. During the summer, E/ET ratios were highest for wetlands for three watersheds (10% higher than unsaturated soil storage), while lowest for the fourth watershed (20% lower than unsaturated soil storage). Uncertainty of the ET partition parameters is strongly influenced by storage volumes, with large storage volumes increasing partition uncertainty. In additional, higher simulated soil moisture increases estimated E/ET. Although unsaturated soil storage accounts for larger surface areas in these watersheds than wetlands, riverine isotopic composition is more strongly affected by evaporation from wetlands. Comparisons of E/ET to measurement-intensive studies in similar ecoregions indicate the methodology proposed here is a useful means of partitioning ET in seasonal, data sparse, regions.

CHAPTER 5

5.2 INTRODUCTION

Evaporation and transpiration are intricately linked components of the water cycle that affect water availability in watersheds worldwide. Large changes in water abundance due to climate change may affect both vegetation (growth and type) and storage (Sugimoto et al., 2002). In mid- to high-latitude watersheds, increasing temperatures are likely to increase storage, lengthen growing seasons, and increase evapotranspiration rates (Woo 1992); however, these changes will unequally affect the timing and relative rates of evaporation and transpiration (Calanca et al., 2006; Abtew and Melesse 2013). This is problematic for hydrologic models in which evaporation and transpiration are commonly simulated as a single lumped component, evapotranspiration (ET). Hydrologic models are required to effectively manage water, particularly in data sparse regions when water usage plans are dependent on estimations of specific flow pathways. Consequently, partitioning ET into its components in hydrologic models is essential to appropriately capture the effects of climate change on water availability.

Energy balance methods can be used to separate ET into its components when one of the components (evaporation or transpiration) is observed. Bowen Ratio Energy Balance (BREB) methods infer evaporation and ET flux from radiation, heat, and temperature measurements at different levels above the surface (Ashktorab et al., 1994; Zhang et al., 2002; Scott et al., 2006). Measurements show seasonal and diurnal patterns in the ET partition are closely related to soil moisture, antecedent precipitation and vegetation (Ashktorab et al., 1994; Zhang et al., 2002; Scott et al., 2006). The required measurements are data intensive and limited to smaller field scales. To reduce measurement intensity, evaporation and transpiration have also been estimated using atmospheric and vegetation parameters (Shuttleworth and Wallace 1985; Lascano et al., 1987; Daamen and Simmonds 1996), soil moisture and flux (Simunek et al., 2008) and soil

surface temperature (Moran et al., 2009). Despite less intensive measurements, such methods remain impractical for application in large-scale hydrologic models because data required for these methods are not readily available.

The stable water isotopes oxygen-18 ($\delta^{18}O$) and deuterium ($\delta^{2}H$) provide an alternative method for evaporation and transpiration estimation, partitioning ET using the fractionating evaporative flux (Yepez et al., 2003; Zhang et al., 2010; Sutanto et al., 2012; Hu et al., 2014). This method combines a mass-balance approach with measurement of the isotopic composition of ET (δ_{ET}), transpiration as xylem/leaf water (δ_x, δ_T), evaporative vapor (δ_E), and the rate of ET flux. The partition is estimated by rearranging the mass-balance to solve for evaporation and transpiration components separately. Regardless of flux measurement, the approach requires isotopic compositions for ET, evaporation, and transpiration. In attempts to reduce measurements, models have been developed to estimate the isotopic composition of evaporation (Craig and Gordon 1965), transpiration (Farquhar and Cernusak 2005; Hu et al., 2014), and ET (Yepez et al., 2003; Williams et al., 2004). Transpiration models have used leaf parameters (Farquhar and Cernusak 2005) and measured compositions (xylem and soil vapour). ET compositions have been estimated using the Keeling plot (Keeling 1961) and vapour isotopic compositions (δ_v). The application of the mass-balance ET partitioning method is dependent on availability of data, and generally not feasible at meso- or macro-scales since it would require significant instrumentation and sample collection.

In macro-scale watersheds, ET has been partitioned on long-term data sets using stable isotope measurements of surface water. Jasechko et al. (2013) applied long-term watershed-scale mass-balances worldwide to assess spatial differences in the annual average partition. Transpiration flux was identified using measurements of discharge and precipitation flux with

isotopic compositions of river, precipitation, and steady-state soil and groundwater. Transpiration composition was inferred from groundwater composition by assuming root-uptake is non-fractionating (Ehleringer and Dawson, 1992). Good et al. (2015) partitioned ET on an annual average basis using continental runoff and atmospheric mass-balance with oceanic waters. To identify the large-scale influence of transpiration on groundwater storage, Evaristo et al. (2016) assumed the long-term xylem composition was equivalent to the intercept of $\delta^{18}O$ and $\delta^{2}H$ on the local meteoric water line. Lastly, a recent large-scale study on the Tibetan Plateau has used high temporal resolution stream water to partition ET with hydrograph separation (Guo et al., 2017). However the majority of these methods do not account for temporal variability (Evaristo et al., 2015; Good et al., 2015; Jasechko et al., 2013) or require significant isotopic sampling (Guo et al., 2017), and, therefore, have limited application to hydrologic models and high-latitude regions in data scarce regions.

The goal of this study is to develop a temporally variable ET partition model requiring only precipitation and riverine compositions of $\delta^{18}O$ and $\delta^{2}H$ as inputs that is suitable for implementation in operational tracer-aided hydrologic models. The ET partitioning model is developed in three steps: first by simulating riverine isotopic composition assuming ET = T in unsaturated soil storage and wetland storage; second by conducting hydrograph separation on the difference between simulated isotopic composition in storage and the observed riverine isotopic composition to determine the required enrichment; and thirdly, by developing an empirical relationship between the required enrichment and air temperature. Application of the empirical model to four northern Canadian watersheds over a multi-year period identifies the temporal variability of ET in these watersheds.

5.3 SITE DESCRIPTION AND DATA COLLECTION

The study watersheds are located on the Canadian Shield in central-northern Manitoba, Canada (above 50°N, Figure 5-1). Four watersheds were selected based on geographic location, physiographic differences (land cover), and the availability of isotopic and discharge data. The areas of the watersheds span the meso-scale spectrum from small (410 km^2) to large (6,109 km^2, Table 5-1). The Sapochi River is a southern tributary of the Odei River.

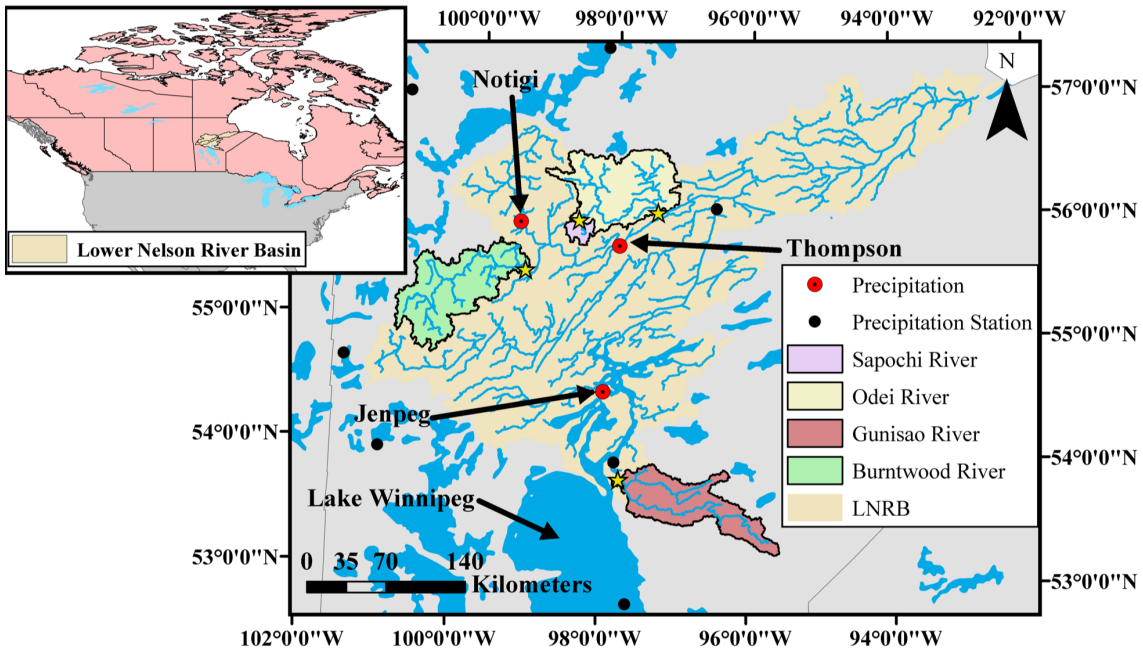

Figure 5-1. The locations of the Sapochi, Odei, Gunisao, and Burntwood River basins within the Lower Nelson River basin. River discharge/isotopic sampling locations (yellow stars), precipitation/groundwater isotopic sampling at corresponding meteorological locations (red circles), and additional meteorological stations (black circles) are also shown.

Table 5-1. Watershed characteristics. Watershed areas are delineated upstream of the sampling location (indicated by coordinates). Average basin slope was determined from a digital elevation model at 30 m resolution (USGS 2016). Surficial geology includes percentages of clay (C), rock (R), till (T), and organic (O) material. Major land cover classes for each watershed were obtained from Geobase (Geobase 2016).

		Sapochi River	Gunisao River	Burntwood River	Odei River
Watershed Area (km^2)		423.2	4409.6	5744.1	6109.3
Latitude		55°54'31"N	53°49'22"N	55°29'44"N	55°59'44"N'
Longitude		98°29'31"W	97°46'29"W	99°13'16"W	97°21'14"W
Average Basin Slope		3.2%	2.2%	4.0%	2.7%
Surficial Geology (C/R/T/O)		51/24/2/23	32/39/0/29	30/47/18/5	59/13/8/20
Land Cover (%)	**Water**	3.7	8.2	11.4	9.5
	Shrub	37.2	15.6	20.7	28.8
	Connected Wetland	11.8	43.5	19.2	14.5
	Disconnected Wetland	9.2	4.9	3.8	7.1
	Broadleaf	12.5	0.1	14.0	9.8
	Conifer	24.6	27.4	29.6	29.9

5.3.1 CLIMATE

The climate of all watersheds is continental sub-arctic. July and August are the wettest months with an average 178 mm – 203 mm of rainfall. Most snowfall occurs in November and March (42 mm – 52 mm total snow water equivalent). Warmer temperatures in transition months (April, May and October) result in mixed liquid/solid precipitation events (29% - 91% monthly rain/precipitation). Approximately one third of annual precipitation is received as snow (Table 5-2, Environment Canada 2016a). Large differences in annual precipitation occur between watersheds, primarily due to differences in snowfall (Table 2). The North American Regional Reanalysis (NARR) and Canadian Precipitation Analysis (CaPA) precipitation values are relatively similar within the Burntwood River to the measurements at Flin Flon, the closest measurement location.

Table 5-2. Climate data for study watersheds. Closest watersheds to each meteorological station and elevation are provided (Environment Canada 2016a; NARR 2016).

Watershed	Odei River	Gunisao River		Burntwood River	
Closest Meteorological Station	Thompson Airport	Cross Lake – Jenpeg	Norway House	Flin Flon	NARR and CaPA
Latitude	55°48'12"	54°32'00"	53°57'00"	54°46'00"	N/A
Longitude	97°51'45"	98°02'00"	97°51'00"	101°53'00"	N/A
Elevation (m.a.s.l.)	224	218.8	223.7	320	N/A
Mean Temperature (°C)	-2.9A	-0.4C	-0.7C	1.0A	1.2
Mean Precipitation (mm)	509.2A	469.4D	532.3C	457.6C	487.8
Mean Rainfall (mm)	340.2A	349.9D	375.8C	344.5C	385.5
Snow Water Equivalent (mm)	169	119.5	156.5	113.1	102.3
Relative Humidity (0600H) (%)	79.3	N/A	72.7	N/A	76.0

*A indicates >30 years of data (WMO 3 and 5 rule), B indicates >25 years of data, C indicates >20 years of data, D indicates >15 years of data

5.3.2 LAND COVER AND SURFICIAL GEOLOGY

Relatively flat topography results in a landscape with high open water and wetland percentages, including headwater lakes, in-stream lakes, and connected and disconnected wetlands (Table 5-1). The percentage of wetlands, shrubs, and broadleaf forest differentiate the catchments. The Gunisao River basin is the most distinct of the basins; here, high percentages of shrub and broadleaf forests present in other watersheds are replaced by wetlands. In all basins, wetlands are a mixture of trees, shrubs, open water, and peat moss. Field surveys indicate that peat moss is also present in at least some areas designated as forest.

Silt, till, clay, and organic materials are the dominant soil types of the watersheds, and are underlain by Precambrian bedrock (GeoBase 2016). The proportion of each soil type spatially varies within each watershed due to physiographic features (e.g., distance from Lake Winnipeg and topographic slope) and depositional processes. The depth of soil to bedrock is spatially

variable within and between watersheds, ranging from zero (exposed bedrock) to greater than 18 m (Flynn et al., 2016).

5.3.3 SAMPLE COLLECTION AND ANALYSIS

River water samples were collected from the watershed outlets of the Gunisao and Burntwood Rivers beginning in 2010, and Sapochi and Odei Rivers in 2011. Grab samples were collected from shore approximately 30 cm below the water surface using a retractable sampling pole. Site accessibility limited sample collection frequency; however, samples encompassed high and low precipitation years. Precipitation samples were collected as composite samples at Thompson Service Center, Jenpeg Generating Station, and Notigi Control Structure on average 12, 5 and 6 times per year, respectively. Groundwater samples were collected at the same locations 22, 5, and 4 times per year respectively. Details of the sampling program are presented in Smith et al. (2016). All water samples were analyzed for $\delta^{18}O$ and $\delta^{2}H$ using a mass spectrometer by InnoTech Alberta, and compared to Vienna Standard Mean Ocean Water 2 (VSMOW2) with precision of ± 0.2 per mille (‰) for $\delta^{18}O$ and ± 1 ‰ for $\delta^{2}H$.

5.3.4 FLOW REGIME OF THE WATERSHEDS

The annual hydrograph is defined by two peak events: a freshet (May and June) and a late summer or early autumn rainfall peak (August and September). In almost a third of the years on record, large late season precipitation events result in discharge events larger than the freshet. The watersheds have over 20 years of daily observed discharge: Sapochi (22 years), Odei (36 years), Burntwood (30 years), and Gunisao (44 years).

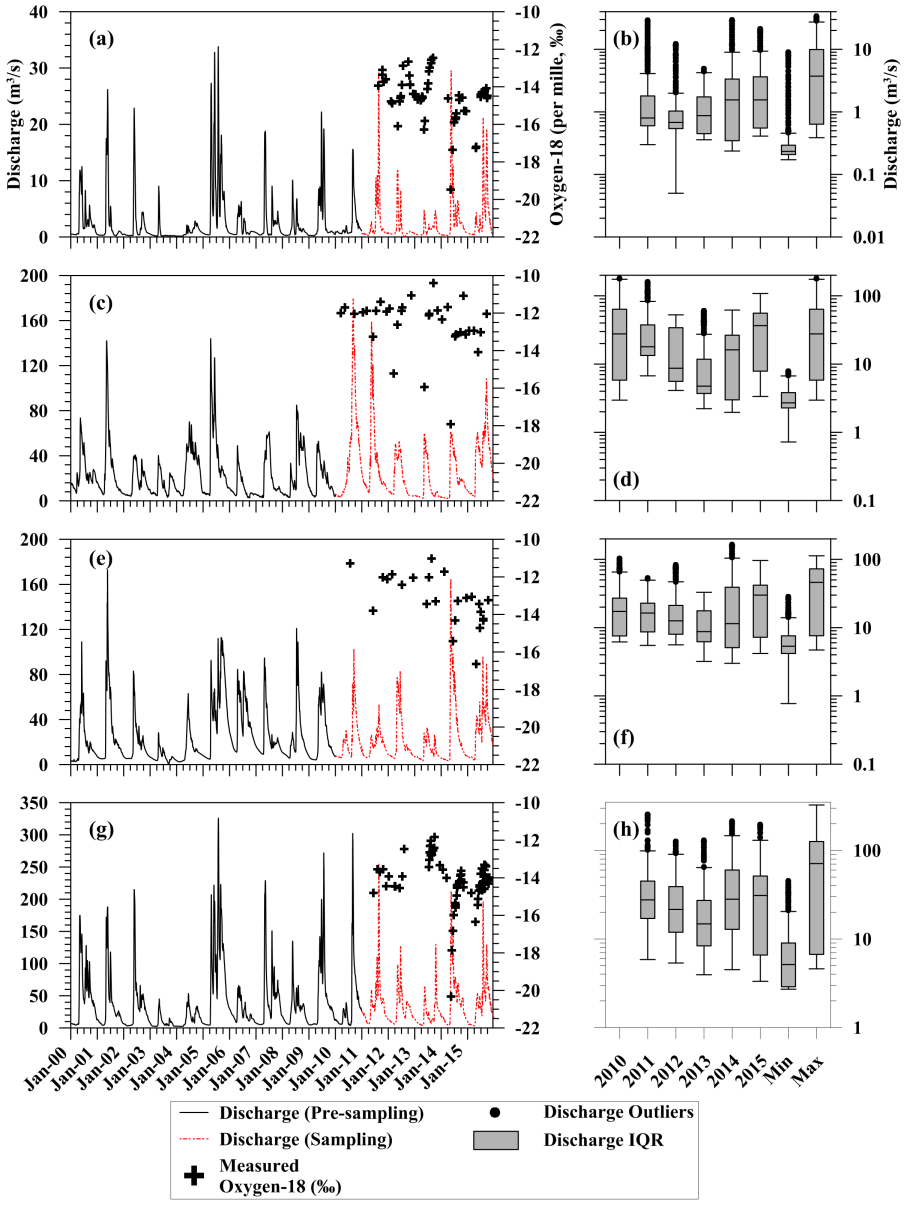

Figure 5-2. Discharge (2000-2015), and boxplots of isotope sampling years compared to historical annual maximum and minimum discharges for the a) Sapochi, b) Gunisao, c) Burntwood, and d) Odei River basins. Hydrographs are separated into isotopic sampling years (red dashed line) and non-sampling years (black solid line). The box plots represent the median, 25th, and 75th discharge percentiles, with whiskers to 1.5 times the interquartile range (IQR). Discharge measurements outside of this range are represented as points on the plots (outliers).

Three of four watersheds (Sapochi, Odei, and Burntwood River) observed their highest discharge in 2005 and lowest in 2003. Minimum and maximum discharge were observed in the Gunisao River basin in 1993 and 2010, respectively. The box plots show variability of discharge throughout the sampling years and the responsiveness of each basin to snowmelt and rainfall. The Sapochi River (Figure 5-2b) has the largest number of outliers relative to the other basins, indicating that the basin is the most responsive. This is also observed at the Odei River (Figure 5-2h), though larger basin size reduces the responsiveness. Isotopic sampling years in the Sapochi and Odei Rivers (black dots) capture average discharge variability. The Burntwood River basin (Figure 5-2f) has relatively stable annual discharge compared to the Odei River basin. Although comparable in size to the Odei River basin, the Burntwood has a greater proportion of lakes which attenuate discharge. Lastly, the Gunisao River basin (Figure 5-2d) is the least responsive, likely resulting from high wetland coverage. Relative to the Burntwood and Odei River basins (of similar size), the Gunisao River has high interannual variability of the IQR. This indicates that the Gunisao River discharge is largely dependent on annual precipitation and has shorter residence times in storage. Average discharge since 2000 has been greater than historical average, coinciding with greater than average precipitation in the region.

5.4 EVAPOTRANSPIRATION PARTITION MODEL DEVELOPMENT

Isotopic composition and discharge were simulated using the Hydrological Evapotranspiration-partition Lumped IsOtopic Simulation (HELIOS) model developed in the numerical matrix software Matlab®. HELIOS is a sub-basin lumped model that expands UMSWIM (Smith et al., 2016) by improving representation of ET and catchment storages, and incorporating δ^2H simulations. HELIOS consists of individual modules for discharge and

isotopic simulations. Specific focus on evaporative fractionation is integrated into the model structure, enriching riverine and storage compositions. Calibration of HELIOS was conducted using a multi-step approach to directly address isotopic equifinality. The first calibration removes fractionation due to evaporation from subsurface storage (not open water) to ensure storages do not simulate water more enriched than observed, as this would result in negative evaporation estimates. The resulting simulations are then assessed for 'under-enriched' water and the required enrichment to correctly estimate stream isotopic compositions. Finally, the amount of required evaporative fractionation is used to inform the ET partition model.

5.4.1 HYDROLOGIC MODULE

HELIOS has five compartments that store and release water in addition to open water storage: unsaturated soil storage, groundwater, ponded water, connected wetlands, and disconnected wetlands (Figure 5-3). Precipitation is added to HELIOS as spatially averaged daily precipitation over the watershed area. The energy balance method is used to estimate snowmelt (Equation A31 - 34) (USACE 1956). Ponded water storage receives water through rainfall and snowmelt (Figure 5-3). Infiltration of ponded water storage to unsaturated soil storage is estimated using the explicit Green-Ampt formulation (Equation A8 - A15; Salvucci and Entekhabi 1994). Unsaturated soil storage is directly connected to groundwater, connected wetlands, and channel storage (Figure 5-3).

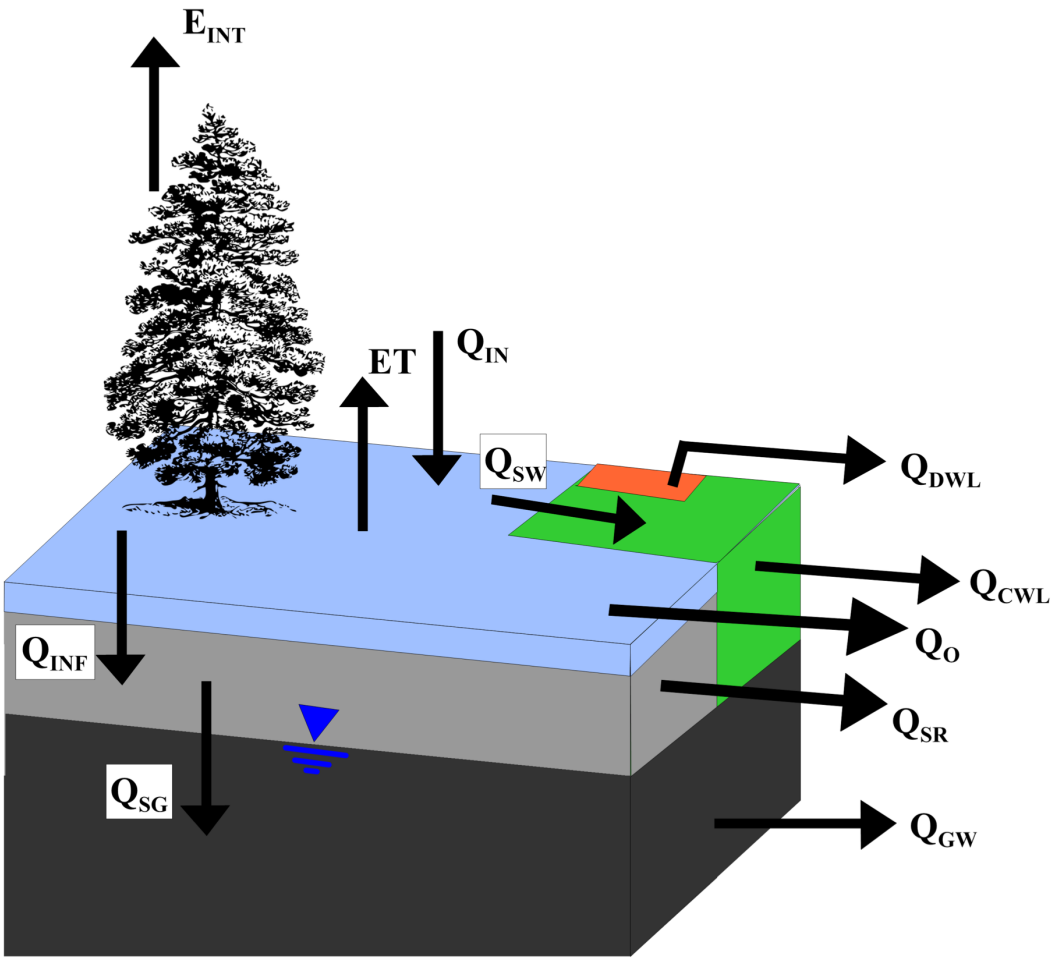

Figure 5-3. Conceptual diagram of the HELIOS model including the five storage compartments: groundwater (dark grey), unsaturated soil storage (grey), ponded water (light blue), connected wetland (green), and disconnected wetland (orange). Flux subscripts are: SG – unsaturated soil to groundwater; INF – ponded water to unsaturated soil; IN - snowmelt and rainfall; SW - unsaturated soil to connected wetlands; DWL - disconnected wetlands to channels; CWL - connected wetland to channels; O - ponded water to channels; SR – unsaturated soil to channels, and GW: groundwater to channels.

Flux between the unsaturated soil storage and groundwater storages (Q_{SG}) (Equation A7) is a non-linear function of moisture and conductivity (Equation A6) limited by vertical flux potential (Equation A5). Horizontal fluxes from unsaturated soil storage, groundwater storage, and connected wetland storage are described using non-linear functions. Horizontal flux from the unsaturated soil storage is a non-linear function of horizontal conductivity (K_{HU}) (Darcy flow,

Equation A1). Groundwater storage horizontal flux is a non-linear function of slope (S), depth to the groundwater table, horizontal conductivity (K_{HS}), and non-linearity of storage (e_{HS}) (Equation A19). Flux from connected wetlands to river channels is estimated using the Dupuit equation for unconfined aquifers (Equation A21). To replicate fill and spill processes (Spence 2007), water is released from ponded water and disconnected wetland storage when maximum storage capacity is exceeded. Open water evaporation is estimated using mass-transfer methods (Equation A29). ET from vegetated surfaces is estimated with the Penman-Monteith model (Equations A25 – 28, Monteith 1965) to account for different transpiration rates. Potential ET (PET) is adjusted to actual ET (AET) using soil moisture and interception evaporation. Leaf and canopy conductance parameters were obtained from studies of similar vegetation types (Stewart 1988; Carlson 1991; Federer et al., 1996). Evaporation of intercepted water (canopy interception) is estimated using the Penman energy balance for consistency with ET (Equation A29) (Penman 1948). Transpiration and evaporation are assumed to change with soil depth (Appendix B).

Water is routed from lumped sub-basins within each watershed to the outlet using the Muskingum method (Equations A35-A39). Routing is necessary due to the attenuation of flow by low topographic relief, channel slopes, in-stream-lakes, and basin size. Lateral channel inflows are added as point sources at the beginning of each reach on a quarter of a day routing step.

5.4.2 ISOTOPIC MODULE

Storage volumes and fluxes estimated by the hydrologic model are used to estimate the isotopic mass-balance on a daily time-step (Appendix C). Isotopic fractionation is accounted for using variations of the Craig and Gordon model (Craig and Gordon 1965), including liquid to vapour, and solid to liquid phase change (Equation C20). Temporal snowmelt fractionation is

essential for source identification (Laudon et al., 2002; Hayashi et al., 2004) and is estimated using the Craig & Gordon model (Equations C12 – C14). The isotopic mixing model is generally fraction dependent (Equation C1); however, if the change in volume (ΔV) is zero, then a time dependent model is used (Equation C2; Gibson 2002). The isotopic mixing model for unsaturated soil storage is depth-dependent, uses the Craig and Gordon (1965) model to estimate total mass flux, and translates flux to depth using an exponential curve. The exponential curve is a function of soil moisture, isotopic groundwater composition (δ_∞) and a storage mixing parameter (P_{EXP}). Low exponents (approaching a minimum of 1) increase mixing and increase observed fractionation with depth. High values (>5) decrease mixing and result in fractionation near surface only (Appendix D). The parameter may be changed when depth-dependent soil measurements are known, otherwise the parameter should be held constant at 1 for consistency with previous models (Barnes & Turner 1998). It was assumed that evaporation and transpiration fluxes occurred from the same storage.

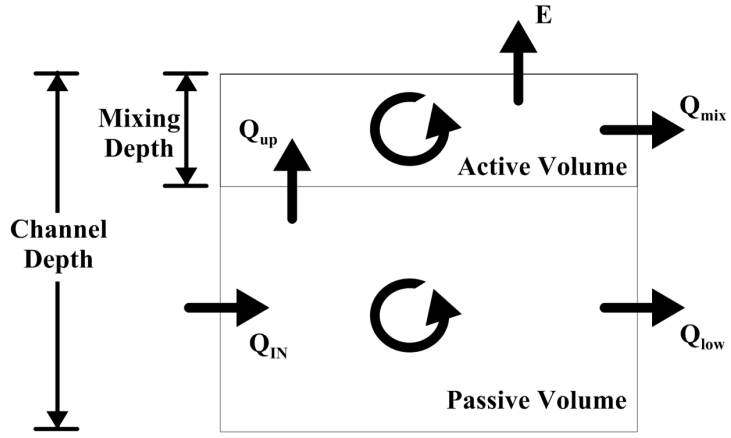

Figure 5-4. Conceptual open water mixing model. Routed discharge (Q_{IN}) enters the passive volume, discharging to the active volume (Q_{up}) or to the next reach (Q_{low}). The mixing equation (Equation C56) is applied to the mixing depth volume. Flux leaving mixing depth volume (Q_{mix}) is combined with Q_{low} at the reach outlet.

Open water storage is split into two volumes: an active portion where fractionation occurs and a passive portion below (Figure 5-4). Full mixing occurs at the end of the reach ($Q_{mix} + Q_{low}$). Isotopic compositions are estimated using mixing models (Equations C1 – C5) for each time-step, where the active volume is replenished using the simulated water balance ($Q_{up} = Q_{mix} + E$).

5.4.3 INPUT DATA REQUIREMENTS

Watershed delineation was accomplished using GreenKenue® with sub-basin areas set to a minimum of 2.5% of the total watershed area. Sub-basin slope was estimated using a digital elevation model (USGS 2016) rasterized to grid cells of 30 m, and the ArcMap percent slope tool. Land cover was determined for sub-basins using Geobase land cover images (10 m resolution) (GeoBase 2016) aggregated into five classes: coniferous forest, broadleaf forest, shrub, wetlands, and water. Wetlands were divided into connected and disconnected classes using an eight-direction connectivity method (Welch et al., in prep), and are considered connected when located adjacent to the river network or other connected wetlands. The percentages of channels lined with wetlands were used to calculate the area through which the wetlands discharge to channels in each sub-basin. Meteorological data used during simulation were obtained from the sources indicated in Table 5-2, with Norway House used for the Gunisao River watershed, and the NARR and CaPA models used for the Burntwood River basin. Observed discharge at catchment outlets was obtained from Environment Canada (Environment Canada 2016b) and Manitoba Hydro (Manitoba Hydro 2016).

5.4.4 DISCHARGE MODEL CALIBRATION

To determine the required enrichment, HELIOS was calibrated assuming ET consisted entirely of transpiration; that is, assuming no fractionation in storage. This removed parameter sets that yield more enriched water than observed prior to any fractionation (i.e., near-surface evaporation dependent storages). The model was calibrated using a multi-objective function with additional constraints based on subsurface isotopic compositions. Simulated groundwater composition ($\delta_{S,GW}$) enrichment was constrained by measured piezometer samples ($\delta_{O,GW}$) such that the ratio of over-enriched simulated groundwater compositions ($\delta_{S,GW}>\delta_{O,GW}$) to total groundwater samples was minimized. Over-enriched simulated groundwater is possible due to improper parameter sets (i.e. incorrect sources). The model was calibrated from 2000-2014 to include diverse hydrological conditions and validated in 2015. A long calibration period was required due to limited temporal resolution of sampling in early isotopic collection years for most watersheds (2010-2013). Discharge calibration was evaluated using a combination of the Nash-Sutcliffe (NSE, peak flow) and Kling-Gupta goodness-of fit (KGE, average error) with log-Nash-Sutcliffe (LNSE, discharge timing), and log-Kling-Gupta goodness-of-fit (LKGE, low-flow average error), applied as a minimization function:

$$\boldsymbol{Min(f) = \sqrt{(1-NSE)^2 + (1-KGE)^2 + (1-LNSE)^2 + (1-LKGE)^2}} \qquad 5\text{-}1$$

Percent deviation was calculated to provide a general estimate of water balance closure since evapotranspiration was not measured. The multi-objective calibration process was conducted as follows:

1) Calibration of primary source flow parameters against measured discharge data. 20,000 Dynamically Dimensioned Search (DDS; Tolson and Shoemaker 2007) simulations were used to calibrate the discharge for each basin, keeping ET partition constant at zero.

2) Parameter sets with simulated riverine isotopic compositions more depleted than measured compositions were identified and retained for analysis.

Evaporation may be inferred using the difference between observed and simulated (more depleted) isotopic compositions, referred to as the required enrichment.

5.4.5 THEORY OF ISOTOPIC EVAPOTRANSPIRATION PARTITIONING

Partitioning ET using tracer-aided watershed modelling exploits the different rates of $\delta^{18}O$ and $\delta^{2}H$ fractionation using the discharge composition at the outlet. Since modeled compositions of water held in non-fractionating storage will not change with the inclusion of fractionation in a model, and open water evaporation fractionation is modelled, the difference between isotopic composition in riverine simulations that neglects evaporation and observed compositions may be equated to actual evaporative fractionation in storages (i.e., unsaturated soil and wetlands). Using measured riverine isotopic compositions, the actual isotopic composition in storage may be estimated as a mass-balance:

$$\boldsymbol{Q_{ob} \cdot \delta_{ob} = Q_G \cdot \delta_G + Q_{Ov} \cdot \delta_{Ov} + Q_{st} \cdot \delta_{st}} \qquad 5\text{-}2$$

where Q is discharge or flux from storage, δ is the isotopic composition ($\delta^{18}O$ and $\delta^{2}H$), and the subscripts denote observed values (*ob*), simulated groundwater (*G*) and overland (*Ov*) flow, and fractionation-affected storage (*st=unsaturated soil + wetland*). Sub-basin routing causes headwater basin waters to reach the outlet at different times. Routing times from sub-basins are estimated at the outlet using probability density function (Ω_R) parameters (i.e., α and β for gamma distribution), calibration, and Muskingum routing. At time t, discharge from source (*, indicating either *G, Ov,* or *st*) is a cumulative distribution of each sub-basin source entering the

channel at time τ <t. Using simulated compositions of groundwater and overland flow, the flux weighted composition ($\delta_{w,*}$) from sub-basin *i* at time *t* may be estimated at the outlet:

$$\boldsymbol{\delta_{w,*}(i,t)} = \frac{\left(\int_0^t \boldsymbol{\Omega(\alpha(i),\beta(i),t-\tau)\cdot Q_*(i,t-\tau)\cdot \delta_*(i,t-\tau)\cdot d\tau}\right)}{\boldsymbol{Q_*(i,t)}} \quad 5\text{-}3$$

Substituting Equations 5-3 into Equation 5-2 for each storage type (*G*, *Ov*, and *st*) provides an equation that may be solved implicitly when high-resolution (daily) stream compositions are available:

$$\sum_{\boldsymbol{i=1}}^{\boldsymbol{SB}} \left(\boldsymbol{\delta_{w,st}(i,t)\cdot Q_{st}(i,t)}\right) = \boldsymbol{Q_{ob}(t)\cdot \delta_{ob}(t)} - \sum_{\boldsymbol{i=1}}^{\boldsymbol{SB}} \left(\left(\boldsymbol{\delta_{w,G}(i,t)\cdot Q_G(i,t)}\right)\right) - \sum_{\boldsymbol{i=1}}^{\boldsymbol{SB}} \left(\boldsymbol{\delta_{w,Ov}(i,t)\cdot Q_{Ov}(i,t)}\right) \quad 5\text{-}4$$

Where *SB* is the total number of subbasins. When high-resolution data are not available, Equation 5-4 may be further simplified by substituting the left hand side (LHS) of Equation 5-4 with the LHS of Equation 5-3 to solve for the instantaneous basin-weighted storage (δ_{st}):

$$\boldsymbol{\delta_{st}(t)} = \left(\boldsymbol{Q_{ob}(t)\cdot \delta_{ob}(t)} - \sum_{\boldsymbol{i=1}}^{\boldsymbol{SB}} \left(\boldsymbol{\delta_{w,G}(i,t)\cdot Q_G(i,t)}\right) - \sum_{\boldsymbol{i=1}}^{\boldsymbol{SB}} \left(\boldsymbol{\delta_{w,Ov}(i,t)\cdot Q_{Ov}(i,t)}\right)\right) / \left(\boldsymbol{Q_{st}(t)}\right) \quad 5\text{-}5$$

Corresponding simulated bulk storage compositions are calculated through mass-balance using simulated unsaturated soil and wetland storage compositions. Using the probability density functions for channel routing, the simulated bulk storage composition (δ_{MV}) is given as:

$$\boldsymbol{\delta_{MV}(t)} = \frac{\left(\sum_{i=1}^{SB}\left(\boldsymbol{\delta_{SL}(i,t)\cdot Q_{SL}(i,t)}\right) + \sum_{i=1}^{SB}\left(\boldsymbol{\delta_{WL}(i,t)\cdot Q_{WL}(i,t)}\right)\right)}{\boldsymbol{Q_{SL} + Q_{WL}}} \qquad 5\text{-}6$$

where *SL* and *WL* are simulated flux (Q) and composition (δ) from unsaturated soil and wetland storage, respectively.

The total cumulative required enrichment (RE) is the difference between δ_{st} and δ_{MV}. When daily δ_{st} are not available, daily average RE may be estimated through regression of RE and Julian day. Selecting the simplest relationship that yields statistically significant parameters (95% confidence) minimizes over-parameterisation of the relationship. For example, regression of RE with Julian day (JD) with a second-order polynomial equation yields:

$$\boldsymbol{RE = a\cdot JD^2 + b\cdot JD + c} \qquad 5\text{-}7$$

where a, b, and c are regression parameters. The rate of change of RE (RE') is equivalent to the difference between daily storage compositions ($C(t) - Co = dC/dt$, Equations C1 – C3). RE' is obtained by taking the derivative of Equation 5-7:

$$\boldsymbol{RE' = 2\cdot a\cdot JD + b} \qquad 5\text{-}8$$

Since enrichment is controlled by evaporative flux, RE' is equivalent to the change in storage composition resulting from evaporation. Storage composition and subsequent fractionation may, however, be influenced by i) precipitation composition, ii) relative humidity (*RH*) (Equations C1 – C3), and iii) temporal changes in the ET rate. These dependencies must be removed from RE' to obtain a direct comparison to ET. The influence of precipitation composition and *RH* values on storage compositions are dependent on storage volume and flux, which may change in time and with parameter sets. The influence of precipitation composition may be removed from RE' by subtracting the normalized average annual precipitation composition. The trend of general evaporative fractionation effect of *RH* on storage (GEF) is estimated using Equation C1, where

evaporation is equal to ET and *f* is one minus the ratio of ET flux to a constant volume. Subtracting GEF yields the required enrichment due to evaporation (REv'). Lastly, temporal ET trends are subtracted from REv'.

The ratio of REv' to ET provides a general partition of evaporation to ET (E/ET). There are three potential scenarios of ET partitioning, i) $\max(\mathrm{REv}') = \max(\mathrm{ET})$, ii) $\min(\mathrm{REv}') = \max(\mathrm{ET})$, and iii) $\mathrm{ET} = \mathrm{constant}$. In the first scenario, the partition of ET is temporally invariant when minimum of REv' and ET occur on the same Julian Day. The second scenario is the inverse of the first, the greatest E/ET occurs at the lowest ET rate. Finally, when ET is constant the greatest E/ET occurs at $\max(\mathrm{RE}')$, similar to the previous scenario; however, variation between maximum and minimum E/ET is damped.

5.4.6 METEOROLOGICALLY-DEPENDENT ET PARTITION

Evaporation and transpiration are highly dependent on meteorological conditions. Establishing a trend of ET partitioning with meteorological conditions allows for temporal-variability of evaporation using variables that directly influence evaporation and transpiration. Theory presented in Section 5.4.5 was applied to four watersheds to determine a partition relationship that is dependent on meteorological variables. Analysis indicated that source contributions affect RE. Groundwater contributions can result in infeasible RE resulting from overly depleted isotopic compositions (Equation 5-5). The effect may be removed by detrending RE (dRE) with the non-fractionating storage contribution fraction (e.g. groundwater) prior to identification of REv'. Source removal of groundwater and normalizing between 0 and 1 revealed non-linear annual changes in dRE (Figure 5-5). The dRE increases rapidly during spring and early summer, and reaches a maximum at the end of summer (August). When insufficient data are available in each calendar year, analysis of dRE must be conducted against Julian day. A

second-order polynomial equation is the simplest regression between dRE and Julian day that is significant (95% confidence level) for all watersheds (R_{adj}^2 between 0.43 and 0.75) and parameters. The relationship may be described as a function of Julian day, dRE(JD). The Burntwood River has one parameter (*a*) that does not meet 95% significance due to insufficient data (Table 5-3). The highest uncertainty observed between the temporal dRE and Julian day regression occurs in the spring freshet, evident in the Gunisao River ($R_{ajd}^2 = 0.26$). Removal of two freshet outliers (Figure 5.5b – red circle) increases the significance of the relationship (from 0.59 to 0.66) though does not significantly change regression parameters. Removing the isotopic precipitation, RH, and ET trends demonstrates that the highest E/ET occurs when ET is low (second scenario in Section 5.4.5) (Figure 5-5e). The trends of E/ET were normalized between 0 and 1 for each watershed to facilitate direct comparison. The perceived early start (Julian Day 110, April 20) of the E/ET trend (Figure 5-5e) is a function of the watershed routing (Equations 5-5 and 5-6) rather than ET. On average, ET was insignificant prior to May.

Table 5-3. Regression analysis of Normalized Detrended Required Enrichment (NdRE) against Julian Day. Values in parentheses are the p-values from 2-sided Student t-test.

Watershed	a	b	c
Sapochi	-1.90×10^{-5} (1.8×10^{-3})	1.0×10^{-2} (2.78×10^{-5})	-8.4×10^{-1} (3.05×10^{-4})
Gunisao	-6.43×10^{-5} (1.3×10^{-2})	3.0×10^{-2} (6.1×10^{-3})	-2.59 (1.1×10^{-2})
Burntwood	-6.84×10^{-5} (7.0×10^{-2})	3.0×10^{-2} (4.5×10^{-2})	-3.04 (5.0×10^{-2})
Odei	-3.60×10^{-5} (5.1×10^{-6})	2.0×10^{-2} (6.40×10^{-7})	-1.90 (1.49×10^{-5})

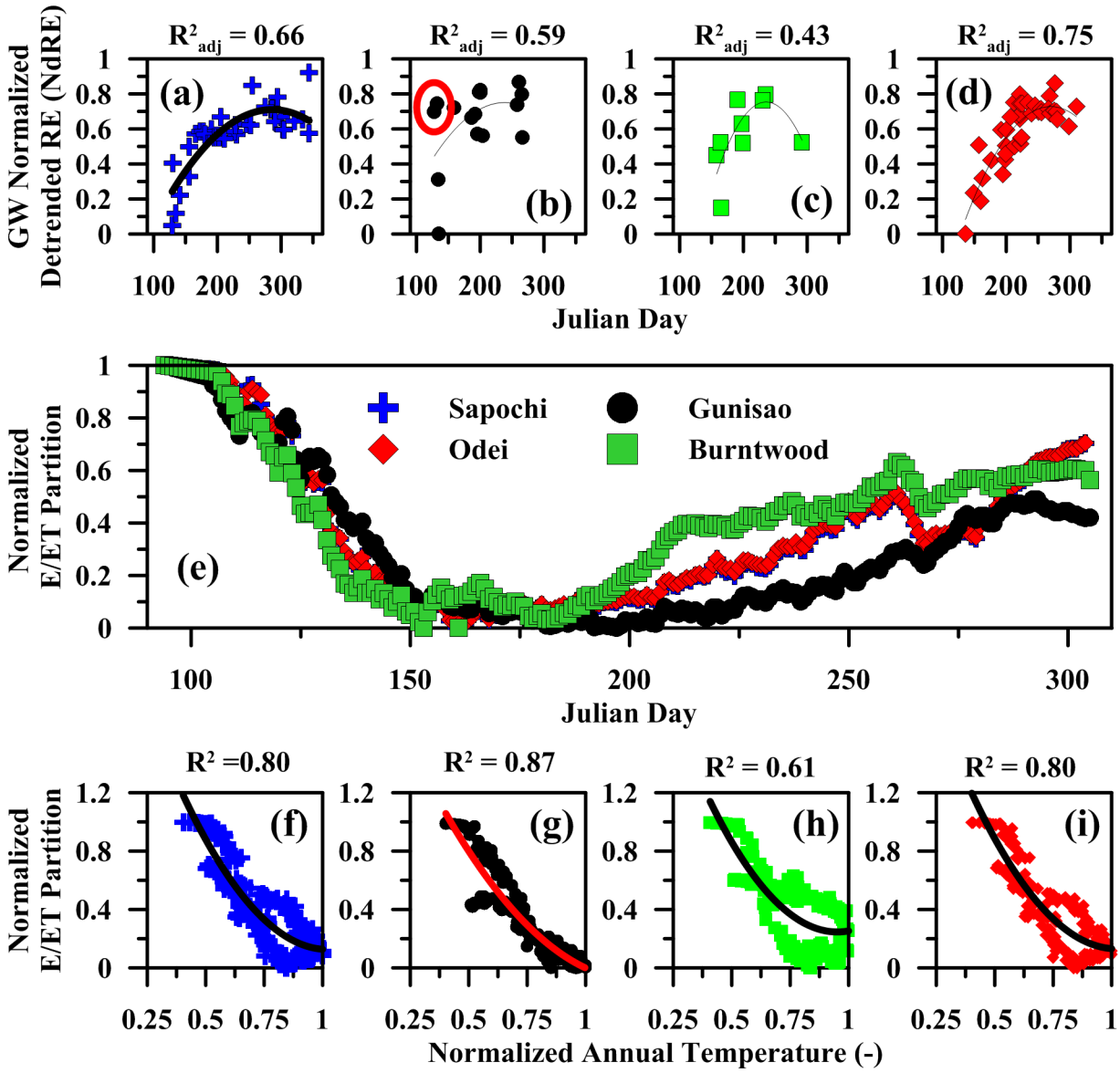

Figure 5-5. Regression of Julian Day and groundwater detrended required enrichment (dRE) for the a) Sapochi, b) Gunisao, c) Burntwood, and d) Odei Rivers. e) Individual watershed E/ET partition by Julian day. Correlation between normalized annual temperature range and E/ET for the f) Sapochi, g) Gunisao, h) Burntwood, and i) Odei Rivers with the R^2 values.

Regressing Julian Day E/ET against meteorological variables (temperature, relative humidity, wind speed, and pressure) reveals that the strongest relationship is to temperature (R^2 values 0.61-0.87; Figure 5-5). The inverse relationships of E/ET to temperature follow a power function. The regressions only provide general temporal trends because they are not specific to

storage volume or mass changes (i.e isotopic precipitation and *RH* effects). Total evaporation is dependent on modelled soil moisture, therefore the magnitude between the extreme E/ET and minimum E/ET are not known until calibration of discharge and isotopic compositions are completed. E/ET can be estimated from temperature independent of units:

$$\frac{\boldsymbol{E}}{\boldsymbol{ET}} = \boldsymbol{f(T)} = \boldsymbol{T^{MA} + Sc} \qquad \lim_{\boldsymbol{T \to 0}} \boldsymbol{f(T) = d.n.e} \tag{5-9}$$

where *MA* is a shape parameter for the magnitude of temporal variability, and *Sc* is a scale parameter correcting the minimum E/ET value. To avoid numerical complexities when temperature approaches $0^{\circ}C$, temperature is standardised:

$$\frac{\boldsymbol{E}}{\boldsymbol{ET}} = \boldsymbol{f(T)} = \left[\frac{\boldsymbol{T - T_{min}}}{\boldsymbol{T_{max} - T_{min}}}\right]^{\boldsymbol{MA}} + \boldsymbol{Sc} \qquad \boldsymbol{T_{min} \leq T_{min}^{actual}} \tag{5-10}$$

where T_{min} and T_{max} are temperature parameters. T_{min} must be less than the minimum observed temperature. Since evaporation cannot be greater than ET, Equation 5-10 has a maximum and minimum:

$$\frac{\boldsymbol{E}}{\boldsymbol{ET}} = \begin{cases} \boldsymbol{1} & \boldsymbol{f(T) > 1} \\ \boldsymbol{f(T)} & \boldsymbol{0 \leq f(T) \leq 1} \\ \boldsymbol{0} & \boldsymbol{f(T) < 0} \end{cases} \tag{5-11}$$

where E/ET has a maximum of 1 and minimum of 0. Sensitivity analysis indicated that the realistic parameter range for *MA* was -0.1 to -2, and for *Sc* between 0 and -1. When *MA* is greater than two, variability is so large that E/ET is binary (only 0 or 1).

The ET partition model (Equation 5-10) was applied to the HELIOS model, calibrated, and evaluated using simultaneous discharge and isotopic observations. The ET partition was applied to three storages: 1) wetlands, 2) unsaturated soils, and 3) ponded water. The influence of ponded water in previous studies (Sutanto et al., 2012) prompted the use of a different partition from unsaturated soils. Calibration discharge was evaluated using the minimization function in Section

5.4.4 and calibration isotopic compositions ($\delta^{18}O$ and $\delta^{2}H$) were evaluated using Nash-Sutcliffe and Kling-Gupta (NSE18, NSE2, KGE18, and KGE2), where 18 and 2 indicate $\delta^{18}O$ and $\delta^{2}H$ simulations, respectively. Discharge and isotopic composition were calibrated using DDS with 20 trials of 2,000 runs (40,000 total runs) from 2000 to 2014; 2015 was simulated as the validation period. The parameter set with the lowest *Min(f)* from each trial was assumed to be behavioral and used in analysis. Uncertainty bounds were determined using the upper and lower bound of all behavioral parameter sets.

5.5 APPLICATION TO FIELD SITES

5.5.1 HELIOS MODEL PERFORMANCE AND SOURCE CONTRIBUTIONS

Calibrated discharge agreed well with observed data when the ET partition model was applied (Table 5-4). As expected, the discharge goodness-of-fit (NSE & KGE) were slightly higher for discharge-only (*Min(f)* < 0.1, Section 5.4.4) than the tracer-aided calibration; however, tracer-aided discharge-isotopic calibration resulted in reduced ranges of behavioral parameters for source contribution (not shown). Observed discharge was generally within the uncertainty bounds of all behavioral simulations at the outlets (Figure 5-6). Spring and summer peak flow events were generally well captured; however, some events were overestimated. In the Sapochi River, overestimation typically occurred during low-intensity, multi-day rainfall events (2012-2013, Figure 5-6a). In the Gunisao and Burntwood rivers, overestimation occurred due to high precipitation events (2011, Figure 5-6b&c). Simulated winter flows were generally representative of the observed discharge; however, they had proportionally higher uncertainty in all basins. While the Burntwood River simulations over-estimated winter flows in three isotopic years (Figure 5-6c), this was not typical of all simulation years (not shown). Increased uncertainty in source contribution (i.e., connected wetlands and groundwater) limited the

identification of the shape of the recession limb, although uncertainty bounds contain measured discharge during the recession limb. The depth of snowmelt was low in 2013 relative to the amount of precipitation received during winter when compared to other years. The underestimation was likely due to over-estimation of sublimation during the winter and evaporation during a longer than average snowmelt period.

Calibrated isotopic compositions also agreed well with observed data when the ET partition model was applied (Table 5-4, Figure 5-7). The simulations of $\delta^{18}O$ and $\delta^{2}H$ were essentially equivalent for KGE (average maximum KGE18: 0.76 and KGE2: 0.75), while NSE goodness-of-fit was higher for $\delta^{18}O$ (average maximum NSE18: 0.56 and NSE2: 0.52, Table 5-4). Tight uncertainty bounds were obtained for simulations during the dominant evaporation months (June-September). The model replicated the observed isotopic depletion induced by snowmelt in all years except 2013. Under-estimation of snowmelt in 2013 led to over-enriched riverine isotopic composition throughout the remainder of the year, and resulted in decreased NSE of $\delta^{2}H$ and $\delta^{18}O$ for the Sapochi, Burntwood, and Odei River basins. The validation year (2015) uncertainty bounds captured the isotopic composition in three of four basins (Sapochi, Odei, and Burntwood), thus indicating the amount of evaporation and evaporative fractionation was appropriate. In contrast, enrichment appeared to be vastly overestimated in the Gunisao River basin. Such extreme enrichment was not observed in other simulated years, and was likely the result of only two enriched precipitation samples being applied as input throughout the year (no further samples collected).

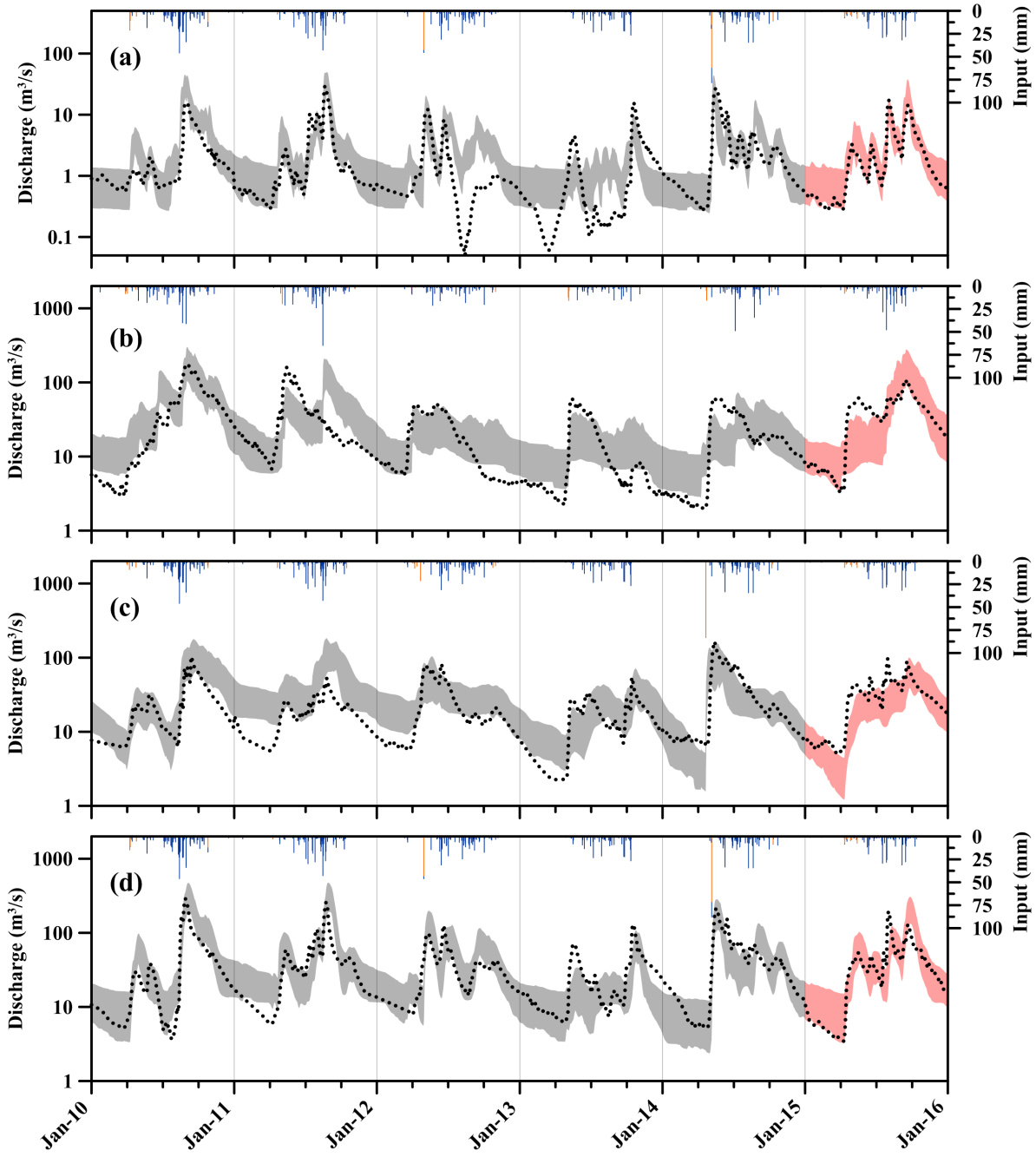

Figure 5-6. Simulated uncertainty bounds for the a) Sapochi, b) Gunisao, c) Burntwood, and d) Odei River basin against the measured discharge. The grey bounds indicate calibration years, and red bounds indicate validation years. Measured precipitation (blue bars) and simulated snowmelt (orange bars) are shown above each subplot.

Table 5-4. Average goodness-of-fit and annual average source component contribution fractions from 2000-2014 for each watershed. Goodness-of-fit metrics are presented for the calibration period only. NSE18 and NSE2 are the Nash-Sutcliffe efficiency of $\delta^{18}O$ and $\delta^{2}H$, respectively. Similarly, KGE18 and KGE2 are the Kling-Gupta efficiency for $\delta^{18}O$ and $\delta^{2}H$, respectively.

	Sapochi	Gunisao	Burntwood	Odei
	Efficiency Criteria			
Nash-Sutcliffe	0.61	0.39	0.37	0.61
Kling-Gupta	0.64	0.67	0.56	0.77
NSE18	0.59	0.38	0.60	0.68
NSE2	0.53	0.34	0.64	0.58
KGE18	0.73	0.70	0.77	0.85
KGE2	0.77	0.71	0.77	0.76
Source Contribution				
Soil (%)	18.4	15.6	19.8	31.6
Connected Wetland (%)	26.1	38.6	54.7	35.7
Disconnected Wetland (%)	5.0	3.1	1.7	4.9
Groundwater (%)	32.1	21.5	6.2	16.4
Overland (%)	18.4	21.2	5.8	11.5

On average, storages that affected the isotopic composition (fractionation dependent storages) accounted for 45-75% of total watershed discharge (unsaturated soil and connected wetlands, Table 5-4). Connected wetlands accounted for 53-73% of the fractionation dependent storage flux (includes unsaturated soil flux to connected wetlands). Overland flow was a large source contribution in each watershed; however, contributions were temporally limited to high input events (i.e. snowmelt and precipitation). Hence, the proportion of total discharge contributed by overland flux was often lower than indicated in Table 5-4. Disconnected wetland contribution was a relatively small portion of the watershed discharge. Similar to overland flow, disconnected wetland contribution only occurred during high input events, generally restricted to snowmelt and late season precipitation. Groundwater contribution was relatively consistent throughout the year, but was a greater proportion of streamflow during winter months when only groundwater and connected wetlands discharged to the channels. The uncertainty of connected wetland and groundwater contribution was greatest during recession limbs (not shown). This was

likely due to inter-annual changes in freezing depths of wetlands and shallow groundwater (assumed to be constant). On average, the simulated peak ET rate during the summer months was between 1.7 and 2.5 mm/day for each of the watersheds.

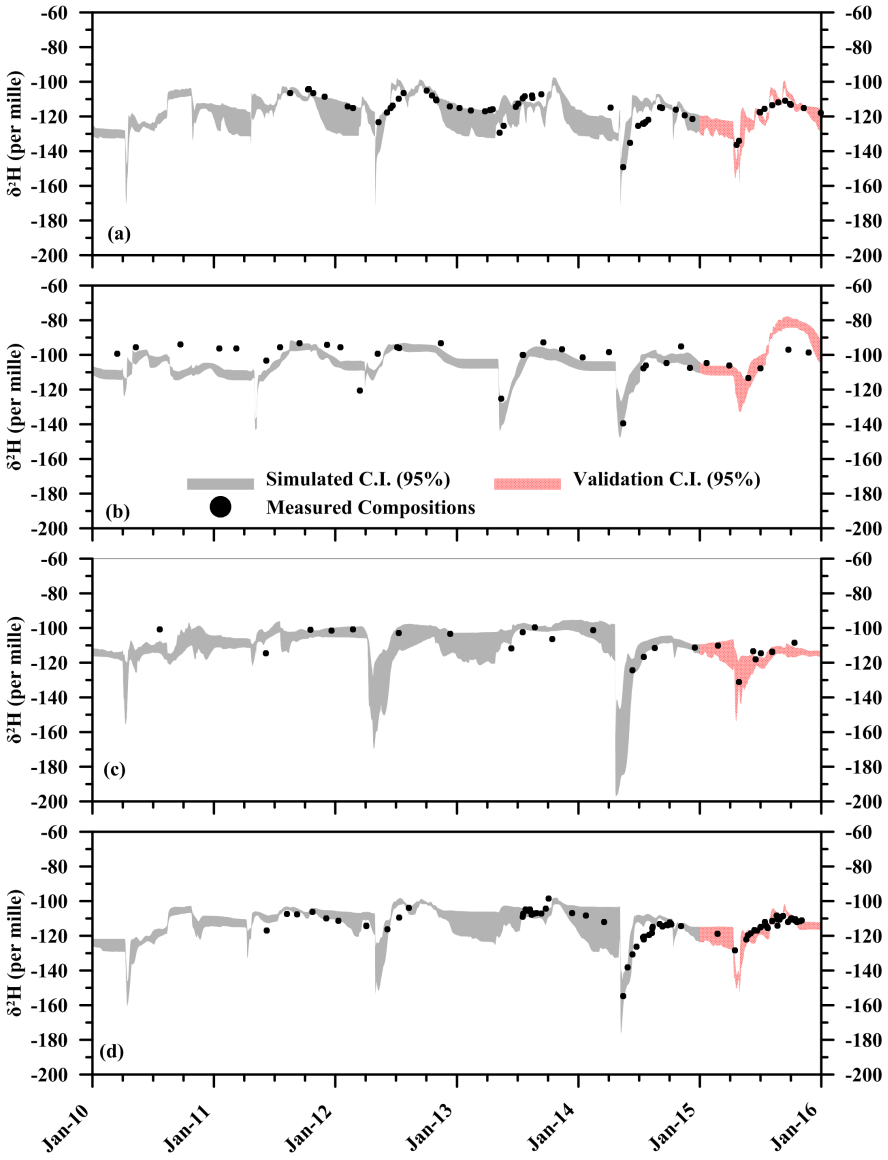

Figure 5-7. Simulated deuterium (a-d) uncertainty bounds for the calibration (grey) and validation (red) years. Measured isotopic compositions (black circles) are shown for the Sapochi (a), Gunisao (b), Burntwood (c), and Odei (d) River basins. Simulations of oxygen-18 are similar and are therefore not shown.

5.5.2 EVAPOTRANSPIRATION PARTITION TREND

The basin-wide partition of E/ET was determined from flux-weighted unsaturated soil and wetland storage partitions (Figure 5-8). The trend followed a general parabolic-shape for each storage, with a higher E/ET during the spring (April and May) and fall (September and October), and lower during the summer (June to August) when transpiration dominated. E/ET was highest for ponded water (when present) in all watersheds, while in three of the four watersheds E/ET was at its lowest in June (July for the other watershed), and wetland storage E/ET was greater than unsaturated soil E/ET. The wetland storage E/ET was significantly higher (90% confidence level) than the unsaturated soil E/ET from July to August. Partition parameters (*MA* and *Sc*) were very similar for the Sapochi, Burntwood, and Odei Rivers, likely because of similar physiography and land cover (Appendix E). The Gunisao had much higher E/ET throughout the year than the other watersheds and the ratio was less variable. For example, in summer the upper uncertainty bound for E/ET was approximately 0.4 in the Gunisao compared to approximately 0.2 in the three other watersheds.

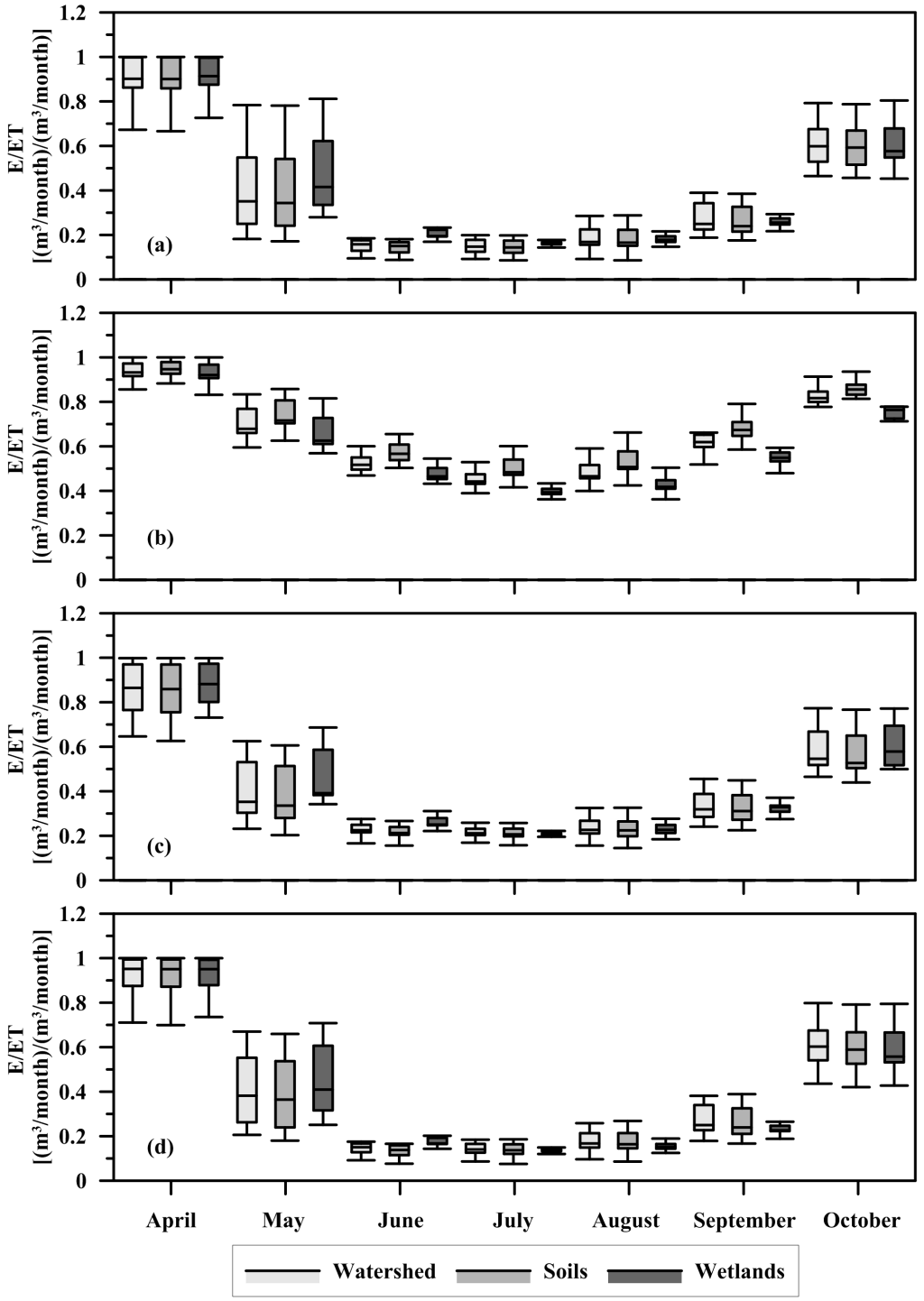

Figure 5-8. Box-plots of the monthly uncertainty bounds for evapotranspiration partition for primary storage components (wetland and unsaturated soils) against the uncertainty bounds for the cumulative evapotranspiration for the basin. Shown on the figure are the a) Sapochi, b) Gunisao, c) Burntwood, and d) Odei River basins. Interquartile ranges (IQR) are set from 25% to 75% and bounded by am IQR factor of 1.5.

High intra-annual variability of the monthly partition was observed for each fractionating storage, and basin-wide E/ET (2000-2015, Figure 5-8). Within the Sapochi, Odei, and Burntwood, the basin E/ET was highly dependent on the volume of soil storage (Figure 5-9), while basin ET partition in the Gunisao was equally dependent on unsaturated soil and wetland storage. Variability was the greatest in the spring and fall, when evapotranspiration rates and temperatures varied the most inter-annually. Based on the temperature dependent model, maximum transpiration (lowest E/ET) was anticipated when temperature was the greatest. However, while temperature did not reach a maximum until August, the lowest E/ET partitions were observed in June. Increases in the partition occurred later in the year (August and September) and coincided with the greatest precipitation events as well as the beginning of abscission. During the growing season (June-August), the average ET partition varied from 0.16-0.56 for unsaturated soils and 0.17-0.46 for wetlands. The basin-wide annual average partition varied from 0.22-0.60.

5.5.3 SOURCES OF EVAPORATION UNCERTAINTY

The uncertainty of E over soils (i.e. shrubs, conifers, broadleaf forest) and wetlands (connected and disconnected) was split into the contributions of different evaporation sources to total E (E_i/E_{Total}, i = unsaturated soil, ponded water, and intercepted water, Table 5-5). Intercepted evaporation was not calibrated with the ET partition because the evaporative effects have no influence on unsaturated soil composition and it does not contribute to streamflow. Higher potential for intercepted evaporation results in the greatest evaporative loss compared to ponded water and unsaturated soil in three of the four watersheds (Table 5-5) and was consistent for soils and wetlands. While ponded water had the highest parameter uncertainty (Appendix E), it accounted for the least E uncertainty (of total E uncertainty) due to the small contribution of

ponded water E and subsequent limited effect of ponded water evaporative fractionation. Generally, the highest uncertainty of evaporation was from unsaturated soil evaporation and subsurface evaporation in wetlands, which varied temporally (not shown). Furthermore, higher uncertainty in unsaturated soil evaporation generally occurred when it accounted for more of the total E (Table 5-5). This source accounted for over 50% of the total partition uncertainty, despite having the most constrained parameter ranges (Appendix E).

Table 5-5. Annual average E/E_{Total} (standard deviation in brackets) over soils (unsaturated soil, intercepted water, and ponded water), and annual average E/E_{Total} over wetlands (soil evaporation, intercepted water) for each watershed.

	Evaporation Source	Sapochi (%)	Gunisao (%)	Burntwood (%)	Odei (%)
Soils	Unsaturated soil evaporation	17.1 (13.9)	64.2 (30.1)	30.5 (27.4)	12.6 (5.5)
	Intercepted water evaporation	80.2 (8.3)	32.2 (3.1)	65.6 (7.8)	83.9 (8.1)
	Ponded water evaporation	2.7 (1.9)	3.6 (0.7)	3.9 (3.5)	3.5 (2.6)
Wetlands	Soil evaporation	36.0 (28.5)	73.1 (21.1)	43.1 (23.6)	36.7 (16.3)
	Intercepted water evaporation	64.0 (0)	26.9 (0)	56.9 (0)	63.3 (0)

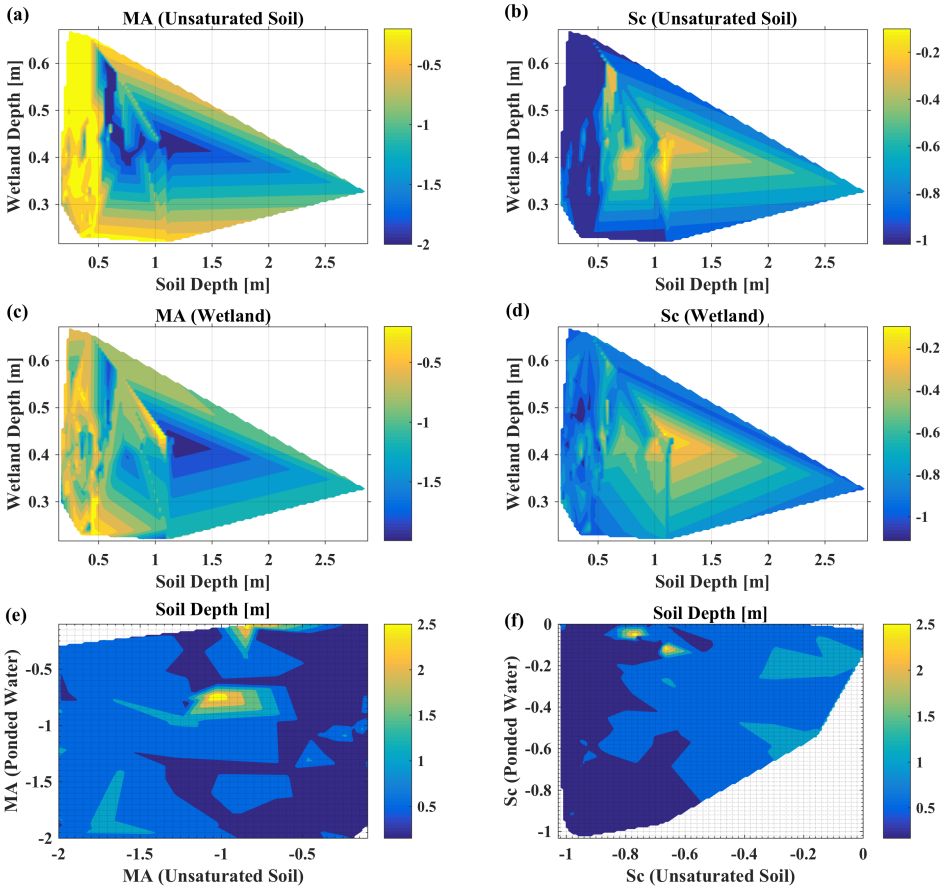

Figure 5-9. The comparison of storage depth with parameter space of a) unsaturated *MA*, b) unsaturated *Sc*, c) wetland *MA*, and d) wetland *Sc*. Parameter space of e) *MA* for unsaturated soils and ponded water against soil depth, and f) *Sc* for unsaturated soils and ponded water against soil depth.

The uncertainty of evaporation from unsaturated soil was a function of both the E/ET partition and estimates of storage. These effects may be separated by identifying the effects of varying storage parameters on partition parameters. The shape parameter (*MA*) for unsaturated soils was simultaneously influenced by unsaturated soil volume and wetland volume (mean storage depth over simulation length, Figure 5-9a). The shape parameter exhibited low sensitivity when the volume of water stored in the unsaturated soil storage was low (<0.5 m), regardless of

wetland volume. As unsaturated soil volume increased, the mean unsaturated shape parameter decreased from -0.25 to -1.07, while the mean unsaturated scale parameter (*Sc*) increased from -0.94 to -0.62 (Figure 5-9b). Soil *MA* was also maximized when wetland volume was near minimum (-0.2) and maximum (-0.7). Wetland *MA* was most uncertain when the unsaturated soil volume was low (Figure 5-9c), however, it similarly decreased as soil volume increased (-0.61 to -1.14). There was no significant change in the scale parameters for ponded water with unsaturated soil volume (Figure 5-9e). It is important to note, however, that there are limited temporal periods for which ponded water storage is greater than 0; therefore, it is difficult to establish the significance of ponded water evaporation on unsaturated soil compositions.

Table 5-6. Auto-regression of the components of unsaturated soil storage and wetland volumes: simulated watershed groundwater tables, soil moisture, and wetland moisture content, to the estimated E/ET of the unsaturated soil and wetland storage. Sign indicates positive or negative correlation and color indicates significance of inclusion to a multi-regression model (p-value green <0.05, red >0.05). US is unsaturated soil E/ET and WL is wetland E/ET.

	Sapochi River		Gunisao River		Burntwood River		Odei River	
	US	WL	US	WL	US	WL	US	WL
Depth to Groundwater Table	-	+	+	+	+	+	-	+
Soil Moisture	+	+	+	+	+	-	+	+
Wetland Moisture	-	-	-	-	-	-	+	-
Unsaturated Soil E/ET	*N/A*	-	*N/A*	-	*N/A*	-	*N/A*	+
Wetland E/ET	-	*N/A*	-	*N/A*	-	*N/A*	+	*N/A*

The influence of individual components of unsaturated soil storage volume and wetland storage volume on the E/ET partition parameters was identified through stepwise linear regression using the variables depth to groundwater table, soil moisture, and wetland moisture

(Table 5-6). The inclusion of a variable in the regression was considered significant when $p < 0.05$ (green shading). A significant positive linear relationship between soil moisture and unsaturated soil E/ET was obtained for all watersheds. A significant relationship between the depth to the groundwater table and unsaturated soil E/ET was only obtained for the Sapochi River. Wetland E/ET was significantly positively related to the depth to the groundwater table and negatively related to wetland moisture for all watersheds. The negative relationship to wetland moisture was merely a function of including the groundwater table. Similar to the relationship of unsaturated soil E/ET and soil moisture, 2-variable regression of the wetland E/ET to wetland moisture were positively correlated. The consistency of simulated moisture on the estimation of E/ET partition indicated that it was the primary influence on the partition parameters.

5.5.4 RIVERINE SENSITIVITY TO STORAGE FRACTIONATION

The routing of unsaturated soil water through connected wetlands (where present) complicated identification of the storage(s) in which evaporation most influenced the isotopic composition of streamflow at catchment outlets. To separate the sources of fractionation, a sensitivity analysis of evaporation on the isotopic composition at the outlet was conducted using the optimum parameters for each trial (20 trials in each watershed). Each trial was conducted twice, changing evaporation (fractionating) to transpiration (non-fractionating) in unsaturated soil storage and then in wetlands. The average changes in simulated isotopic composition were calculated for each storage for the isotope sampling period (2011-2014). The dependence of evaporation on storage volume and land cover percentages was removed by calculating ratios of evaporation to storage volume and area (E/S/A) (Figure 5-10).

A log-linear relationship between isotopic change and evaporation change per storage volume was identified for unsaturated soil and wetland storages (Figure 5-10). The greatest rate of change in riverine composition was observed when the E/S/A ratio was small, and the least rate of change occurred when the E/S/A was high. Decreasing evaporation in wetlands exerted greater influence on stream isotopic composition, with the rate of change almost twice as high for wetlands (0.42) compared to unsaturated soils (0.25). The rate of change was the most pronounced when E/S/A was low. Additionally, the relationship was much stronger for wetlands (R^2=0.93) than unsaturated soils (R^2=0.54) due to complex mixing of unsaturated soil water and ponded water.

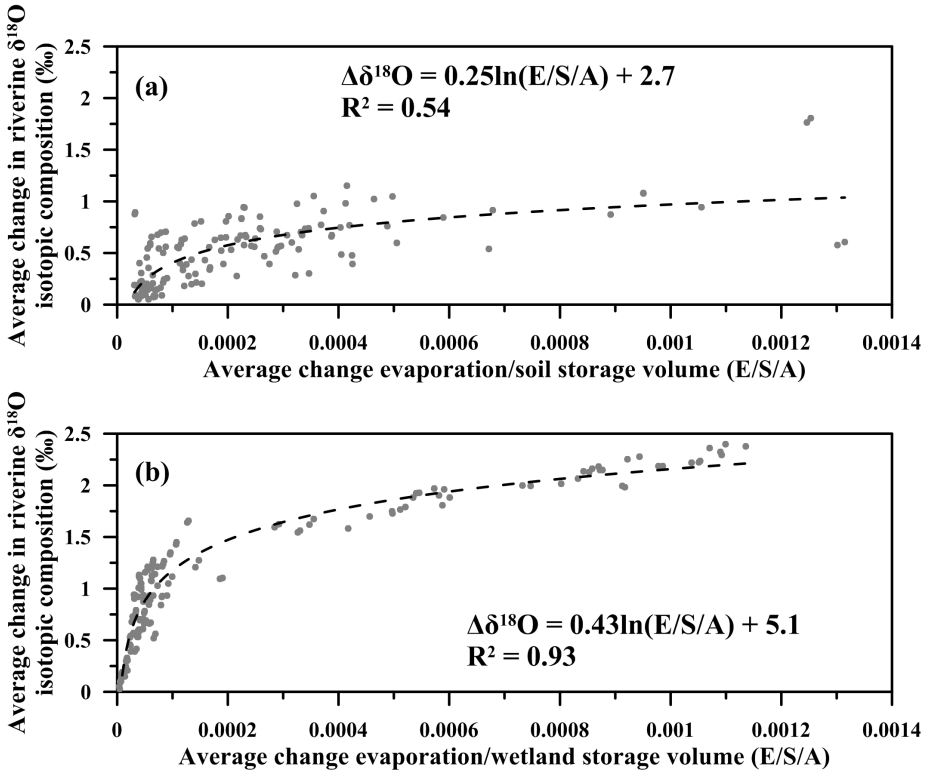

Figure 5-10. Relationship between the change in evaporation and change in simulated riverine isotopic composition for a) unsaturated soil storage, and b) wetland storage. Evaporation is normalized by storage volume and surface area.

5.6 DISCUSSION

5.6.1 ASSESSMENT OF BASIN AND STORAGE ET PARTITIONING

The observed discharge and isotopic compositions of streamflow at catchment outlets are well captured by incorporating an ET partition model that is a function of air temperature. In contrast to previous studies, this study uses isotopic differences of river samples and model calibration to verify the accuracy of the ET partitioning method rather than observations of two of the three components (evaporation, transpiration, and evapotranspiration) (Kool et al., 2014). The total ET estimated within each watershed was comparable to the BOREAS study (same location), which estimated average summer ET ~2 mm/day (Amthor et al., 2001). Calibrated mean watershed ET partitions for the Sapochi, Odei, and Burntwood River basins during the growing season are comparable to studies conducted in forested and shrub regions (0.07-0.4) using stable water isotopes (Kelliher et al., 1992; Kostner 2001; Gibson and Edwards, 2002; Stannard and Weltz 2006; Sutanto et al., 2012; Domec et al; 2012; Raz-Yaseef et al., 2012; Gabrielli 2016), though few studies are situated in high-latitudes. Significantly higher E/ET ratios are, however, estimated in the Gunisao River in this study. Vegetation in the Gunisao basin is predominantly shrubs or shrub wetlands and more analogous to open canopy crop cover, which may result in higher evaporation (Kool et al., 2014; Gabrielli 2016). Higher proportions of herbed wetland rather than shrub wetland may be the cause of increases in E/ET for the Burntwood and Gunisao (0.31 and 0.6, respectively) relative to the Sapochi and Odei basins (0.21 and 0.22 respectively). Herbed wetlands have lower LAI than shrub wetlands (Barbour and Billings 2000) which typically results in higher evaporation rates (Gabrielli 2016). The Burntwood likely has a lower E/ET than the Gunisao due to a greater proportion of treed area (higher LAI) in the watershed (Table 5-1).

Though temperature has previously been used to estimate unsaturated soil evaporation (Allen 1990; Peñuelas et al., 2009; Deol et al., 2012), RH, canopy coverage, and moisture content of the subsurface are also known to be important. Using our temperature-dependent ET partition model, spring simulations following the freshet over-estimated isotopic measurements. This may be due to the use of general trends of δ_A and RH, and limited inclusion of vegetation parameters. For example, during the spring, low δ_A and low RH (<60%) result in much greater fractionating effects than when δ_A is high (>20‰). Combining RH with the temperature-ET model may improve spring estimation; however, this would only be justifiable when additional data are available to aid model calibration (Abtew and Melesse 2013). In addition, inclusion of RH into the temperature-dependent model would need to consider height-dependence as average RH is higher in dense forests (e.g. Amazon rainforest) within the canopy than above it (Lowman and Rinker 2004). This has the potential to reduce the sensitivity of evaporative fractionation in unsaturated soil storage below the canopy. The RH within the canopy of the Boreal watersheds in this study is likely not as affected due to lower canopy density (Brooks and Kyker-Snowman 2008). Canopy coverage and ground vegetation (e.g., Sphagnum moss) may potentially be used to spatially adjust the ET partition with leaf area index (Booth and Loheide 2010) and moisture content, where such data are available. Inclusion of ground vegetation may result in greater spatial variability of E/ET due to varying moisture content and water retention (e.g., peat material, McCarter and Price 2012).

5.6.2 IMPLICATIONS FOR MODELLING

Calibrating a tracer-aided model with storage and isotopic fractionation parameters reintroduces storage parameter equifinality, although it facilitates more accurate estimation of isotopic fractionation within storage. Separation of ET into its components limits the amount of

fractionation within a storage compartment by avoiding fractionation of transpired water. Incorrect estimation of evaporative fractionation within storage may result in incorrect identification of primary flow components, similar to the effect of temporally dependent precipitation (McDonnell et al., 1991). For example, partitioning ET results in temporal increases in water sourced from wetland and groundwater storages compared to those previously identified for the Sapochi and Odei Rivers (Smith et al., 2016). Inclusion of the ET partition and other improvements (separation of connected and disconnected wetlands) reduces uncertainty of isotopic composition (δ^2H and $\delta^{18}O$) during ET-dominated months and in simulated flows.

The E/ET partition is highly dependent on the estimated moisture content and subsurface storage volume. Consequently, higher uncertainty of either simulated moisture content or storage volume increases the uncertainty of estimated E/ET and its parameters. The higher uncertainty during periods of increased storage depth during modelling may be explained through mass-balance, where large volumes or inflows dampen the fractionation effects of evaporation (Gibson et al., 1993; Gibson 2002). Therefore, reduction of uncertainty of the partition parameters may be achieved most simply with more accurate storage volume estimates for the store with the greatest volume. Despite positive correlations, it remains difficult to establish the sensitivity of parameters for ponded water partitioning that are the most uncertain due to the limited periods ponded water is present within the simulations in these catchments. Further modelling of ponded water conditions may be considered as open water evaporation over soil, while considering the reduction of available radiation energy within the soil. In addition, improved estimation of snowmelt fractionation may reduce uncertainty during spring when variably enriched snowmelt may influence identification of sources (Taylor et al., 2002; Penna et al., 2013).

Parameterisation and calibration of estimated E/ET are contingent on the availability of water moving between storages (i.e. ponded water, wetland, and unsaturated soil), and within storage (moisture content, Table 5-6). As it is infeasible to parameterise E/ET for all degrees of saturation in all storages, including the degree of saturation (and subsequent storage depth) in a general watershed E/ET partitioning model is likely to reduce the model parameterisation. The increase in E/ET as soil moisture increases identified in this study has also been observed using alternative assessment methods (Stannard and Weltz 2006; Raz-Yaseef et al., 2012). The high correlation between storage conditions indicates further reduction of parameterisation may be possible through the incorporation of storage properties (e.g. porosity, density), such that storages that present less resistance to evaporation (wetlands) result in higher E/ET (Sutanto et al., 2012).

Riverine enrichment observed at a catchment outlet depends on the primary source of evaporation within a catchment and the influence of evaporation on water in storage. As widespread (spatial and temporal) sampling across all storages is not feasible, it is useful to identify the storage where measurement will most constrain uncertainty (Tetzlaff et al., 2008). Assessment of the change in riverine isotopic composition indicates that wetlands proportionally account for the greatest riverine enrichment. In addition, higher parameter uncertainty in wetlands, and the sensitivity of riverine composition to wetland composition changes, suggests that wetland sampling would provide the greatest reduction in hydrological modelling uncertainty. Furthermore, sampling within wetlands would reduce uncertainty in identifying the source waters contributing to fall streamflow (Hinton et al., 1994; Laudon et al., 2004).

5.7 CONCLUSIONS

This study provides a new method for partitioning ET at the catchment scale using the isotopic composition of river water and air temperature. In seasonal basins, E/ET is highly correlated to temperature, and follows a parabolic trend from spring to fall. Calibration of a tracer-aided model with a temperature dependent ET partition indicates distinct differences in E/ET between storages. Ponded water yields the greatest E/ET ratios (highest evaporation), while unsaturated soil storages generally have the lowest E/ET ratio (most transpiration). Wetlands yielded higher E/ET than in unsaturated soils despite lower interception evaporation, due to higher subsurface water availability and ensuing subsurface evaporation. Higher moisture content results in higher E/ET, and large storage volumes increase the uncertainty of the partition. Evaporation from different storages does not influence stream compositions equally. Rather, evaporative fractionation in wetlands has a proportionally greater effect on the riverine isotopic composition than that in unsaturated soils. In catchments where soil moisture data are available, the methods presented here may be used to further constrain the temperature-dependent ET partition model with subsurface moisture with the implicit solution (Equation 5-3). Simplifications to ET partitioning methods are particularly useful for application in meso- and macroscale watersheds with limited data available. Partitioning ET has further significance in the assessment of the ages of catchment water fluxes. Historically, transit time models have not partitioned ET, rather assumed transpiration flux and evaporation flux occur from the same source water. The temperature-dependent model for ET partitioning provides a means for assess ET partition flux ages independently, and establish how long-term climate changes may affect both the partition and water storage.

5.8 ACKNOWLEDGEMENTS

The authors would like to thank Manitoba Hydro, Water Survey of Canada, and Innotech Alberta for sample collection and analysis. We acknowledge funding for sampling from Manitoba Hydro, Water Survey of Canada, and the Natural Sciences and Engineering Research Council (NSERC) through a Collaborative Research and Development Grant and Post-graduate Scholarship - Doctoral Program (PGS-D, A.A.S.).

5.9 REFERENCES

Abtew, W., Melesse, A. 2013. *Evaporation and Evapotranspiration: Measurements and Estimations*. Springer Netherlands.

Allen, A.J. 1990. Measurement and estimation of evaporation from soil under sparse barely crops in Northern Syria. *Agricultural and Forest Meteorology*. **Volume 49**: 291-309.

Amthor, J., Chen, J., Clein, J., Frolking, S., Goulden, M., Grant, R., Kimball, J., King, A., McGuire, A., Nikolov, N., Potter, C., Wang, S., Wofsy, S. 2001. Boreal forest CO_2 exchange and evapotranspiration predicted by nine ecosystem process models: Intermodel comparisons and relationships to field measurements. *Journal of Geophysical Research*, **Volume 106(D24)**: 623-648.

Ashktorab, H., Pruitt, W. O. Paw, K. T. 1994. Partitioning of evapotranspiration using lysimeter and micro-Bowen-ratio system. *Journal of Irrigation and Drainage Engineering*, **Volume 120(2)**: 450-464.

Barbour, M.G., Billings, D.W. 2000. *North American terrestrial vegetation*. Cambridge University Press, UK.

Barnes C.J., Turner J.V. 1998. Chapter 5: Isotopic Exchange in Soil Water, *in Isotope Tracers in Catchment Hydrology*. Elsevier. Amsterdam.

Booth E.G., Loheide, S.P. 2010. Effects of evapotranspiration partitioning, plant water stress response and topsoil removal on the soil moisture regime of a floodplain wetland: implications for restoration. *Hydrological Processes*. **Volume 24**: 2934-2946.

Brooks R.T., Kyker-Snowman, T.D. 2008. Forest floor temperature and relative humidity following timber harvesting in southern New England, USA. *Forest Ecology and Management*. **Volume 254**: 66-73.

Calanca P., Roesch, A., Jasper, K., Wild, M. 2006. Global warming and the summertime evapotranspiration regime of the alpine regions. *Climate Change*. **Volume 79**: 65-78. DOI: 10.1007/s10584-006-9708-4.

Carlson, T. 1991. Modelling stomatal resistance: an overview of the 1989 workshop at the Pennsylvania State University. *Water Resources Research*, **Volume 54**: 109-106.

Craig, H., Gordon, L. 1965. Deuterium and oxygen-18 variations in the ocean and marine atmosphere. *Stable Isotopes in Oceanographic Studies and Paleotemperatures*, pp. 9-130.

Daamen, C.C., Simmonds, L.P. 1996. *Soil Water, Energy and Transpiration - A Numerical Model of Water and Energy Fluxes in Soil Profiles and Sparse Canopies*, Reading: University of Reading.

Deol, P., Heitman, J.L., Amoozegar, A., Ren T., Horton R. 2012. Quantifying non-isothermal subsurface soil water evaporation. *Water Resource Research*. **Volume 48:** 1-11.

Domec, J-C., Sun, G., Noormets, A., Gavazzi, M.J., Treasure, E.A., Cohenm E., Swenson, J.J., McNulty, S.G., King, J.S. 2012. A comparison of three methods to estimate evapotranspiration in two contrasting loblolly pine plantations: age-related changes in water use and drought sensitivity of evapotranspiration components. *Forest Science*. **Volume 58(5)**: 497-512.

Ehleringer, J.R., Dawson, T.E. 1992. Water uptake by plants: perspectives from stable isotope composition. *Plant, Cell & Environment*, **Volume 15**: 1073-1082.

Environment Canada, 2016a. Past Weather and Climate. [Online] Available at: http://climate.weather.gc.ca/historical_data/search_historic_data_e.html [Accessed 2016]

Environment Canada, 2016b. Hydrometric Data. [Online] Available at: http://www.wsc.ec.gc.ca/applications/H2O/index-eng.cfm?stype=location [Accessed 2016].

Evaristo, J., Jasechko, S., McDonnell, J.J., 2015. Global separation of plant transpiration from groundwater and streamflow. *Nature*. **Volume 525**: 91-94. DOI: 10.1038/nature14983.

Farquhar, G.D. & Cernusak, L.A. 2005. On the isotopic composition of leaf water in the non-steady-state. *Functional Plant Biology*, **Volume 32(4)**: 293-303.

Federer, C.A., Vorosmarty, C., Fekete, B. 1996. Intercomparison of methods for calculating evaporation in regional and global water balance models. *Water Resource Research*, **Volume 30**: 2315-2321.

Flynn, D., Kurz D., Alfaro, M., Graham, J., Arenson, L. 2016. Forcasting Ground Temperatures under a Highway Embankment on Degrading Permafrost. *Journal of Cold Regions*

Engineering. **Volume 30(4)**: 4016002-1-20. DOI: 10.1061/(ASCE)CR.1943-5495.0000106.

Gabrielli, E.C. 2016. Partitioning Evapotranspiration in Forested Peatlands within the Western Boreal Plain, Fort McMurrary, Alberta, Canada. *Theses and Dissertations (Comprehensive)*. Paper 1820.

GeoBase. 2016. [Online] Available at: http://www.geobase.ca/geobase/en/ [Accessed 2014].

Gibson J., Edwards, T.W.D. 2002. Regional water balance trends and evaporation-transpiration partitioning from a stable isotope survey of lakes in northern Canada. *Global Biogeochemical Cycles*. **Volume 16(2)**: 10-1-14. DOI: 10.1029/2001GB001839.

Gibson, J.J., Edwards, T.W.D., Bursey, G.G. 1993. Estimating Evaporation Using Stable Isotopes: Quantitative Results and Sensitivity Analysis for two catchments in Northern Canada. *Nordic Hydrology*. **Volume 24**: 79-94.

Gibson, J. 2002. Short-term evaporation and water budget comparisons in shallow Arctic lakes using non-steady isotope mass-balance. *Journal of Hydrology*, **Volume 264**: 242-261.

Good, S.P,. Noone, D., Bowen, G. 2015. Hydrologic connectivity constrains partitioning of global terrestrial water fluxes. *Science*. **Volume 349**: 175-177.

Guo, X., Tian, L., Wang, L., Yu, W., Qu, D. 2017. River recharge sources and the partitioning of catchment evapotranspiration fluxes as revealed by stable isotope signals in a typical high-elevation arid catchment. *Journal of Hydrology*. **Volume 549:** 616-630. DOI:10.1016/j.jhydrol.2017.04.037

Hayashi, M., Quinton, W. L., Pietroniro, A. Gibson, J. 2004. Hydrologic functions of wetlands in a discontinuous permafrost basin indicated by isotopic and chemical signatures. *Journal of Hydrology*, **Volume 296**: 81-97.

Hinton, M.J., Schiff, S.L., English, M.C. 1994. Examining the contributions of glacial till water to storm runoff using two- and three-component hydrograph separations. *Water Resources Research*. **Volume 30**: 983-993. DOI: 10.1029/93WR03246

Hu, Z., Wen, X., Sun, X., Li, L., Yu, G., Lee, X., Li, S. 2014. Partitioning of evapotranspiration through oxygen isotopic measurements of water pools and fluxes in a temperature grassland. Journal of *Geophysical Research: Biogeosciences*, **Volume 119**: 358-371.

Jasechko, S. Sharp, X., Gibson, J.J., Birks., Yi, Y., Fawcett, P.J. 2013. Terrestrial water fluxes dominated by transpiration. *Nature*, **Volume 496**: 347-350.

Keeling, C.D. 1961. The concentration and isotopic abundances of carbon dioxide in rural and marine air. *Geochimica et Cosmochimica Acta*, **Volume 24**: 277-298.

Kelliher, F.M., Kostner, B.M.M., Hollinger, D.Y., Byers, J.N., Hunt, J.E., McSeveny, T.M., Meserth, R., Weir, P.L., Schulze, E.-D. 1992. Evaporation, xylem sap flow, and tree transpiration in a New Zealand broad-leaved forest. *Agricultural and Forest Meteorology*. **Volume 62**: 53–73.

Kool, D., Agam, N., Lazarovitch N., Heitman, J.L., Sauer, T.J., Ben-Gal, A., 2014. A review of approaches for evapotranspiration partitioning. *Agricultural and Forest Meteorology*. **Volume 184**: 56-70.

Kostner, B. 2001. Evaporation and transpiration from forests in Central Europe-relevance of patch-level studies for spatial scaling. *Meteorology and Atmospheric Physics*. **Volume 76**: 69–82.

Lascano, R.J., Van Bavel, C.H.M., Hatfield, J.L., Upchurch, D.R. 1987. Energy and water balance of a sparse crop: simulated and measured soil and crop evaporation. *Soil Science Society of America Journal*, **Volume 51**: 1113-1121.

Laudon, H., Hemond, H.F., Krouse, R., Bishop, K.H. 2002. Oxygen-18 fractionation during snowmelt: Implications for spring flood hydrograph separation. *Water Resources Research*, **Volume 38(11)**: 40.1-40.10.

Laudon, H., Seibert, J., Köhler, S., Bishop, K. 2004. Hydrological flow paths during snowmelt: Congruence between hydrometric measurements and oxygen 18 in meltwater, soil water, and runoff. *Water Resources Research*. **Volume 40**: W03102-1-9. DOI: 10.1029/2003WR002455.

Lowman, M.D., Rinker, H.B. 2004. Forest Canopies, 2nd ed. Elsevier.

McCarter, C.P.R., Price, J.S. 2014. Ecohydrology of Sphagnum moss hummocks: Mechanisms of capitula water supply and simulated effects of evaporation. *Ecohydrology* **Volume 7**: 33–44.

McDonnell, J.J., Stewart, M.K., Owens, I.F. 1991. Effect of catchment-scale subsurface mixing on stream isotopic response. *Water Resources Research*. **Volume 27**: 3065–3073.

Manitoba Hydro, 2016. Hydrological Data. [Online] Available at: https://www.hydro.mb.ca/hydrologicalData/static/ [Accessed 2016].

Monteith, J. L. 1965. Evaporation and environment. *Symposia of the Society for Experimental Biology*, **Volume 19**: 205-224.

Moran, M.S., Scott, R., Keefer, T., Emmerich, W., Hernandez, M., Nearing, G., Paige, G., Cosh, M., O'Neill, P. 2009. Partitioning evapotranspiration in semiarid grassland and shrubland ecosystems using time series of soil surface temperature. *Agricultural and Forest Meteorology*, **Volume 149**: 59-72.

National Oceanic and Atmospheric Administration, 2016. NCEP North American Regional Reanalysis: NARR. [Online] Available at: http://www.esrl.noaa.gov/psd/data/gridded/data.narr.html

Penman, H.L. 1948. Natural evaporation from open water, bare soil, and grass. *Royal Society of London Proceedings*, **Series A**: 193:120-145.

Penuelas, J., Rutishauser, T., Filella, I. 2009. Phenology feedbacks on climate change. *Science* **Volume 324**: 887–888.

Raz-Yaseef, N., Yakir, D., Schiller, G., Cohen, S. 2012. Dynamics of evapotranspiration partitioning in a semi-arid forest as affected by temporal rainfall patterns. *Agricultural and Forest Meteorology*. **Volume 157**: 77–85.

Salvucci, G.D., Entekhabi, D. 1994. Explicit expressions for Green-Ampt (delta function diffusivity) infiltration rate and cumulative storage. *Water Resources Research*, **Volume 30**: 2661-2661.

Scott, R. L., Huxman, T.E., Cable, W.L., Emmerich, W.E. 2006. Partitioning of evapotranspiration and its relation to carbon dioxide exchange in a Chihuahuan Desert shrubland. *Hydrological Processes*, **Volume 20**: 3227-3243.

Shuttleworth, W. J., Wallace, J. S. 1985. Evaporation from sparse crops - an energy combination theory. *Quarterly Journal of the Royal Meteorological Society*, **Volume 111**: 839-855.

Šimůnek, J., Šejna, M., Saito, H., Sakai, M., van Genuchten, M. 2008. *The HYDRUS-1D Software Package for Simulating the Movement of Water, Heat, and Multiple Solutes in Variably Saturated Media, Version 4.08*, Riverside: University of California Riverside.

Smith, A.A., Welch, C., Stadnyk, T.A. 2016. Assessment of a lumped coupled flow-isotope model in data scarce Boreal catchments. *Hydrological Processes*. **Volume 30**: 3871-3884. DOI:10.1002/hyp.10835

Spence, C., 2007. On the relation between dynamic storage and runoff: A discussion of thresholds, efficiency, and function. *Water Resources Research*, **Volume 43**: 1-11. DOI:10.1029/2006WR005645.

Stannard, D.I., Weltz, M.A. 2006. Partitioning evapotranspiration in sparsely vegetated rangeland using a portable chamber. *Water Resources Research*. **Volume 42**: 1–13.

Stewart, J. B. 1988. Modelling surface conductance of pine forest. *Agricultrual and Forest Meteorology*, **Volume 43**: 17-43.

Sugimoto, A., Yanagisawa, N., Naito, D., Fujita, N., Maximov, T.C. 2002. Importance of permafrost as a source of water for plants in east Siberian taiga. *Ecological Research* **Volume 17**: 493-503. DOI: http://dx.doi.org/10.1046/j.1440-1703.2002.00506.x.

Sutanto, S. J., Wenninger, J., Coenders-Gerrits, A. M., Uhlenbrook, S. 2012. Partitioning of evaporation into transpiration, soil evaporation and interception: a comparison between isotope measurements and a HYDRUS-1D model. *Hydrology and Earth System Sciences*, **Volume 16**: 2605-2616.

Taylor, S., Feng, X., Renshaw, C.E. 2002. Isotopic evolution of snowmelt 2. Verification and parameterization of a one-dimensional model using laboratory experiments. *Water Resource Research*. **Volume 38:** 36-1-8. DOI: 10.1029/2001WR000815.

Tetzlaff, D., McDonnell, J.J., Uhlenbrook, S., McGuire, K.J., Bogaart, P.W., Naef, F., Baird, A.J., Dunn, S.M., Soulsby, C. 2008. Conceptualizing catchment processes: simply too complex? *Hydrological Processes*. **Volume 22**: 1727–1730.

Tolson, B. A., Shoemaker, C. A. 2007. Dynamically dimensioned search algorithm for computationally efficient watershed model calibration. *Water Resource Research*, **Volume 43**. W01413-1-16. DOI:10.1029/2005WR004723.

USACE. 1956. Snow Hydrology, Portland: s.n.

USGS. 2016 USGS Digital Elevation Models [Online] Available at http://data.geocomm.com/dem/ [Accessed 2016].

Welch, C., Smith, A.A., Stadnyk, T.A. in prep. Physiographic controls on the isotopic composition of river water in 16 boreal catchments, Canada.

Williams, D.G., Cable, W., Hultine, K., Hoedjes, J.C.B., Yepez, E.A., Simonneaux, V., Er-Raki, S., Boulet, G., de Bruin, H.A.R., Chehbouni, A., Hartogensis, O.K., Timouk, F. 2004. Evapotranspiration components determined by stable isotopes, sap flow and eddy covariance techniques. *Agricultural and Forest Meteorology*, **Volume 125**: 241-258.

Woo, M. 1992. Impacts of climate variability and change on Canadian wetlands. *Canadian Water Resources Journal*, **Volume 17(1)**: 63-69.

Yepez, E.A., Williams, D.G., Scott, R.L., Lin, G. 2003. Partitioning overstory and understory evapotranspiration in a semiarid savanna woodland from the isotopic composition of water vapor. *Agricultural and Forest Meteorology*, **Volume 119**: 53-69.

Zhang, S., Wen, X., Wang, J., Yu, G., Sun, X. 2010. The use of stable isotopes to partition evapotranspiration fluxes into evaporation and transpiration. *Acta Ecologica Sinica*, **Volume 30**: 201-209.

Zhang, Y., Liu, C., Shen, Y., Kondoh, A., Tang, C., Tanaka, T., Shimada, J. 2002. Measurement of evapotranspiration in a winter wheat field. *Hydrological Processes*, **Volume 16**: 2805-2817.

CHAPTER 6: EXAMINATION OF STORAGE VARIANT TRANSIT TIME DISTRIBUTIONS IN HIGHLY SEASONAL WATERSHEDS

Aaron Smith[1,2], Chani Welch[1], Tricia Stadnyk[1]

[1]Department of Civil Engineering, University of Manitoba, Winnipeg, Manitoba

[2]Department of Geosciences, University of Aberdeen, Aberdeen, UK

This manuscript has been submitted to Water Resources Research

This chapter examines the application of time-variant transit time distributions in northern watersheds, dominated by intra-annual changes in sub-surface flow paths and seasonality of vegetation growth which temporally vary the partition of evapotranspiration (ET). The use of a temperature-dependent ET partition model, developed in Chapter 5, is essential for independent analysis of evaporation and transpiration flux ages. Stable water isotopes $\delta^{18}O$ and $\delta^{2}H$ are used in conjunction with StorAge Selection (SAS) functions to separately estimate transit time distributions of discharge, evaporation, transpiration. These distributions provide insights to long-term storage availability and the potential impacts of climate change on both storage availability and the partition of ET.

CHAPTER 6

6.1 ABSTRACT

Seasonal evapotranspiration (ET) greatly influences sub-surface storage availability in northern watersheds where freeze-thaw cycles inter- and intra-annually change the volume of water accessible to vegetation (via transpiration) and evaporation. StorAge Selection (SAS) functions are one way that changes in subsurface transport may be related to changes in watershed storage. In northern latitudes, changes to effective watershed storage due to freeze-thaw cycles must also be considered. Here we decompose the SAS functions to include time-varying maximum potential storage and evapotranspiration partitioning. Maximum potential storage is estimated using monthly time-steps of storage-discharge relationships. A simple two-parameter ET partition equation is applied to independently assess evaporation and transpiration age using two distributions. The mean effective subsurface storage during winter was between 560 mm and 1030 mm, compared to 81 mm to 333 mm during summer. Storage volumes were directly related to mean discharge age, with the youngest water discharged during summer. Mean evaporation age was approximately one month, while mean transpiration age ranged from two to three years. Independently assessing evaporation and transpiration distributions provides a first-order estimate of the influence of each flux on the storage-discharge transit time.

CHAPTER 6

6.2 INTRODUCTION

Northern watersheds are strongly influenced by seasonal changes in water flux and availability. Climate warming-induced changes affecting high latitude regions include decreasing permafrost coverage, and lengthening frost-free periods, which act to increase subsurface water storage and subsequent annual evapotranspiration (ET) (Abtew and Melesse 2012). ET and water storage are positively correlated, in that increased subsurface storage results in increasing ET flux (Jung et al., 2010; Zhang et al., 2016). In hydrologic modelling, ET is often conceptualised as a lumped variable incorporating the two components: evaporation (E) and transpiration (TR). However, the ratio of E to TR is influenced by soil moisture and recent precipitation influence (Sutanto et al., 2012; Zhang et al., 2016; Smith et al., submitted). Differing availability of water for E and TR suggests that the components independently affect the volume of water in storage. Furthermore, in high-latitude environments the partition of ET into its components changes on a temporal basis and therefore may restrict the availability of water to either E or TR (Smith et al., submitted). Such differences may be observable in the ages of evaporated and transpired water, and may have a considerable impact on the estimated age of water in storage, influencing perceived flow paths in transit time analysis (Botter 2012).

Time-invariance in storage-discharge relationships has been identified as a limiting assumption in lower-latitude watersheds, with increases in total catchment storage decreasing the estimated transit time at the outlet (e.g. van der Velde et al., 2012; Harman 2015). Transit time modelling has been adapted to include temporal-variability of the mean transit time with: 1) functions of temporal catchment mixing (Klaus et al., 2015); 2) moving window and high resolution data (Birkel et al., 2012; Birkel et al., 2015); 3) hydrological modelling including lumped and distributed model storage estimation (Soulsby et al., 2015; van Hujigevoort et al., 2016); 4) time-variant parameters of distributions (Hrachowitz et al., 2010); 5) “waiting”

functions for temporal storage release (Botter et al., 2011); 6) StorAge Selection (SAS) functions (Harman 2015); and 7) dual storage STorage Outflow Probability (STOP) functions (van der Velde et al., 2012; van der Velde et al., 2015). The latter three methods modified the conceptual model of estimating catchment transit time introduced by Niemi (1977) to include temporal variance of storage. The conceptual difference is based upon 1) conservation law, 2) closure relationships (solving the conservation law) and 3) functions for selection from storage. SAS and STOP explicitly aimed to reproduce dynamic conditions where high antecedent storage results in newer water exiting the watershed at a faster rate. Such modifications are ideal for watersheds with permafrost and seasonal frozen ground because of the role of seasonal storage changes on the reproduction of catchment flow pathways in the model (Heidbuchel et al., 2012; van der Velde et al., 2015), though few studies have attempted simulation in basins with these conditions (Tetzlaff et al., 2015).

The mass-balance conceptualisation of time-variant functions has directly incorporated time-variance of ET selection, which is essential for understanding watershed mean transit time (Ali et al., 2014). ET flux has a much shorter transit time than storage-discharge since water used for both E and root uptake occur from near surface storages (van der Velde et al., 2015). Time-variant methods using stable water isotopes, however, have not addressed the differences in the transit time of E relative to TR, rather, accounting for evaporative fractionation within the ET distribution (Benettin et al., 2017). The separation of ET using stable water isotopes is dependent on the assumption that TR does not preferentially remove light or heavy isotopes from storage (Ehleringer and Dawson 1992), and that atmospheric conditions govern evaporative fractionation of soil water (Craig and Gordon 1965). Temporal variation in the ratio of E/ET in northern basins is likely to further affect the estimation of catchment transit time.

CHAPTER 6

The goals of this research are to 1) identify temporal changes in available water storage, 2) adapt a time-variant transit time model to include E and TR separately using ET partitioning, and 3) apply the time-variant transit time model to a catchment to identify the influence of TR distribution and age on the isotopic composition of water at the catchment outlet. We identify temporal differences in available storage by developing monthly storage-discharge relationships from precipitation, ET, and observed discharge. Implementation of a temperature-dependent ET partition model enables assessment of isotopic fractionation effects in storage. We apply a variety of transit time distributions to E and TR fluxes to identify the influence of distribution selection on the estimated ages. These methods are applied to a northern Canadian watershed with annual freeze thaw cycles and temporal variability of the ET partition.

6.3 SITE DESCRIPTION

The lower Nelson River Basin (LNRB), in northern Manitoba, Canada, is of interest to watershed practitioners due to significant water usage in the region, and highly seasonal hydrology (Smith et al., 2015). The Sapochi River basin (55^{o}54' N, 98^{o}29' W) is a relatively small (391 km^{2}) northern Canadian watershed located within the Boreal forest region of the Canadian Shield (Figure 6-1). It has a long-term discharge record (1993 to present) and isotopic measurements (oxygen-18, $\delta^{18}O$, and deuterium, $\delta^{2}H$, 2011 to present). The basin receives on average 542 mm of annual precipitation, with approximately 70% of total precipitation falling as rainfall. Total water loss due to ET and sublimation is estimated at 348 mm from long-term water balance estimates.

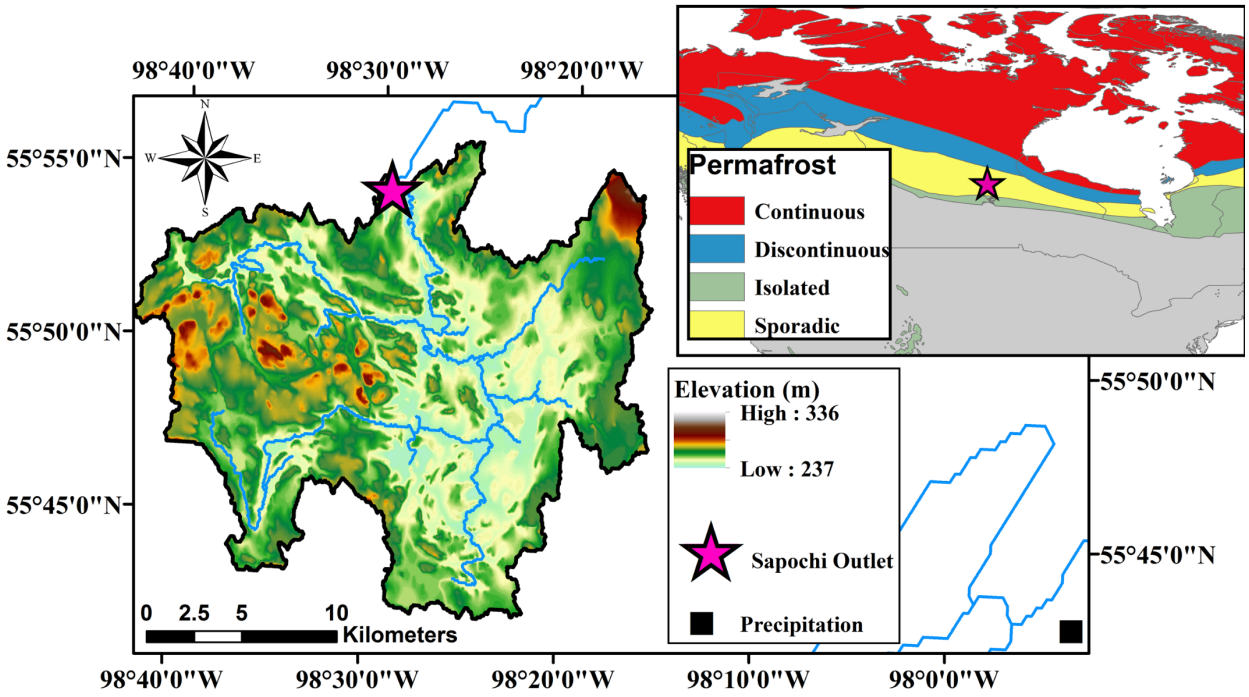

Figure 6-1. The topography and channels of the Sapochi River basin with the riverine measurement location (purple star) and precipitation measurement location (black square) at Thompson Airport. The subset figure indicates the location of the Sapochi River in the lower Nelson River basin and North America. The colour bands indicate permafrost distribution.

Catchment land cover and physiography are described in detail in other studies in the area (Smith et al., 2015, 2016, submitted). Soils in the basin consist of generally shallow layers of silt, till, clay, and organic materials, with occasional outcropping of the underlying Precambrian bedrock. Land cover in the basin is a mixture of shrubs (37%), coniferous forests (24.6%), wetlands (21%), broadleaf forests (12.5%), and lakes (3.7%). The Sapochi River has been studied with tracer-aided models (stable water isotopes) to assess the source waters (Smith et al., 2015), and to identify the temporal trends of ET partitioning on a catchment scale (Smith et al., submitted). These studies have identified rapid overland flow events in response to snowmelt and precipitation events as storages fill up. Meteorology is measured 43km from the basin outlet at the Thompson Airport (Figure 6-1), a class A Environment Canada meteorological station (WMO standards, Environment Canada 2016). Composite samples of rainfall (approximately

monthly) and snowpack (on average twice per year, including depth-dependent) have been collected since 2010 and analysed with a precision of ±1.0 per mille (‰) for δ^2H and ±0.2‰ for $\delta^{18}O$ to the Vienna Standard Mean Ocean Water 2 (VSMOW2) standard. Sampling of stream flow compositions followed the sampling program described in Smith et al. (2015).

6.4 MODIFICATION OF TIME-VARIANT TRANSIT TIME FUNCTIONS FOR HIGH-LATITUDE WATERSHEDS

Application of simple hydrologic models, such as transit time distributions, to high-latitude watersheds is generally more complex than mid-latitude watersheds, predominantly due to seasonal freezing of the sub-surface (changing storage) and snowmelt processes. However, estimation of time-variant transit time is dependent on the probabilistic selection of water from storage (via StorAge Selection functions, SAS), and therefore initial approximation of changes in watershed storage is essential to inform SAS functions. Furthermore, stable isotope composition used in SAS functions may temporally vary in storage due to evaporative effects. SAS functions are modified to incorporate: 1) intra-annual changes in storage availability and 2) seasonal changes in evaporative fractionation of riverine isotopic compositions.

6.4.1 INFERRING SEASONALITY IN WATERSHED STORAGE FROM DISCHARGE

6.4.1.1 SEPARATING OVERLAND FLOW AND STORAGE DISCHARGE

StorAge selection functions (SAS) inherently assume temporal changes to probability distributions for discharge and ET due to storage. Observed basin discharge data are readily available; however, storage is difficult to measure consistently at high spatial and temporal resolutions. To overcome this issue, techniques that correlate storage to discharge have been developed using hydrologic modelling and observed discharge (Kirchner 2009). Such methods, however, are unable to account for rapid overland flow (i.e., when discharge is not directly proportional to precipitation) and temporally changing storage potential (i.e., due to freezing);

both of which are frequently experienced in high-latitude basins. It is first necessary to separate discharge into the portion generated by overland flow versus the portion released from storage. The portion of discharge released from storage (i.e., observed storage discharge, Q_S) is obtained from observed discharge, Q_{Obs}:

$$\boldsymbol{Q_S(t) = Q_{Obs}(t) - Q_{Obs}(t) \cdot F_{Ov}(t)} \quad 6\text{-}1$$

where $F_{Ov}(t)$ is the fraction of observed discharge resulting from overland flow. The fraction of observed discharge from overland flow may be obtained from a lumped hydrologic model. Storage-discharge relationships may then be directly applied to $Q_S(t)$ and overland flow (i.e., $Q_{Ov}(t) = Q_{Obs}(t)\, F_{Ov}(t)$), where overland flow storage effectively becomes channel attenuation.

6.4.1.2 APPLICATION OF TEMPORALLY VARIANT STORAGE-DISCHARGE RELATIONSHIPS

Watershed discharge is related to changes in storage through the rate of change of Q_S and ET leaving storage, and precipitation or snowmelt entering storage (Kirchner 2009). The change in Q_S is given by

$$\boldsymbol{\frac{\partial Q_S}{\partial t} = \frac{\partial Q_S}{\partial S}\frac{\partial S}{\partial t} = \frac{\partial Q_S}{\partial S}(P - ET - Q)} \quad 6\text{-}2$$

where $\partial Q_S/\partial t$ is the rate of change of Q_S with time, $\partial S/\partial t$ is the rate of change of storage with time, and $\partial Q_S/\partial S$ is the rate of change of Q_S with change in storage. If precipitation and ET are negligible relative to flow in each time-step, Equation 6-**Error! Reference source not found.** may be generalised to

$$\boldsymbol{g(Q_S) = \frac{-\frac{dQ_S}{dt}}{Q_S} = \frac{dQ_S}{dS}} \quad 6\text{-}3$$

which directly equates storage to discharge through the function $g(Q_S)$. Integration of Equation 6-3 and solving for storage reveals that $g(Q_S)$ must always be positive, therefore the storage

relationship may only be calculated using the recession limb hydrograph. Finally, storage is related to Q_S through a power law relationship:

$$\boldsymbol{g(Q) = a \cdot Q^{b-1}} \quad 6\text{-}4$$

where a is the intercept and b is the slope of the log-log relationship of dQ_S/dt and Q_S. Substitution of the right hand side of Equation 6-3 into Equation 6-4, rearranging and integration yields:

$$\int \boldsymbol{dS} = \int \boldsymbol{\frac{1}{a} \cdot Q^{1-b} dQ} \quad 6\text{-}5$$

and is solved as:

$$\boldsymbol{S - S_o = \frac{1}{a} \cdot \frac{1}{2-b} \cdot Q^{2-b}} \quad 6\text{-}6$$

where S_o is a constant of integration.

Discharge data are commonly collected on a daily time step; a temporal scale at which ET is non-negligible during the summer months. Hourly data may be estimated by smoothing over a three-day polynomial discharge regression. In addition, daily precipitation may be assumed to have a uniform intensity over 24 hours for the hyetograph. Large basins with low topography can result in extended recession periods with the maximum slope of the recession limb occurring after a 'transition' period following the peak flow. For example, in the Sapochi, the maximum slope of the recession limb has been estimated to commonly occur up to one week after the hydrograph crest (Smith et al., submitted). These transition periods are consistent with routing attenuation rather than storage release. The transition period inhibits interpretation of the relationship between discharge and its rate of change, as it has abnormally low change in discharge despite high discharge rates. The transition period may be eliminated by identifying the second order differential of discharge (d^2Q/dt^2) and ensuring positive values following a peak event are not considered.

Air temperatures consistently below freezing during the winter months in high-latitude basins seasonally freezes soil water, thereby decreasing storage and constraining flow paths (typically November through March, or later). Rather than assessing a static trend for Q_S and dQ_S/dt, monthly variation in temperature can be used to estimate frozen soils (Tetzlaff et al., 2015; Flynn et al., 2016), reducing scatter in the storage-discharge relationship and revealing meaningful storage changes over time. As shown by Kirchner (2009), higher scatter will likely occur during low discharge periods; therefore, dQ_S/dt should be binned for each month, with the size of the bins determined by the conditions of the first order Taylor-series expansion error (standard error of $dQ_S/dt \leq ½$ of the mean dQ_S/dt) starting from highest Q_s. Storage as a function of Q_s is obtained by integrating the daily slope and intercept of the log-log relationship of $\bar{Q}_S$ and $\overline{dQ_s/dt}$. Temporal variability of storage contributing to discharge is identified by comparing the storage volumes in different periods to a standard discharge. For example, frozen soil reduces effective storage (mobile water) in winter relative to summer; therefore, more water must be stored in winter to produce the same discharge as during summer. For SAS functions, relative changes in watershed 'wetness' are defined through changes in storage relative to average storage. For simplicity, storage is standardised by the daily mean storage (i.e., $S_N = \frac{S-\mu(S)}{\sigma(s)}$), reducing the impact of storage availability on SAS functions.

6.4.2 MATHEMATICAL DERIVATION OF EVAPORATION FRACTIONATION IN STORAGE SELECTION FUNCTIONS

6.4.2.1 TEMPORAL VARIABILITY OF TRANSIT TIME DISTRIBUTIONS WITH STORAGE

Transit time distributions (TTD) are used to approximate mixing and transport patterns at the catchment scale. Historically, TTDs translate input (entering storage at time $t_i<t$) as a probability of its exit at time t. SAS functions transpose the probability distribution to storage,

tracking parcels of water and estimating the probability of water parcels of age $T=t-t_i$ leaving storage relative to their age and storage, rather than t. In time-variable studies, inputs are identified and generally referred to as water parcels in storage with age τ (Harman 2015; van der Velde et al., 2015). Expanding the conservation equation from Niemi (1977) and Botter et al. (2011) to explicitly include overland flow (Section 6.4.1.1), E, and TR with the change of storage over time gives the change in storage with time as

$$\frac{\partial S_T}{\partial t} = J_T(T,t) - \sum_{j=1}^{n} Q_{S_{Tj}}(T,t) - \sum_{j=1}^{n} Q_{Ov_{Tj}}(T,t) - \sum_{j=1}^{n} E_{T,j}(T,t) - \sum_{j=1}^{n} TR_{T,j}(T,t) - \frac{\partial S_T}{\partial T} \quad 6\text{-}7$$

where J_T is water entering storage, $Q_{S_{Tj}}$ is outflow from storage, $Q_{Ov_{Tj}}$ is overland flow, and E_{Tj} and TR_{Tj} are evaporation and transpiration fluxes, respectively. Equation 6-7 describes the flow path of all water parcels; however, complex systems prevent tracing of individual parcels of water. Harman (2015) suggested that the conservation law may be solved using age-ranked storage. In this method, the probability of water selected from age-ranked storage columns is determined using a distribution

$$\overleftarrow{p(T,t)} = \Omega_{Q_s}(S_T,t) \quad 6\text{-}8$$

where $\Omega_{Q_s}(S_T,t)$ is a cumulative distribution function (i.e. $\sum S_T = 1$) and $\overleftarrow{p(T,t)}$ is a backward TTD (also been referred to as the reverse TTD (van der Velde et al., 2012), or the condition exit time TTD (Botter et al., 2011). Conservation equation fluxes may be decomposed into two parts, total flux and probability of water selection ($\overleftarrow{p(T,t)}$), to describe the contribution of water of age $\tau < t$ to total flux. Reformulation of Equation 6-7 with probability functions of storage age selection provides

$$\frac{\partial S(t) \cdot \overleftarrow{p_S(T,t)}}{\partial t} = -Q_S(t) \cdot \overleftarrow{p_Q(T,t)} - Q_{Ov}(t) \cdot \overleftarrow{p_Q(T,t)} - E(t) \cdot \overleftarrow{p_E(T,t)} - TR(t) \cdot \overleftarrow{p_{TR}(T,t)} - \frac{\partial S(t) \cdot \overleftarrow{p_S(T,t)}}{\partial T} \quad 6\text{-}9$$

where $J_T(T,t)$ is not shown for simplicity and is assumed to have an age of zero, and the subscripts for backward transit times (Q_S, Q_{Ov}, E, TR, and S) denote storage-discharge, overland discharge, E, TR, and storage, respectively. With this formulation, a variety of distributions for $\overleftarrow{p(T,t)}$ may be used to describe the selection of water from storage; including uniform, exponential, and gamma distributions (Harman 2015).

6.4.2.2 TIME-VARIANT ET PARTITIONING

Transit time modelling has generally been conducted with lumped ET rather than its independent components for two reasons: 1) measurement limitations for E and TR across wide spatial and temporal scales, and 2) limited methodology for ET partitioning using isotopic approaches. Here, the latter is addressed through ET partitioning within TTDs (Equation 6-9), thus allowing E and TR to vary independently through time. Two methods are directly applicable to ET partitioning within time-variant transit time functions without introducing significant complexities: 1) ET mass-balance, and 2) temperature-dependent partitioning.

ET mass balance requires daily time-steps and corresponding isotopic compositions of atmospheric fluxes to identify flux components

$$ET(t)\delta_{ET}(t) = E(t) \cdot \int_0^t \overleftarrow{p_E(T,t)}\delta_E(T,t)dT + TR(t) \cdot \int_0^t \overleftarrow{p_{TR}(T,t)}\delta_{TR}(T,t)dT \quad 6\text{-}10$$

where δ_E is the evaporation vapour composition, δ_{TR} is the xylem or soil water isotopic composition (assumed to be equal), and δ_{ET} is the vapour ET composition. δ_{ET} can be estimated using the Keeling plot (i.e., CO_2 estimated in the atmosphere) with the intercept of the inverse of

vapour composition (δ_v) and mixing ratio (Kahmen et al., 2008; Zhang et al., 2010). Rearranging the mass-balance (Equation 6-10), total E can be estimated using δ_E, δ_{TR}, δ_{ET}, and ET (modified from Zhang et al., 2010) and assuming a $\overleftarrow{p(T,t)}$ of E and TR

$$\boldsymbol{E(t) = \frac{\left(\int_0^t \overleftarrow{p_{TR}(T,t)}\delta_{TR}(T,t)dT - \delta_{ET}(t)\right)}{\int_0^t \left(\overleftarrow{p_{TR}(T,t)}\delta_{TR}(T,t) - \overleftarrow{p_E(T,t)}\delta_E(T,t)\right)dT} ET(t)} \quad 6\text{-}11$$

or with measured TR compositions ($\delta_{TR,M}$)

$$\boldsymbol{E(t) = \frac{\delta_{TR,M}(t) - \delta_{ET}(t)}{\delta_{TR,M}(t) - \int_0^t \overleftarrow{p_E(T,t)}\delta_E(T,t)dT} \cdot ET(t)} \quad 6\text{-}12$$

The difference in the application of Equation 6-11 and Equation 6-12 is what is calibrated: use of Equation 6-11 during modelling facilitates calibration of $\overleftarrow{\int_0^t \overleftarrow{p_{TR}(T,t)}\delta_{TR}(T,t)dT}$ to $\delta_{TR,M}$, whereas Equation 6-12 directly applies $\delta_{TR,M}$ to best estimate E(t) while $\overleftarrow{p_{TR}(T,t)} \cdot \delta_{TR}(T,t)$ is calibrated to $\delta_{TR,M}$ to ensure water and mass-balance. When separate vapour and atmospheric measurements are not available there is insufficient flux evidence of a flux gradient of δ_{ET} to δ_E in the Keeling methods, resulting in $\delta_{ET} = \delta_E$ and ET = E; therefore the method (Equations 6-10 to 6-12) is not applicable.

The second method of partitioning ET within SAS functions is more parameterised; however, it only requires riverine and precipitation isotopic measurements for $\delta^{18}O$ and $\delta^{2}H$ and air temperature

$$\boldsymbol{\frac{E}{ET} = ETp = \left(\frac{Temp - Temp_{min}}{Temp_{max} - Temp_{min}}\right)^{MA} + Mc} \quad 6\text{-}13$$

where $Temp_{min}$ and $Temp_{max}$ are temperature normalisation parameters, MA is a shape parameter, and Mc is a scale parameter (Smith et al., submitted). MA and Mc are calibrated by simultaneous optimisation of the storage evaporative enrichment of riverine $\delta^{18}O$ and $\delta^{2}H$, which are linearly correlated (Craig 1961). To prevent mathematical errors, $Temp_{min}$ must be less than or equal to

the minimum observed temperature over the simulation period. Previous use of temperature-dependent partitioning for the Sapochi River basin and other similar basins found *MA* is generally between -0.1 and -0.5, and *Mc* is between -0.85 and -1 (Smith et al., submitted). The temperature-dependent ET partition model was developed within a tracer-aided model, which assumed a relationship between potential ET (PET) and actual ET (AET) through soil moisture. Soil moisture may be estimated for SAS functions by relating the storage volume (Section 6.4.2) to soil moisture (van der Velde et al., 2015). Here, we define the relationship of PET to AET through the probability of storage occurrence using a normal distribution to describe storage volume

$$\boldsymbol{SM_{JD}(t) = \Omega_{SM}(\overline{S_{JD}}, \sigma_{JD}) \cdot (S_{max} - S_{min}) + S_{min}} \quad 6\text{-}14$$

where $\Omega_{SM}(\overline{S_{JD}}, \sigma_{JD})$ is a cumulative distribution function, $\overline{S_{JD}}$ is mean Julian day storage, σ_{JD} is Julian day standard deviation, and S_{max} and S_{min} are parameters with values between zero and one. Inter-annual Julian day storages are normalised by the daily mean to yield the probability of $\overline{S_{JD}}$ and σ_{JD} on a given day. When S_{max} is known (assumed or calibrated), S_{min} may be solved for by substituting Equation 6-14 into the long-term water balance

$$\boldsymbol{\sum (P - Q) = \sum SM_{JD}(t) \cdot PET} \quad 6\text{-}15$$

where S_{min} must be less than S_{max}. When S_{max} is equal to S_{min}, temporal variability of storage does not influence the relationship of AET to PET and Equation 6-14 is simplified to a constant value (S_{min}).

6.4.2.3 EVAPORATIVE FRACTIONATION OF WATER PARCELS IN STORAGE

Similar to the discharge distribution, the E distribution in the conservation equation (Equation 6-9) selects water using the age-ranked distribution. Evaporation is known to isotopically fractionate due to preferential removal of lighter water (H^1 and O^{16} rather than H^2

and O^{18}), thereby changing the isotopic composition of water remaining in a parcel. To identify how the isotopic composition of a parcel changes with time, we apply mass to the conservation equation, accounting for outflow, changes in volume, and changes in mass. Since water age (T) is the same for a single parcel then the mass-balance may be simplified to

$$\frac{\boldsymbol{dV_T(t)}}{\boldsymbol{dt}}\boldsymbol{\delta_s(t)} = \boldsymbol{I_T(t)\cdot\delta_I(t)\cdot\chi(T) - Q(t)\cdot\delta_s(t)\cdot\overleftarrow{p_Q(T,t)} - E(t)\cdot\delta_E(t)} \\ \boldsymbol{\cdot\overleftarrow{p_E(T,t)} - TR(t)\cdot\delta_{TR}(t)\cdot\overleftarrow{p_{TR}(T,t)} - \frac{d\delta_s\,(t)}{dt}V_T(t)} \quad \text{6-16}$$

where $V_T(t)$ is the volume of a parcel of water, $I(t)$ is the input flux, δ_I is the initial isotopic composition, $Q(t)$ is flux to the stream, $E(t)$ is evaporation, $TR(t)$ is transpiration flux, and δ_S, δ_E and δ_{TR} are the storage, evaporative vapour and transpiration isotopic compositions, respectively. Input to a storage parcel is limited by a Dirac function ($\chi(T)$) that ensures water only enters instantaneously, at time t_i. On a daily time-step, the isotopic composition of $TR(t)$ may be assumed to be equivalent to the xylem water. Xylem water is replenished via root-uptake, which does not alter the isotopic composition of water removed from storage (i.e., non-fractionating). Where all water fluxes are known, δ_E and δ_s are the only unknowns. δ_E may be described as a function of the isotopic composition of storage and atmospheric resistance (Craig and Gordon 1965)

$$\boldsymbol{\delta_E(T,t) = \frac{\delta_s(t) - RH(t)\cdot\delta_A(t) - \varepsilon(t)}{1 - RH(t) + \varepsilon_K(t)/1000}} \quad \text{6-17}$$

where RH is relative humidity, δ_A is atmospheric isotopic composition, ε is total equilibrium fractionation, and ε_k is the kinetic fractionation. δ_A can be estimated assuming isotopic equilibrium with precipitation (δ_P) (Horita and Wesolowski 1994). Total equilibrium fractionation is the sum of equilibrium fractionation (ε^*) and kinetic fractionation. Kinetic fractionation (ε_k) may be obtained from (Gonfiantini 1986):

$$\boldsymbol{\varepsilon_k(t) = n \cdot C_k \cdot \theta \cdot (1 - RH(t))} \quad \text{6-18}$$

where n is the effect of wind turbulence on ambient moisture (e.g., 0.5 for fully turbulent and 1 for stagnant, Gat 2010), C_k is the ratio of molecular diffusivity (O^{18}/O^{16} and H^2/H^1), and θ is the influence of humidity advection on ambient moisture (e.g. 0.88 for North American Great Lakes and 1 for small lakes, Gat 2010). δ_s may be solved by substituting Equation 6-17 and Equation 6-18 into Equation 6-16.

The appropriate solution to Equation 6-16 depends on whether the system is time-dependent ($\Delta V=0$), or fraction dependent ($\Delta V \neq 0$) over a time-step, dt (Gibson 2002). Since a parcel is labelled at the time it enters storage (t_i), its volume will only decrease with time; therefore, the solution through all time may be described using the fraction-dependent solution of δ_S

$$\boldsymbol{\delta_s(t + dt) = \delta_{ss}(t) + (\delta_s(t) - \delta_{ss}(t)) \cdot f(t)^{\frac{E(t) \cdot \overleftarrow{p_E(T,t)} \cdot (m(t)-1)}{\Delta S}}} \quad \text{6-19}$$

where f is the change in volume over a time-step $\left(0 \leq \left(f(t) = \frac{S(t+dt)}{S(t)}\right) \leq 1\right)$, $\delta_{ss}(t)$ is the steady-state composition, and $E(t) \cdot \overleftarrow{p_E(T,t)}$ is the evaporation from the parcel. When f(t)<1, the isotopic composition of the parcel approaches $\delta_{ss}(t)$

$$\boldsymbol{\delta_{ss}(t) = \frac{\left(E(t) \cdot \overleftarrow{p_E(T,t)}\right) \cdot m(t) \cdot \left(RH(t) \cdot \delta_A(t) + \varepsilon(t)\right)}{E(t) \cdot \overleftarrow{p_E(T,t)} \cdot (m(t) - 1) - TR(t) \cdot \overleftarrow{p_{TR}(T,t)} - Q(t) \cdot \overleftarrow{p_Q(T,t)}}} \quad \text{6-20}$$

where $E(t) \cdot \overleftarrow{p_E(T,t)}$ is controlled by atmospheric conditions through δ_A, RH, and ε.

Atmospheric effects on a parcel may be obtained by substituting Equation 6-20 into Equation 6-19 for each time $t>t_i$ until the storage parcel is infinitely small. However, steady-state isotopic composition $\delta_{ss}(t)$ changes over time as δ_A, RH, and ε change with time ($t_i \leq \xi \leq t$), where ξ is some time between when the parcel of water entered storage and the current time-

step, complicating direct estimation of Equation 6-19 at any time $t>t_i$. Solution may be simplified by developing an infinite series based on atmospheric effects. For example, through three time-steps,

$$\begin{aligned}\boldsymbol{\delta_s(t+3\cdot dt)} = &\boldsymbol{(\delta_s(t_i)-\delta_{ss}(t_i))\cdot f(t)^{A(t)}\cdot {f_{t+1}}^{A(t+dt)}{f_{t+2}}^{A(t+2\cdot dt)}}\\ &\boldsymbol{+\big(\delta_{ss}(t_i)-\delta_{ss}(t+dt)\big){f_{t+1}}^{A(t+dt)}{f_{t+2}}^{A(t+2\cdot dt)}}\\ &\boldsymbol{+\big(\delta_{ss}(t_i+dt)-\delta_{ss}(t_i+2\cdot dt)\big){f_{t+2}}^{A(t+2\cdot dt)}+\delta_{ss}(t_i+2\cdot dt)}\end{aligned} \quad 6\text{-}21$$

where t+3·dt is three time-steps from t_i. A(t) describes the changes that atmospheric conditions have on the isotopic composition of a parcel,

$$\boldsymbol{A(t)=\frac{E(t)\cdot\overleftarrow{p_E(T,t)}\cdot(m(t)-1)}{E(t)\cdot\overleftarrow{p_E(T,t)}+TR(t)\cdot\overleftarrow{p_{TR}(T,t)}+Q(t)\cdot\overleftarrow{p_Q(T,t)}}} \quad 6\text{-}22$$

Using the mathematical principle of exponents, $y^{\log_y(x)}=x$, all volume fractions may be rearranged to have the same base. Using these principles, the isotopic composition of water in storage at any time after t_i is simplified into two terms: the current time-step deviation (Equation 6-19), and the long-term isotopic steady-state,

$$\begin{aligned}\boldsymbol{\delta_s(T,t)} = &\boldsymbol{\left[\sum_{\xi=t_i+1}^{t-1} {f_i}^{g(\xi,t)}\big(\delta_{ss}(\xi-1)-\delta_{ss}(\xi)\big)\right]+\delta_{ss}(t)+f(t)^{A(t)}(\delta_{ss}(t-1)}\\ &\boldsymbol{-\delta_{ss}(t))}\end{aligned} \quad 6\text{-}23$$

where $g(\xi,t)$ is the cumulative atmospheric effect on storage defined with A(ξ) and f(t)

$$\boldsymbol{g(\xi,t)=A(\xi)+\sum_{j=\xi+1}^{t} A(j)\cdot\log_{f_i} f_j} \quad 6\text{-}24$$

The functions A(ξ) and g(ξ) influence the degree of water parcel fractionation: when evaporation is zero, no fractionation occurs (i.e., δ_S(t+dt) = δ_S(t)), and when evaporation is the total flux

selected from a parcel, maximum potential fractionation occurs (i.e., $f^{(m-1)}$ where $m \geq 1$). The isotopic compositions for all parcels of water in storage at time *t* are solved independently using Equations 6-21 to 6-24.

6.5 APPLICATION OF SAS FUNCTIONS TO THE SAPOCHI RIVER BASIN

6.5.1 FLUX DISTRIBUTION SELECTION

The SAS time-variant model (Harman 2015) was selected to demonstrate the application of ET partitioning and storage fractionation in TTD modelling. To apply this model, distributions were required for each flux: storage-discharge, overland-discharge, E and TR. The gamma distribution was used to estimate storage-discharge age and overland-discharge age as it has previously been shown to best represent watershed discharge relationships (Kirchner et al., 2001; Harman 2015). The fractions of storage-discharge and overland-flow discharge were obtained from a previously calibrated tracer-aided model of the Sapochi River basin (Smith et al., submitted). E and TR were estimated using three combinations of distribution models to best hypothesize the selection of water from storage. The selection of these distributions was based on the "two water worlds" hypothesis, where mobile water is readily available (younger), and immobile water is tightly bound and not easily replenished (older) (McDonnell 2014). The exponential distribution hypothesizes that younger water is preferentially selected, while also providing information on the relative influence of older, less mobile water. For the exponential distribution, a lower MTT indicates less influence of older water, while a higher MTT indicates relatively equal preference of young and old water. The gamma distribution provides an additional hypothesis of preferential young water (low shape parameter) versus more complex mixing of older water (high shape parameter). Finally, the uniform distribution tests the hypothesis of volumetric selection of water from storage. Comparison of distributions from

storage to a screened piezometer (i.e., mobile water only) provides an estimation of mobile versus immobile water selection. Estimated older water from a distribution indicates some potential selection from tightly bound, immobile water, whereas younger water indicates a preference for more readily mobile water. The distributions were tested using three model combinations: 1) exponential distribution for E and TR (E^eTR^e), 2) exponential for E and uniform for TR (E^eTR^u), and 3) gamma for E and uniform for TR (E^gTR^u).

6.5.2 PARAMETERISATION OF SAS FUNCTIONS

Monthly storage-discharge and overland-discharge curves were developed using 4 % of the samples in each month to develop appropriate bins: 4 % was necessary to meet conditions of the first order Taylor-series expansion error. Spring and summer months (May-July) consistently experienced greater changes in storage-discharge (i.e., ln(-dQ/dt)) for the same observed discharge as late summer and fall (August–October) (Figure 6-2a). There is a progressive shift downward (i.e., decreasing intercept) from early to late summer and fall before transitioning to the 'cluster' of winter flows. The relatively low flow during winter months limits the identification of distinct differences between months without further information (e.g., depth of frozen ground or ground temperatures). Examination of overland-discharge relationships did not show the same monthly variability as storage-discharge (Figure 6-2b). As anticipated, the greatest discharge and change in discharge from overland-storage was observed during freshet periods (April-May), as well as during large rain events (i.e., August).

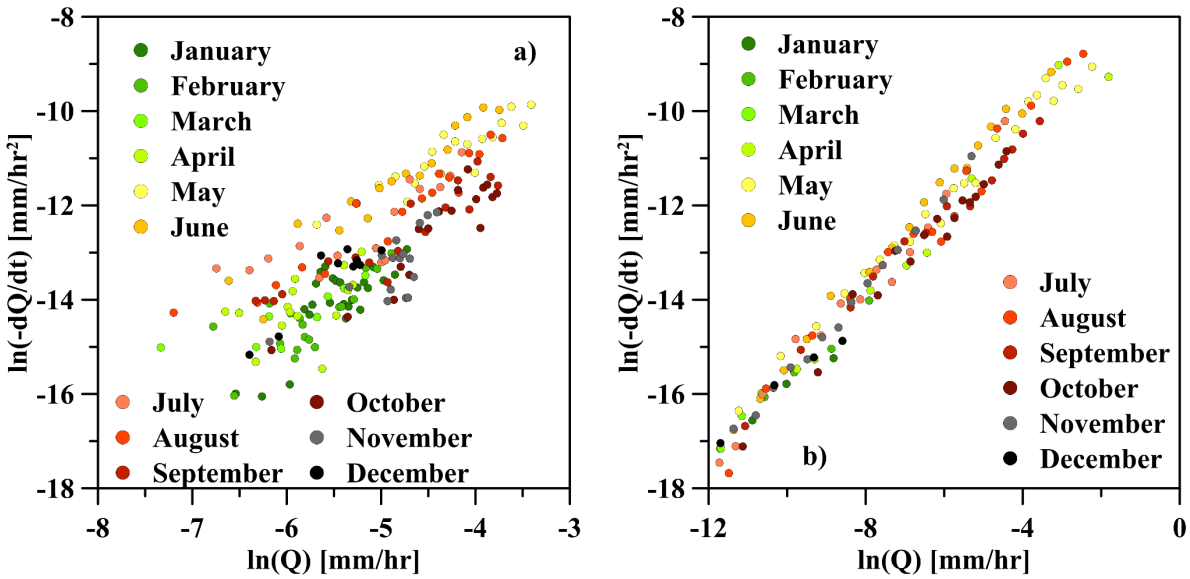

Figure 6-2. a) Recession plot of ln(Q) and ln(-dQ/dt) for storage flow water and b) ln(Q) and ln(-dQ/dt) for overland flow water. Shown are the averaged dQ/dt for each month, binned by 4% of the total number of discharge observations.

Regression of $\overline{dQ/dt}$ and $\bar{Q}$ identified the slope, intercept, and significance of the storage- and overland-discharge relationships; and hence, quantifiable changes in monthly storage (Table 6-1). The slope and intercepts were significant to 99% confidence, yielding R^2 values between 0.54 and 0.96. R^2 values were typically low for winter months (January–March) due to high variability of $\ln(-dQ_S/dt)$ for low flows (Figure 6-2a). The summer months (June–September) yielded relatively consistent slope and intercept values, indicative of limited changes in available subsurface storage capacity (Table 6-1). Shoulder season values (October-November and April-May) indicated rapid changes in available subsurface storage capacity. Estimation of storage with the slope and intercept (Equation 6-6) shows that more water is required in storage during the winter (December-March) than during summer (June-September) to produce an equivalent discharge.

Table 6-1. Regression parameters for slope and intercept (corresponding p-values) with the adjusted R^2. Parameters are included for each month as well as annual overland flow.

	Slope (p-value)	Intercept (p-value)	Adjusted R^2 Value
January	1.54 (2.6×10^{-6})	-5.60 (4.5×10^{-4})	0.61
February	1.15 (1.9×10^{-4})	-7.79 (3.4×10^{-5})	0.54
March	0.74 (1.0×10^{-2})	-9.98 (2.0×10^{-4})	0.62
April	1.38 (5.1×10^{-10})	-6.05 (1.8×10^{-8})	0.85
May	0.89 (3.9×10^{-10})	-7.17 (4.7×10^{-17})	0.80
June	1.24 (5.9×10^{-15})	-5.54 (4.6×10^{-15})	0.93
July	1.21 (2.8×10^{-12})	-5.98 (1.1×10^{-12})	0.87
August	1.31 (2.6×10^{-17})	-5.64 (5.3×10^{-17})	0.96
September	1.22 (9.1×10^{-15})	-6.68 (1.0×10^{-16})	0.93
October	1.79 (3.9×10^{-15})	-4.56 (7.8×10^{-11})	0.94
November	1.81 (2.9×10^{-9})	-4.35 (5.7×10^{-5})	0.95
December	1.34 (1.4×10^{-7})	-6.21 (4.5×10^{-7})	0.86
Overland	0.93 (9.3×10^{-16})	-6.41 (3.3×10^{-14})	0.99

Application of SAS functions within the Sapochi River requires 18 parameters: 11 for storage-discharge, three for overland-discharge distributions, one each for E and TR distributions, and two for ET partitioning (Table 6-2). The high-degree of parameterisation of the storage-discharge and overland-discharge distributions is a result of monthly variable parameters for the storage-discharge distribution (10 parameters). The temporal variability of storage-selection shape parameters (α_Q) is consistent with the storage-discharge relationship, while no temporal variability is observed for storage-overland-discharge (Figure 6-2). Since the storage-discharge relationship is non-stationary for seven months (October-May), α_Q are likely not the

same and should be changed in time similar to Hrachowitz et al. (2010). It is assumed that storage-discharge water is consistently older than overland-discharge water, therefore α_{Ov} must be less than or equal to min(α_Q).

Storage-scale parameters (λ and ΔSc) are time-invariant for both storage-discharge and overland-discharge distributions because storage is normalised by daily values (Section 6.4.2). Scale parameters control the importance of temporal variation in watershed 'wetness' to the response of the watershed storage. Values of ΔSc that are much larger than the deviation of storage (S_N) damp the impact of 'wetness' variability. Calibration of ΔSc must be greater than maximum storage, $\overline{S_N}$, to prevent mathematical errors in gamma distributions.

Table 6-2. Parameterisation of the three model combinations, including storage-discharge, overland-discharge, E, and TR distributions and parameters for ET partitioning. Initial parameter ranges are provided for all three combinations; parameter subscripts denote their representative flux, E is evaporation, TR is transpiration, Q is storage-discharge, and Ov is overland-discharge.

	Parameters	E^eTR^e	E^eTR^u	E^gTR^u
Storage-Discharge	α (9 parameters)	[0.1 – 5.0]*		
	λ	[-400.0 – 0.0]		
	ΔSc	[5.0 – 20.0]		
Overland-Discharge	α	[0.1 – 5.0]		
	λ	[-400.0 – 0.0]		
	ΔSc	[12.0 – 20.0]		
Evaporation	α^e or α^g	[10 – 100]	[10 – 100]	[0 – 0.1]
Transpiration	α^e or S^u	[0 – 800]	[0 – 800]	[0 – 800]
ET flux partition	Ma	[0.1 – 0.5]		
	Mc	[0.0 – 1.0]		

* independent parameter from Oct to May

E and TR distributions require only shape parameters since scale parameters are directly used to inform storage 'wetness'. The gamma distribution for E is the only distribution that explicitly uses the storage scale parameters, while the exponential and uniform distributions select water based solely on age. The parameter ranges for E and TR distributions were selected to have the same range of transit time between combinations. Isotopic parameters n, C_k, and θ

(Equation 6-18) are obtained from the previously calibrated tracer-aided model (Smith et al., submitted). Parameterization of the distributions additionally provides an estimate of the volume of water in storage that is directly responsible for a flux –the effective volume. A small effective volume may indicate either a small watershed storage capacity, or a small portion of the total storage contributing to discharge. Conversely, a large effective volume may indicate a larger volume of storage, or more equal contribution from all storages.

6.5.3 SAS FUNCTION CALIBRATION PROCEDURE AND ASSESSMENT

Calibration of the time-variant transit time solution using SAS functions was conducted using Matlab® and the Dynamically Dimensioned Search (DDS) algorithm (Tolson and Shoemaker 2007) using 25 trials of 3000 runs (75,000 total runs). Calibrations were conducted using three ET distribution combinations (i.e., $E^eTR^e, E^eTR^u, E^gTR^u$) for two scenarios of soil moisture (Equation 6-14): 1) constant ratio of AET to PET (non-dependent soil moisture, nSOM), and 2) varying ratio of AET to PET (fully dependent, SOM). In nSOM, S_{max} is equal to S_{min} so the ratio of AET to PET is constant with time, whereas with SOM, S_{max} is equal to 1 and S_{min} is solved for, changing the ratio of AET to PET with time. Runs were evaluated with a minimisation function comprised of the Nash-Sutcliffe efficiency (NSE) (Nash and Sutcliffe 1970) and Kling-Gupta efficiency (KGE) (Kling et al., 2012) criteria for oxygen-18 (subscript 18) and deuterium (subscript 2) of modelled and measured riverine composition

$$\boldsymbol{f(Min) = \sqrt{(1 - NSE_{18})^2 + (1 - NSE_2)^2 + (1 - KGE_{18})^2 + (1 - KGE_2)^2}} \qquad 6\text{-}22$$

The calibration period was synonymous with riverine isotopic measurement (i.e., 2011-2015). Following calibration, a sensitivity analysis of TR distribution parameters (α_T) was conducted by evaluating δ_T against isotopic values (assumes water must be mobile) reported from a shallow

piezometer (δ_{GW}). The sensitivity analysis was completed to assess the effect of TR loss on storage and storage-discharge age. Parameters for the other distributions were set as the optimised parameters from calibration.

SAS function calibration and sensitivity was conducted using rainfall, temperature, and relative humidity data from Thompson Airport (Environment Canada 2016), and ET and snowmelt flux and isotopic compositions from the HELIOS model (Smith et al., submitted). The first isotopic year was replicated five times in the model to produce a 5-year spin-up of isotopic compositions prior to model simulation. Water selected with age older than simulation and spin-up length was set equal to storage-weighted average (uniform selection from storage), which then considers long-term E fractionation (Harman 2015). Confidence intervals (95 %) were calculated for simulations meeting acceptable efficiency using likelihood functions.

6.5.4. TIME-SERIES ASSESSMENT OF WATER FLUX AGE AND ISOTOPIC COMPOSITION

The mean age of E varied the most substantially with the E distribution (Figure 6-3a-c). The temporal variability of E age increased, and average age decreased, when E distribution parameters decreased (not shown). The upper uncertainty bounds for the mean age of E were younger than 60 days for exponential models, increasing to almost 80 days for the gamma model. The average maximum E and TR ages differed between distribution combinations: 30 d, 38 d, and 33 d for E and 700 d, 512 d, and 469 d for TR for the E^eTR^e, E^eTR^u, and E^gTR^u models, respectively. The exponential distribution resulted in relatively constant TR age with time (E^eTR^e, Figure 3d), whereas uniform distributions (E^eTR^u; E^gTR^u) resulted in highly variable age. Without calibration to measured transpired water, riverine isotopic compositions were not sensitive to TR distribution parameters during TR-dominated periods.

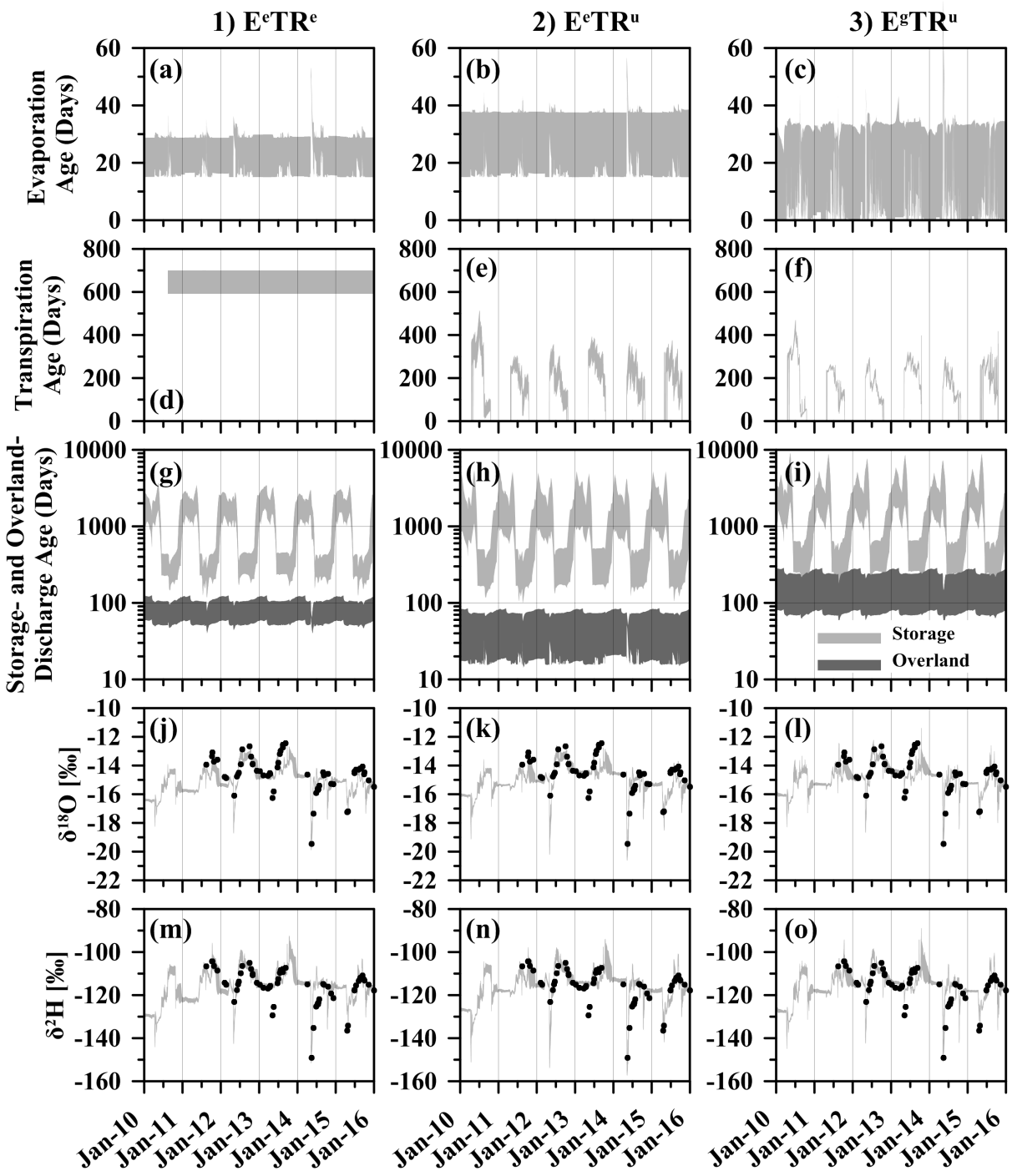

Figure 6-3. Model combinations 1) E^eTR^e, 2) E^eTR^u and 3) E^gTR^u with 95% confidence bounds of the age of a-c) evaporation, d-f) transpiration g-i) storage-discharge and overland flow age at the outlet with j-l) simulated oxygen-18 and, m-o) simulated deuterium.

Storage-discharge mean age (Figure 6-3g: light grey) changed drastically between models, most notably between E^eTR^u and E^gTR^u. Using the gamma distribution for E, selection from storage resulted in older water leaving storage in both summer and winter months. The mean storage discharge age during the summer was 1.7 times older for E^gTR^u than E^eTR^e, decreasing to 1.6 times older during the winter. Similar proportional changes for storage-discharge occurred between E^gTR^u and E^eTR^u, with the former 1.2 and 1.3 times older for summer and winter, respectively. Similar differences between TR ages were produced by the models, though the mean TR age trend was opposite (E^gTR^u<E^eTR^u<E^eTR^e, Table 6-3). Mean overland discharge age also varied between model combinations (Figure 6-3g-i, Table 6-3) as a result of hysteresis of winter storage-discharge (E^eTR^u<E^eTR^e<E^gTR^u). Mean E age has an opposite trend to the overland-discharge age (E^gTR^u<E^eTR^e<E^eTR^e, Table 6-3). Using the gamma distribution (for E), α_Q changed more gradually during winter, resulting in younger water released during early winter rather than during rapid spring discharge.

Table 6-3. Mean values of storage-discharge and overland-discharge water age. Mean age is averaged for summer (May to October) and winter (November to April).

Age Distribution		E^eTR^e	E^eTR^u	E^gTR^u
Storage-Discharge	Summer	426	605	736
	Winter	2574	3172	4154
Overland-Discharge	All seasons	82	46	161
Evaporation	Summer	23.6	27.6	19.8
Transpiration	Summer	611.6	224.8	204.2

Each model combination captured the general trends in riverine isotopic composition (Figure 6-3j-o). For SOM, optimised trial minimisation functions resulted in ranges of 1.04 to 1.08 for E^eTR^e, 1.15 to 1.45 for E^eTR^u, and 1.11 to 1.32 for E^gTR^u combinations. Since SOM simulations had consistently lower minimisation function results than nSOM simulations, analysis was conducted using SOM simulations only. Substantial inter-annual variability was

observed within the watershed: summer compositions increased between 2011 and 2013, and were relatively depleted in 2014 and 2015. Late 2012 and early 2013 isotopic compositions were over-estimated, indicating the isotopic composition of precipitation observed at Thompson did not reflect the isotopic composition of precipitation within the basin. Under-estimation of snowmelt in 2013 resulted in over-estimation of isotopic composition by the model, and likely strongly affected isotopic composition for the entire year due to under-estimated storage. Correction of snowmelt input based on freshet peak analysis (2010-2015 peaks) increased the 2013 snowmelt flux and resulted in more accurate estimation of freshet and annual composition (not shown).

6.5.5 SUB-SURFACE STORAGE PARAMETERISATION

Calibration resulted in similar trends for optimised parameters for all three model combinations. Some parameters were highly sensitive and greatly reduced the parameter space (λ_Q and λ_{Ov}, Figure 6-4a&e), while others were less sensitive (ΔSc_{Ov}, Figure 6-4f). Despite lower sensitivity, optimum ΔSc_{Ov} was similar for all model combinations (Figure 6-4f). The SAS functions for storage-discharge and overland-discharge (i.e. gamma distributions) were constant for all model combinations, therefore parameters were directly comparable. Higher parameter variability existed between storage-discharge parameters (Figure 6-4a&b) than between overland-discharge parameters (Figure 6-4e&f). This was expected due to greater-than-observed intra-annual variability in storage-discharge relationships relative to overland-discharge (Figure 6-2). Low values of ΔSc for both storage-discharge and overland-discharge, in addition to near zero values of λ (Figure 6-4a), indicated that the watershed was sensitive to intra-annual changes in storage. The gamma distribution shape parameter, α_Q, was the only parameter that varied temporally (Figure 6-4d), increasing during months with the greatest decrease in storage

identified from storage-discharge relationships (Section 6.4.1). High α_Q indicated preferential selection of older water from December to February, while α_Q decreased as temperatures began to warm in spring. Each model combination resulted in an unusual peak in α_Q during May, which in some cases was greater than the winter value (Figure 6-4d). Selection of older water during May (increase of α_Q) depleted the isotopic composition at the outlet relative to lower α_Q values (not shown). E^gTR^u resulted in a vastly different selection of water compared to the other combinations. α_Q^g did not greatly increase until February (i.e., the coldest month of the year), and then gradually declined thereafter; while α_Q^e increased rapidly during early winter (October-January), and gradually declined toward spring.

Parameters for E, TR, and the partition, were consistent when the same SAS function for E or TR was used between model combinations. The α_E optimised toward the minimum parameter range for both the exponential and gamma distribution (Figure 6-4g), indicating that E preferentially removes younger water from soils. TR parameters for the uniform distribution were consistent regardless of E distribution selection (E^gTR^u and E^eTR^u), optimised at 250 mm (Figure 6-4h). Dependence on the variability of storage resulted in high variability of TR age despite the low value. The exponential TR distribution (E^gTR^e) optimised toward the maximum of the parameter range, resulting in almost uniform selection of TR water from all water ages. Consequently, a constant TR age was estimated (Figure 6-3d). Optimisation of partition parameters was consistent for each combination, with approximately the same sensitivity as α_E (Figure 6-4g).

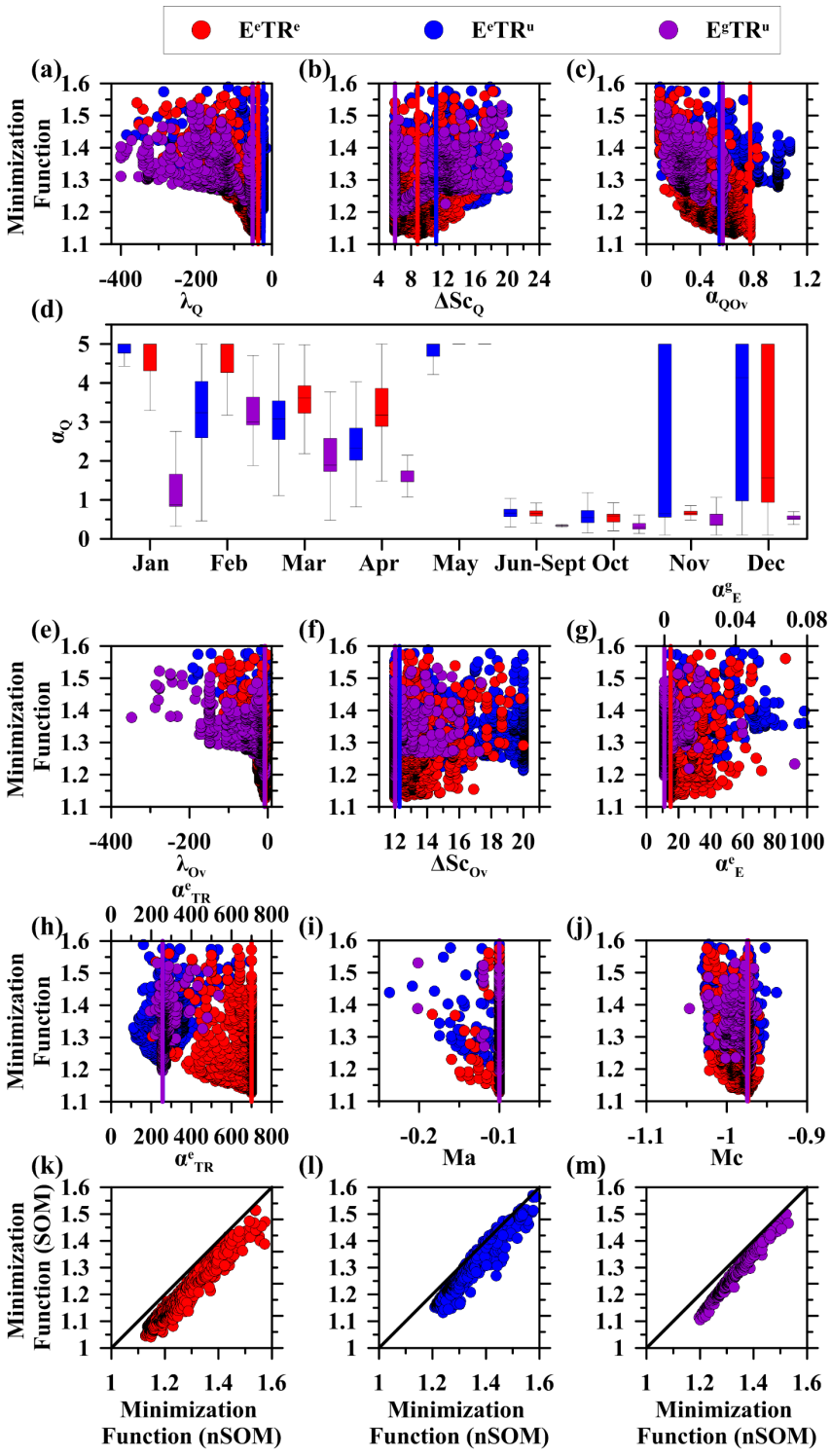

Figure 6-4. Transit time parameters for SAS functions and overland flow using the gamma distribution (λ, ΔSc) for the three ET model combinations. Evaporation partition parameters (Ma and Mc) are shown as scatter plots. Box-and-whisker plots represent the uncertainty of α_Q monthly (25th and 75th percentiles with whiskers to 1.5·IQR). Calibrations with and without soil moisture ET correction are compared in subplots k-m for each combination.

The importance of the temporal variability of the relationship between PET to AET with soil moisture was determined through the comparison of calibration with and without soil moisture correction (SOM vs nSOM, Equation 6-20). For each model combination, nSOM consistently had higher minimization function values than SOM. Differences between SOM and nSOM were most prevalent for E^gTR^u (Figure 6-4k-m). As the efficiency criteria decreased, the difference between SOM and nSOM optimisation increased. This indicates that the distributions were sensitive to temporal changes in the difference of PET to AET. Since soil moisture was generally lowest during the summer, ET (and subsequently evaporative fractionation) was greatly reduced during this period (Equations 6-14 and 6-15).

6.5.6 ESTIMATED STORAGE AGE

The effective storage volume (μ_S) of any flux distribution may be estimated using the parameters α, λ, and ΔSc ($\mu_S(\alpha, \lambda, \Delta Sc)$) (Harman 2015). When λ is negative, larger effective storage indicates a decrease in total storage available due to the distribution selecting from a larger range of storage ages. Substantial differences between the effective mean storage volumes were observed between model combinations used in calibration (Table 6-4). For each combination, a distinct increase in effective storage was apparent from summer to winter. Smaller effective storage during summer indicated that a smaller portion of total volume accounted for discharge, as compared to during winter. This is also observed with overland-discharge, where the smaller effective mean volume indicated that overland discharge uses a much smaller portion of the total storage volume. The hypothesized distribution for E and TR has a large influence on the estimated effective volume of water available for each flux. As the effective transpiration volume increased (i.e. E^eTR^e and E^eTR^u), the effective volume for

evaporation also increased. As volume for effective evaporation decreased (i.e. E^eTR^u and E^gTR^u), however, effective volume for transpiration decreased.

Table 6-4. Effective mean volume of water (mm) used in transport for summer (June-November) and winter (December-May) for storage-discharge, overland-discharge, E, and TR for the optimum calibration.

	Season	E^eTR^e (mm)	E^eTR^u (mm)	E^gTR^u (mm)
Storage-Discharge	Summer	184.5	333.8	81.2
	Winter	1030.0	962.1	558.7
Overland-Discharge	N/A	56.2	60.6	55.2
Evaporation	N/A	16.8	21.4	0.1
Transpiration	N/A	0.4	160.6	153.4

6.5.7 SENSITIVITY ANALYSIS OF TRANSPIRATION (δ_{TR}) CALIBRATION

To further examine how TR distributions influenced the riverine isotopic composition, TR (simulated δ_{TR}) was recalibrated using measured isotopic compositions of shallow soil water at one location in the vicinity of the catchment (~40 km away). Parameters for storage and E distributions were held constant at the optimum calibrated values. Recalibration results (blue bands, 95% bounds of TR sensitivity) were appreciably different from the original calibration (dark grey bands) for TR age (Figure 6-5a-c), TR composition (Figure 6-5d-f), and riverine composition (Figure 6-5g-i). Estimates of TR age from recalibration decreased for each model combination, although the most significant decrease occurred when the exponential distribution was used for TR: from 650 days to 160 days. The sensitivity analysis indicated that a local optimum occurred at 650 days, while 160 days was the observed global optimum (not shown). Substantial declines in mean age were also observed for E^eTR^u (130 days, Figure 6-5b) and E^gT^u (100 days, Figure 6-5c). TR composition was comparable to soil composition, particularly when the gamma distribution was used for evaporation. None of the model combinations were able to estimate the very depleted compositions in 2013, however, this was likely due to under-estimation of snowmelt flux. Optimisation of TR composition to soil composition strongly

influenced mean TR age, which was highly sensitive to TR distribution parameters. Recalibration of TR resulted in selection of younger water, which resulted in fractionation of older water via E (recall age-ranked storage E distributions). Since older water was released during the winter, riverine compositions in the following summer were greatly influenced (on average 0.5‰ increase in $\delta^{18}O$).

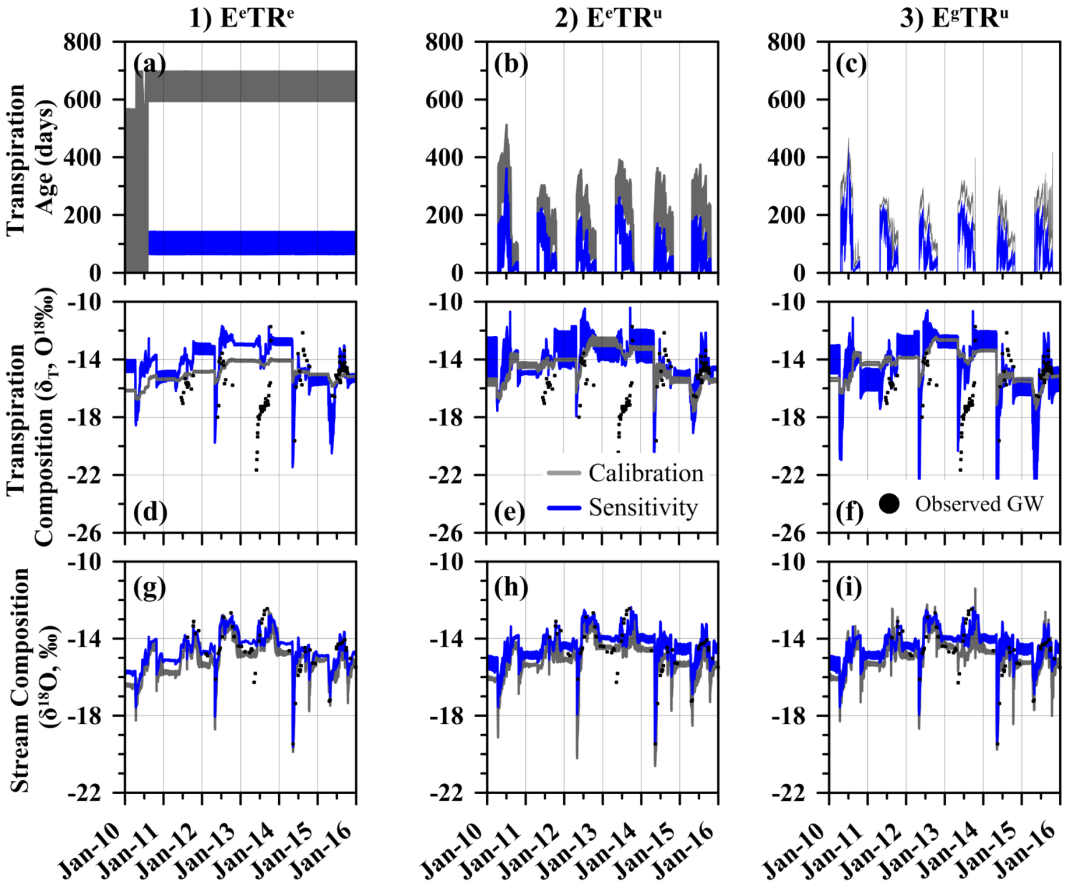

Figure 6-5. Comparison of sensitivity analysis of TR parameters using the best parameter sets from calibration (1.04, 1.15, and 1.11 for E^eTR^e, E^eTR^u, and E^gTR^u minimisation functions). Subplots a-c compare the TR age of calibration and sensitivity analysis for each combination (1) E^eTR^e, 2) E^eTR^u, 3) E^gTR^u). TR compositions (Figure 6-5d-f) are the flux weighted compositions of TR removed from soil (d: E^eTR^e, e: E^eTR^u, f: E^gTR^u). Riverine compositions (Figure 6-5g-i) of oxygen-18 for each combination (g: E^eTR^e, h: E^eTR^u, i: E^gTR^u) are compared for calibration and sensitivity analysis. Blue bands show the 95% confidence interval for transpiration sensitivity, dark grey shows 95% confidence intervals from calibration.

6.6 DISCUSSION

6.6.1. ASSESSING THE STORAGE CAPACITY OF A HIGH-LATITUDE WATERSHED

Only a limited number of studies have estimated transit times in watersheds undergoing freezing, likely due to the complexities of intra-annual changes in storage (Tetzlaff et al., 2015). Here we present a method by which the change in effective storage may be incorporated into transit time analysis. Storage-discharge regressions and estimated effective mean storage volume show intra-annual changes act to decrease water movement during winter months. The development of time-variant solutions for transit time analysis enabled further analysis of freeze-thaw cycles by introducing time-variable storage. The inclusion of temporal changes to the storage-discharge shape parameter (α_Q) adjusts water selection age with decreasing storage since this reduces the probability that younger water (i.e., likely more mobile and nearer to the surface) is contributing to the stream. It is this more surficial, younger water that is most likely to be influenced by annual freeze-thaw of the soils. An increase in discharge gamma distribution parameters (α_Q) during winter relative to summer increases the effective volume in transit, and indicates that older water is more readily discharged than younger water in winter. This is consistent with point measurements in road embankment studies near Thompson (Flynn et al., 2016), which have shown near surface (i.e., newest water) has the greatest potential for freezing. That said, younger water has potential to exit the basin in winter via shallow soil pathways (Granger et al., 1984; Laudon et al., 2004). For some of the combinations (E^eT^e and E^eT^u), it is not physically realistic that water selection changes rapidly from new to old water between October (low α_Q, Figure 6-4d) and November (high α_Q) since it is unlikely the watershed undergoes rapid freezing (DeGaetano et al., 2001).

During winter, the storage-discharge uncertainty bounds ranged from two to 27 years ($E^{g}T^{u}$). The maximum storage-discharge age is considerably longer than the accepted period (five years) of information $\delta^{2}H$ or $\delta^{18}O$ may provide (McGuire and McDonnell 2005). High uncertainty during winter months may be attributed to structural model limitations. Fractionation of ground-freeze-up (Posey and Smith 1957) is not considered within the model, and may result in more depleted isotopic compositions from soil as the sub-surface storage and open water freeze during early winter, and gradual reintroduction of depleted late fall precipitation compositions. Enrichment during the spring is likely overshadowed by snowmelt fractionation and associated depleted compositions (Laudon et al., 2002; Taylor et al., 2002; Carey & Quinton, 2004). Addressing inter-annual variability of sub-surface freezing may also further reduce the uncertainty of simulated storage-discharge age during the winter. Storage-discharge relationships (Equation 6-13) were stationary inter-annually. Under a changing climate, freeze-up is likely to occur later, the extent of permafrost is likely to decrease (Yi et al., 2007), and total available storage and discharge likely to increase (Lyon et al., 2010; Walvoord et al., 2012). Consideration of groundwater temperature can likely explain the inter-annual extent of subsurface freezing (Woo 2012). Finally, lake stratification and turnover during the spring and fall months may also influence the isotopic composition of the stream. Lake turnover may result in a rapid influx of depleted water from the hypolimnion, thereby resulting in underestimation of our estimates of evaporation. The fractionation of some of the cold weather processes (i.e. freeze-thaw and lake turnover) may influence the estimation of evaporation and transpiration water ages by the introduction of more depleted waters into storage.

6.6.2 EFFECT OF ET PARTITIONING USING SAS FUNCTIONS ON MEAN WATER AGE

The use of different distributions for SAS functions (i.e., uniform, exponential, gamma) strongly affects how water is removed from storage and has major implications for the age estimation of water influenced by evaporative enrichment (Botter 2012). The separation of ET and use of different distributions for E and TR provides an initial estimate of how each flux may influence catchment transit time estimations. Application of a temperature-dependent ET partition model resulted in calibrated empirical parameters that replicated hydrological processes in soils found independently in previous modelling of the watershed (Smith, et al., submitted). As the temperature-dependent E/ET partition equation is intended for large-basins, E/ET variability that occurs at small spatial and temporal scales may be obscured in favour of watershed averaged E/ET. The method may also benefit from the further separation of non-fractionating TR into interception E and TR to limit total water loss from soils (Sutanto et al., 2012). Daily E/ET variability may not be observed in the Sapochi River watershed due to mixing, land cover spatial heterogeneity, and riverine attenuation that occurs in watersheds of this size (Smith et al., submitted). The areal threshold below which small-scale (vegetation specific) ET partitioning may be required may be determined using mass-balance and temperature dependent ET partition methods in data-rich watersheds of varying sizes.

Implementation of multiple distributions for E and TR was an effective tool to test water source hypothesis. Regardless of the distribution, E age was consistently younger water, which indicates a preference toward mobile water. This was exemplified further with the gamma distribution and preferential selection of water even younger than the exponential distribution. Conversely, the TR age was consistently older water. While the exponential distribution indicated selection of water, very young to very old (older than the simulation length), the uniform distribution implied a relatively equal mix of young and old water, with a much younger

median TR age (75-350 days). All TR hypotheses (i.e., exponential and uniform) were still, however, estimated to be older than the available mobile water present in the piezometer (Figure 6-5). This likely indicates some mixing of mobile and immobile water for root-uptake, however, without xylem water sampling further testing of these hypotheses is limited.

Calibrating riverine compositions using evaporative fractionation resulted in sensitive TR distribution parameters. As Botter (2012) surmised, calibration of TR resulted in different storage age changes with different distributions; however, the change in storage age with TR distribution was equally influenced by the E distribution (Figure 6-5). Sensitivity analysis demonstrated that riverine $\delta^{18}O$ is insensitive to TR distributions during the summer months, but is strongly influenced during ice-on periods. This indicates that there is high sensitivity to E distributions during the summer months, while TR influences are delayed until winter months. With the empirical approach, appropriate soil measurements may be used to calibrate to measured δ_T compositions, thereby improving understanding and estimation of storage-discharge age. When data are available for the mass-balance method, this raises an interesting question: what is the impact of using observed δ_T or simulated δ_T in the mass-balance (Equation 6-8 and 6-9)? Using measured data would likely provide an improved estimate of E; however, calibration of the TR distribution (Section 6.5.5) may substantially change storage-discharge compositions. Though screened piezometers have limited application for sampling transpiring water, they provide a general estimate of the water available for root-uptake (Ehleringer and Dawson 1992; Dawson and Ehleriner 1998; Eggemeyer et al., 2008). Depth-dependent samples may improve the understanding of TR distributions and would eliminate the invasive nature of xylem water sampling (Goodger et al., 2005), although it may only be applicable to temperate forests and grasslands (Evaristo et al., 2015). The application of various sampling regimes would likely

require the concurrent use of age-ranked distributions and depth ranked distributions for direct correlation of measurements.

6.7 CONCLUSIONS

High-latitude watersheds contain challenging hydrological processes, which increase the significance of seasonal E effects during short growing seasons, and act to decrease storage availability during freeze-up periods. The modification of time-variant transit time modelling for time-variant storage potential (freeze-thaw cycles) and differences in E and TR flow paths can be achieved through varying distribution parameters to select older 'available' water and partitioning ET using stable water isotopes. The dual calibration of oxygen-18 and deuterium was used to identify temporal variability of E fractionation, which aided in ET partitioning. A comparison of the mean storage-discharge age to E and TR distributions shows dependence of storage age on E distribution during the summer, and TR distribution during the winter. Lower air temperatures drove vastly differing storage availability between winter and summer. Winter storage-discharge drew from a larger storage of water though yielded less discharge. Mean storage-discharge age increased for all seasons when mean E age decreased. The selection of the TR distribution had a significant impact on both E age and storage age when calibrated to independent data. A single 'best' TR or E distribution may not be identified from this analysis as the selection of distributions is interdependent. That said, the separation of ET into its components within SAS presented here provides a platform on which this may be achieved with measured vegetation and soil data. The approach of watershed storage simulation is useful for water practitioners as it provides insights into both short and long-term water availability. Additionally, the parsimonious nature of the model provides a simple and fast means of storage estimation.

6.8 ACKNOWLEDGEMENTS

The authors thank the Manitoba Hydro and Water Survey of Canada crews in Thompson, MB for sample collection and maintenance of on on-site equipment. Funding from the Natural Sciences and Engineering Research Council (NSERC) of Canada Collaborative Research and Development Grant and Post-graduate Scholarship Doctoral Program (PGS-D) from NSERC aided this project. We would also like to thank InnoTech Alberta for sample analysis.

6.9 REFERENCES

Abtew, W., Melesse, A. 2013. *Evaporation and Evapotranspiration: Measurements and Estimations*, Springer Netherlands.

Ali, G., Birkel, C., Tetzlaff, D., Soulsby, C., McDonnell, J. J., Tarolli, P. 2014. A comparison of wetness indices for the prediction of observed connected saturated areas under contrasting conditions. *Earth Surface Processes and Landforms*, **Volume 39**: 399-413.

Benettin, P., Soulsby, C., Birkel, C., Tetzlaff, D., Botter, G., Rinaldo, A. 2017. Using SAS functions and high-resolution isotope data to unravel travel time distributions in headwater catchments. *Water Resources Research*, **Volume 53(3)**: 1864-1878. DOI: 10.1002/2016WR0202117.

Birkel, C., Soulsby, C., Tetzlaff, D. 2015. Conceptual modelling to assess how the interplay of hydrological connectivity, catchment storage and tracer dynamics controls nonstationary water age estimates. *Hydrological Processes*, **Volume 29**: 2956-2969.

Birkel, C., Soulsby, C., Tetzlaff, D., Dunn, S., Spezia, L. 2012. High-frequency storm event isotope sampling reveals time-variant transit time distributions and influence of diurnal cycles. *Hydrological Processes*, **Volume 26**: 308-316.

Botter, G. 2012. Catchment mixing processes and travel time distributions. *Water Resources Research*, **Volume 48(5)**: W05545-1-15. DOI: 10.1029/2011WR011160.

Botter, G., Bertuzzo, E., Rinaldo, A. 2011. Catchment residence and travel time distributions: The master equation. *Geophysical Research Letters*, **Volume 38(11)**: L1403-1-6. DOI: 10.1029/2011GL047666.

Carey, S.K., Quinton, W.L. 2004. Evaluating snowmelt runoff generation in a discontinuous permafrost catchment using stable isotope, hydrochemical and hydrometric data. *Nordic Hydrology*, **Volume 35**: 309-324.

Craig, H. 1961. Isotopic Variations in Meteoric Waters. *Science*, **Volume 133(3465)**: 1702–1703. DOI:10.1126/science.133.3465.1702.

Craig, H., Gordon, L. 1965. Deuterium and oxygen-18 variations in the ocean and marine atmosphere. *Stable Isotopes in Oceanographic Studies and Paleotemperatures*: 9-130.

Dawson, T.E., Ehleriner, J.R. 1998. The role of plants in catchment-level hydraulic processes: Insights from stable isotope studies. In: C. Kendall & J. J. McDonnell, eds. Isotope Tracers in Catchment Hydrology. Amsterdam: Elsevier: 165-202.

DeGaetano, A.T., Cameron, M.D., Wilks, D.S. 2001. Physical Simulation of Maximum Seasonal Soil Freezing Depth in the United States Using Routing Weather Observations. *Journal of Applied Meteorology*, **Volume 40**: 546-555.

Eggemeyer, K.D., Awada, T., Harvey, F.E., Wedin, D.A., Zhou, X., Zanner, C.W. 2008. Seasonal changes in depth of water uptake for encroaching trees Juniperus virginiana and Pinus ponderosa and two dominant C4 grasses in a semiarid grassland. *Tree Physiology*, **Volume 29**: 157-169.

Ehleringer, J.R., Dawson, T.E. 1992. Water uptake by plants: perspectives from stable isotope composition. *Plant, Cell & Environment*, **Volume 15**: 1073-1082.

Evaristo, J., Jasechko, S., McDonnell, J.J. 2015. Global separation of plant transpiration from groundwater and streamflow. *Nature*, **Volume 525**: 91-94.

Flynn, D.J., Kurz, D., Alfaro, M., Arenson, L.U. 2016. Forecasting ground temperatures under a highway embankment on degrading permafrost. *Journal of Cold Regions Engineering*, **Volume 30**: 04016002-1-20. DOI: 10.1061/(ASCE)CR.

Gat, J. 2010. *Isotope Hydrology: A study of the water cycle*, Imperial College Press, London.

Gibson, J.J. 2002. Short-term evaporation and water budget comparisons in shallow Arctic lakes using non-steady isotope mass-balance. *Journal of Hydrology* **Volume 264**: 242-261.

Gonfiantini, R. 1986. Environmental isotopes in lake studies. In: P. Fritz & J. C. Fontes, eds. Handbook of Environmental Isotope Geochemistry. New York: Elsevier, pp. 113-168.

Goodger, J.Q.D., Sharp, R.E., Marsh, E.L., Schachtman, D.P. 2005. Relationships between xylem sap constituents and leaf conductance of well-watered and water-stressed maize across thee xylem sampling techniques. *Journal of Experimental Botany*, **Volume 103**: 2389-2400.

Granger, R.J., Gray, D.M., Dyck, G.E. 1984. Snowmelt infiltration to frozen prairie soils. *Canadian Journal of Earth Sciences*, **Volume 21**: 669-677.

Harman, C. 2015. Time-variable transit time distributions and transport: Theory and application to storage-dependent transport of chloride in a watershed. *Water Resources Research*, **Volume 51(1)**: 1-30. DOI: 10.1002/2014WR015707.

Heidbuchel, I., Troch, P.A., Lyon, S.W., Weiler, M. 2012. The master transit time distribution of variable flow systems. *Water Resources Research*, **Volume 48(6)**: W06520-1-19. DOI: 10.1029/2011WR011293.

Hortia, J., Wesolowski, D. 1994. Liquid-vapour fractionation of oxygen and hydrogen isotopes of water form the freezing to the critical temperature. *Geochimica et Cosmochimica Acta*, **Volume 58(16)**: 3425-3437.

Hrachowitz, M., Soulsby, C., Tetzlaff, D., Malcolm, I.A., Schoups, G. 2010. Gamma distribution models for transit time estimation in catchments: Physical interpretation of parameters and implications for time-variant transit time assessment. *Water Resources Research*, **Volume 46(10)**: W10536-1-15. DOI: 10.1029/2010WR009148.

Jung, M., Reichstein, M., Ciais, P., Seneviratne, S.I., Sheffield, J., Goulden, M.L., Bonan, G., Cescatti, A, Chen, J., de Jeu, R., Dolman, A.J., Eugster, W., Gerten, D., Gianelle, D., Gobron, N., Heinke, J., Kimball, J., Law, B.E., Montagnani, L., Mu, Q., Mueller, B., Oleson, K., Papale, D., Richardson, A.D., Roupsard, O. 2010. Recent decline in the global land evapotranspiration trend due to limited moisture supply. *Nature*, **Volume 467**: 951-954.

Kahmen, A., Simonin, K., Tu, K.P., Merchant, A., Callister, A., Siegwolf, R., Dawson, T.E., Arndt, S.K. 2008. Effects of environmental parameters, leaf physiological properties and leaf water relations on leaf water δ18O enrichment in different Eucalyptus species. *Plant Cell and Environment*, **Volume 31**: 738-751.

Kirchner, J. 2009. Catchments as simple dynamical systems: Catchment characterization, rainfall-runoff modelling, and doing hydrology backward. *Water Resources Research*, **Volume 45(2)**: W02429-1-34. DOI: 10.1029/2008WR006912.

Kirchner, J.W., Feng, X., Neal, C. 2001. Catchment-scale advection and dispersion as a mechanism for fractal scaling in stream tracer concentrations, *Journal of Hydrology,* **Volume 254(1–4)**: 82–101. DOI:10.1016/S0022-1694(01)00487-5.

Klaus, J., Chun, K.P., McGuire, K.J., McDonnell, J.J. 2015. Temporal dynamics of catchment transit times from stable isotope data. *Water Resources Research*, **Volume 51**: 4208-4223.

Kling, H., Fuchs, M., Paulin, M. 2012. Runoff conditions in the upper Danube basin under an ensemble of climate change scenarios, *Journal of Hydrology,* **Volume 424–425**: 264–277. DOI:10.1016/j.jhydrol.2012.01.011.

Laudon, H., Hemond, H.F., Krouse, R., Bishop, K.H. 2002. Oxygen-18 fractionation during snowmelt: Implications for spring flood hydrograph separation. *Water Resources Research*, **Volume 38(11)**: 40.1-40.10.

Laudon, H., Kohler, S., Siebert, J., Bishop, H. 2004. Hydrological flow paths during the spring flood: congruence between hydrometric measurements and oxygen-18 in snow melt,

soil water, and runoff. *Water Resource Research*, **Volume 40(3)**: W03102-1-9. DOI: 10.1029/2003WR002455.

Lyon, S.W., Laudon, H., Seibert, J., Mörth, M., Tetzlaff, D., Bishop, K.H. 2010. Controls on snowmelt water mean transit times in northern boreal catchments. *Hydrological Processes*, **Volume 24**: 1672-1684.

McDonnell, J. 2014. The two water worlds hypothesis: ecohydrological separation of water between streams and trees? *Water*, **Volume 1(4)**: 323-329.

McGuire, K.J., McDonnell, J.J. 2006. A review and evaluation of catchment transit time modelling. *Journal of Hydrology*, **Volume 330**: 543-563.

Nash, J.E., Sutcliffe, F.V. 1970. Fiver flow forecasting through conceptual models: Part 1- A discussion of principles. *Journal of Hydrology*, **Volume 10:** 282-290.

Niemi, A.J. 1977. Residence time distributions of variable flow processes. *International Journal of Applied Radiation and Isotopes*, **Volume 28**: 855-860.

Posey, J.C., Smith, H.A. 1957. The equilibrium distribution of light and heavy waters in a freezing mixture. *Journal of the American Chemical Society*, **Volume 79**: 555-557.

Smith, A.A., Delavau, C.J., Stadnyk, T.A. 2015. Identification of geographical influences and flow regime characteristics using regional water isotope surveys in the lower Nelson River, Canada. *Canadian Water Resource Journal*, **Volume 40(1)**: 23-35.

Smith, A., Welch, C., Stadnyk, T. 2016. Assessment of a lumped coupled flow-isotope model in data scarce Boreal catchments. *Hydrological Processes*, **Volume 30(21)**: 3871–3884. DOI:10.1002/hyp.10835.

Smith, A.A., Welch, C., Stadnyk, T.A. Submitted. Assessing seasonality and uncertainty in evapotranspiration partitioning using a lumped tracer-aided model.

Soulsby, C., Birkel, C., Geris, J., Dick, J., Tunaley, C., Tetzlaff, D. 2015. Stream water age distributions controlled by storage dynamics and nonlinear hydrologic connectivity: Modelling with high-resolution isotope data. *Water Resource Research*, **Volume 51**: 7759-7776.

Sutanto, S.J., Wenninger, J., Coenders-Gerrits, A.M., Uhlenbrook, S. 2012. Partitioning of evaporation into transpiration, soil evaporation and interception: a comparison between isotope measurements and a HYDRUS-1D model. *Hydrology and Earth System Sciences*, **Volume 16**: 2605-2616.

Taylor, S., Feng, X., Willaism, M., McNamara, J. 2002. How isotopic fractionation of snowmelt affects hydrograph separation. *Hydrological Processes*, **Volume 16**: 3683-3690.

Tetzlaff, D., Buttle, J, Carey, S.K., McGuire, K., Laudon, H., Soulsby, C. 2015. Tracer-based assessment of flow paths, storage and runoff generation in northern catchments: a review. *Hydrological Processes*, **Volume 29**: 3475-3490.

Tolson, B.A., Shoemaker, C.A. 2007. Dynamically dimensioned search algorithm for computationally efficient watershed model calibration. *Water Resource Research*, **Volume 43(1)**: W01413-1-16. DOI:10.1029/2005WR004723.

van der Velde, Y., Heidbüchel, I., Lyon, S.W., Nyberg, L., Rodhe, A., Bishop, K., Troch, P.A. 2015. Consequences of mixing assumptions for time-variable travel time distributions. *Hydrological Processes*, **Volume 29**: 3460-3474.

van der Velde, Y., Torfs, P.J.J.F., van der Zee, S.E.A.T.M., Uijlenhoet, R. 2012. Quantifying catchment-scale mixing and its effect on time-varying travel time distributions. *Water Resource Research*, **Volume 48(6)**: W06536-1-13. DOI: 10.1029/2011WR011310.

van Hujigevoort, M.H.J., Tetzlaff, D., Sutanudjaja, E.H., Soulsby, C. 2016. Using high resolution tracer data to constrain water storage, flux and age estimates in a spatially distributed rainfall-runoff model. *Hydrological Processes*, **Volume 30(25)**: 4761-4778. DOI: 10.1002/hyp.10902.

Walvoord, M.A., Voss, C.I., Wellman, T.P. 2012. Influence of permafrost distribution on groundwater flow in the context of climate-driven permafrost thaw: example from Yukon Flats Basin, Alaska, United States. *Water Resources Research*, **Volume 48(7)**: W07524-1-17. DOI: 10.1029/2011WR00233.

Woo, M. 2012. Permafrost Hydrology. Springer Link

Yi, S., Woo., M., Altaf Arain, M. 2007. Impacts of peat and vegetation on permafrost degradation under climate warming. *Geophysical Research Letters*. **Volume 34(6)**: L16504-1-5. DOI: 10.1029/2007GLO30550

Zhang, S., Wen, X., Wang, J., Yu, G., Sun, X. 2010. The use of stable isotopes to partition evapotranspiration fluxes into evaporation and transpiration. *Acta Ecologica Sinica*, **Volume 30**: 201-209.

Zhang, Y., Peña-Arancibia, J.L., McVicar, T.R., Chiew, F.H.S., Vaze, J., Liu, C., Lu, X., Zheng, H., Wang, Y., Liu, Y.Y. Miralles, D.G., Pan, M. 2016. Multi-decadal trends in global terrestrial evapotranspiration and its components. *Nature Scientific Reports*, **Volume 6(1)**: 19124. DOI: 10.1038/srep19124.

CHAPTER 7: CONCLUSIONS

7.1. SUMMARY AND MAJOR FINDINGS

7.1.1. IDENTIFICATION OF PRIMARY FLOW COMPONENTS IN HIGH-LATITUDE WATERSHEDS

The stable isotopes of water (δ^2H and $\delta^{18}O$) and discharge were used with statistical analysis and tracer-aided modelling to identify the primary stream flow components in the headwaters of the lower Nelson River basin (Chapters 3 to 5). Two model versions (Chapter 4 and 5) were used to help explore differences in the primary flow components contributing to stream flow in four headwater basins, each exhibiting various physiographic features and climate patterns. Selection of headwater basins with distinct physiography helped to investigate the diversity of flow paths in this region.

Observed riverine isotopic compositions assisted in identifying the amount each source water was contributing to streamflow from rain, snowmelt, groundwater, and evaporation pan samples using the LEL, LMWL, and LML. The method was applied in the lower Nelson River Basin (Chapter 3), a high latitude watershed north of Lake Winnipeg (>50^o) where both discharge and isotopic composition were measured in numerous headwater catchments. Precipitation and groundwater were more enriched than global precipitation trends (slope of 7.47 relative to a global average of 8, though near to that of Canada (7.8)), indicating a semi-arid climate. A potentially significant influence of evaporation on water in storage was shown with lower mixing line slopes in the headwater basins (4.2) relative to the main stem rivers (4.41, 6.92 and 8.02). Main channels had low variability regardless of discharge anomaly; however, high

and low discharge in the headwater basins experienced seasonal variability of $\delta^{18}O$ due to differences in physiographic features. $\delta^{18}O$ in high flow anomalies revealed a dependence on rapid flow paths while low flow anomalies were consistent with wetland discharge. Normal to high discharge was due to multiple flow paths (rapid, wetland, among others), thus identified a minimum of three total storages: soil water (comprising rapid flow), wetland storage, and groundwater (long-term stable flow).

A conceptual lumped tracer-aided model (UMSWIM, Chapter 4) was used to estimate fluxes from the three storages in two headwater basins (Sapochi and Odei River basins) by simulating $\delta^{18}O$ and discharge. Soil water storage fluxes were the primary component (43-60%), followed by groundwater storage (19-54%) and wetland storage (3-21%) although groundwater and wetland contributions were inadequately separated during winter in each basin. Uncertainty in soil water contributions was highly correlated to the precipitation flux, indicating dependence of soil storage on the total precipitation. High uncertainties during spring and high precipitation events indicate that two primary fractionating storages have different components of their flow paths: soil water has a slower flow (unsaturated zone), and rapid flow (overland flow); and wetlands are distinct between annually available discharge (connected wetlands) and sporadic discharge (disconnected flow). Fluxes from connected wetlands (26-55%) were generally the highest component of discharge for four watersheds (Sapochi, Gunisao, Burntwood, and Odei River Basins; Chapter 5). Separation of the soil storages revealed relatively high proportions of rapid/overland flow (6-21%) and unsaturated (soil water) flow (6-32%). The overland flow contributions were isolated to temporal periods of high precipitation where infiltration was limited (e.g., snowmelt on frozen soil and high precipitation periods). Groundwater (6-32%), and disconnected wetland (2-5%) storages were consistently the lowest proportion of discharge.

Simultaneous simulations of discharge and stable water isotopes (δ^2H and $\delta^{18}O$) has identified that a significant proportion of source water was present in subsurface regions critical for evapotranspiration fluxes. Furthermore, the large proportion of discharge originating from near surface water storage indicate that there is likely high sensitivity of water storages to changes in meteorological conditions and fluxes (e.g. precipitation, temperature, relative humidity, wind, etc.).

7.1.2. ESTABLISHING A NEW METHOD FOR ET PARTITIONING

Tracer-aided model simulations (i.e. discharge, δ^2H, and $\delta^{18}O$) were used in conjunction with isotope hydrograph separation to identify intra-annual trends of E/ET to the inverse of air temperature. The components of ET were further separated into observable fractionation at the outlet (unsaturated storage evaporation and open water evaporation), and non-observable or non-fractionating at the outlet (transpiration and intercepted evaporation) for the soil and wetland storages. Fractionation dominated storages were independently parameterised in tracer-aided simulations to separate physiographic differences within modelled watersheds.

Application of the ET partition model indicated that the partition generally followed a parabolic trend, with highest transpiration during summer months (June-August) and highest evaporation during the shoulder seasons (April, May, September, and October; Chapter 5). The change in fractionation showed different magnitudes of E/ET for different storage. E/ET was generally higher in wetland storage than in unsaturated soil storage. Ponded water storage yielded the highest E/ET, though ponded water storage was not always present and total evaporation was minimal. Additionally, simulations with higher soil moisture in either wetland or unsaturated soil storages resulted in higher evaporation. Minimum E/ET occurred during the early summer (June) when the growing season begins, as opposed to end of summer when

temperatures were the highest. The greatest temporal uncertainty of E/ET occurred during the shoulder seasons (spring and fall), having the greatest inter-annual variability of ET flux and vegetation conditions (i.e. time of budding and abscission). The partitioning of ET aided in both understanding evaporation and transpiration effects on storage at the watershed scale, and separating temporal changes in storage due to external sources (other than evapotranspiration; Chapters 5&6). The high negative correlation to temperature and positive correlation to soil moisture of unsaturated soil evaporation indicated sensitivity of storage in regional watersheds to changes in atmospheric conditions. Using the partitioning method, further effects of evaporation and transpiration on storage may be ascertained through preferential flow path and flux age identification.

7.1.3. IDENTIFICATION OF EVAPORATION AND TRANSPIRATION FLUX AGES

Storage-discharge, overland discharge, and the partition of ET were used in a time-variant transit time model using three different distributions to assess the influence of each flux on the age of water in storage (Chapter 6). Existing SAS functions were modified to include ET partitioning, transit time distributions for multiple independent fluxes (storage-discharge, overland-discharge, E, and TR), and time-variability of storage availability (frozen-ground conditions). Riverine isotopic compositions (δ^2H and $\delta^{18}O$) were used to calibrate the model to investigate the temporal influences of evaporation and transpiration age on storage and mean watershed transit times.

Simulation using combinations of storage selection distributions (e.g. gamma, exponential, or uniform) revealed how the age of evaporation and transpiration fluxes influence the isotopic composition in storage. Evaporation flux comprised much younger water (1-70 days) than transpiration (2-3 years). Simulations of the ET partition showed similar partition rates to those

identified by lumped tracer-aided modelling, with transpiration dominating the vapour flux in summer when evapotranspiration flux is the greatest. Changing the distribution used for evaporation or transpiration fluxes significantly altered the respective estimates of mean flux age, but did not greatly change the age of the other flux. Preferential selection of very young water for evaporation greatly influenced mean storage-discharge age as it limited the replenishment of younger water to storage. Decreases in mean transpiration flux age (i.e. selection of younger water) resulted in large enrichments to riverine isotopic compositions during the winter months. This enrichment resulted from older evaporative flux, which counter-acted younger transpiration flux, which was released during winter. Reducing unsaturated soil evaporation will decrease the age of transpired water and additionally decrease the mean age of storage-discharge water. This has large implications for water management, as decreasing the mean age of storage-discharge indicates less reliable long-term storage, more preferential flow paths, and a faster and larger (precipitation) event-based responses.

7.2. LIMITATIONS AND FUTURE WORK

This research specifically focused on identifying methods to assess changes in water availability due to evaporation and transpiration in high-latitude data sparse regions. Although the work presented here has aided in the understanding of data-scarce, high-latitude watersheds, some limitations remain. This highlights that future research areas may both further advance the methods presented, and aid in future modelling attempts within these and other, similar watersheds. Limitations include: data availability, interactions between soil and vegetation, complexities of lake hydrology, and sub-surface freeze-thaw cycles.

7.2.1. HIGH LATITUDE WATERSHED DATA AVAILABILITY

Inherent issues with modelling attempts in high-latitude regions include the limited data for model validation (beyond model efficiency) of simulated flow paths, in addition to the limited resolution of model input (and therefore uncertainty in model input). Concerns regarding model input uncertainty have been examined through the regional estimation of isotopic composition in precipitation, relative to other more local or static input compositions (Delavau et al., 2017). Both temporal and spatial variability of precipitation were found to be important to process identification and flow path contributions. Chapter 4 identified a strong relationship of precipitation composition to the uncertainty of unsaturated soil contribution to the river discharge. Similar to the limitations raised by Delavau (2016), more frequent and spatially variable isotopic sample collection may help to further reduce model uncertainty with storage contribution, and therefore the ET partition (Holmes 2016). The lack of depth-dependent groundwater sampling and samples from different subsurface hydrologic units resulted in some soil storage equifinality. This subsequently led to higher uncertainty in the ET partition. Further tracer-aided hydrological calibration with soil isotopic data will likely help reduce uncertainty in isotopic, discharge, and E/ET estimation. However, the spatial domain and lack of accessibility in many high-latitude watersheds increases the difficulty of large-scale sampling programs. The modelling completed in Chapter 5 helped to identify hydrologic units that may benefit from more rigorous sampling to help further constrain future tracer-aided modelling.

Another limitation inherent in this research was the number of isotopic streamflow samples per year, which resulted in intra-annual analysis but not inter-annual comparisons. Although additional evapotranspiration partitioning frameworks were outlined for more comprehensive riverine sampling regimes (Chapter 5), there is little that the current general trend of ET partitioning may describe for long-term trends without analysis of inter-annual variability of

evaporative fractionation and ambient conditions. For this reason, there is a need to identify the relationship of E/ET with multiple conditions to establish the nature of multiple changing conditions. It is recommended that future studies consider high-latitude regions with more consistent long-term data (i.e. weekly or bi-weekly for 2 or more years, e.g. Guo et al., 2017) to directly identify inter-annual changes of evaporation fraction due to:

- Relative humidity (*RH*)
- Ambient atmospheric composition (δ_A)
- Potential evapotranspiration flux (*PET*)
- Soil moisture (*SM*)

In particular, the headwater basins of the Mackenzie River basin should be considered as ideal study locations given the large hydrometric-isotopic datasets available, and the land cover similarities (i.e. wetlands) to the LNRB. It is possible that such similarities of land cover may allow for direct comparison of the E/ET relationship between the headwaters in the Mackenzie and Lower Nelson River basins as a pseudo-validation exercise.

7.2.2. INTERACTIONS OF SOIL AND VEGETATION

Due to the large-scale nature of the tracer-aided modelling, the direct identification of transpiration fluxes from different soil and vegetation types was not feasible. Vegetation units were aggregated for the sole estimation of unsaturated soil and wetland ET partitions. Chapter 5 identified significant differences in the ET partition of the unsaturated soils and wetlands between watersheds as likely signs of differences in vegetation and soil conditions. However, separation may not be addressed even through small-scale studies due to significant unidentified heterogeneity of both soil and vegetation, as this is amplified at smaller scales. At larger scales, high-resolution satellite imagery may further constrain vegetation influences on ET partitioning

through refined temporal classification of vegetation and canopy density, minimizing some observed effects of vegetation heterogeneity via larger scale mixing. Additional watershed simulations may identify large-scale effects of vegetation types on the ET partition, and create the possibility of spatially mapping the ET partition over large-scale watersheds.

Calibration methods provide an indirect estimate of the E and TR ages and their influence on discharge water age over large spatial scale with limited data. These methods provide a first estimate of the influence of E, TR, and E/ET where direct measurement may not be feasible. However, validating E and TR flux age over large spatial scales remains. Direct measurement of soil and xylem isotopic samples in addition to riverine isotope samples could provide further validation of root-uptake through the calibration.

7.2.3. IMPORTANCE OF EVAPORATIVE FRACTIONATION IN LAKE HYDROLOGY

There is a need to address the complexities of lake hydrology within basin-wide ET partitioning to limit potential over-fractionation of sub-surface storage. While open water fractionation was accounted for in all open water areas (Chapters 4 and 5), lumped models are limited in including lakes in models as a result of not accurately defining the location of the lake (Birkel et al., 2011). Higher lake residence times (>1 year) increase the evaporative fractionation of a well-mixed lake (Gat 2010); however, high-latitude lakes generally experience biannual lake turnover (shoulder seasons), which reduce the long-term (inter-annual) lake enrichment (Gibson et al., 2002). Furthermore, there is little evidence of evaporation fractionation due to open water within the tracer-aided modelling (Chapters 4 and 5); however, it is unclear whether this results from the channelized lakes assumption (short residence times) or due to the small lake percentages (<10%, Gibson and Edwards 2002). For these reasons, there is a need to better identify the residence times and stratification of these lakes in hydrologic modelling (*also see*,

Holmes 2016 recommendations) potentially using density-dependent methodologies developed for thermal stratification (Kirillin and Shatwell 2016) in conjunction with ET partitioning methods. Separation of lakes storages into epilimnion and hypolimnion storages would limit the mixing of lake volume and allow for further constraint of the separation of evaporative fractionation from sub-surface storages (i.e. unsaturated soils and wetlands) from open water evaporative fractionation. Furthermore, the consideration and incorporation of lake hydrology into the E/ET partition methodology may widen the application to catchments influenced by hydraulic regulation (e.g. hydroelectric dams).

7.2.4. FREEZE-THAW CYCLES

Lastly, hydrological processes in high-latitude watersheds are complicated by both permafrost and intra-annual soil freeze-thaw cycles. These conditions limit infiltration, lateral sub-surface flow, and reduce sub-surface storage availability. There is significant need for tracer-aided modelling of such processes at various spatial and temporal resolutions, including the depth of frost penetration, as increasing temperatures due to climate change influence the spatial heterogeneity of permafrost influence. As identified in Chapter 6, there is significant intra-annual variability in sub-surface storage, notably during the shoulder seasons, but additionally during the winter months. However, this analysis identified large scatter due to inter-annual differences, which may be resolved through measurement of the water content and subsurface temperature for the degree and depth of freezing (Azmatch et al., 2012). Research conducted with tracer-aided modelling (Chapters 4 and 5) simplified freeze-thaw estimations by using air temperature, but were limited in subsurface freezing extent estimation. Uncertainty in the ET partition of the shoulder seasons (spring and fall) further points to ground freeze-thaw cycles as a significant process to be addressed in ET partitioning. In addition to discharge, freeze-thaw cycles

potentially effect soil isotopic compositions during spring freshet by gradually releasing ice-bound late fall precipitation compositions that have been isotopically fractionated. While these processes may be masked by snowmelt fractionation, the influence of thaw-induced fractionation on the ET partition should be examined further.

The work completed in this thesis presents a significant step forward in temporal ET partitioning estimation in data-scarce high-latitude watersheds, while providing insights to some dominant processes within these regions and highlighting future work that may further constrain estimation methods. Constraining and identifying large-scale watershed processes, notably evaporation and transpiration, using tracer-aided modelling is essential for long-term water management and planning. Changes in fluxes will influence the storage response within these basins, potentially decreasing the transit time and increasing the storage responsiveness to annual changes in precipitation, exacerbating flood and drought conditions.

7.3. REFERENCES

Azmatch, T.F., Sego, D.C., Arenson, L.U., Biggar, K.W. 2012. Using soil freezing characteristic curve to estimate the hydraulic conductivity function of partially frozen soils. *Cold Regions Science and Technology*, **Volume 83-84**: 103-109.

Birkel, C., Tetzlaff, D., Dunn, S.M., Soulsby, C. 2011. Using lumped conceptual rainfall-runoff models to simulate daily isotope variability with fractionation in a nested mesoscale catchment. *Advances in Water Resources*, **Volume 34**: 383-394.

Delavau, C.J., Stadnyk, T.A., Holmes, T. 2017. Examining the impacts of estimated precipitation isotope ($\delta^{18}O$) inputs on distributed tracer-aided hydrological modelling. *Hydrology and Earth System Science*. **Volume 21**: 2595-2614. DOI:10.5194/hess-2016-539.

Delavau, C.J. 2016. Development of precipitation $\delta^{18}O$ isoscapes for Canada and application within a tracer-aided hydrological model. *PhD Thesis*. University of Manitoba.

Gat, J., 2010. Isotope Hydrology: A study of the water cycle. London. Imperial College Press.

Gibson, J.J. 2002. Short-term evaporation and water-budget comparisons in shallow Arctic lakes using non-steady isotope mass-balance. *Journal of Hydrology*, **Volume 264**: 242-261.

Gibson, J.J., Edwards, T.W.D. 2002. Regional water balance trends and evaporation-transpiration partitioning from a stable isotope survey of lakes in northern Canada. *Global Biogeochemical Cycles*, **Volume 16(2)**: 10-1–10-14.

Gibson, J.J., Prepas, E.E., McEachern, P. 2002. Quantitative comparison of lake throughflow, residency, and catchment runoff using stable isotopes: modelling and results from a regional survey of Boreal lakes. *Journal of Hydrology*, **Volume 262**: 128-144.

Guo, X., Tian, L., Wang, L., Yu, W., Qu, D. 2017. River recharge sources and the partitioning of catchment evapotranspiration fluxes as revealed by stable isotope signals in a typical high-elevation arid catchment. *Journal of Hydrology*, **Volume 549**: 616-630.

Holmes, T. 2016. Assessing the value of stable water isotopes in hydrologic modelling: A dual-isotope approach. *Master of Science Thesis.* University of Manitoba.

Kirillin, G., Shatwell, T. 2016. Generalized scaling of seasonal thermal stratification in lakes. *Earth-Science Reviews*, **Volume 161**: 179-190.

APPENDIX A: HELIOS HYDROLOGIC MODEL EQUATIONS

Model Process	Method	Numerical Model	EQN
Unsaturated Zone		$\boldsymbol{K_{HU}} = K_{HU} \cdot \left(\frac{\theta}{\phi}\right)^{e_{HU}}$	A1
		$\boldsymbol{Q_R} = \boldsymbol{K_{Hu}} \cdot S \cdot GWT \cdot 2 \cdot CL$	A2
		$\boldsymbol{Q_{SR}} = Q_R \cdot (1 - WLC)$	A3
		$\boldsymbol{Q_{SW}} = Q_R - Q_{SR}$	A4
		$\boldsymbol{ASSV} = (\phi - \theta) \cdot GWT \cdot A$	A5
		$\boldsymbol{PRE} = K_h \cdot \left(\frac{\theta}{\phi}\right)^{a_u} \cdot A$	A6
		$\boldsymbol{Q_{SG}} = (PRE - ASSV)$	A7
Infiltration	**Explicit Green-Ampt**	$\boldsymbol{\psi_f} = \frac{2 \cdot b + 3}{2 \cdot b + 6} \cdot \psi_{ae}$	A8
		$\boldsymbol{\psi_f^*} = \psi_f(\phi - \theta)$	A9
		$\boldsymbol{T_{peak}} = \frac{K_v \psi_f^*}{\left(w(w - K_v)\right)}$	A10
		$\boldsymbol{f(T_{peak})} = T_{peak} \cdot w$	A11
		$\boldsymbol{T_{comp}} = \frac{f(T_{peak})}{K_v} - \frac{\psi_f^*}{K_v} \cdot \ln\left(1 - \frac{f(T_{peak})}{\psi_f^*}\right)$	A12
		$\boldsymbol{t_e} = 1 - T_{peak} - T_{comp}$	A13
		$\boldsymbol{T^*} = \frac{\psi_f^*}{K_v}$	A14
		$\boldsymbol{Q_{INF}} = K_v \cdot \left(\left(1 - \frac{\sqrt{2}}{3}\right) t_e + \frac{\sqrt{2}}{3} \cdot \sqrt{T^* \cdot t_e + t_e^2} + \frac{\sqrt{2}-1}{3} T^* \cdot (\ln[\![(t]\!]_e + T^*) - \ln T^*) + \frac{\sqrt{2}}{3} T^* \left(\ln [\![(t]\!]_e + \frac{T^*}{2} + \sqrt{T^* t_e + t_e^2}\right) - \ln \frac{T^*}{2}\right)\right)$	A15
Throughfall	**Water-balance**	$\boldsymbol{P_{th}} = P - R_{int}$	A16
Interception	**BROOK90**	$\boldsymbol{R_{int}} = 0.15 \cdot LAI$	A17
Ponded Water and Disconnected Wetlands	**Fill-and-spill**	$\boldsymbol{Q_o} = \max\{0, V_p - V_{pMAX}\}$	A18

APPENDIX A

Saturated Zone		$\boldsymbol{Q_{GW}} = K_{HS} \cdot (S + M_C \cdot M_s)^{a_s} \cdot (d_{GW}) \cdot 2 \cdot CL$	A19
		$\boldsymbol{M_s} = \frac{d_{GW}}{TD}$	A20
Connected Wetlands	**Dupuit Unconfined Aquifer Equation**	$\boldsymbol{Q_{CWL}} = K_w \cdot \frac{h_o^2 - h_r^2}{W_{width}} \cdot CL \cdot h_o$	A21
		$\boldsymbol{W_{width}} = \boldsymbol{A/CL}$	A22
		$\boldsymbol{d_e} = \boldsymbol{W_{width}} \cdot \boldsymbol{S}$	A23
		$\boldsymbol{h_o} = \boldsymbol{d_e} + \boldsymbol{d_w}$	A24
Evapotranspiration	**Penman-Monteith**	$\boldsymbol{ET} = \frac{\left(\Delta \cdot (K + L) + \rho_a \cdot c_a \cdot C_{at} \cdot e_a^* \cdot (1 - RH)\right)}{\rho_w \cdot \lambda_v \cdot (\Delta + \gamma \cdot (1 + C_{at}/C_{can}))}$	A25
		$\boldsymbol{C_{at}} = \frac{v_a}{6.25 \cdot \left[\ln\left(\frac{z_m - z_d}{z_o}\right)\right]^2}$	A26
		$\boldsymbol{C_{can}} = f_s \cdot LAI \cdot C_{leaf}$	A27
		$\boldsymbol{C_{leaf}} = C_{leaf}^* \cdot f_k(K_{in}) \cdot f_p(\Delta\rho_v) \cdot f_T(T_a) \cdot f_\theta(\Delta\,\theta)$	A28
Intercepted Evaporation	**Penman**	$\boldsymbol{ET} = \frac{\left(\Delta \cdot (K + L) + \rho_a \cdot c_a \cdot C_{at} \cdot e_a^* \cdot (1 - RH)\right)}{\rho_w \cdot \lambda_v \cdot (\Delta + \gamma)}$	A29
Open Water Evaporation	**Mass-Transfer**	$\boldsymbol{E} = (b_o + b_1 \cdot v_a) \cdot (e_s - e_a)$	A30
Snowmelt	**Energy Balance**	$\boldsymbol{Q_{cc}} = -c_i \cdot \rho_w \cdot h_m \cdot (T_s - T_m)$	A31
		$\boldsymbol{Q_{m2}} = \theta_{ret} \cdot h_s \cdot \rho_w \cdot \lambda_f$	A32
		$\boldsymbol{\theta_{ret}} = -0.0735 \cdot \left(\frac{\rho_s}{\rho_w}\right) + (2.67\times10^{-4}) \cdot \left(\frac{\rho_s^2}{\rho_w}\right)$	A33
		$\boldsymbol{Q_{m3}} = (h_m - \theta_{ret} \cdot h_s) \cdot \rho_w \cdot \lambda_f$	A34
River Attenuation	**Muskingum Routing**	$\boldsymbol{Q_{Out2}} = Q_{IN2} \cdot R_o + Q_{IN1} \cdot R_1 + Q_{out} \cdot R_2$	A35
		$\boldsymbol{R_o} = \frac{-K_M \cdot X_M + 0.5 \cdot \Delta t}{D}$	A36
		$\boldsymbol{R_1} = \frac{K_M \cdot X_M + 0.5 \cdot \Delta t}{D}$	A37
		$\boldsymbol{R_2} = \frac{K_M - K_M \cdot X_M - 0.5 \cdot \Delta t}{D}$	A38
		$\boldsymbol{D} = K_M - K_M \cdot X_M + 0.5 \cdot \Delta t$	A39

K_{HU}: Saturated hydraulic conductivity of the unsaturated storage, θ: soil water content, ϕ: soil porosity, e_{HU}: non-linearity of unsaturated conductivity, S: Basin Slope, GWT: groundwater table, CL: channel length, Q_R: total unsaturated flux, Q_{SR}: unsaturated flux to river, WLC: percent wetland lined channels, Q_{SW}: unsaturated flux to the river, ASSV: available vertical flux, PRE: vertical flux potential, Q_{SG}: vertical flux from unsaturated to saturated, ψ_f: wetting-front suction, b: soil spacing, ψ_{ae}: air entry pressure, K_v: vertical hydraulic conductivity, w: rainfall intensity, T_{peak}: time to peak, t_e: effective time, T_{comp}: compression time, T^*: Characteristic time, Q_{INF}: recharge potential P_{th}: throughfall precipitation, P: precipitation, R_{int}: interception volume, LAI: leaf area index, V_p: volume of ponded water, Q_o: overland flux, K_{HS}: saturated conductivity, M_c: Moisture content , M_s: Moisture content effect on saturation slope, a_s: non-linearity of saturated soils, d_{GW}: depth of saturated storage, TD: total depth of storage, K_w: wetland conductivity, W_{width}: wetland width, h_o: relative wetland depth, h_r: river depth, A: area, d_e: elevation difference, d_w: storage wetland depth, Δ: slope of vapour pressure curve, K: shortwave radiation, L: longwave radiation, ρ_a air density, c_a: specific heat of air C_{at}: atmospheric conductance, e_a^*: vapour pressure at

APPENDIX A

saturation at evaporative surface, RH: relative humidity, ρ_w: water density, λ_v: latent head of vapourization, γ: psychrometric constant, C_{can}: canopy conductance, v_a: wind speed, z_m: wind speed measurement height, z_d: zero plane displacement, z_o: roughness height, C_{leaf}^*: maximum leaf conductance, $f_k(K_{in})$: light factor on stomatal opening, $f_\rho(\Delta\rho_v)$: vapour-pressured deficit on stomatal opening, $f_T(T_a)$: air temperature on stomatal opening, $f_\theta(\Delta\theta)$: leaf water content on stomatal opening, C_{leaf}: leaf conductance, e_s: saturated vapour pressure, e_a: actual vapour pressure, c_i: heat capacity of ice, h_m: snow water equivalent depth, T_s: surface temperature, T_m: snow temperature θ_{ret}: water retention of snow, h_s: depth of snow λ_f: latent heat of melting, ρ_s, density of snow, K_M: Muskingum routing parameter, X_M: Muskingum storage parameter, Δt: Routing time-step

APPENDIX B: DEPTH-DEPENDENT EVAPORATION AND TRANSPIRATION

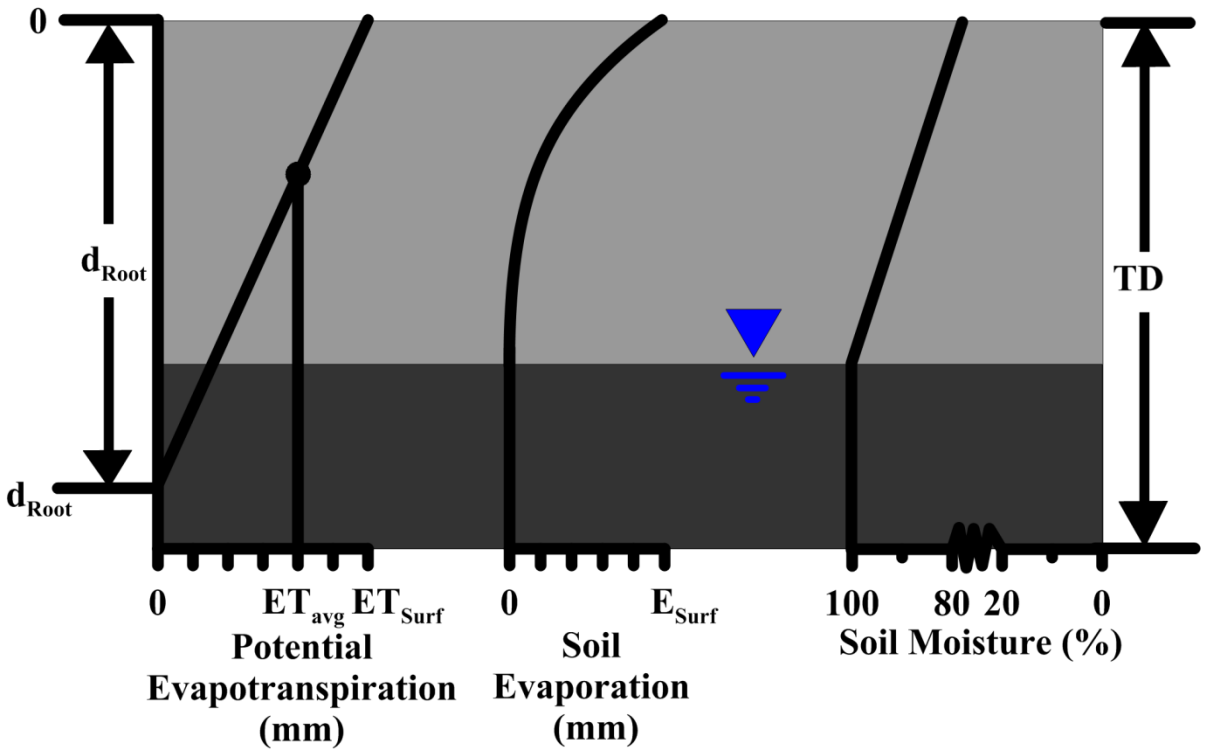

Figure B1: Conceptual model of evapotranspiration (ET) and evaporation estimation with depth. Total depth of the storage is shown as TD. Potential ET is assumed to decrease linearly with depth (left), where ET decreases from the surface, from ET_{surf} at d_{root}=0 to 0 at d_{root}=max. Soil moisture decreases linearly from the groundwater table (100%) to the surface. The surface soil moisture is a function of the unsaturated soil depth and average saturation. PET is partitioned with depth where evaporation is a function of soil moisture and PET to establish a non-linear curve with depth. Evaporation is maximum as the surface (E_{surf}) and decreases with depth to the groundwater table (0).

APPENDIX C: HELIOS ISOTOPIC MODEL EQUATIONS

Isotope Process	Method	Mathematical/Empirical Model	Equation
Isotope Mixing Models	**Fraction Dependent**	$\boldsymbol{C(f)} = C_{ss} - (C_{ss} - C_o)f^{\frac{-(m-1)E+IN}{\Delta V}}$	C1
	Time Dependent	$\boldsymbol{C(t)} = C_{ss} - (C_{ss} - C_o)e^{-\frac{(Em+O)t}{V}}$	C2
	Complete mixing (no E)	$\boldsymbol{C(t)} = \delta_{IN} - (\delta_{IN} - C_o)f^{-\frac{IN}{\Delta V}}$	C3
	Steady-State	$\boldsymbol{C_{ss}} = \frac{E \cdot m \cdot (RH \cdot \delta_A + \varepsilon) + IN \cdot \delta_{IN}}{E \cdot (m-1) + IN}$	C4
		$\boldsymbol{m} = \frac{1}{1 - RH + \varepsilon_k}$	C5
Unsaturated Mixing	**Exponential Distribution**	$\boldsymbol{C(f,z)} = \frac{A \cdot C(f) \cdot P_1^2 + (B - A \cdot P_1^2) \cdot \delta_\infty}{B}$	C6
		$\boldsymbol{A} = \left(\frac{1}{2} \cdot S_M \cdot (z^2 - z_t^2) + MSs(z - z_t)\right)$	C7
		$\boldsymbol{B} = (S_M \cdot z + P_1 \cdot S_M \cdot z_t + P_1 \cdot MSs) \cdot z \cdot e^{-\frac{P_1 \cdot z_t}{z}} - e^{-P_1} \cdot z \cdot (S_M \cdot z \cdot (P_1 + 1) + P_1 \cdot MSs)$	C8
		$\boldsymbol{MSs} = M \cdot 2 - 1$	C9
		$\boldsymbol{S_M} = \frac{1 - MSs}{z_{GwT}}$	C10
Ponded Water Mixing	**Complete Mixing**	$\boldsymbol{C(t)} = \frac{V_p \cdot \delta_p + R \cdot \delta_R + M \cdot \delta_M}{V_f}$	C11
Snowmelt Fractionation	**Craig-Gordon Model**	$\boldsymbol{\alpha_s} = \frac{\frac{1}{\alpha} - (1 - RH)}{1 - RH}$	C12
		$\boldsymbol{b} = \frac{RH}{1 - RH}$	C13
		$\boldsymbol{\delta_M} = \frac{1}{\alpha_s} \cdot f_s^{\alpha_a} \cdot (\delta_{sn} \cdot \alpha_s - \delta_A \cdot b) + (\delta_A \cdot b)$	C14
Atmospheric Compositions	**Temperature Dependent Model**	$\boldsymbol{\delta_A} = \frac{\delta_P - \varepsilon^*}{\alpha^*}$	C15
Equilibrium Separation		$\boldsymbol{\varepsilon^*} = (\alpha^* - 1) \cdot 1000$	C16

Liquid Vapour Equilibrium		$\boldsymbol{\alpha^*} = \frac{\left(\left(e^{6.71\cdot\frac{W}{1000}}\right)\cdot\left(e^{0.35\cdot\frac{W^3}{1000}}\right)\right)}{e^{\frac{7.69}{1000}}\cdot\left(e^{1.67\left(\frac{W^2}{1000}\right)}\right)}$	C17
		$\boldsymbol{W} = \frac{10^3}{T_a + 273.15}$	C18
Kinetic Separation		$\boldsymbol{\varepsilon_k} = n \cdot C_k \cdot \theta \cdot (1 - RH)$	C19
Evaporation Composition		$\boldsymbol{\delta_E} = (C(t) - RH \cdot \delta_A - \varepsilon) \cdot m$	C20

C_{ss}: Isotopic steady-state, C_o: Initial isotopic composition, *f*: volume fraction, z : groundwater table or point of interest, MSs : estimated soil moisture at the surface (≥ 0), S_M : moisture slope (linear), Zt : depth to water moisture (generally will be 0), P1 : exponential mixing parameter.

APPENDIX D: DEPTH-DEPENDENT SOIL ISOTOPIC FRACTIONATION

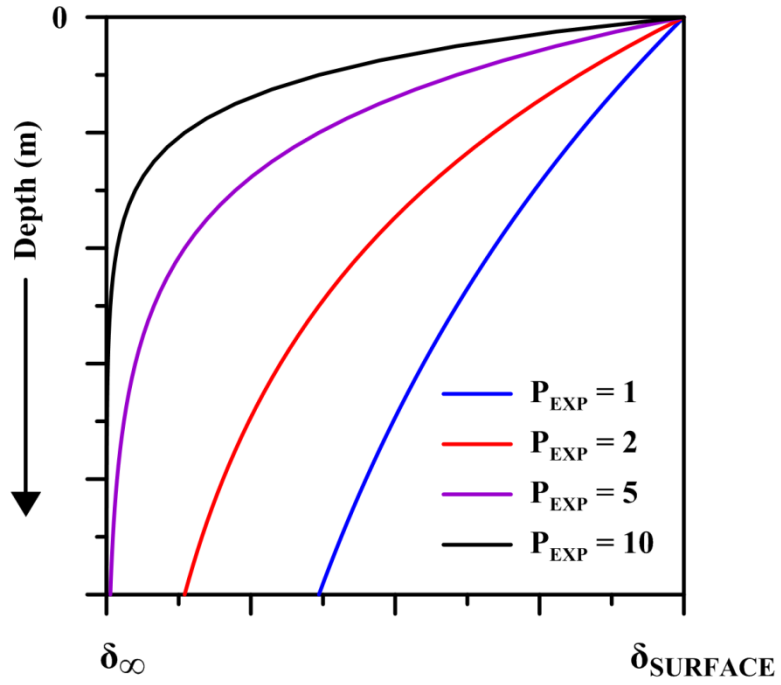

Figure D1: Estimated isotopic composition as a function of storage depth and P_{EXP}.

APPENDIX E: EVAPOTRANSPIRATION PARTITION PARAMETER SENSITIVITY

Table E: ET partition parameter sensitivity given as mean ± standard deviation calibration values. MA adjusts the temporal variability of E/ET and Sc adjusts the minimum E/ET at maximum temperatures.

	Parameter	Sapochi	Gunisao	Burntwood	Odei
Unsaturated Soils (No Ponded water)	***MA***	-0.16±0.12	-1.60±0.50	-0.46±0.38	-0.13±0.05
	Sc	-0.96±0.02	-0.48±0.24	-0.86±0.13	-0.97±0.03
Unsaturated Soils (Ponded Water present)	***MA***	-0.86±0.59	-1.26±0.51	-1.00±0.64	-0.82±0.67
	Sc	-0.55±0.31	-0.19±0.18	-0.36±0.34	-0.48±0.30
Wetlands	***MA***	-0.60±0.43	-1.17±0.51	-0.79±0.39	-0.57±0.40
	Sc	-0.86±0.13	-0.56±0.25	-0.82±0.14	-0.84±0.14